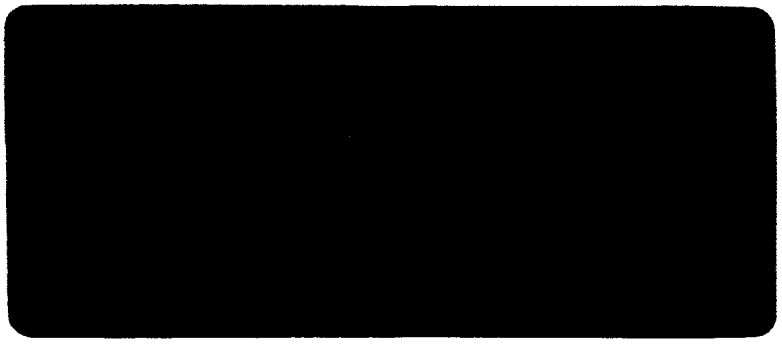

GPO PRICE $ _____

CFSTI PRICE(S) $ _____

Hard copy (HC) 6.00

Microfiche (MF) 1.50

ff 653 July 65

JET PROPULSION LABORATORY
CALIFORNIA INSTITUTE OF TECHNOLOGY
PASADENA, CALIFORNIA

FINAL DESIGN REPORT

FOR

DEPLOYABLE LARGE AREA

SOLAR ARRAY STRUCTURE

RYAN

AERONAUTICAL COMPANY

REPORT NO. 20869-2

5 MAY 1966

This work was performed for the Jet Propulsion Laboratory, California Institute of Technology, pursuant to a subcontract issued under Prime Contract NAS 7-100 between the California Institute of Technology and the United States of America represented by the National Aeronautics and Space Administration.

Jet Propulsion Laboratory

Contract No. 951107

PAGES 231

TABLE OF CONTENTS

LIST OF ILLUSTRATIONS

LIST OF ILLUSTRATIONS (Continued)

LIST OF TABLES

1.0 INTRODUCTION

This report presents the results of the Phase II, Detail Design activities for a Prototype Deployable Large Area Solar Array Supporting Structure conducted by the Ryan Aeronautical Company for the Jet Propulsion Laboratory under Contract No. 951107.

The purpose of the Phase II program was to extend the array concept as established under the Phase I activities to a detail design, prepare engineering drawings and specifications and to conduct supporting technical analysis to insure conformance of the final design with the desired contract objectives.

Section 3.0 of this report contains a functional description and illustration of the major elements of the array and the proposed installation of the array to a hypothetical spacecraft. Sections 4.0 through 9.0 contain supporting technical data.

2.0 SUMMARY

The design, technical analysis and preparation of engineering drawings for a Deployable Large Area Solar Array Support Structure have been accomplished in accordance with the Phase II (Design Phase) requirements of JPL Contract 951107. The final configuration reflects in detail the concept selected at the conclusion of the Phase I (Concept Evaluation Phase) activity. No major problem areas are evident that indicate the inability of the design to fulfill the functional objectives of the program.

The following is a summary of structural and thermal characteristics of the design as compared with contract requirements. The calculated structural weight based on substrate unit area is greater than contract requirements, but reflects a design which is based on controlled tolerance sheet thicknesses, reliability in fulfilling mission requirements and the use of present state-of-art materials.

	Actual Design	Contract Reqm'ts
Solar Cell Area/Panel	51 ft^2	Approx. 50 ft^2
Structure Weight Per Unit Area of Solar Cells	.417 to .462 lbs/ft^2	$< .3 lbs/ft^2$
- Static Requirements -		
Substrate Radius of Curvature	6 in. min.	6 in. min.
- Dynamic Requirements -		
Angular Change of Solar Cell Substrate/unit length	$< .3$ Degree/in.	< 1 Degree/in.
Variation in First Mass Moment of Array and Support Structure for Stowed Position	$\pm 5.1\%$	$< \pm 5\%$
Undamped First Cantilever Frequency of Deployed Array Structure	0.55 cps	Between 0.5 & 5.0 cps

	Actual Design	Contract Requirements
Variation in Ratio of Stiffness to Mass of Deployed Array Structure	$\pm$4.3%	$< \pm$10%
- Thermal Requirements-		
Resistance to Sterilization	300°F	295°F
Emissivity of Rear Surface of Substrate	.90	> .8

3.0 DESIGN DISCUSSION

The array concept, shown schematically in Figure 3-3 and in detail by Ryan drawings 208V001 through 208V013, is designed to deploy a minimum of 200 ft^2 of solar cell area. This area is divided into four sections of approximately 50 ft^2 each. These sections, which are approximately 3 ft x 18 ft, will be referred to as deployable solar panels. The panels are deployed and supported by extendable beams. The beams and solar cell substrate are stowed on a cylindrical drum which is driven by an electric motor to deploy or retract the solar panels. The support beams are designed to flatten as they approach the drum thus making wrapping possible.

The individual panel and support concepts presented here will be divided into seven basic areas for purposes of discussion. These areas are:

Support Beam
Substrate
Support Structure
Actuation
Electrical Provisions
Mount Provisions

These areas are discussed individually in the following pages. This discussion will be limited to a description of the final design since the preliminary development report (Reference 8) explores the history of the design and substantiates choices made.

3.1 Support Beam (Reference Ryan Drawing 208V007)

The cross-sectional shape of the beam and substrate attachment is shown diagramatically in Figure 3-4. The entire assembly is shown in detail on Ryan drawing 208V007. The top and bottom sections are identical except for the substrate attach strip which is seamwelded to the lower portion, and the doubler strips which are attached to the inboard end of the top section. Both sections are joined as indicated at their faying surfaces by seamwelds along the entire length. The inboard end of the beam assembly is deformed to a flat surface and permanently held in this shape by seamwelding the two caps together and adding a doubler. The reason for this end design is to facilitate attachment to the drum by providing a preflattened beam assembly

which will mount flush with the substrate storage drum. The outboard end of the beam attaches directly to a cross member leading to the beam on the opposite end of the panel assembly. The substrate attach strip mentioned previously contains precisely located slots which will be controlled with respect to mating slots in the substrate and opposite hand beam. This control will be accomplished by means of coordinated tooling. The purpose of these slots is part of the scheme of substrate attachment to the beam. A formed sheet metal part containing fingers is inserted into these slots (Ryan Drawing 208V012). The fingers are bent 90° to accomplish fastening and the part then forms a connector with sufficient flexibility to follow the rolled assembly and sufficient strength to transfer the loads from the substrate to the beam.

The material used for the beam was .006 sheet Ti 6AL-4VA. The beam will be formed by first seamwelding the flat upper and lower halves together. A tool will then be inserted between the two layers to expand the sheets to required height and control the curvature of the upper and lower surfaces. Forming tools will next be placed on each side of the section to completely control the shape of the section. The entire assembly of prestressed beam and forming tools will be heat treated as sufficient temperature and for sufficient time to allow the material of the beam to creep to the shape set by the tools. After the assembly is cooled, the tools are removed without changing the shape of the creep formed beam.

The beam is stowed by rotating the substrate storage drum which reels in the beam. Pressure from the drum causes the beam to flatten in successive element lines as the two parts contact at the drum tangent point. The longitudinal bending strength of the beam is greatly reduced in the flattened area and easily conforms to the shape of the outside dia. of the drum. As the direction of drum rotation is reversed, the pressure on the beam is removed as each element passes the tangent point and the beam returns to its original shape. It should be noted briefly here, as explained fully in Reference 8, that the beam design is a balance between beam cross-sectional shape and material thickness and strength that will produce the required beam properties but is still capable of deforming to a flat configuration without permanent set.

3.2 Substrate (Reference Ryan Drawings 208V005 and 208V013)

Two versions of substrate construction are shown on the referenced drawings. Drawing 208V005 shows the substrate divided into four modules with provisions for attaching. Drawing 208V013 shows a one-piece substrate. Each of these configurations will be described here but the one-piece substrate will be presented only as an alternate.

3.2.1 Modular Substrate

The basic material of the substrate is #113 resin impregnated fiberglass cloth. The major portion of the module is .003 inch thick. Areas .50 inch wide along each side are built up to .012 inch in thickness. Slots are added in these areas to accommodate the previously explained method of connecting to the extendable beam, (Section 3.1). The ends of the substrate are provided with piano-type hinge halves which, by the use of a fiberglass hinge pin, accomplish the attachment of one module to another and to the outboard cross beam. The inboard end of the substrate is terminated by adding a 1/8" dia. fiberglass rod along its width to reduce the possibility of handling damage.

The back surface of the substrate contains 1/2" dia. pads for protecting the fragile solar cells. The pads are made from silicone foam and faced with .002 inch thick teflon sheet. Four of the modules attached end to end by the use of removable 1/8"dia. fiberglass hinge pins and secured to the extendable beams by sheet metal connectors (Drawing 208V012) provide the surface for mounting twelve 18 x 34 solar cell groups as required by JPL specification. This area accommodates 51 ft^2 of solar cells/panel as a minimum. Additional space is available on each module for mounting cells in the amount of .38 ft^2 or 1.53 ft^2/panel or 6.12 ft^2 per array. Approximately 3 ft^2 of area is available per panel also by extending substrate from the present inboard end still further inboard to meet the drum. This would provide 4.35 ft^2/panel or 17.4 ft^2 per array.

As the beam and substrate storage drum rotates and retracts the beams, the attached substrate follows the beam and is wrapped around the outside of the drum for approximately six turns and is stowed in this position

until the deployment command reverses this process and extends beams and substrate.

3.2.2 Continuous Sheet Substrate (Refernece Ryan Drawing 208V015)

This substrate is also constructed from .003 in. resin-impregnated fiberglass cloth. Damper pads of identical material and pattern as described (Section 3.2.1) cover the rear surface of the substrate. The width is extended to provide .20 in. overlap on the beam attach surface for use in bonding directly to the beam strip. The outboard end extends to overlap the outboard cross beam and bond in place. The inboard end is unattached and is stiffened by a 1/8 " dia. fiberglass rod laminated into the fiberglass cloth.

3.3 Roller Drum

The outside of the roller drum is set by JPL specification to a minimum of 1 ft dia., since the minimum bend radius for the substrate is limited to 6 inches. The drum consists of a cylindrical .025 sheet magnesium skin 43.1 in. long. Approximately 30% of the area of this skin is removed by lightening holes. The skin has an access door provided for electrical harness access and also attach provisions for the extendable beams. Each end of the drum assembly is fabricated from a honeycomb sandwich flanged at the O.D. to provide rivet attachment to the skin. A machined magnesium hub is mounted at the center of this sandwich at each end and supports the static and dynamic loads of the drum assembly. These hubs act as an axle for rotation and transfer loads to the support structure. The area of the drum which supports the beams is reinforced at one end by an .025 magnesium stiffener and at the other end of the drum by an .025 magnesium bulkhead which also acts as a guide for the electrical harness. The center of the guide bulkhead supports a spool which is part of the electrical harness provisions and will be discussed in Section 3.6. A machined magnesium spur gear is riveted to one end of the drum and provides the method of driving the drum.

3.4 Support Structure (Reference Ryan Drawing 208V006)

Each end of the roller drum is encompassed and supported by a magnesium sheet metal structure defined by the referenced drawing. This structure serves also as a housing for leaf spring loaded rollers which restrain the beam (Section 3.5). Mounting bosses are attached to the sides of the assembly for the installation of beam support guides (Reference Ryan drawing 208V004). Flanges are used on the outside surface of the structure to provide for mounting the assembly on the spacecraft and a screw hole pattern on the left-hand assembly is provided for installation of the drive motor (Section 3.5). The outboard end of each assembly is constructed as a torque box by tieing the two sides together with bulkheads. This part of the assembly transfers loads, imposed by the extended beam, to a cross beam which ties the two assemblies together and furnishes a good load path. This cross beam, which is permanently attached, and three other hat section beams, which are removed after the assembly is installed in the spacecraft, are shown on Ryan drawing 208V001.

3.5 Actuation System

The primary elements in the actuation system are: deployable beam, roller drum, spring rollers, beam guides, drive gears, drive motor and gear box unit and shut-off switch. The construction of the major items is explained in other sections but the forementioned elements will be brought together here to describe their functions as an integrated system.

The roller drum mounted in bearings is the assembly that attaches to the beam and actually pulls the beam in for retraction or will push the beam out for extension. To accomplish this action the drum is rotated on its bearings by the drive motor working through a spur gear which is attached to one end of the drum assembly. To start the retraction cycle, the motor rotates the drum which pulls on the attached beams and causes the beams to start wrapping around the drum. This wrapping must be preceeded by a change in shape of the beam cross section. This change in shape is caused by the pressure of the drum upon the

beam at the tangent point as previously explained in Section 3.1. Further rotation of the drum causes the beam to be pulled through the guides until approximately 5 1/2 revolutions accomplish complete retraction.

The position and extension direction of the beam is determined by beam guides (Reference drawing 208V004), which are shaped to the contour of the beam at the transition area. These beam guides must react loads imposed by the beam at full extension and also follow the changing position of the drum tangent point as successive layers are added or removed. The guide is pivoted at the outer end to accomplish this position change. A cross shaft which is rotated by the beam travel on a friction wheel causes rotation of a cam support (Reference drawing 208V004-59 and -60) and provides a means of reacting beam loads at any position along the total travel of the beams.

The guide (Reference drawing 208V004) is fabricated from resin impregnated fiberglass cloth laminated to .040 thickness and reinforced by magnesium formers. The friction of the faying surface is reduced by applying a liner of .020 teflon.

During retraction, friction in the system will have no adverse effect on the beam wrapping characteristics since the pull of the drum on the beam causes a tension condition in the wrapped layers and no buckling of the beam will occur. Extending the beam by reversing the motor rotation and therefore the drum rotation will cause the drum to push on the flattened and coiled beam which is stabilized radially on the drum.

Spring loaded rollers are used to furnish the radial support and are located 22 places around the circumference of the coiled beam. The springs are leaf-type .012 titanium sheet and the rollers are epoxy coated magnesium, (Reference drawing 208V006-3). The reaction of the low-friction rollers holds the beam tightly coiled preventing buckling and allowing extension.

The drive motor is a D.C. unit with an integral planetary gear reduction cage. The motor speed is 12,000 RPM and the speed reduction ratio of the gear box is 639.9. The gear box output shaft RPM $= \frac{12,000}{639.9} =$

18.75 RPM. The ratio of drive pinion gear dia to spur gear dia is $\frac{10}{.75} =$ 13.35:1. This produces a roller drum RPM of $\frac{18.75}{13.35} = 1.41$ RPM and a lineal beam extension rate of 4.43 ft/minute. The torque capability of the motor is 1 in-oz. The torque multiplication ratio of the gear box is 262 in.-oz. The torque multiplication from the drive pinion gear to the sput gear is 13.35 x 262 = 3,498 in-oz. or 219 in-lbs of torque is supplied to the roller drum.

The motor is furnished with ball temperature bearings and the gear train lubricated with G.E. versalub G 300. A radio noise filter is provided in the cable. Magnetic shielding is available by the use of a conetic material if later required but is not furnished on this unit.

The maximum in and out position of the beam is sensed by a shut-off switch assembly (Reference Ryan drawing 208V011). This assembly consists of aluminum tumblers which allow the roller drum to turn through 1990° before actuating a double throw micro-switch to shut off the motor.

3.6 Electrical Provisions

An electrical layout was made using the available area and geometry of the structure shown in Figure 3-3. A general description of the buildup is as follows:

1. The solar array consists of four blades
2. Each blade consists of four 55.8 x 36.64 panels
3. Each panel consists of three electrical strings (cell groups)
4. Each string (cell group) consists of four electrical modules
5. Each electrical module consists of 22 submodules
6. Each submodule consists of ten 2 cm x 2 cm cells
7. The electrical connections are ten cells in parallel and 88 cells in series for each string
8. Each string is terminated with four blocking diodes, as shown below:

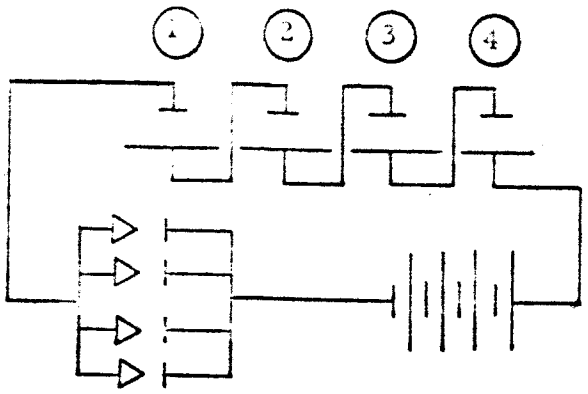

With the cells connected as described above, electrical characteristics of each cell group are as follows, for the conditions noted:

1. At 28°C and rated power input of 140 mw/cm^2 with a 10% efficient cell - 40.48 VDC @ 1.156 A= 46.8 watts output
2. At 59°C and rated power input of 140 mw/cm^2 with a 10% efficient cell - 37.31 VDC @ 1.156 A= 43.12 watts output

The quantities of cells required for the previously described electrical units are as follows:

1.	Submodules	10 cells (all parallel)
2.	Module	220 cells (22 in series)
3.	Cell group (string)	880 cells (88 in series)
4.	Panel	2,640 cells (3 strings in parallel)
5.	Blade	10,560 cells (4 panels in parallel)
6.	Solar array	42,240

The power outputs for these units are:

1.	Cell group	43.125 watts
2.	Panel	129.375 watts
3.	Blade	517.5 watts
4.	Solar array	2,070 watts

Notes:

The substrate area required is 205.4 ft^2

The cell area required is 188.9 ft^2

Packing factor = 91.9%

The number of cells per sq ft = 206

Individual cells area including spacing = .664 in^2

The foregoing layout was investigated to check the feasibility of the geometry to produce 2,000watts. The 2,070 - watt output of this layout proves its feasibility. This electrical design is submitted as one which is compatible with the selected mechanical design and spacecraft electrical requirements using the specified 18 x 34 modules. Additional area is available with the present design to a total of 217.4 ft^2 as noted in Section 3.2.

An area .6 wide is furnished along the length of the substrate for routing flat electrical leads.

The method of providing for the rotation of the drum in routing the harnesses outside the panel assembly and attaching to a fixed point is shown on Ryan drawing 208V008. Eight #22 wires are attached to a fiberglass strip which will serve as a spring carrier. This flat harness is spirally wrapped around a spool inside the drum assembly in a retainer, created by the placement of structural bulkheads in the drum (Section 3.3). One end of the harness is terminated in an electrical connector secured to the drum. Access to this connector may be obtained by removal of the access door in the drum. It is here that the electrical feed from the cells is connected. The opposite end of the harness feeds through the spool and is secured to the panel assembly support structure. An electrical connector is also provided at this end of the harness for connecting to the spacecraft. The spool, previously mentioned, has its position permanently fixed by insertion of a plug (Reference drawing 208V006). This same plug is used to wind the spiralled harness to a compact coil for its stowed position so as to eliminate vibration problems during the boost phase. When the panel assembly is deployed, the rotating drum causes the tightly wound spiral to unwind gradually during the 5-1/2 turns of the drum. Retracting the panel reverses this process.

3.7 Mounting Provisions (Reference Ryan Drawing 208V002)

The referenced drawing illustrates four solar panel assemblies mounted in one plane. The 52-inch dia. circle shown as spacecraft structure was JPL design criteria as set forth by JPL drawing J4190680. The mount structure, which adapts the solar panel

assemblies to this dia., is shown on the referenced drawing. This structure is riveted construction and is fabricated from .032 magnesium sheet. Design of the part was directed to reducing deflection to a minimum since it was important to minimize the dynamic load amplification to the panel assemblies. This was accomplished by closed intersecting torque boxes which serve to beam the load from adjacent panel assemblies to a cantilevered torque box which transfers the load to the spacecraft. The mount can be readily understood by referring to drawing 208V002. A machined fitting at the base of the mount provides a bolt pattern for attachment to the spacecraft.

Panel assemblies are installed on the mounts by mating the channels on each part and sliding the panel assemblies inboard until the bolt patterns align. Attach bolts are then installed to complete the structural tie.

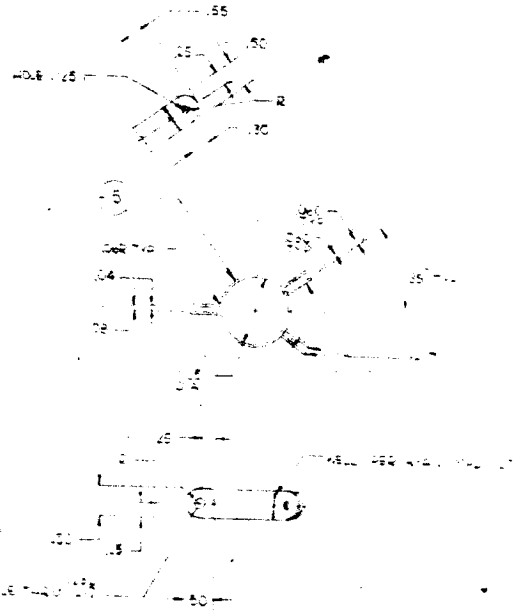

DETAIL - II HINGE PIN

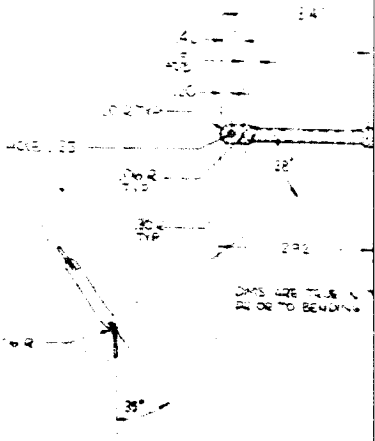

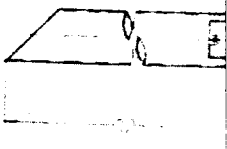

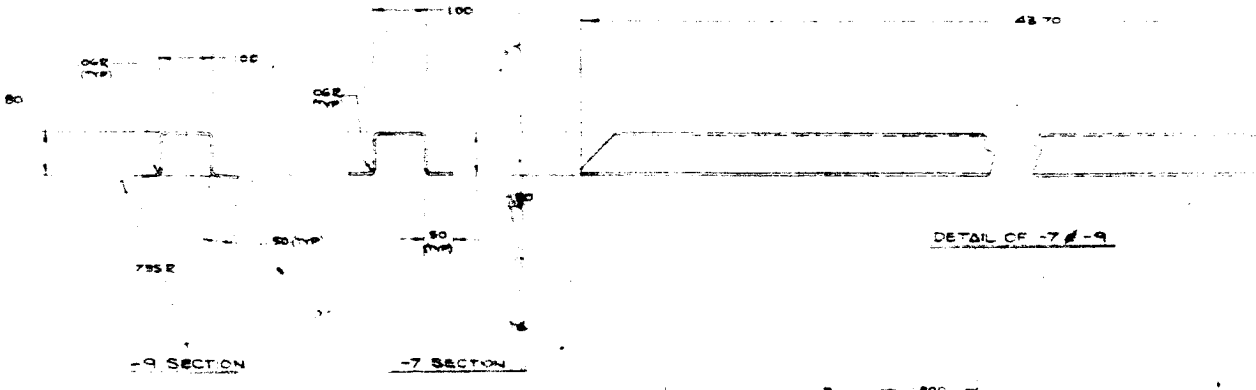

DETAIL OF -7 & -9

-9 SECTION

-7 SECTION

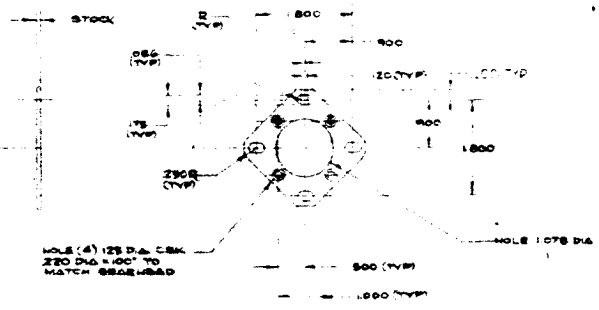

DETAIL OF -5

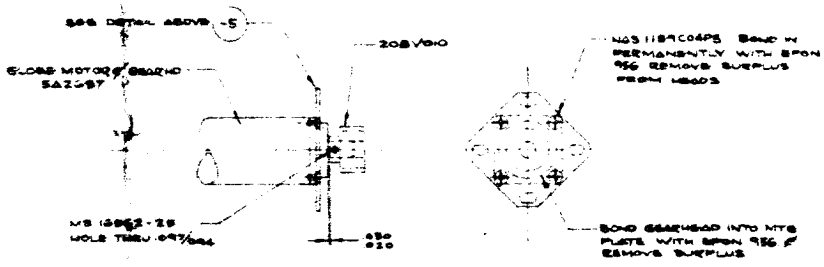

-3 ASSY

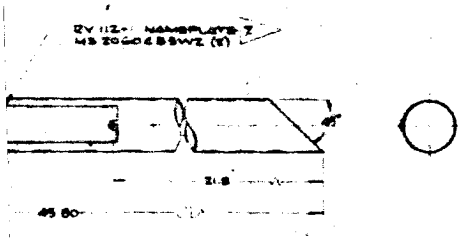

DETAIL OF -21

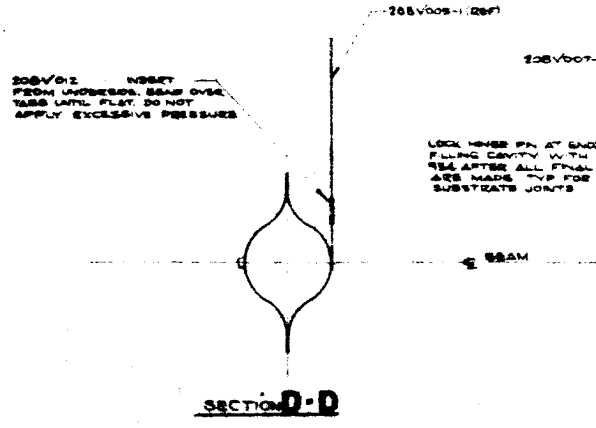

SECTION D-D

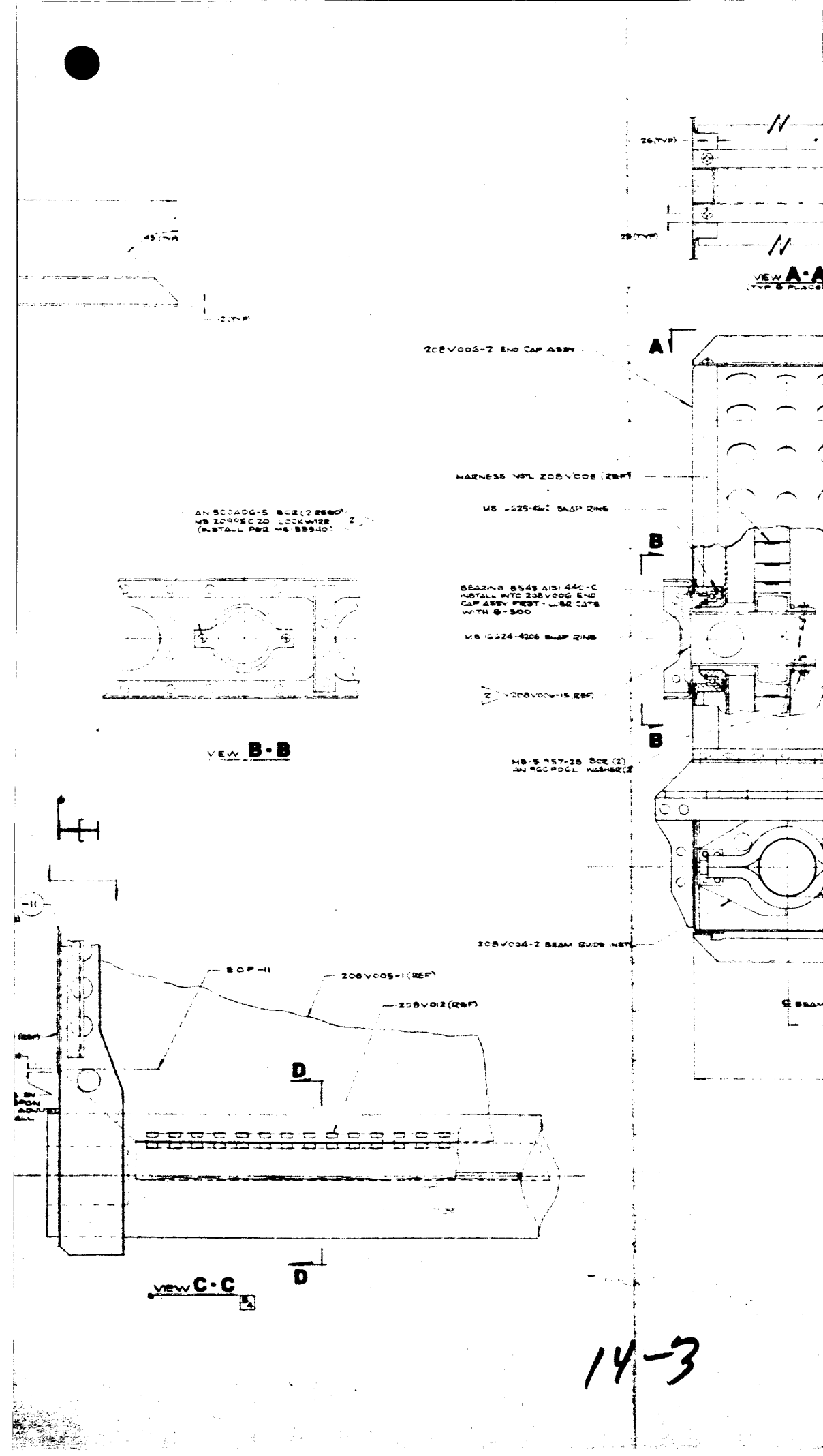
26 (TYP)
29 (TYP)
VIEW A-A
208V006-2 END CAP ASSY
A
HARNESS INSTL 208V008 (REF)
MS 9225-4012 SNAP RING
AN 500ADG-5 SCR (2 REQD)
MS 20995C20 LOCKWIRE
(INSTALL PER MS 33540)
B
BEARING 8548 AISI 440-C
INSTALL INTO 208V006 END
CAP ASSY FIRST - LUBRICATE
WITH Ø-300
MS 9224-4206 SNAP RING
208V004-15 (REF)
VIEW B-B
MS 9557-28 SCR (2)
AN 960 PDGL WASHER (2)
208V004-2 BEAM GUIDE INSTL
208V005-1 (REF)
208V012 (REF)
D
VIEW C-C

14-3

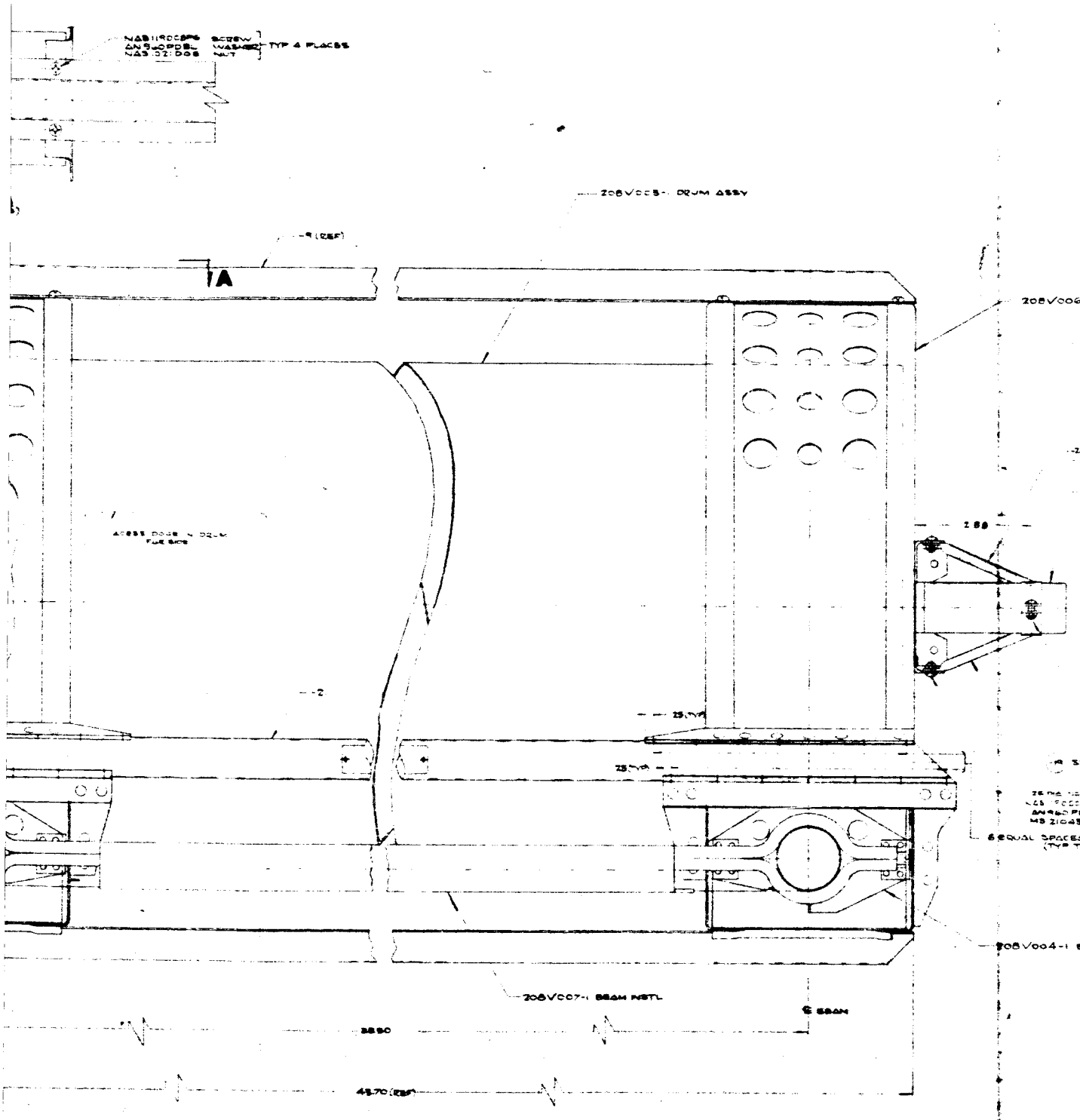

(-1) DEPLOYABLE SOLAR PANEL ASSEMBLY

14-4

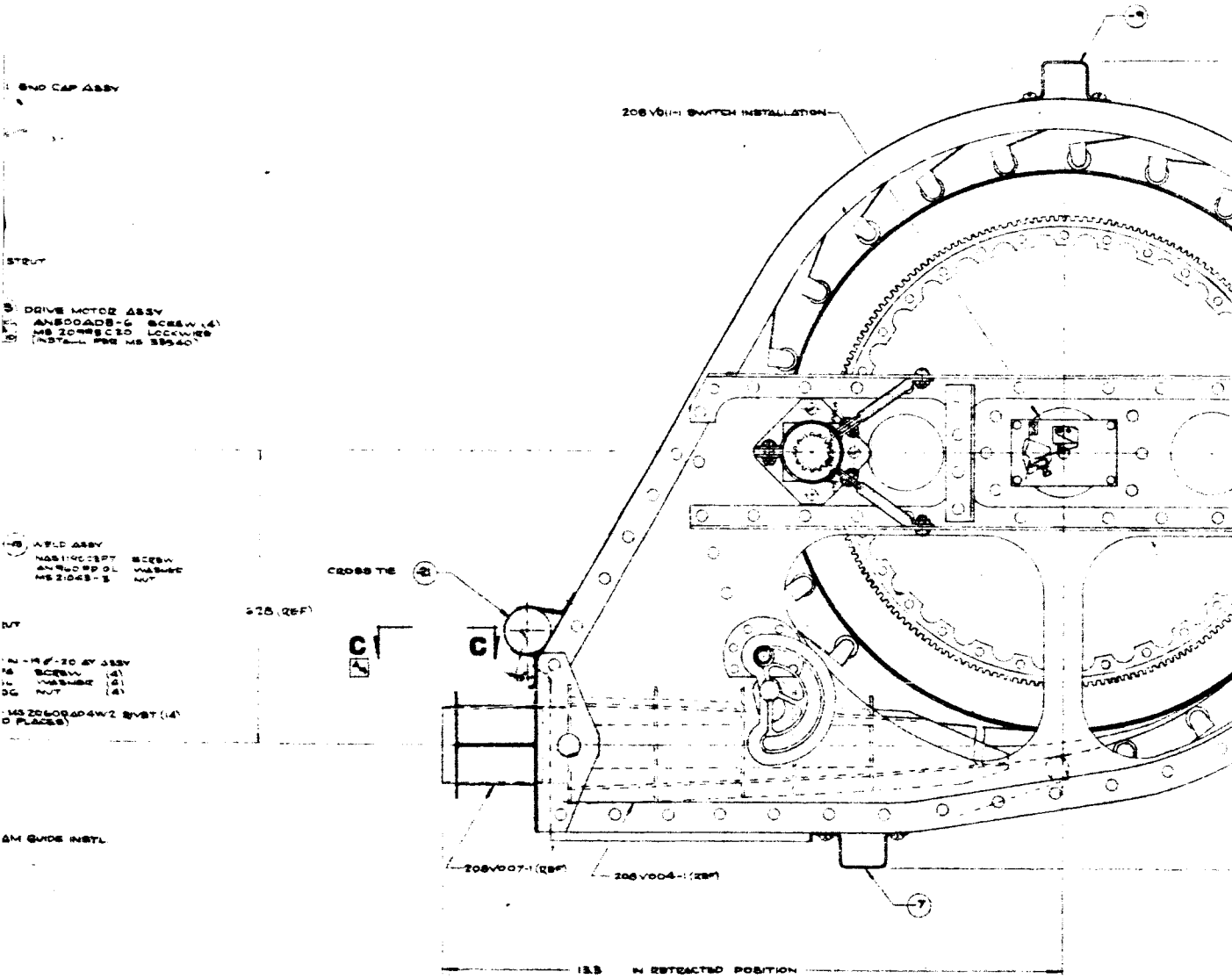
208V011-1 SWITCH INSTALLATION
CROSS TIE
208V007-1
208V004-1
133 IN RETRACTED POSITION

14-5

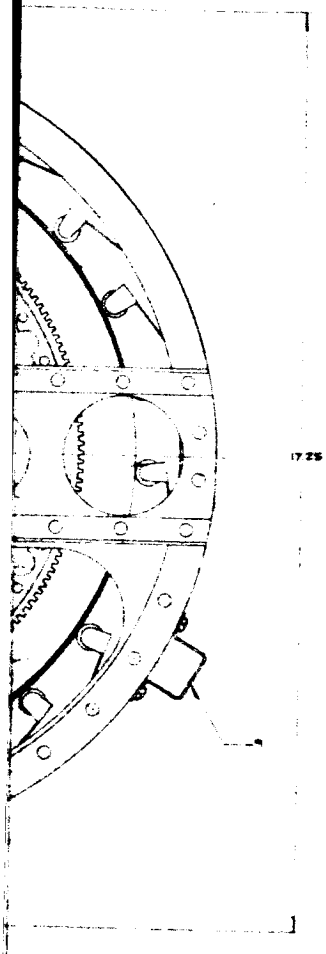

17.25 (REF)

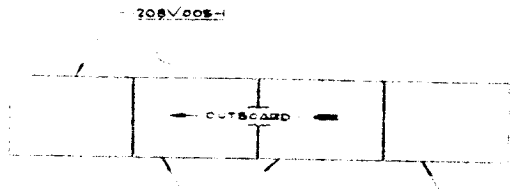

VIEW SHOWING RELATIVE POSITIONS OF SUBSTRATE ASSEMBLIES IN DEPLOYED CONDITION

NOTES:

1. MAY BE PURCHASED FROM GLOBE INDUSTRIES: DAYTON 4 OHIO
2. SEE 208V008 FOR INSTALLATION INSTRUCTIONS
3. ALL PROCESSES TO BE IN ACCORD WITH RYAN SPEC 208 S 002
4. HEAT TREAT TO T8 AFTER FORMING
5. ANODIZE WITH DOW 17 TYPE I PER MPD-102
6. SEE ALSO CHEMICAL AND PAINT CO. PITTSBURG CALIF.
7. ADD THE FOLLOWING INFORMATION TO NAME-PLATE:
   NAME OF PART: DEPLOYABLE SOLAR PANEL
   SERIAL NO.: 1, 2, 3, 4 (AS APPLICABLE)
   PART NO.: 208V001
   CONTRACT NO.: NAS 7-100/951107
   MARK OUT "FSN"

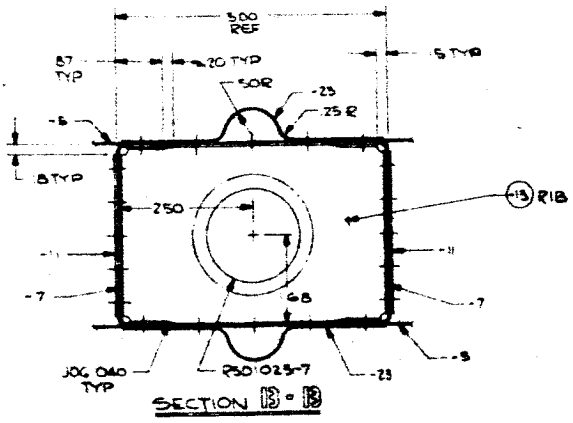

SECTION B-B

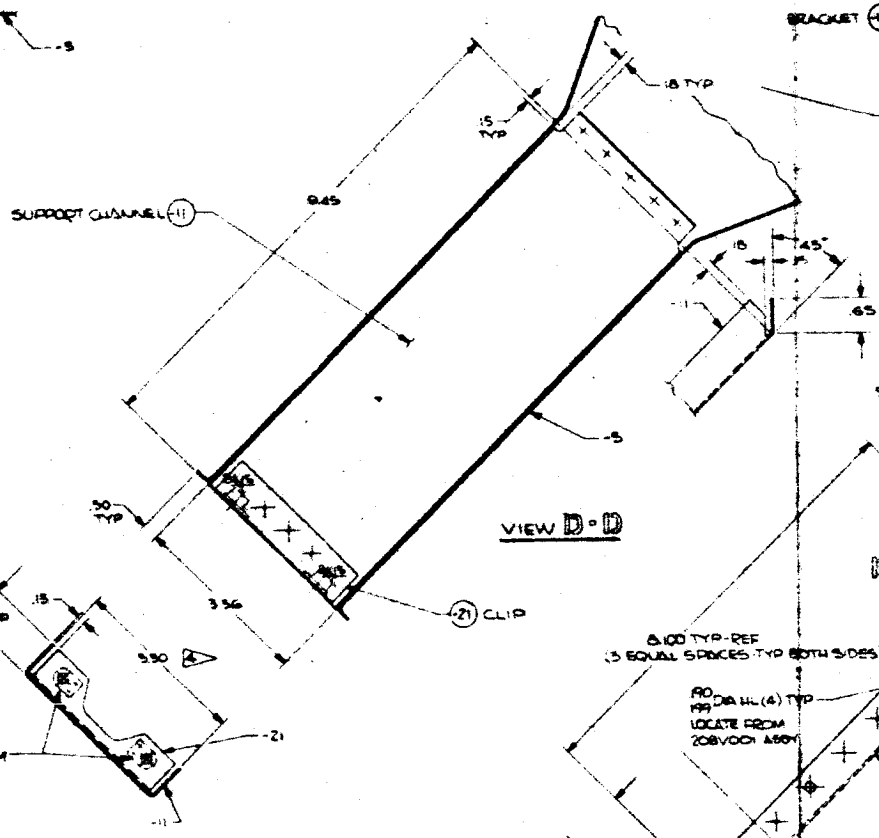

VIEW D-D

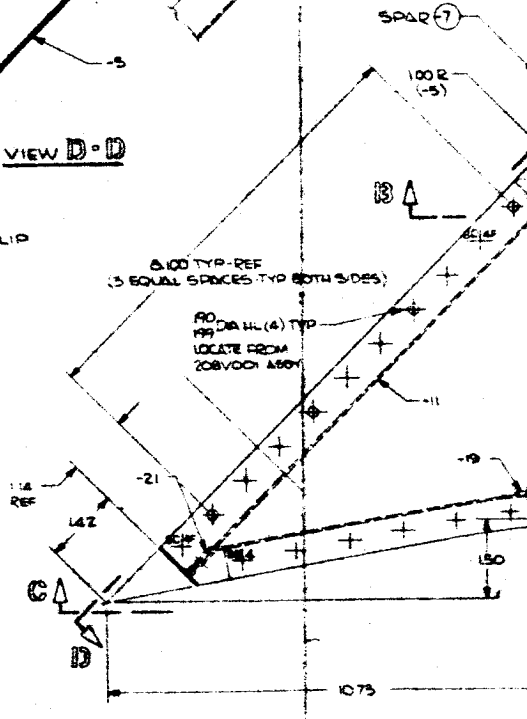

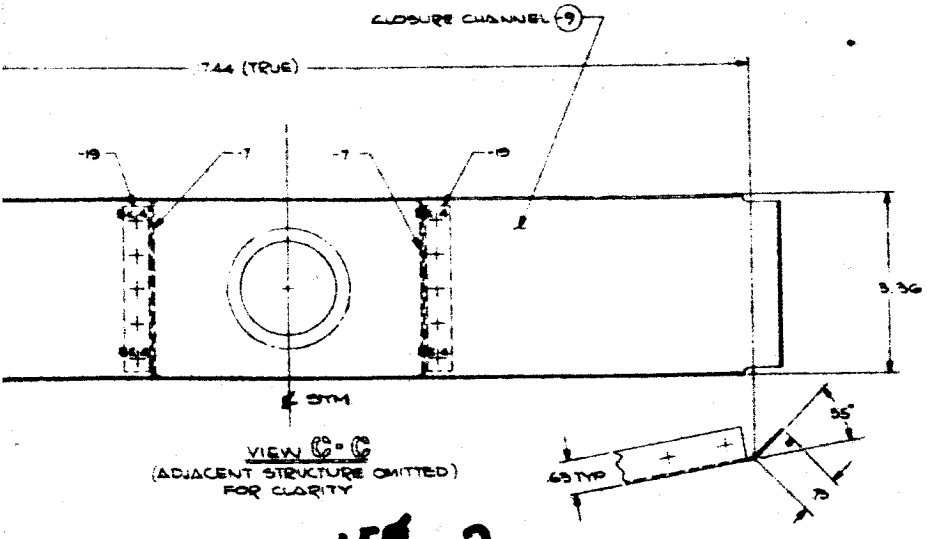

VIEW C-C
(ADJACENT STRUCTURE OMITTED FOR CLARITY)

-3 SUPPORT

158-2

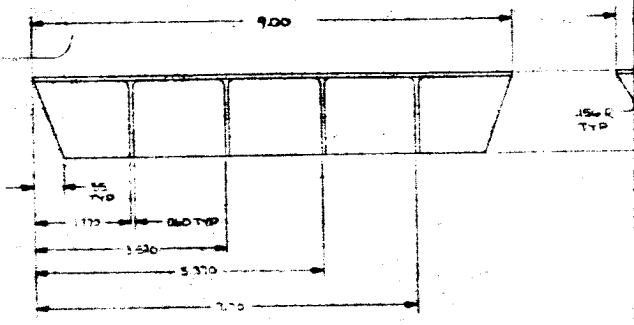

DETAIL -15

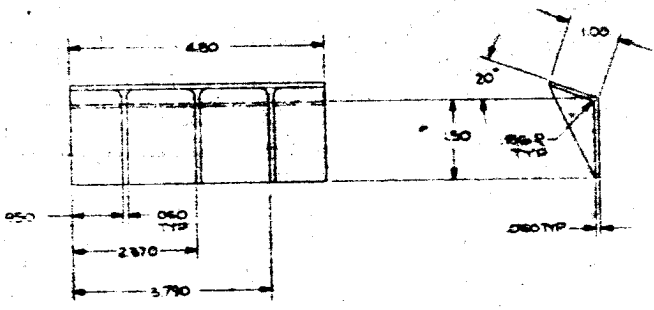

DETAIL -17

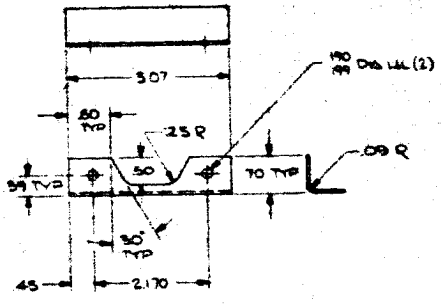

DETAIL -21

15-1

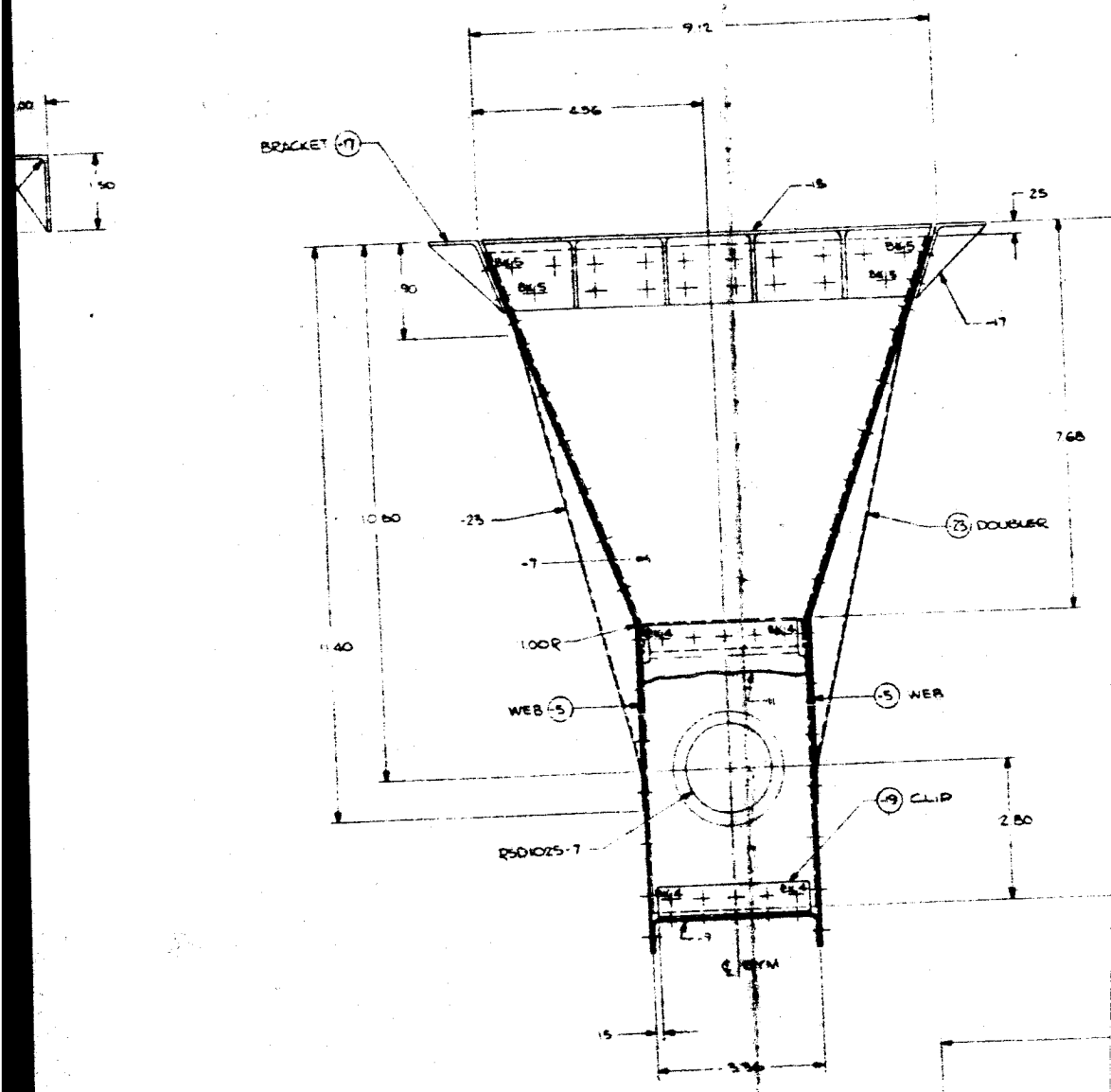
9.12
4.56
BRACKET -17
-15
.25
.90
-17
7.68
10.60
-25
-7
-23 DOUBLER
11.40
100R
WEB -5
-5 WEB
-9 CLIP
R5D1025-7
2.80
15
SECTION A-A
.15 TYP
.15 TYP
3.10
.50
.09 R
.65
DETAIL -19

16-3

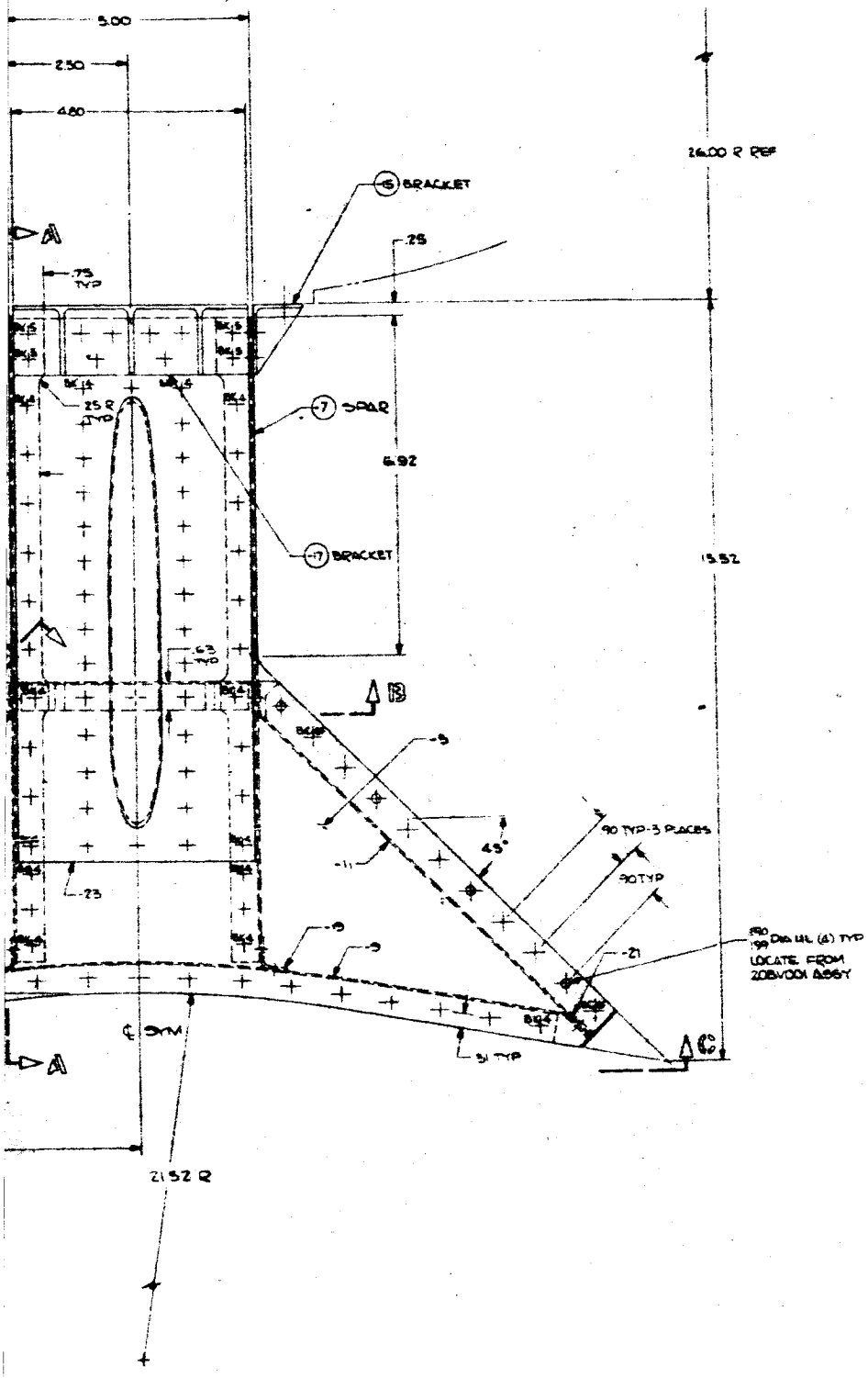

PLAN VIEW

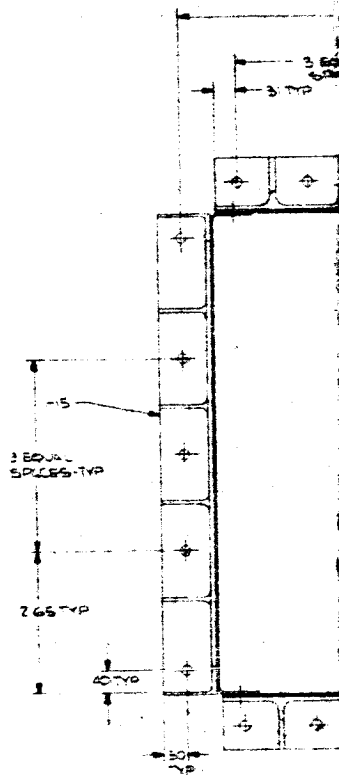

SECTION
(SHOWING
- INSTL
4 PLACES

20BV001

STRUCTURE ASSEMBLY

15-4

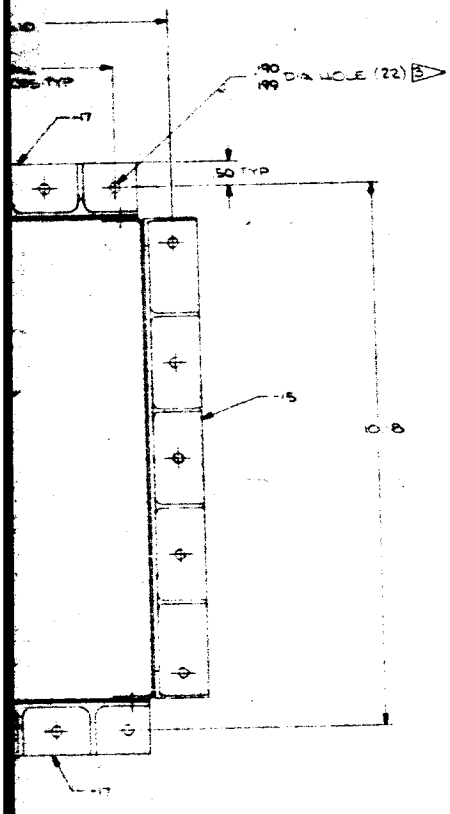

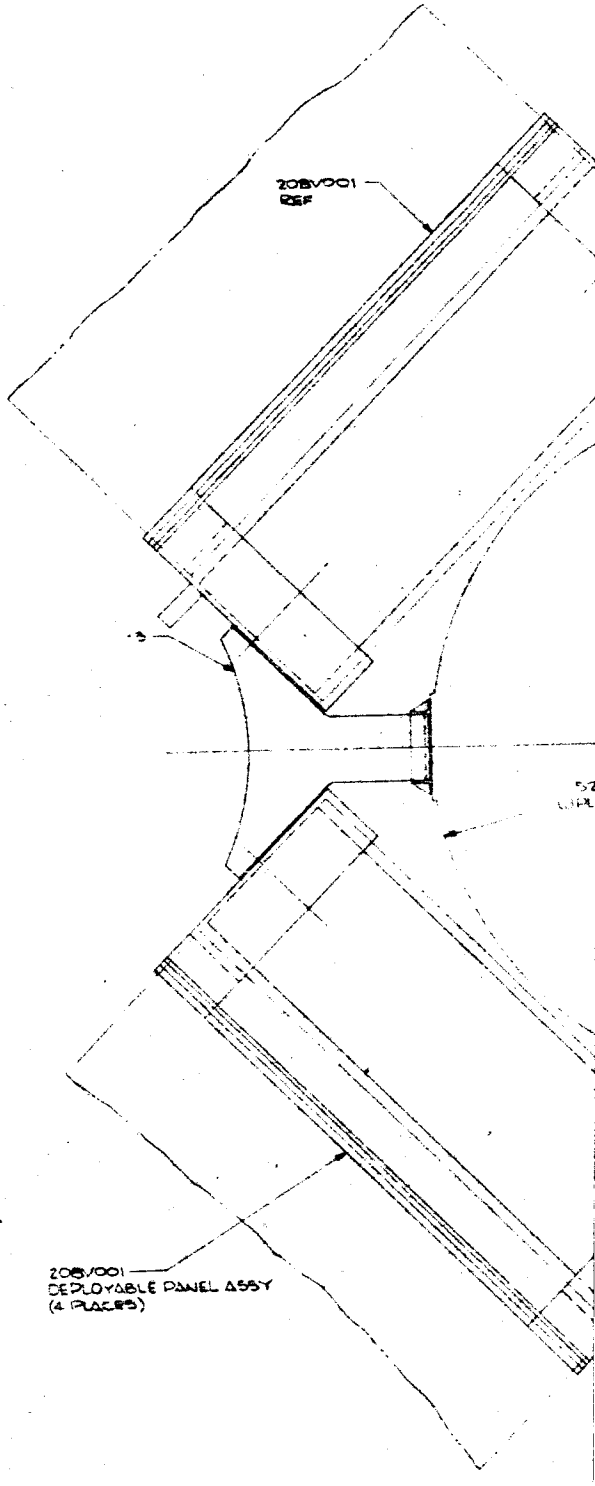

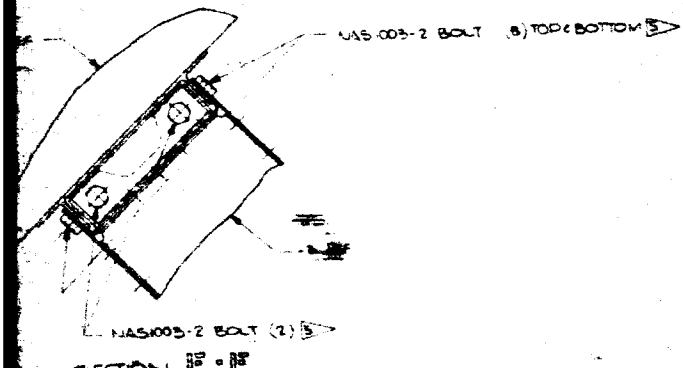

SECTION
(TYP 8 PLACES)

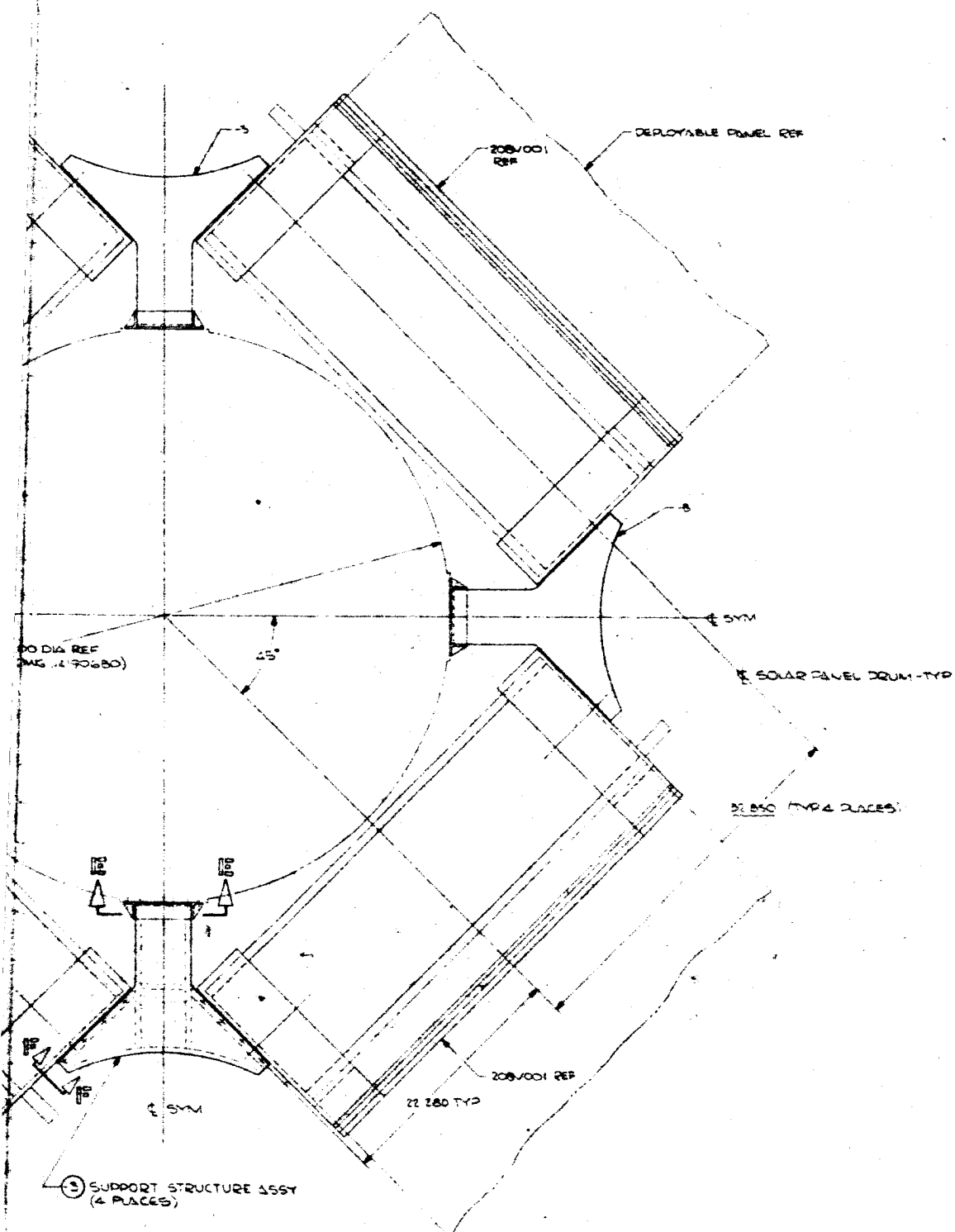

-1 SOLAR ARRAY INSTL

SCALE 1/4

NOTES:

1. EDGE DISTANCE FOR NO. 4 RIVETS TO BE .25 EXCEPT AS SHOWN.
2. EDGE DISTANCE FOR NO. 5 RIVETS TO BE .31 EXCEPT AS SHOWN.
3. ATTACHMENT HARDWARE FOR -1 INSTL TO BE FURNISHED BY CUSTOMER
4. MATING DIMENSION $\pm\frac{.01}{.00}$. TO ALLOW FITNESS OVER ATTACH FLANGES OF 208V001.
5. TORQUE TO 20-25 IN LBS.
6. BEND RAD. TO BE .09
7. RELIEF RAD. TO BE .12.
8. ALLOWABLE MACHINE MISMATCH FROM DIMENSIONS INDICATED TO BE -.000 TO +.030.
9. SHEET STOCK TOL $\pm\frac{.03}{.00}$.
10. ALL PROCESSES TO BE IN ACCORD WITH CYAN SPEC 208S002
11. ANODIZE ALL DETAILS WITH DOW 7 TYPE I PER MPD 102
12. REMOVE 208V001-7 & -9 CHANNELS ON INSTL.

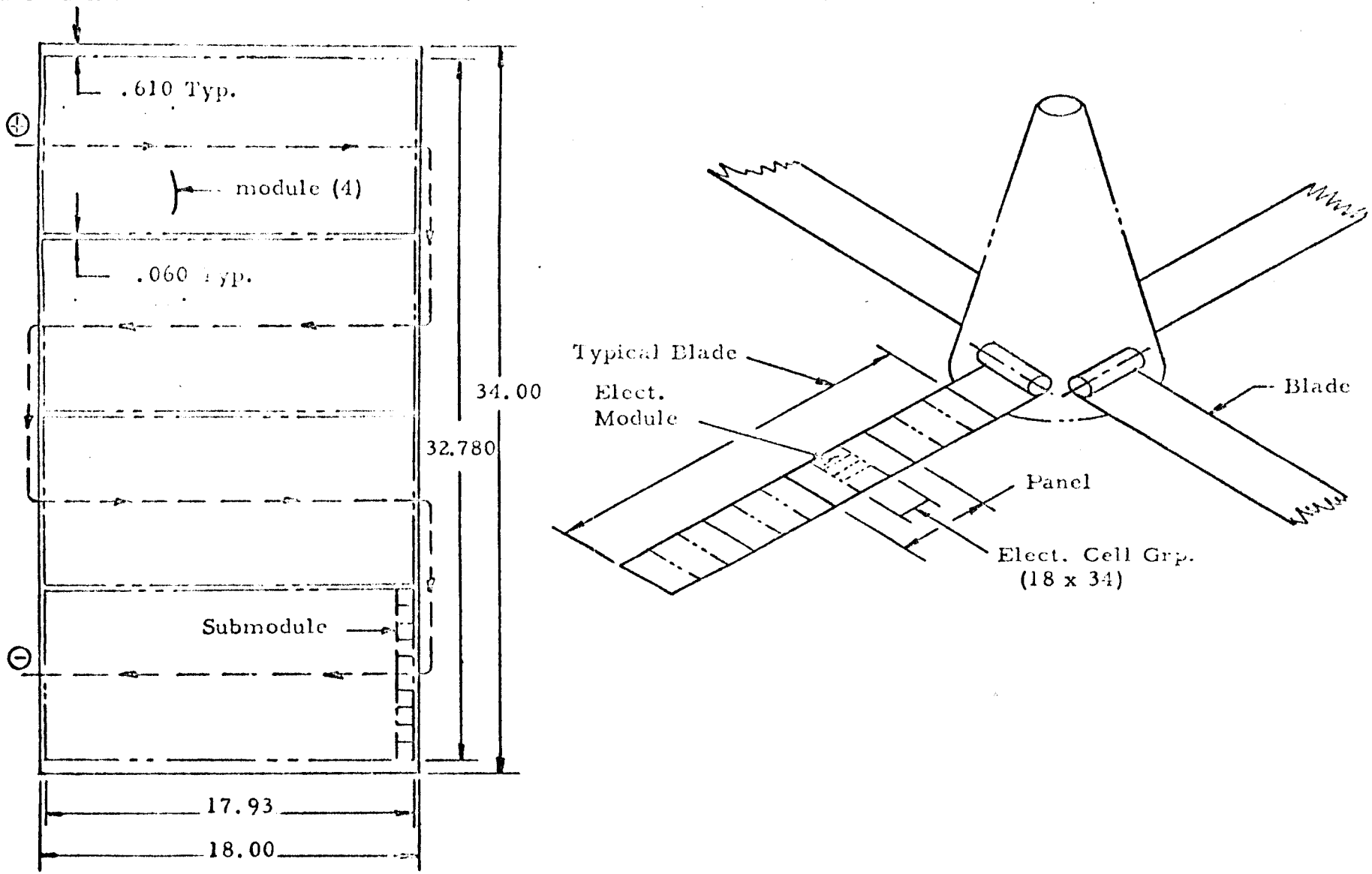

(18 x 34) Electrical String

Figure 3-3 Solar Array

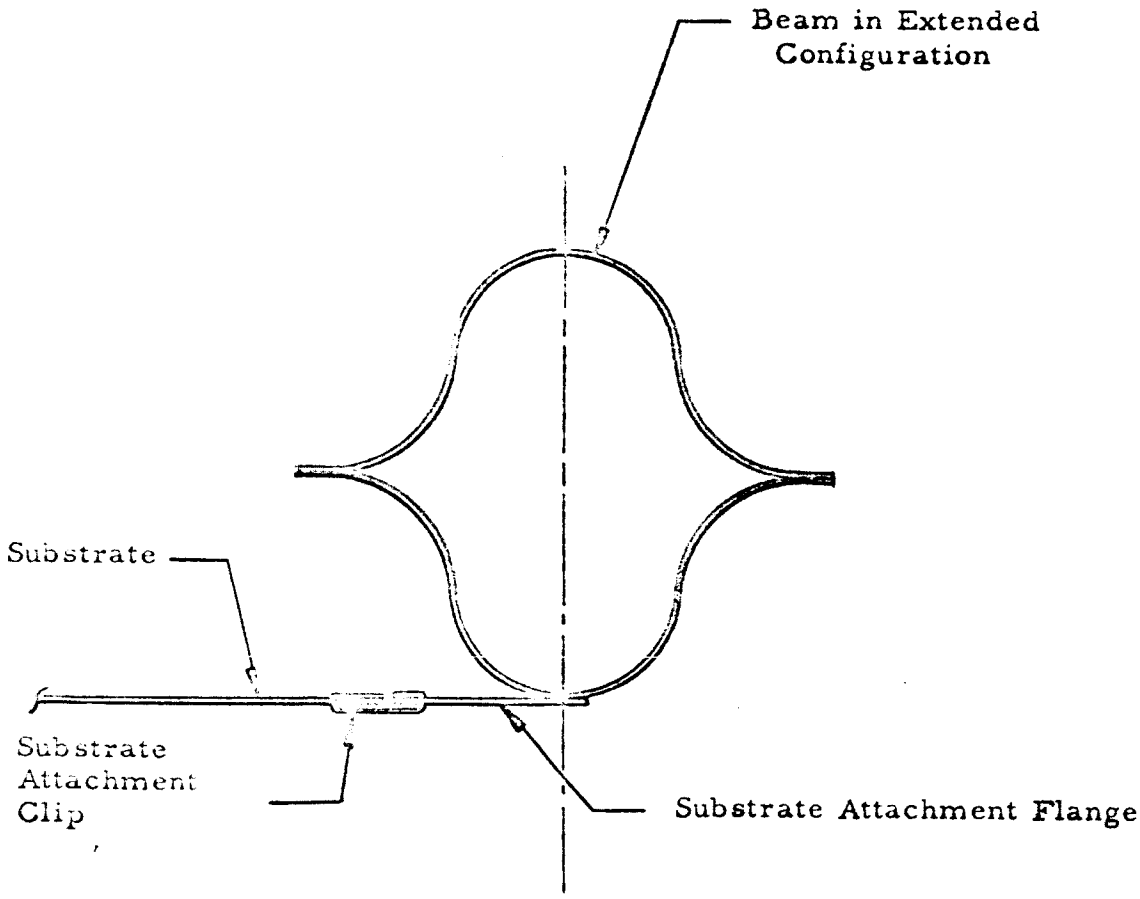

Section Thru Deployable Beam

Figure 3 - 4

Table 4-1

Drawing List -- Jr. Deployable Solar Panel

208V001	Deployable Panel Assembly			
208V002	Solar Array Installation-Support Structure--Deployable Solar Panel			
208V003	Drum Assembly	"	"	"
208V004 Sht 1 & 2	Beam Guide Installation	"	"	"
208V005	Substrate Assembly	"	"	"
208V006	End Cap Assembly	"	"	"
208V007	Beam Installation	"	"	"
208V008	Harness Installation	"	"	"
208V009	Gear-Drum Drive	"	"	"
208V010	Gear-Motor Drive	"	"	"
208V011	Switch Installation	"	"	"
208V013	Substrate Assembly-Alternate	"	"	"
208S001	Assembly and Adjustment Instructions	"	"	"

4.0 DESIGN CRITERIA

The design criteria utilized in the detail design and analysis of the Deployable Large Area Solar Array Structure are taken in whole from the data and information presented in the Statement of Work of the pertinent contract.

4.1 Configuration Design Criteria

No provisions shall be required on the array structure to support unrelated spacecraft components such as power regulating zener diodes, cold gas attitude control systems and/or vernier solar pressure vanes.

During the launch phase, the array structure shall remain within the envelope shown on JPL Drawing No. J-4190680 (Sheet 1). This drawing reflects the available packaging regions for a broad range of typical Mariner spacecraft systems under study for use in the 1969 - 197X era. The drawing depicts a standard Surveyor class shroud on an Atlas-Centaur vehicle. The spacecraft is arbitrarily defined to be an octagonal frame, fifty-eight inches across on the major diagonal. Primary array structure attachment to the spacecraft may be accomplished along any of the corners or vertical edges of the hypothetical spacecraft frame.

The basic array structure shall be designed to have a minimum number of different components. This requires that the total array structure be composed of not more than four sub-elements or panels.

Total available surface for solar cell mounting shall be between one hundred fifty and four hundred square feet. For initial planning and conceptual study purposes, a target area of two hundred square feet shall be assumed. The geometry of the array structure shall be based upon a rectangular modular solar cell array of 18 inches x 34 inches, having a weight of 0.30 pound per square foot. This weight shall include cells, filters, modular wiring, and secondary cabling.

Any mechanical latch points or devices located on the cell surface shall not shade the solar cell surface when the array structure is oriented

$\pm 5^{\circ}$ from the normal incidence angle of illumination.

4.2 Structural Design Criteria

Under the hypothetical environmental conditions set forth in the Environmental Criteria for a useful life of eighteen months:

1. The array structure shall have the capability of surviving normal ground handling during fabrication, assembly, qualification testing and storage. The array structure shall also have the capability of being repaired when subject to minor damage.
2. The array structure shall have the capability of surviving all dynamic loads, including transportation, cruise course correction, and retromaneuver at planetary encounter. It is implicitly assumed that the array structure will be in the undeployed configuration during launch and in the deployed configuration during course correction motions. Depending upon the nature of the array structure (deployed or undeployed), either configuration may or may not be used during the retromaneuver. The retromaneuver thrust shall not be used to initiate or power the retraction, if required, of the array structure. Upon the completion of the retromaneuver, the array structure shall be in the deployed configuration suitable for power production.
3. The rear surface of the array structure shall be designed to minimize heat radiation traps in order to minimize local front surface hot spots.
4. All array structure components shall have provisions for pressure equalization between internal elements and the external flight environment.
5. To preclude real or potential degradation of the solar cells mounted upon the array structure, the curvatures induced in the cells shall be limited as follows:
   a. The radius of curvature of the undeployed or stowed array structure shall at no time be less than six inches.
   b. Under dynamic conditions, the angular change of the

cell substrate per unit length shall be less than 1.0 degree/inch.

6. To avoid servoelastic coupling of the array structure and hypothetical spacecraft control system, the inertial and response characteristics for the array structure shall be as follows:

   a. During powered flight (boost, retro), due to allowable tolerance variations in the fabrication process, the first mass moment of the array structure (undeployed or deployed) shall vary less than 5% as measured about the spacecraft centerline (boost axis).

   b. If deployed, the array structure shall further have the following characteristics:

      1. The undamped first cantilever natural frequency of the array structure shall be between 0.5 and 5.0 cps.

      2. The ratio of damping to critical damping in the first cantilever mode shall be in the range .15 to 0.7.

      3. In the first cantilever mode of the array structure, the ratio of generalized stiffness to generalized mass (k/m) shall vary less than 10% due to all allowable tolerance variations in the fabrication processes.

   c. During cruise phase (including course correction maneuver), the requirements shall be as defined in Paragraphs 6,b,1 and 6, b, 3.

7. Structural criteria given below are stated in terms of limit loads (yield design loads). Induced stress levels shall be computed for all loading conditions stated in Paragraphs 7,a and 7, b. Critical conditions shall be clearly identified and carefully evaluated. Margins of safety on stresses induced by these limit design loads as follows:

$$M.S. = \frac{Y.S.}{L.S.} - 1 \geq 0$$

$$M.S. = \frac{U.S.}{1.25\,(L.S.)} - 1 \geq 0$$

where M.S. = Margin of Safety
L.S. = Stresses resulting from Limit Loads
Y.S. = Yield Stress
U.S. = Ultimate Stress

The yield and ultimate stress values shall be those for the appropriate material as given in the latest editions of MIL-HDBK-5 and MIL-HDBK-17.

a. Thermal Cycling: this cycling represents the effects of spacecraft orbit about a planet as well as spacecraft attitude reorientations associated with mid-course corrections. The design limit thermal loads for this array structure are equivalent to the levels experienced during the following test environment:

1. Pressure - The maximum pressure shall be 10^{-4} mm Hg.

2. Free space background - The free space background or heat sink shall be simulated by a blackened wall having a total absorptivity or greater than 0.80 at liquid nitrogen temperatures, as viewed from the array structure surface.

3. Heat Cycling - A heat input to the array structure surface of 80 watts per square foot shall be held until temperatures stabilize. The electrical power source shall then be turned off for a 1-1/2-hour period. The subsequent step changes in electrical power input from 0 to 80 watts per square foot defines the start of a cycle. Periods of applied electrical power shall be for a 1-1/2-hour duration. Periods of non-applied electrical power shall be for a 1-1/2-hour duration. (see Figure 4-1). The array structure shall be subjected to 10 periods of applied heater power for a total test time of approximately 40 hours.

b. Limit Structural Design Loads: the following table contains the

applicable limit accelerations for use in the determination of the appropriate limit loads. These accelerations define the environment at the array structure-spacecraft interface. The array structure shall be checked for structural adequacy under both static and vibratory criteria. Static and vibratory loads are not to be superimposed for design purposes.

Condition	Static	
	Long.	Lat.
a. Max. q & Mach. 1	4g	3g
b. Booster Burnout	12g	2g
c. Booster Tailoff	2g	0
d. Cruise Maneuver	0.2g	.05g
e. Retro Burner	6g	1g

Condition	Vibratory		
	Level	Range (cps)	Rate Minute/Octave
a. Max. q & Mach 1	-	-	-
b. Booster Burnout	1.6g rms	2-20	1 min/oct
	4.0g rms	20-200	1 min/oct
	Noise 0.2g 2/cps	200-2000	180 seconds
c. Booster Tailoff	-	-	-
d. Cruise Maneuver	0	-	-
e. Retro Burner	0.8g rms	2-20	0.5 min/oct
	2.0g rms	20-200	0.5 min/oct
	Noise $0..2g^2$/cps	200-2000	180 seconds

4.3 Thermal Design Criteria

All components shall meet the following sterilization requirements:

a. Withstand exposure to 3 thirty-six hour periods of heat at 145°C (295°F) in dry nitrogen (a total of one hundred eight (108) hours.

b. Withstand exposure to a gas mixture of 12% ethylene oxide, 88%

freon gas for ten hours at a relative humidity between 30% and 50%.

The temperature at any point on the solar cell surface, as a function of solar irradiance, shall be less than the values defined in Figure 4-2. This is a maximum temperature for any position on the front surface of the array structure. These temperatures may be achieved by requiring that exposed surfaces on the rear and edges of the array structure have a total hemispherical emissivity of greater than 0.80 in the temperature range of -30°C and 80°C.

The rear surface of the array structure shall be designed to minimize heat radiation traps in order to minimize local front surface "hot spots".

Thermal cycling represents the effect of spacecraft orbit about a planet as well as spacecraft attitude reorientations associated with cruise course corrections. The design limit thermal loads for this array structure are equivalent to the levels experienced during the following test environment:

a. Pressure - The maximum pressure shall be 10^{-4} mm Hg.
b. Free Space Background - The free space background or heat sink shall be simulated by a blackened wall having a total absorptivity of greater than 0.80 at liquid nitrogen temperatures as viewed from the array structure surface.
c. Heat Cycling - A heat input to the array structure surface of 80 watts per square foot shall be held until temperatures stabilize. The electrical power source shall then be turned off for a 1-1/2-hour period. The subsequent step changes in watts/square foot define the start of a cycle. Periods of applied electrical power shall be for a 1-1/2-hour duration. Periods of non-applied electrical power shall be for a 1-1/2-hour duration. The array structure shall be subjected to ten periods of applied heater power for a total test time of approximately forty hours.

4.4 Material Design Criteria

The cell mounting surface shall be capable of being cleaned with solvents

or mild acid etching techniques prior to cell mounting.

The cell mounting surface shall be fabricated of or coated with a material that is an electrical insulator. This material shall be capable of withstanding the rigors of cell-mounting techniques. This material shall survive and be capable of repair, in the event that a damaged or defective cell must be removed. The insulation resistance shall be greater than 100 megohms, measured at a test potential of 200 VDC between the cell mounting surface and any metallic portion of the substrate.

The use of any material shall be predicated upon the proven ability of the material to withstand the deep space environment for a time in excess of eighteen months.

All components shall meet the following sterilization requirements:

a. Withstand exposure to three thirty-six hour periods of heat at 145°C (295°F) in dry nitrogen, a total of one hundred eight (108) hours.

b. Withstand exposure to a gas mixture of 12% ethylene oxide, 88% freon gas for ten hours at a relative humidity between 30% and 50%.

The exposed surfaces on the rear and edges of the array structure shall have a total hemispherical emissivity of greater than 0.80 in the temperature range of -30°C to 80°C.

Magnetic materials shall not be used in any of the array structure components, except when array structure reliability is affected by use of such materials.

4.5 Weight Design Criteria

A design objective shall be to keep the weight of the array structure and deployment mechanisms below 0.6 pound per square foot, including

solar cells, cabling and wiring.

The solar cell array shall have a weight of 0.30 pound per square foot. The weight shall include cells, filters, modular wiring and secondary cabling.

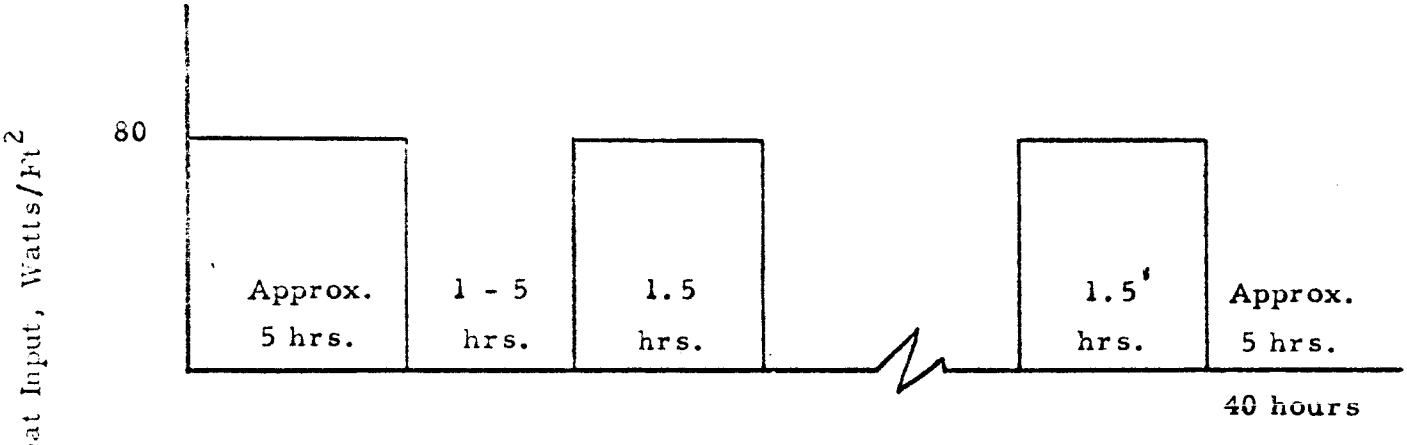

Figure 4-1 Periods of Electrical Power

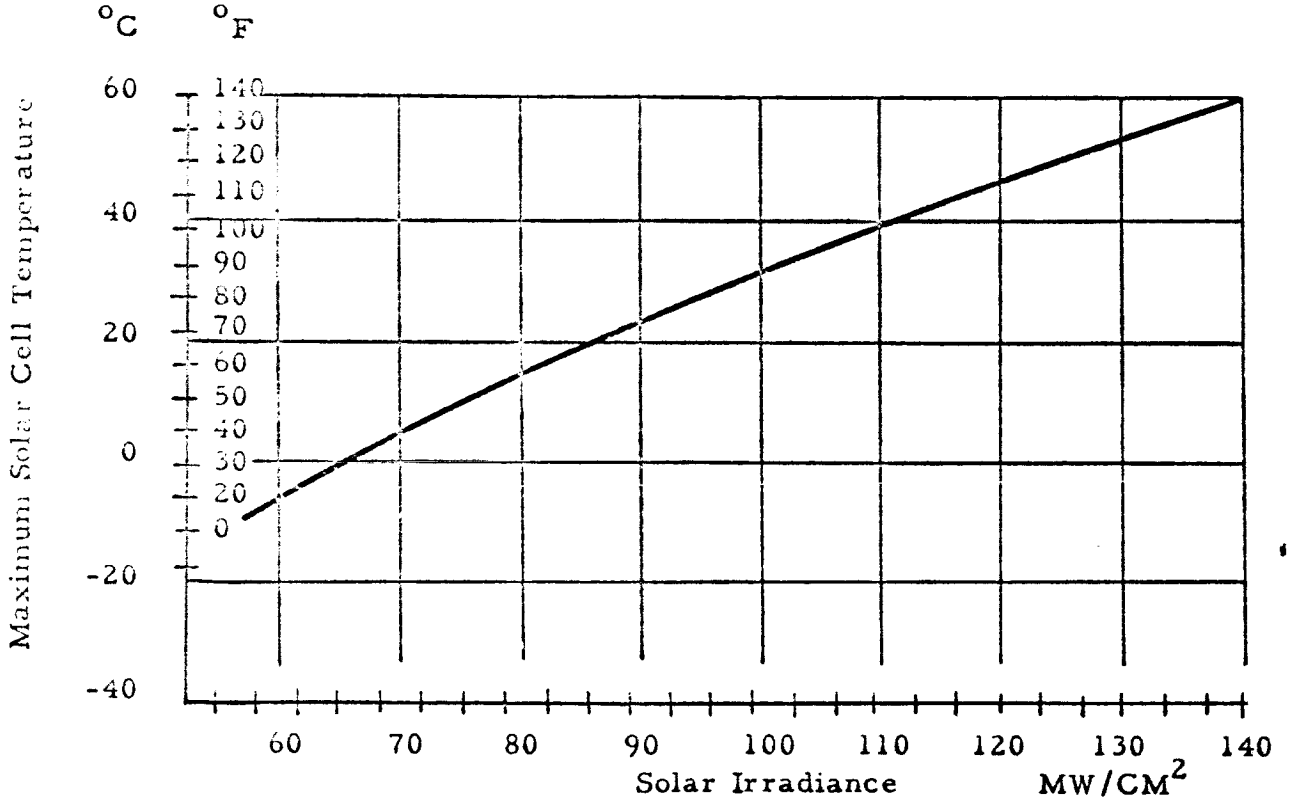

Figure 4-2 Solar Irradiance vs Maximum Solar Cell Temperature

5.0 STRESS ANALYSIS

Analysis is presented for critical loading/environment conditions only. Analysis is based on average sheet thicknesses with the exception of beam analysis which is based on minimum sheet thicknesses. Dynamic loads are treated as static loads. Where vibration loads are concerned, elastic buckling of any one element of a composite cross-section is treated as an ultimate failure to assure that fatigue due to "oil-canning" action will be eliminated.

Design loads used for analysis are derived from limit accelerations given in the JPL statement of work. Dynamic environment is not coupled with static load environment (See Section 4.0).

Yield Design Loads = Limit

Ultimate Design Loads = 1.25 x Limit

5.1 Axial Load In Wrap Drum

The critical condition occurs during launch with the drum assembly, on its supports, vibration excited along the longitudinal axis. A dynamic transmissibility of 5:1 at 2/3 f_n ($f_n \cong$ 300 cps) is considered for analysis. An excitation "g" level of 4 rms in the 20-200 cps range is given in the design criteria. Temperatures are considered to be greater than 75°F. One half total axial load is reacted at each drum end.

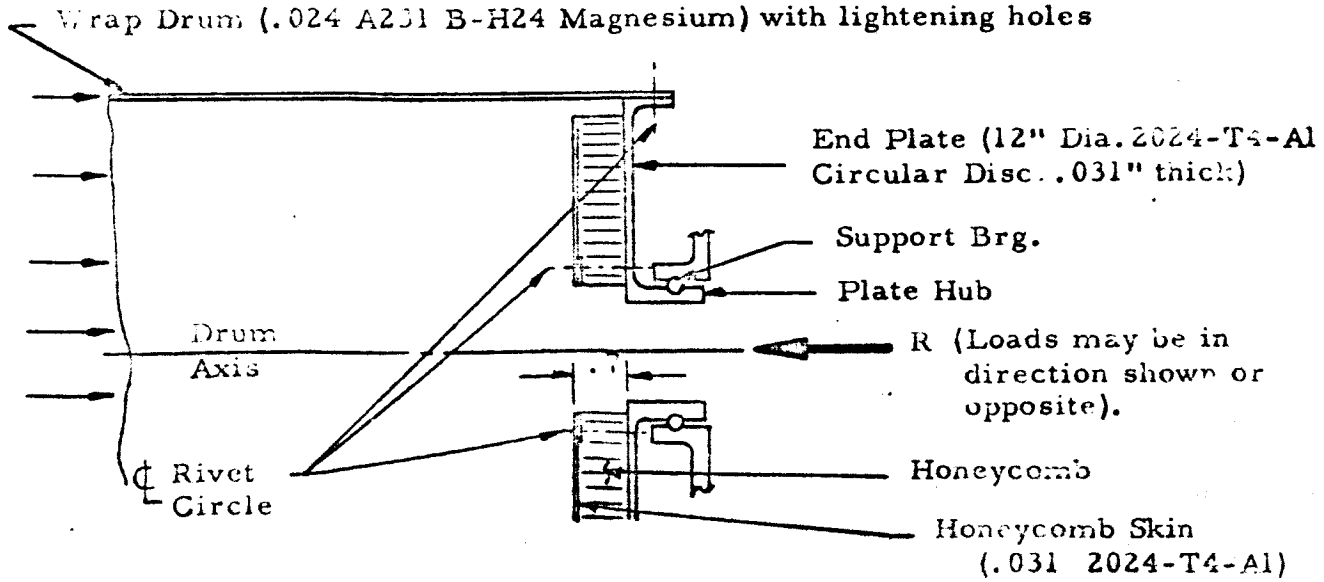

One End of Drum

$$R = \frac{W(g)}{2} = \frac{33.3\ (4 \times 1.414 \times 5)}{2} = 470.8 \text{ lbs limit}$$

Brg. thrust allowable = 4000 lbs limit (Reference 1, Brg. No. B545)

$$M.S. = \frac{\text{Thrust Allow.}}{R} \quad -1 \rightarrow \underline{\text{HIGH}}$$

The axial load is transferred from the wrap drum to the support brg by a circular honeycomb plate. Radial moment restraint offered by the wrap drum is considered negligible, allowing the plate to be analyzed as simply supported at the outside edge and loaded uniformly along the inside edge. Reference 2, page 198, case 14 is used for analyzing the plate for stresses and maximum deflection.

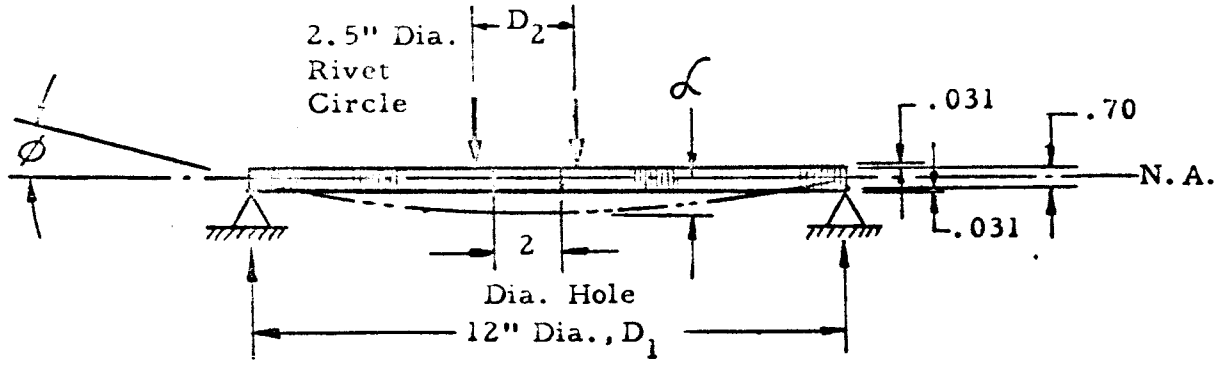

$$I_{n.a.} = .77 \times 10^{-2} \text{ in}^4/\text{in}_1$$

The thickness of a solid plate of equivalent stiffness is calculated as,

$$t_e = (12\ I)^{1/3} = (12 \times .77 \times 10^{-2})^{1/3} = .452 \text{ in}$$

The maximum stress occurs at the inside edge of the plate. The equivalent stress for the honeycomb plate is calculated as follows neglecting moment restraint provided by the plate hub,

$$f_{b_c} = \frac{3R}{2\pi\left(\frac{1}{\mu}\right)\left(t_e\right)^2}\left[\frac{2\left(\frac{D_1}{2}\right)^2\left(\frac{1}{\mu}+1\right)}{\left(\frac{D_1}{2}\right)^2-\left(\frac{D_2}{2}\right)^2}\log\frac{\left(\frac{D_1}{2}\right)}{\left(\frac{D_2}{2}\right)}+\left(\frac{1}{\mu}-1\right)\right]\left(\frac{.35}{.452/2}\right)$$

$$\mu = \frac{E_{avg}}{2G} - 1 \quad \text{(Using values given in Reference 3)}$$

$$\mu = \frac{10.6 \times 10^7}{2 \times 4 \times 10^7} - 1 = .33$$

$$f_{b_c} = \frac{3 \times 470.8}{2\pi\left(\frac{1}{.33}\right)\left(.452^2\right)} \left[\frac{2\left(\frac{12}{2}\right)^2 \left(\frac{1}{.33} + 1\right)}{\left(\frac{12}{2}\right)^2 - \left(\frac{2.5}{2}\right)^2} \log \frac{\left(\frac{12}{2}\right)}{\left(\frac{2.5}{2}\right)} + \left(\frac{1}{.33} - 1\right) \right] \left(\frac{.35}{.452/2}\right)$$

$$f_{b_c} = 363 \left[8.43 \log 4.8 + 2.03 \right] (1.55)$$

$$f_{b_c} = 363 \left[8.43 \times .68124 + 2.03 \right] (1.55) = 4373 \text{ psi yield}$$

$F_{c_y} = 34000$ psi for 2024-T4 Alclad Heat treated by user (Reference 3)

$$\text{M.S.} = \frac{F_{c_y}}{f_b} - 1 = \frac{34000}{4373} - 1 = +\underline{6.77}$$

The above M.S. is large, however, minimum deflection is a prime requirement to assure small dynamic amplification factors.

The maximum deflection of the honeycomb plate is calculated as,

$$\delta = \frac{3R\left[\left(\frac{1}{\mu}\right)^2 - 1\right]}{4\pi E_{avg}\left(\frac{1}{\mu}\right)^2 t_e^3} \left\{ \frac{\left[\left(\frac{D_1}{2}\right)^2 - \left(\frac{D_2}{2}\right)^2\right]\left(3 \cdot \frac{1}{\mu} + 1\right)}{\left(\frac{1}{\mu} + 1\right)} - \frac{4\left(\frac{D_1}{2}\right)^2\left(\frac{D_2}{2}\right)^2\left(\frac{1}{\mu} + 1\right)}{\left(\frac{1}{\mu} - 1\right)\left[\left(\frac{D_1}{2}\right)^2 - \left(\frac{D_2}{2}\right)^2\right]^2} \left(\log \frac{D_1/2}{D_2/2} \right)^2 \right\}$$

$$= \frac{3 \times 470.8\left[\left(\frac{1}{.33}\right)^2 - 1\right]}{4\pi \times 10.6 \times 10^7 \left(\frac{1}{.33}\right)^2 (.452)^3}\left\{\frac{\left[\left(\frac{12}{2}\right)^2 - \left(\frac{2.5}{2}\right)^2\right]\left(3 \cdot \frac{1}{.33} + 1\right)}{\left(\frac{1}{.33} + 1\right)}\right.$$

$$\left. + \frac{4\left(\frac{12}{2}\right)^2 \left(\frac{2.5}{2}\right)^2 \left(\frac{1}{.33} + 1\right)}{\left(\frac{1}{.33} - 1\right)\left[\left(\frac{12}{2}\right)^2 - \left(\frac{2.5}{2}\right)^2\right]} \left(\log \frac{\frac{12}{2}}{\frac{2.5}{2}}\right)^2 \right\}$$

$$= 102.3 \times 10^{-7} \left\{86.22 + 12.97 \quad (\log 4.8)^2\right\}$$

$$\delta = 102.3 \times 10^{-7} \left\{86.22 + 12.97 \quad (.68124)^2\right\} = .95 \times 10^{-3} \text{ in.}$$

The deflection of the plate induces radial rotation of the wrap drum end. The magnitude of rotation is calculated using Reference 4.

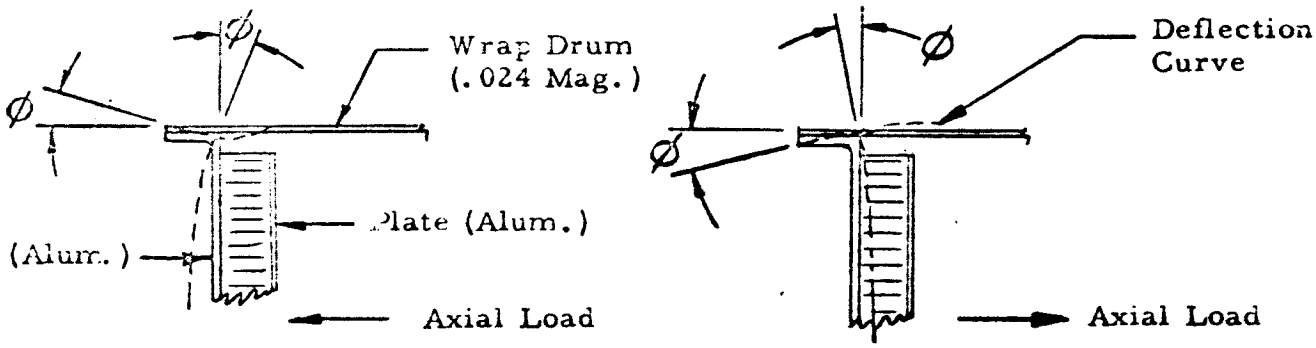

$$\phi = K_R \times \frac{R \cdot \left(\frac{D_1}{2}\right)}{E_{avg} t_e^3}$$

$K_R = 1.06$ by extrapolation

$$\phi = 1.06 \times \frac{470.8 \left(\frac{12}{2}\right)}{10.6 \times 10^{7} (.452)^{3}} = .3 \times 10^{-3} \text{ Radians} = .018 \text{ Degrees}$$

From Reference 2, page 271, case 11 the moment required to produce radial rotation, ϕ, is calculated as,

$$M_o = \phi \times \frac{E_{avg}\, t^3}{12(1-\mu^2)} \times \left[\frac{3(1-\mu^2)}{\left(\frac{D_1}{2}\right)^2 t^2} \right]^{.25}$$

$$= .30 \times 10^{-3} \times \frac{6.5 \times 10^{6} \times (.024)^3}{12(1-.35^2)} \times \left[\frac{3(1-.35^2)}{\left(\frac{12}{2}\right)^2 (.024)^2} \right]^{.25}$$

$$M_o = 30 \times 10^{-3} \times \frac{6.5 \times 10^{6} \times (.024)^3}{12 \times .8775} \times 3.37 = 0.36 \text{ in-lbs/in}$$

The assumption that the outside plate edge has negligible moment restraint is valid.

Radial bending stress in drum end,

$$f_{b_1} = 2 \frac{M_o}{t} \left[\frac{3(1-\mu^2)}{\left(\frac{D_1}{2}\right)^2 t_2} \right]^{(.25)^2} = 2 \times \frac{.36}{.024} (3.37)^2 =$$

$= 341$ psi yield

The above bending stress is added to the axial stress in the drum end,

$$f_c = f_b + \frac{R}{\pi D_1 t} = 341 + \frac{470.8}{\pi \times 12 \times .024} =$$

$$f_c = 341 + 520 = 861 \text{ psi yield}$$

M.S. $\longrightarrow$ HIGH

The radial bending stress in the end plate at the outside edge is less critical than in the drum and therefore no stresses are computed.

The axial load is transferred from the wrap drum to the end plate by means of shear in rivets,

$$\text{Rivet Shear} = \frac{R}{\text{No. of Rivets}} = \frac{1.25 \times 470.8}{48} = 12.3 \text{ lbs. ult.}$$

Let vibration shear allow. at endurance limit = 20% of static brg. allow. (Reference 16) for 3/32 BB Rivet = (163 x 1.18) x .20 = 38.5 lbs.

$$\text{M.S.} = \frac{38.5}{12.3} - 1 = +\underline{2.13}$$

Axial load (when in one direction) is transferred from the end plate into the support brg. through tension in rivets and shear in the honeycomb core. Rivets are used to eliminate local peel in the end plate - honeycomb core adhesive bond.

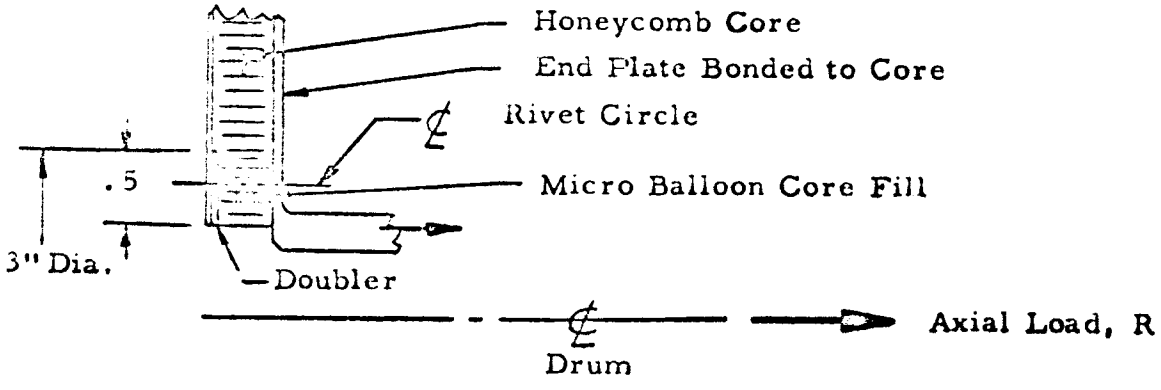

$$\text{Rivet Tension} = \frac{R}{\text{No. of Rivets}} = \frac{1.25 \times 470.8}{10} = 58.9 \text{ lbs. ult./Rivet}$$

Let vibration tension allowable at endurance limit = 20% of calculated tension allowable (Reference 3 and 13, page 167) $\cong$ .20 (1.4 x 363) = 101.6 lbs. for 1/8 BC rivets.

$$\text{M.S.} = \frac{101.6}{58.9} - 1 + \underline{.72}$$

Maximum shear in the honeycomb core is considered to be on a 3 in. dia. circle,

$$f_s = \frac{R}{\text{Shear Area}} = \frac{1.25 \times 470.2}{3 \times .65} = 91.8 \text{ psi. ult.}$$

$\text{Shear Allowable}_{(\min)} = 110$ psi. (Reference 5) for 3/16 Hexcell x 3.1 lbs/ft^3 honeycomb core

$$\text{M.S.} = \frac{110}{91.8} - 1 + \underline{.20}$$

5.2 Torsion in Wrap Drum

The wrap drum is designed for two considerations resulting from torsion transferred over the drum length between beams during substrate extension and retraction. The torque design considerations as set forth by the Ryan Aeronautical Company are given as,

a. Torsional deflection shall be no greater than the allowable fabrication tolerance between the substrate-to-beam attach clip and slot in substrate of .005 to .010 in. This condition is set forth so no shear is induced in the substrate resulting in substrate buckling and possible damage to the solar cells.

b. Total lateral displacement of the substrate shall be less than one-half inch when in the extended position.

c. Wrap drum thickness shall be no less than .020 in. for handling and fabrication purposes.

The preliminary development report suggested a wrap drum with 30% of the surface area reduced with lightening holes. Analysis is based on a differential design torque resistance to wrapping of 66 in.- lbs. (See Figure 11-1). Wrap drum temperatures are considered equal to beam temp. (150°F) with the substrate retracting prior to retro-rocket firing near Mars.

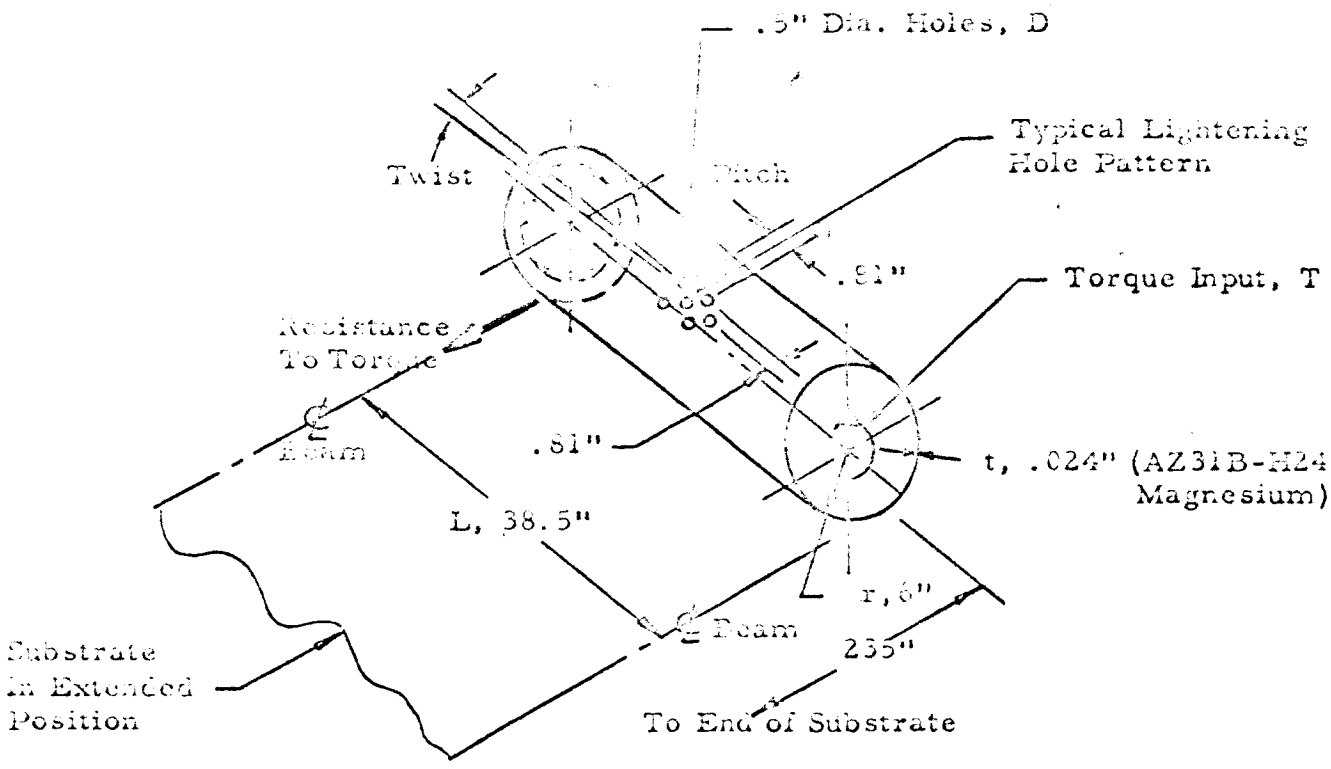

The above wrap drum with holes is reduced to an equivalent torque drum without holes by calculating an effective sheet thickness, $t_{(eff)}$ using Reference 6.

$$t_{(eff)} = t \quad (1 \quad - \quad \text{area reduction by holes}) \quad x \quad e$$

Where sheet efficiency factor, e , is computed by the empirical EQN,

$$e = \left[1.14 - \frac{\text{Pitch}}{2570\, t} - \frac{D}{\text{Pitch}} \right]$$

$$= \left[1.14 - \frac{.8}{2570 \times .02} - \frac{.5}{.8} \right]$$

$$e = \left[1.14 - .0156 - .625 \right] = .50$$

$$t_{(eff)} = .024 \left(1 - \frac{\frac{\pi}{4}(.5)^2}{.81 \times .81} \right) \times .50 = .024 \ (1 - .30) \times .50 = .0084 \text{ in.}$$

$$\text{Torsion Deflection} = \frac{TL}{GJ} \times r$$

$$J = 2\pi r^3 t_{(eff)} = 2\pi (6)^3 \times .0084 = 11.4 \text{ in.}^4$$

$$G = 2.4 \times 10^6 \text{ psi (Reference 3)}$$

$$\text{Torsion Deflection} = \frac{66 \times 38.5}{2.4 \times 10^6 \times 11.4} \times 6 = 0.00056 \text{ in. on wrap drum surface}$$

and total lateral displacement of substrate $= 0.00056 \left(\frac{235}{38.5}\right) = .0034$ in.

The following curve shows the relationship of torsion deflection to drum weight savings by (1) varying lightening hole dia, (2) varying hole pitch and (3) reducing sheet thickness.

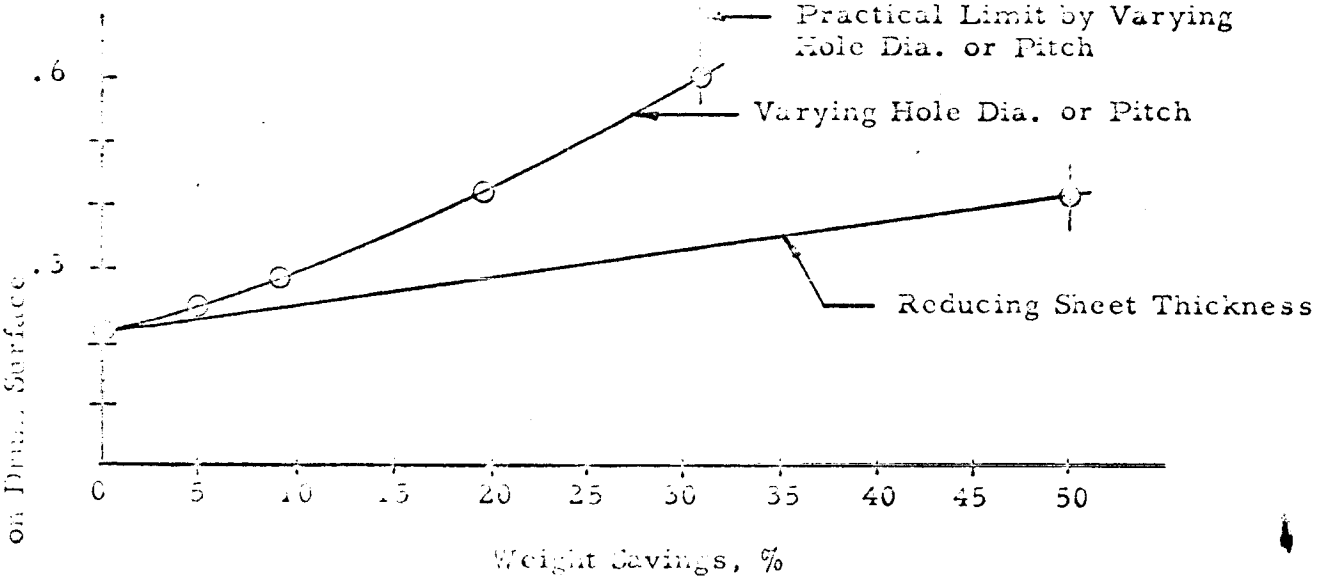

Wrap drum torsion stress and elastic buckling allowables are calculated using Reference 7. (Section 6.1.3 and Figure 6.3.1, respectively).

$$f_s = \frac{(T)r}{J} = \frac{(1.25 \times 66) \times 6}{11.4} = 43 \text{ psi ult}$$

$$F_{s_{cr}} = K_s E \left(\frac{t_e}{L}\right)^2 \cdot \frac{\quad}{12(1 - \mu^2)}$$

$K_s = 1000$ for clamped edges

$E = 6.4 \times 10^6$ psi for AZ31B-H24 Mag. at 150° F

$\mu = .35$

t_e is the effective sheet thickness based on an equivalent $I_{N.A.}$

$= (1 - \text{Area Reduction by Holes})^{1/3} \times t$

$= (1 - .3)^{1/3} \times .024 = .021$

$$F_{s_{cr}} = 1000 \times 6.4 \times 10^6 \left(\frac{.021}{38.5}\right)^2 \cdot \frac{\pi^2}{12\left(1 - .35^2\right)}$$

$$F_{s_{cr}} = 1000 \times 6.4 \times 10^6 \left(\frac{.021}{38.5}\right)^2 \times .937 = 1748 \text{ psi}$$

M.S. $\longrightarrow$ HIGH

5.3 Attachment of Substrate and Beam to Wrap Drum and Substrate to Beam in Area of Wrap Drum

The critical condition occurs during cruise maneuver between Earth and Mars. The substrate is in the extended position and is subjected to an in-plane shear due to a steady-state acceleration of .05g. The spacecraft is considered to be in the Earth's vicinity. Substrate temperature is considered at 150° F.

Shear is not transferred from the substrate to the beams until lateral deflection of the beams occur, thereby compensating for dimensional tolerances between the substrate-to-beam attach clip and slot in substrate of .005 in. min. Analysis is first based on an assumption that loads are transferred by shear and bending in the beam to reaction areas at the beam support and shear attachments of beam to wrap drum. The beam support is assumed to act only as a pivot support, not providing moment restraint in the lateral plane.

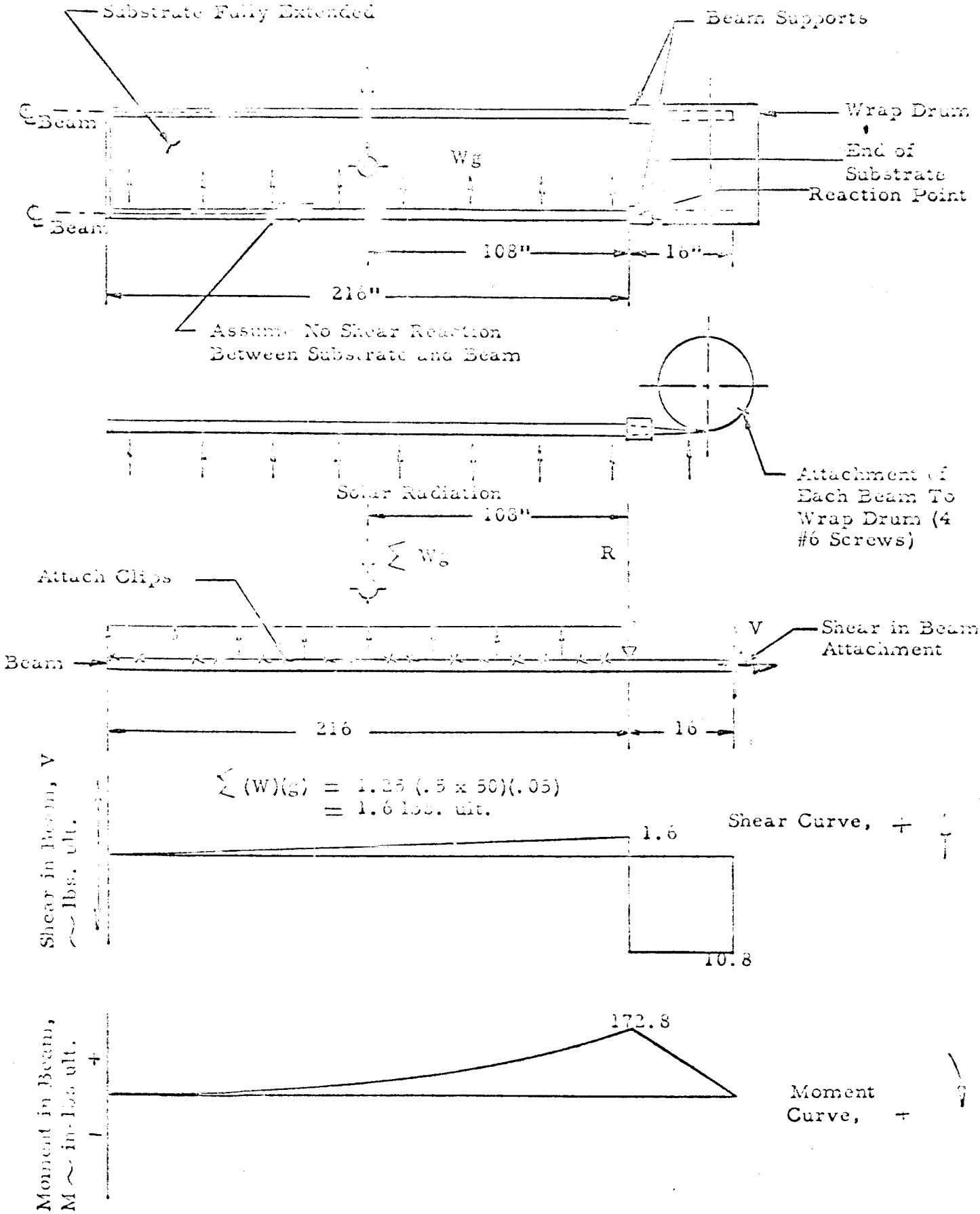

$$\sum (W)(g) = 1.25\ (.5 \times 50)(.05) = 1.6 \text{ lbs. ult.}$$

If the assumption that one beam transfers all the load in bending is valid, lateral deflection of the beam must be less than that required to accumulate an axial tolerance of .005 in.

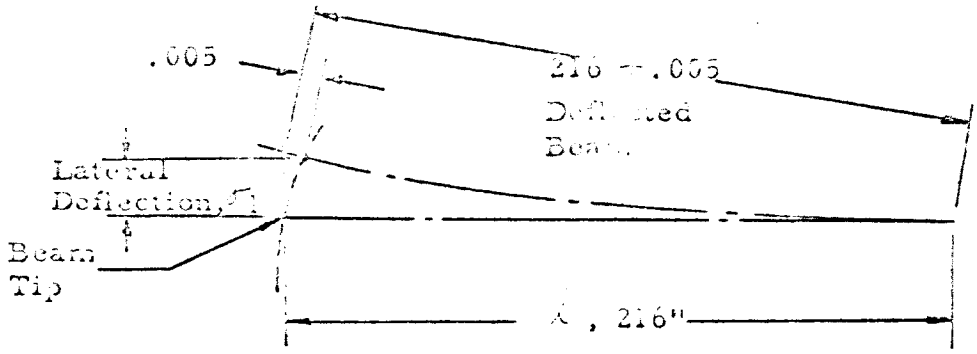

$$\sigma_1 = \left[(216.005)^2 - (216)^2 \right]^{1/2} = \underline{\underline{1.5}} \text{ in. before shear clip begins to carry load}$$

Deflection, σ_2, due to load (Reference 2, page 100, case 3)

$$\sigma_2 = \frac{(W)(\ell)^4}{8\,EI}$$

where $E = 14.6 \times 10^6$ psi for 6AL-4V annealed titanium at 250°F (Reference 3)

$I = .0335$ in^4 (See Section 5.11)

$$\sigma_2 = \frac{\left(\frac{1.6}{216}\right)(216)^4}{8 \times 14.6 \times 10^6 \times .0335} = 4.1 \text{ in.}$$

Therefore, the beam carries $\frac{1.5}{4.1} = 37\%$ of the load in bending before shear is transferred into the substrate at the attach clips.

Shear in #6 screws at attachment of beam to wrap drum is calculated by resolving moment, M, as a couple for the two conditions,

$$\text{Shear} = \frac{M}{(\text{Beam Spacing})(\text{No. of Screws})} + \frac{M(.37)}{(16)(\text{No. of Screws})}$$

$$\text{Shear} = \frac{172.8\,(1 - .37)}{(3.5)(4)} + \frac{172.8\,(.37)}{(16)(4)} = 1.71 \text{ lbs ult/screw}$$

Shear allowable for #6-32 AN507 screw = 246 lbs (Reference 12) BRG on .072 sheet.

M.S. $\rightarrow \underline{\underline{H}}$ H

Shear in substrate at attach clips assuming total shear transferred through clips,

$$\text{Shear} = \frac{V(Q)}{I} = \frac{1.0\left(2\pi rt \times \frac{38.5}{2}\right)}{\left[2\left(2\pi rt\right)\left(\frac{38.5}{2}\right)^2\right]} = .04 \text{ lbs/in. ult.}$$

$$f_{br} = \frac{(\text{Shear})(\text{Clip Spacing})}{(\text{Bearing Area})}$$

if a .009 fiberglass doubler is used, the total brg. thickness of the substrate is .012in.

$$f_{br} = \frac{(.04)(.6)}{(.012 \times .005)} = 400 \text{ psi ult}$$

Let F_{br} = 11.9% of 95% of F_{br} of a 1/8 in. thick 112 glass cloth laminate at 150°F (Reference 9, Figures 2-22, 4-4 and Table 2-7) = .119 x .93 x 23300 = 2579 psi.

$$\text{M.S.} = \frac{2579}{400} - 1 + \underline{5.45}$$

Based on Ryan test data (See Section 11.3) at 300°F,

$$F_{br} = \frac{\text{Shear Allow}_{\text{Brg.}} \text{ (Clip Spacing)}}{\text{(Bearing Area)}}$$

$$= \frac{(.95)(.6)}{(.012 \times .005)} = 9500 \text{ psi}$$

$$\text{M.S.} = \frac{F_{br}}{f_{br}} - 1 \longrightarrow \underline{\text{HIGH}}$$

Shear in Substrate,

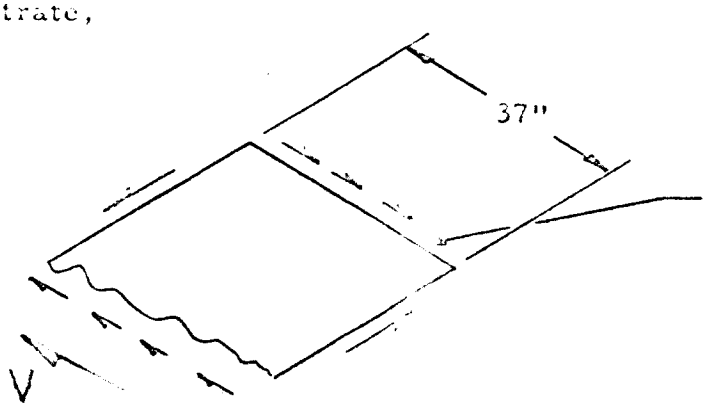

Shear Flow

$$q = \frac{V}{36.5} = \frac{\quad}{36.5} = .04 \text{ lbs/in.,ult}$$

$$q_{cr} = K_s E_c \left(\frac{t}{b}\right)^2 \cdot \frac{\quad^2}{12(\quad - \mu^2)}$$

$K_s = 5.35$ for edges simply supported (Reference 11, Figure 22)

$E_c = 1.1 \times 10^6$ psi

$\mu = .10$ based on 112 epoxy impregnated glass cloth at 150°F(Ref. 9)

$q_{cr} = 5.35 \times 1.1 \times 10^6 \left(\frac{.006}{.37}\right)^2 = .15$ lbs/in., This is the allowable before the solar cells become shear loaded.

$$M.S. = \frac{q_{cr}}{q} - 1 = \frac{.15}{.04} - 1 = + \underline{2.75}$$

5.4 Tension in Substrate-to-Beam Attach Clips

The critical condition occurs during cruise maneuver between Earth and Mars. The substrate is in the extended position and is subjected to a .2g steady-state acceleration normal to the substrate plane. The loads are carried by the substrate acting as a diaphram which induces tension in the clips attaching the substrate to the beam. Substrate temperature is considered at 150°F. (Reference 8, Figure 25) maximum at the attachment to the clips. Clip temperature is considered at 200°F.

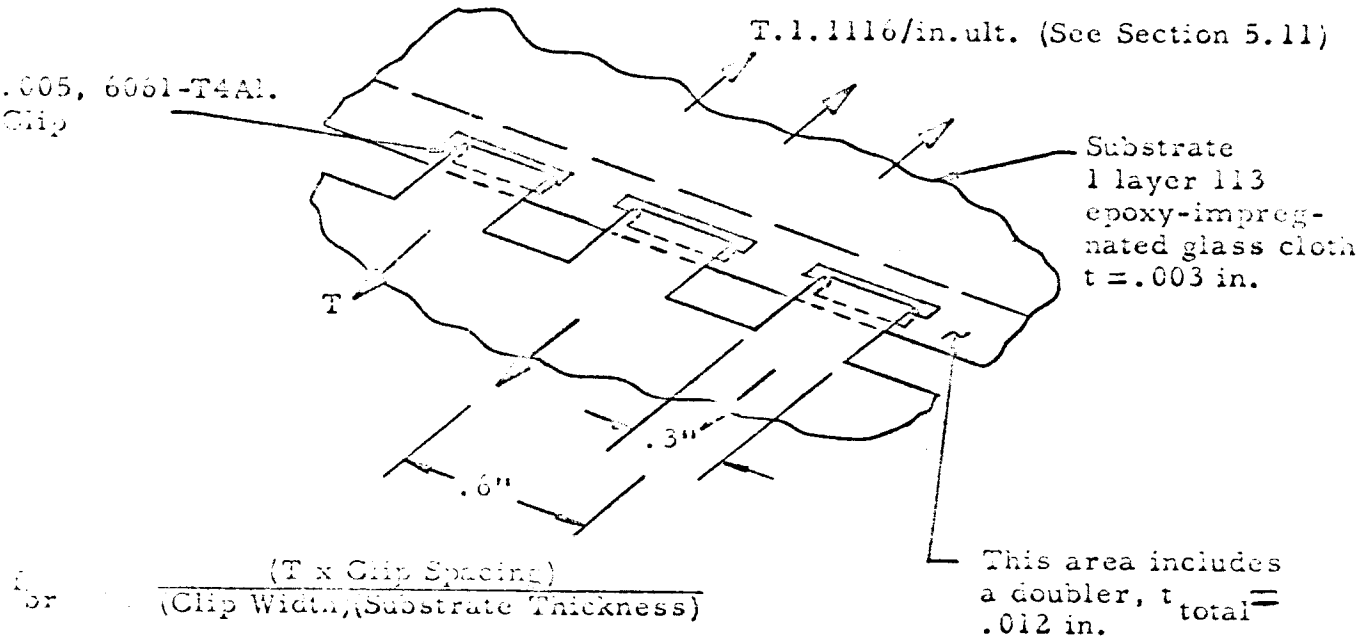

$$f_{br} = \frac{(T \times \text{Clip Spacing})}{(\text{Clip Width})(\text{Substrate Thickness})}$$

$$f_{br} = \frac{(1.11 \times .6)}{(.3)(.012)} = 185 \text{ psi}$$

F_{br} = 2579 psi, (Reference 9) and 4028 psi minimum (From Ryan Test Data)

$$\text{M.S.} = \frac{F_{br}}{f_{br}} - 1 = \frac{4028}{185} - 1 \longrightarrow \underline{\text{HIGH}}$$

$$\text{Shear out of Substrate} = \frac{\left(\frac{T}{1.25}\right)(\text{Clip Spacing})}{(\text{Shear Area})} = \frac{\left(\frac{1.11}{1.25}\right)(.6)}{(2 \times .25 \times .012)}$$

$$= 89 \text{ psi yield}$$

Shear Allowable at proportional limit for 150°F = .93 x 1650 = 1535 psi
(Reference 9, Table 2.[illegible]) M.S. $\longrightarrow$ HIGH

Bending-Tension in Clip,

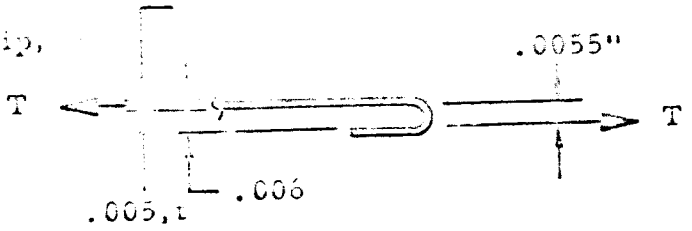

$$f_{bt} = \frac{(T \times \text{Clip Spacing})}{(\text{Clip Width})(\text{Clip Thickness})} + \frac{(.0055\,T \times \text{Clip Spacing})\left(\frac{t}{2}\right)}{(\text{Clip Width})(t)^3/12}$$

$$= \frac{(1.11 \times .6)}{(.3)(.005)} + \frac{(.005 \times 1.11 \times .6)\left(\frac{.005}{2}\right)}{(.3)(.005)^3/12}$$

$f_{bt} = 44.4 + 292.8 = 337$ psi ult

$F_{t_u} = .93 \times 42000 = 39060$ psi for 6061-T4 at 200°F (Reference 3)

M.S. $\longrightarrow$ HIGH

5.5 Bending in Wrap Drum

The critical condition occurs during launch with the drum assembly vibration excited normal to the longitudinal axis. A dynamic transmissibility of 12.5:1 based on a structural damping ratio of .04 (due to substrate wrapped around drum acting as damping material) with the drum vibrating in a fundamental mode ($f_n \cong 200$ cps) is considered for analysis an excitation g level of 4 RMS in the 20-200 cps range is given in design criteria. Temperatures are considered to be no greater than 75°F.

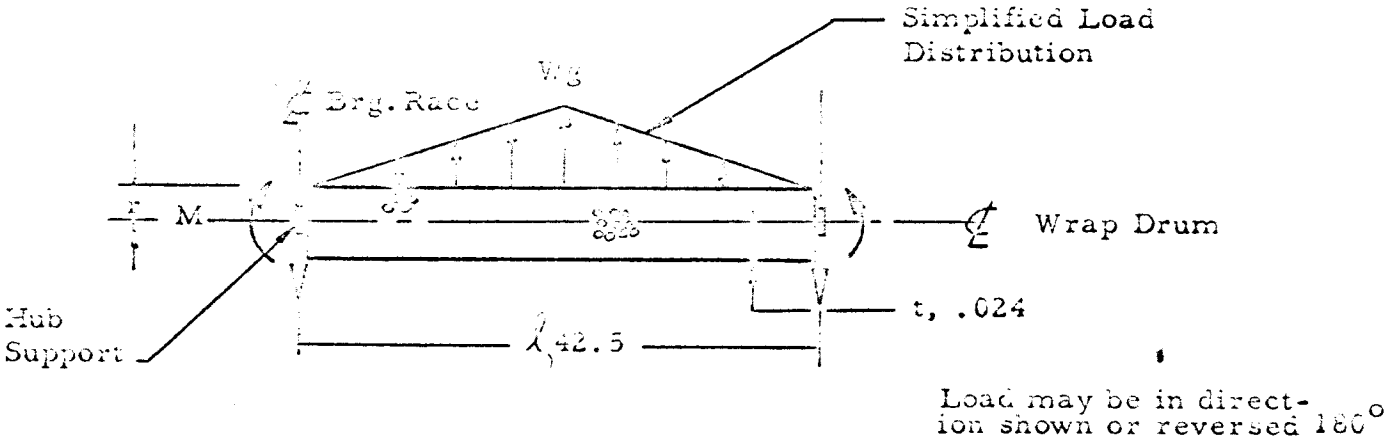

Due to the smaller stiffness at the hub support relative to that of the wrap drum, bending stress in the drum is based on a no-moment restraint condition at the hub supports. Analysis is based on AZ61B-F24 Magnesium Sheet.

$$f_{bc} = \frac{Mr}{I_{(eff)}}$$

$$M = \frac{(Wg)(\ell)^2}{12} \quad \text{at mid-length (Reference 2, Pg. 104, case 17)}$$

$$M = \frac{\left(\frac{17}{42.5} \times 4 \times 1.414 \times 12.5 \times 1.25\right)(42.5)^2}{12} = 5321 \text{ in.-lbs ult}$$

$$I_{(eff)} = \pi (r)^3 \left[t\,(1 - \text{hole area reduction})\right] = \pi(6)^3\left[.024(1-.3)\right]$$

$$I_{(eff)} = 11.4 \text{ in.}^4$$

$$f_{bc} = \frac{5321 \times 6}{11.4} = 2800 \text{ psi ult}$$

$f_{b_t} = 1.9 \times 2800 = 5320$ psi ult due to stress concentration around holes (Reference 2, pg. 344, case 5)

$$F_{bc} = .9038\, E_{avg} \left(\frac{t_e}{\ell}\right)^2 \cdot K \times 1.3 \quad \text{(Reference 7, pg. 5.7)}$$

$$Z = \frac{\ell^2}{\pi t_e} \left(1 - \mu^2\right)^{1/2}$$

t_e is the effective sheet thickness based on an equivalent

$$t_{N.A.} = (1 - \text{Area Reduction By Holes})^{1/3} \times t$$

$\mu = .35$ for AZ31B-H24 Mag.

$$Z = \frac{(42.5)^2}{6 \times .021} \left(1 - .35^2\right)^{1/2} = 1.34 \times 10^4$$

$$\frac{r}{t_e} = \frac{6}{.021} = 286, \quad K = 3 \times 10^3$$

$$F_{bc} = .9038 \times 6.4 \times 10^6 \left(\frac{.021}{42.5}\right)^2 \times 3 \times 10^3 \times 1.3 = 5416 \text{ psi}$$

$$M.S. = \frac{F_{bc}}{f_{bc}} - 1 = \frac{5416}{2800} - 1 = +\underline{0.93}$$

5.0 Analysis of Beam Guide Sleeve

The critical condition occurs during cruise maneuver between Earth and Mars. The substrate is in the extended position and is subjected to a .2g steady-state acceleration normal to the substrate plane. Guide sleeve temperature is considered no greater than a possible beam temperature of 250°F (Reference 8, Table .13 for bare blue oxidized beam).

A reaction at the forward former of 6.2 lbs ult due to an in-plane steady-state acceleration of .05g on the substrate (see analysis "Attachment of Substrate and Beam to Wrap Drum", this report) is considered less critical than the conditions presented here.

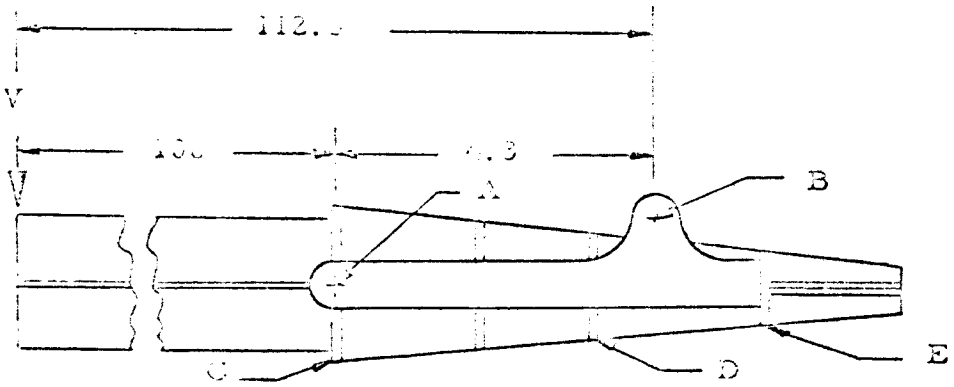

$V = .2g \times .5\#/ft^2 \times 25\ ft^2 = 2.5\#$ yield (Reference 8, Substrate Studies

Load @ A $= \frac{2.5\# \times 112.3\ in}{4.3\ in.} = 65.4\#$ yield

Load @ B $= \frac{2.5\# \times 108\ in}{4.3\ in} = 62.8\#$ yield

The load @ A is transmitted by C (front former) and the load @ B is transmitted by D and E (formers). The load @ A is reacted by two .25 dia. pins with a .14 lightening hole through center. Roark, page 299 (Reference 2) gives the circumferential stress as $S = K \frac{2P}{wb}$; K is a coefficient that depends on the ratio a/b and is given in table form. $S = 10.1 \quad 1/2 \quad \frac{2(65.4)}{.125} = 1660\#/in.^2$

$F_{ty} = 29$ KSI AZ31B-H24 Mag. (Reference 3) For at 62% of room temp = 250°F)

$F_{ty} = 18.0$ KSI

B support = A tube 5/16 O.D. x 3/16 I.D.

Then $S = 10 \cdot \frac{1}{2}$ $\frac{2(12.8)}{(1.5)}$ = 2050 #/in^2 yield

M.S. ⟶ HIGH

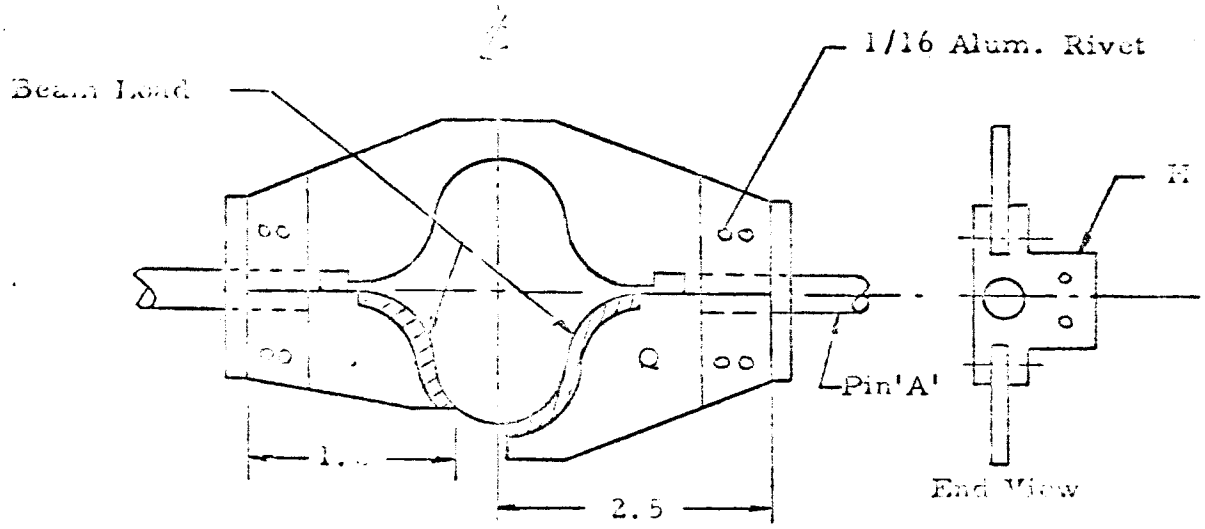

Front Former 'C'

Parts P & Q of the front former react load @ 'A' (65.4#) and the load is distributed as shown. Thus P reacts $\frac{65.4}{2}$ = 32.7# & Q reacts 32.7#.

The plate P & Q are retained by two (2) rivets in each part and the rivets are in double shear. Reference 2, page 297 gives the case for eccentric loading of a rivet joint.

$Q = P_{et_1} / \Sigma r^2$ consider Q and let the load P act 2/3 dis. to ℄ which would be the extreme case then P = 32.7#, e = 1.675, r_1 = .175,

$\Sigma r^2 = r_1^2 + r_1^2 = .062$

$\therefore Q = \frac{32.7 \times 1.675 \times .175}{.062}$ = 153.5# yield = 192 lbs ult

Double Shear Allow. for $\frac{3}{32}$ B

Rivet = 406 lbs (Reference 16)

M.S. = $\frac{406}{192} - 1 = +1.11$

The support is attached to the side plate by two (2) 1/16" dia rivets in singel shear

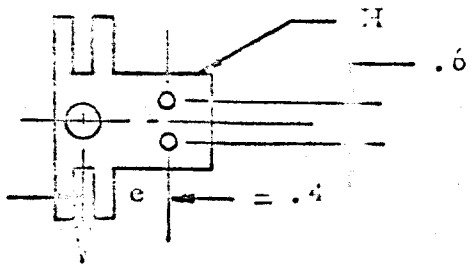

The case for eccentric loading of a rivet joint (Reference 2, page 297),

$$Q = Pe\ r_1 / \Sigma r^2 \text{ where } e = .4,\quad r_1 = .3,\quad P = 32.7, \&$$

$$\Sigma r^2 = .3^2 + .3^2 = .18$$

$$\therefore\ Q = \frac{32.7 \times .4 \times .3}{.18} = 21.8\#\ \text{yield} = 27\ \text{lbs ult}$$

M.S. $\longrightarrow$ HIGH

Part Q of the front former may be considered as a beam fixed in part H, as Q is riveted and bonded.

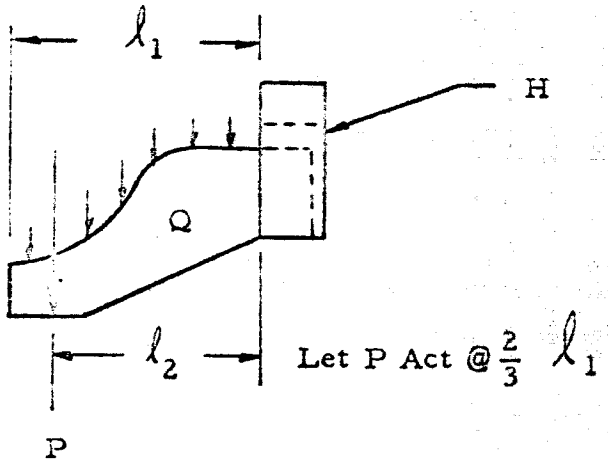

P = 32.7# yield

Then take I@ ℓ_2

$I = \frac{1}{12} bh^3$ Where b = .1 & h = .5

$I = .0010\ in^4$

$\delta = \frac{P \ell_2^3}{3EI}$ (Reference 2, page 100, case #1)

$E = 6.3 \times .0^{6}$ (Reference 3) for AZ31B-H24 Mag at 250° F

Then $\delta = \frac{32.7 \times 1.3^{3}}{3 \times 6.3 \times 10^{6} \times .0010} = \underline{.0038}$ in.

Beam analysis at open part of front former. The substrate deflection = .22 in. (See Section 5.11) and the substrate membrane stress induces a distributed load along the beam of ..1 #/in ult (See Section 5.11).

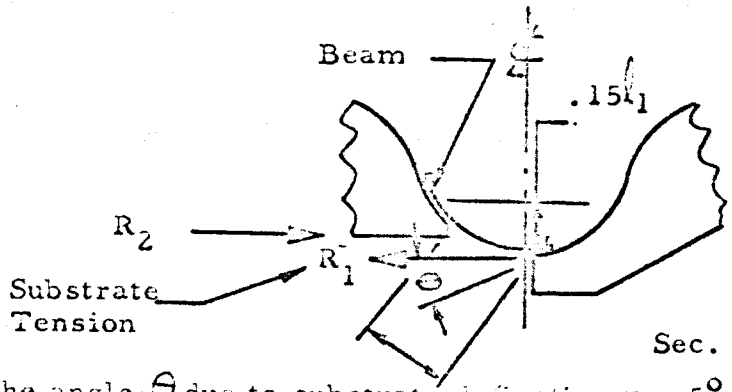

The angle θ due to substrate deflection = .5° approximately. Thus, the load may be said to act at 90° to $\not\subset$. Sec. A may be considered as a beam fixed at both ends with a differential shear R_1 and R_2.

Then $\delta = \frac{M \ell^2}{6EI}$ (Reference 2)

$M = \frac{1}{2} (V \ell_2)$

Let $V = 3R_1$ which is 3" wide sec. of the substrate. This load will be considered to act on a 1" sec. of the beam.

$\therefore I = \frac{1}{12} (t)^3$ t=.0065"

$M = \frac{1}{2} (3 \times 1.1 \times .15) = .25$ in.lbs ult

$I = \frac{1}{12} (.0065)^3 = .023 \times 10^{-6}$

$\delta = \frac{.25 (.4)^2}{6 \times 14.5 \times 10^{6} \times .023 \times 10^{-6}} = .020$ in.

Then $f_b = \frac{6M}{t^2} = \frac{6 \times .25}{(.0065)^2} = 35503$ psi ult

M.S. $\longrightarrow$ HIGH

The load at point B was shown to be 62.8# yield, but, this reaction may be $\pm$ and would be reacted at former D & E

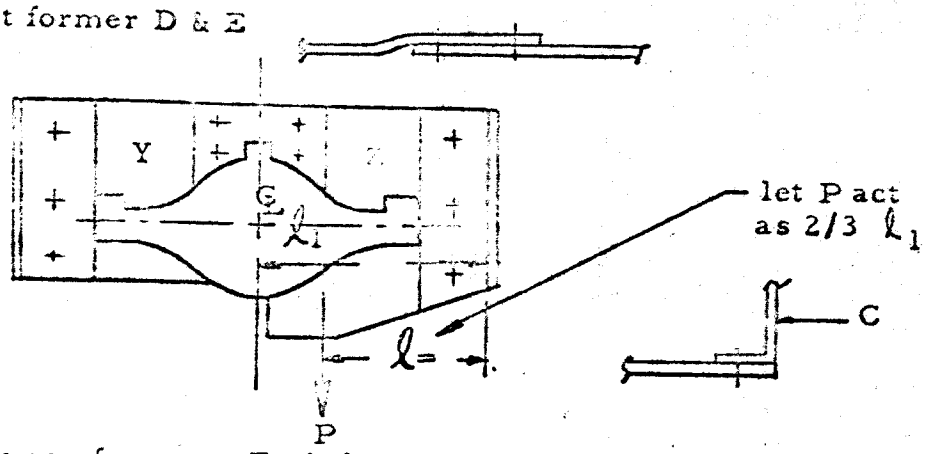

With $\frac{1}{2}$ load (31.4#) on ea. former. Each former may then be considered in the same manner as the front former. It will be noted that formers D & E are made of two parts, Y & Z, which are fixed at the $\mathcal{E}$ by 4 rivets. Also, former 'D' is fixed to former 'E' by a channel 'C' at each end.

Then $P = \frac{31.4}{2} = 15.7\#$ yield

I is taken @ $\ell_2 = \frac{1}{12}\ bh^3$ where $b = .05$ & $h = .5$

$$\ell_2 = \frac{2}{3} \times 1.93 = 1.28 \text{ in.} \qquad I = \frac{1}{12}\ (.05)(.5)^3 = .00052 \text{ in.}^4$$

$$\delta = \frac{P\ \ell_2^3}{3EI} = \frac{(15.7)(1.28)^3}{(3)(6.3)(10^6)(.00052)} = .0026 \text{ in.}$$

$$f_s = \frac{M}{I/c} = \frac{(15.7)(1.28)}{.00052/.25} = 9662 \text{ psi yield}$$

$$\text{M.S.} = \frac{17980}{9662} - 1 = + \underline{.86}$$

The load on the beam at 'B' is the same as 'A' less the solar cells

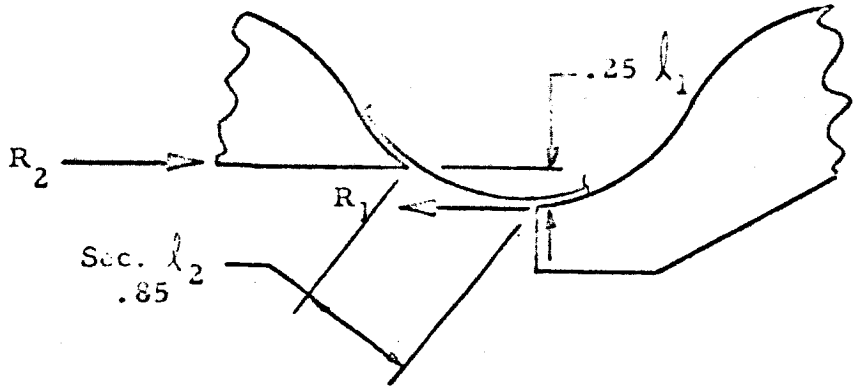

Weight at sec. considered = total weight — solar cells = 5.7507# — 4.469#

= .2817#

The load density = $\frac{.28\#}{(38)(10)}$ = .000736 #/in.^{2} @ 1g

= .0001472 #/in.^{2} @ .2g

= .000184#/in.^{2} Ult

5.7 Wrap Drum Subjected to External Radial Pressure

This condition exists during launch if the stowed substrate is excited in the fundamental mode of vibration. Loads are derived from dynamic analysis presented in Section 6.1. Temperatures are considered to be no greater than 75°F. Analysis is made considering the condition when the five wrapped layers of substrate are vibrating in phase.

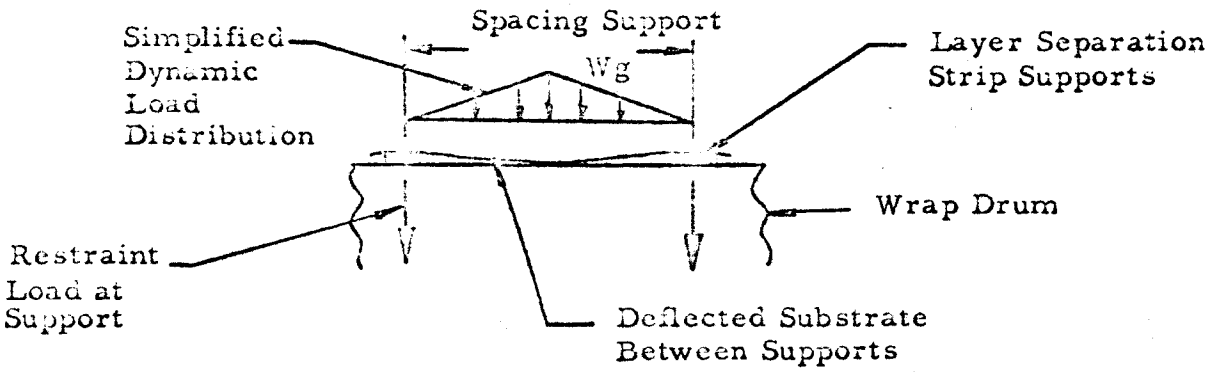

The resultant load at supports is calculated using the equation for sinusoidal vibration. If we consider a support spacing increase from 4 to 6 in., f_n is reduced from 285 cps by the square root of the relation for beam deflection.

$$f_n = 285 \left[\left(\frac{4}{6}\right)^4\right]^{1/2} = 233 \text{ cps, consider 200 cps.}$$

Maximum deflection, δ , is increased as follows assuming no increase in peak dynamic output acceleration,

$$\delta = .009 \left(\frac{6}{4}\right)^4 = .046 \text{ in.}$$

Then, output acceleration, g,

$$= \frac{\delta (2\pi f)^2}{386.4} = \frac{.046(2\pi \times 200)^2}{386.4} = 188 \text{ g (0-peak)}$$

Resolving the load distribution into a uniform distribution,

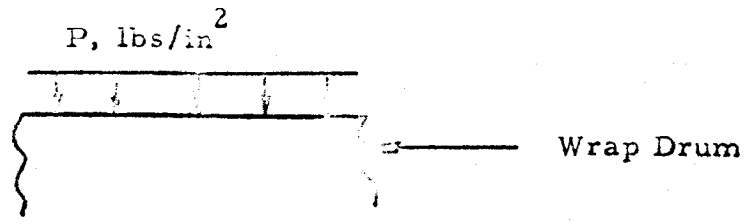

$$P = \frac{1}{2}(wg) = \frac{1}{2}\left(\frac{.3}{144} \times 1.25\right) = .25 \text{ lbs/in.}^2 \text{ ult.}$$

For 4 substrate wrap layers vibrating in phase,

$$P = 4 \times .25 = 1.0 \text{ lbs/in.}^2 \text{ ult.}$$

The allowable elastic buckling of the wrap drum is calculated for .025 AZ31B-H24 Magnesium Sheet first assuming no intermediate stabilizing rings. Analysis is based on Reference 2, page 318, case Q.

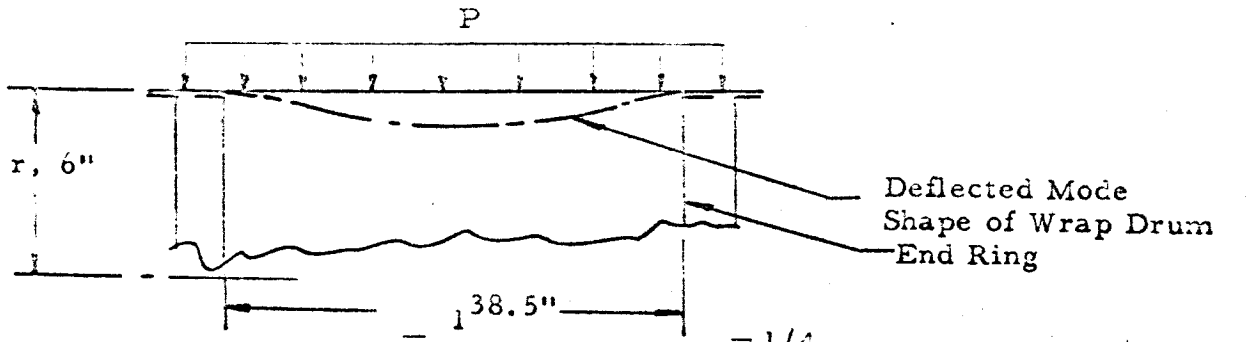

$$P_{cr} = .807 \times \frac{Et^2}{\lambda r}\left[\left(\frac{1}{1-\mu^2}\right)^3 \frac{t^2}{r^2}\right]^{1/4} = .807 \times \frac{6.5 \times 10^6 \times .025^2}{38.5 \times 6} \times \left[\left(\frac{1}{1-.35^2}\right)^3 \frac{.025^2}{6^2}\right]^{1/4}$$

$P_{cr} = 0.99$ lbs/in.^{2}, which is reduced due to the presence of 30% area lightening holes as follows,

$$P_{cr} = 0.99 \quad (.7)(.7)^{1/4} \quad = 0.28 \text{ lbs/in.}^2$$

The required capability of the end rings to provide the support necessary is calculated as,

$$P = 1.0 \left(\frac{38.5}{2}\right) = 19.3 \text{ lbs/in. ult.}$$

$$P_{cr_{(\text{end rings})}} = 457 \text{ lbs/in. yield (Reference 8, page 132)}$$

Then, $$M.S. = \frac{0.28}{1.0} - 1 \longrightarrow \text{Negative}$$

Therefore it is suggested that the wrapped substrate vibration mode inducing this magnitude of external radial pressure be eliminated.

5.8 Substrate Deflection for Stowed Condition

This analysis is conducted to determine if the 1/8 inch thick substrate spacer strips are sufficient to prevent contact of respective substrate layers or the inner layer with the wrap drum during dynamic excitations. Solar cell damage could result if contact were to occur.

The condition occurs during launch vibration excitation at fundamental frequency. The critical case is during the radial "Breathing Mode" for which analysis is presented in Section 6.1. Temperatures are no greater than 75°F. In-plane (axial motion) of one substrate layer with respect to another is negligible since attachment of the substrate to the wrapped beams prevent this motion.

Analysis presented is based on a spacing of 6 inches between substrate spacer strips. Radial loads and deflections for the modified spacing condition (Section 6.1 was based on a 4 inch spacing) are presented in Section 5.7.

Outer Wrapped Layer:

The critical condition occurs with the two outer layers vibrating out of phase.

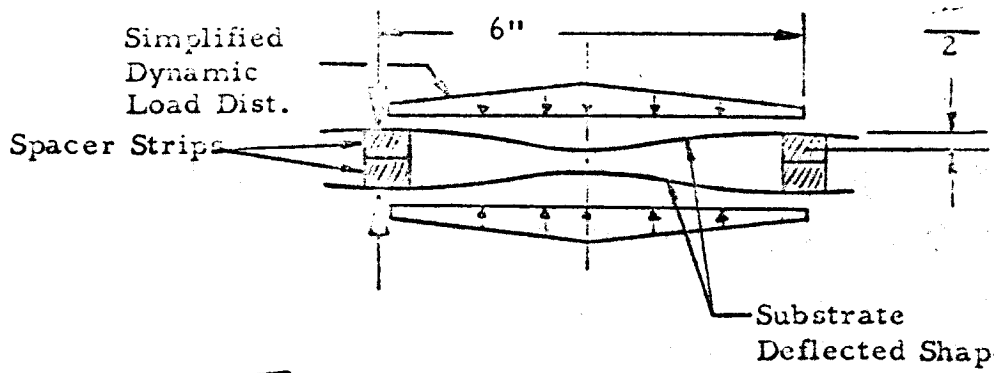

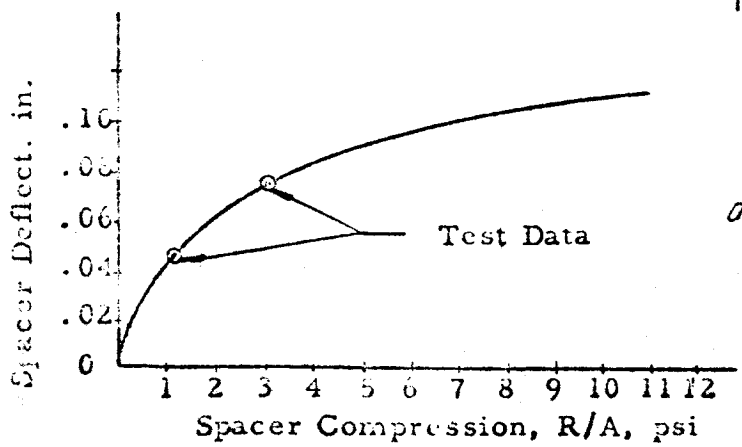

$$f = \left[f_{(\text{substrate})}\right] + \left[f_{(\text{spacer strip})}\right]$$

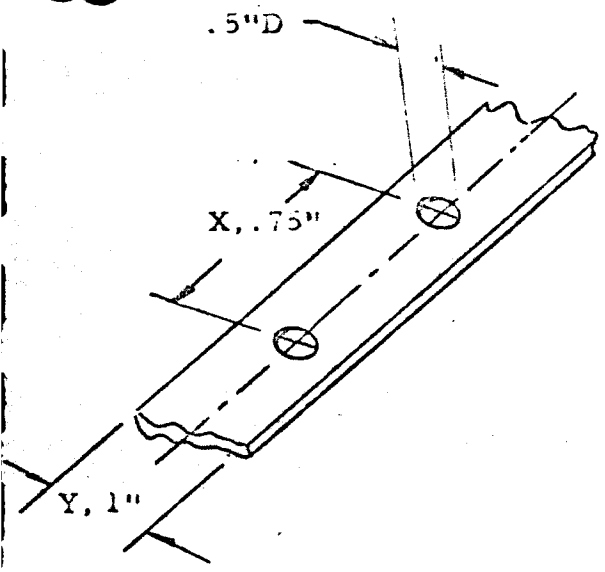

Silicone Sponge
Spacer Strip

$$R = (2P)\left(\frac{6}{2}\right) = (2 \times .25)(3) = 1.5 \text{ lbs/in.}^{\text{radial}} \text{ ult.}$$

$$A = \left[1 - \frac{D^2}{X \cdot Y}\right] \cdot Y = \left[1 - \frac{\pi \times .5^2}{4 \quad .75 \times 1}\right]$$

$$\times \quad 1 = .74 \text{ in.}^2/\text{in.}^{\text{radial}}$$

$$\frac{R}{A} = \frac{1.5}{.74} = 2.03 \text{ psi ult}$$

Then,

$$\delta = [2 \times .046] + [.005] = .147 \text{ in.}$$

Permissable $\delta < .125$ in.

Inner Vibrating Layer:

The critical condition occurs with the 4 wrapped layers vibrating in phase.

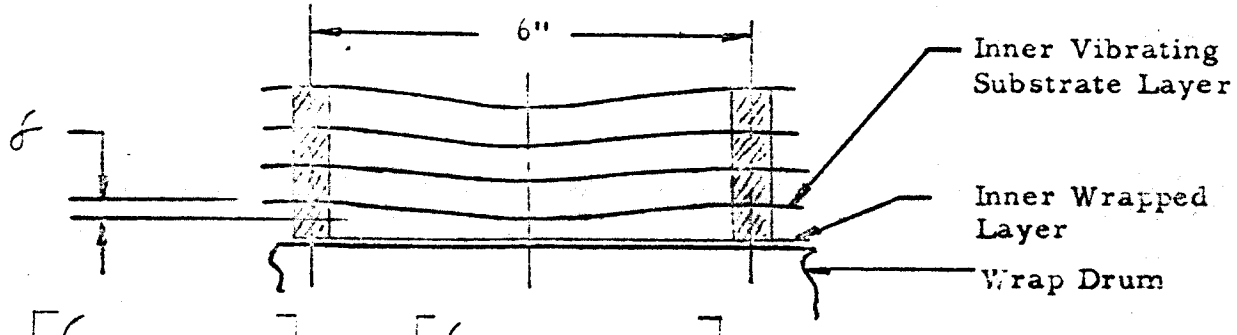

$$\delta = [\delta_{(\text{substrate})}] + [\delta_{(\text{spacer strip})}]$$

$$R = (4P)\left(\frac{6}{2}\right) = (4 \times .25)(3) = 3 \text{ lbs/in.}^{\text{radial}} \text{ ult}$$

$$A = .74$$

$$\frac{R}{A} = \frac{3}{.74} = 4.05 \text{ psi. ult.}$$

$$\delta = [.046] + [.078] = .124 \text{ in.}$$

Permissable $\delta <$ [illegible] in.

The above analysis shows that solar cell damage is evident for a 6 inch distance between spacer strips with the substrate vibrating in the radial "Breathing Mode". Therefore, it is suggested that this mode be eliminated by forcing the substrate into a frequency mode above the 200 cps. sinusoidal vibration range and into the noise spectrum range. This is accomplished through the use of spot spacers as shown in the following sketch.

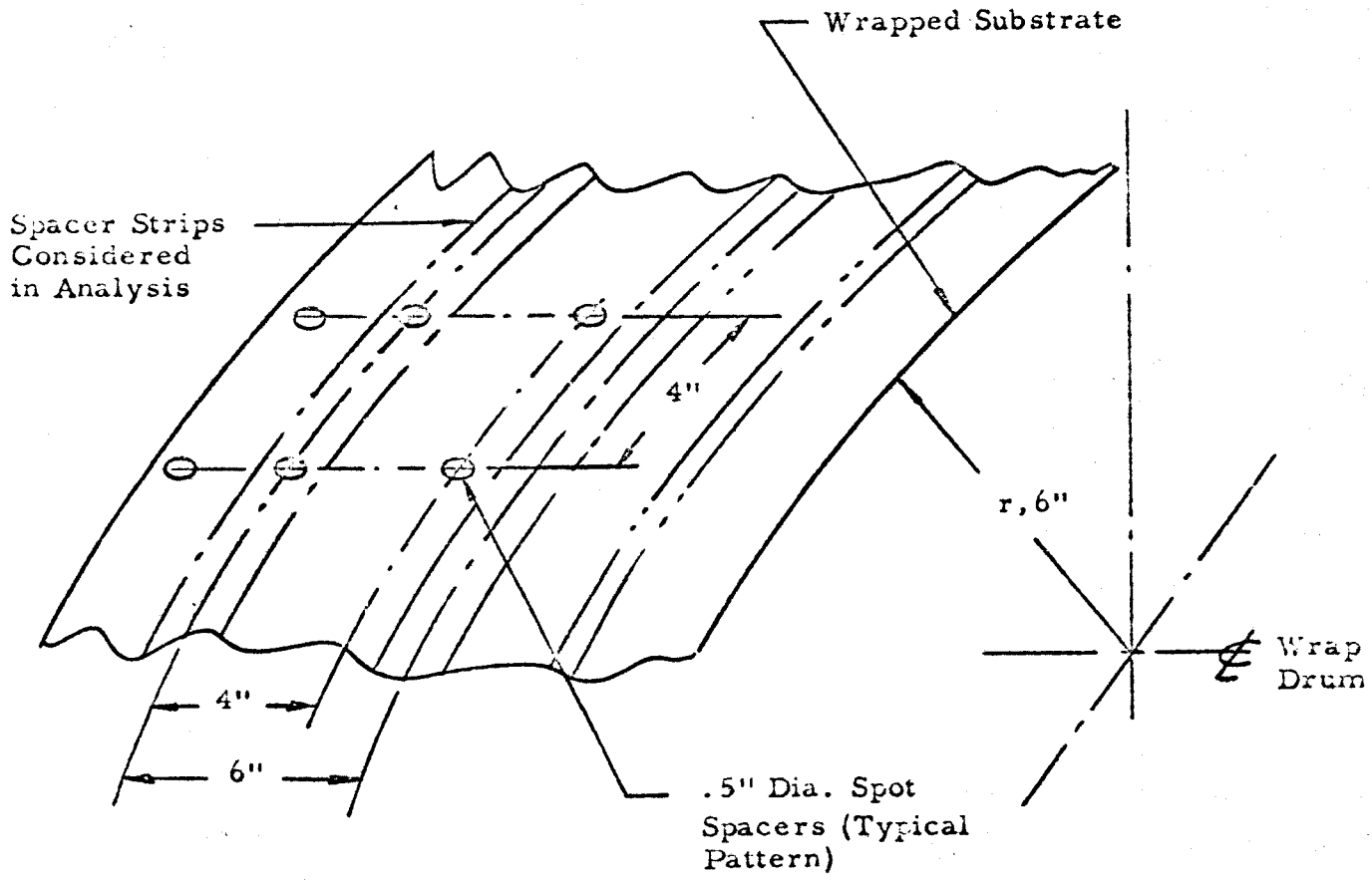

5.9 Analysis of Support Structure

Analysis is presented for launch environment. Temperatures are considered no greater than 75°F. The bracket is designed to limit deflections for the critical loading conditions presented.

This is necessary to validate the assumption used for dynamic analysis that dynamic load transfer from the spacecraft interface to the wrap drum is for a rigid body; ie. a dynamic transmissability. of 1.

Steady-state thrust load,

The static load V = 1/2 (W)(g) where W is the total calculated weight less the support structure.

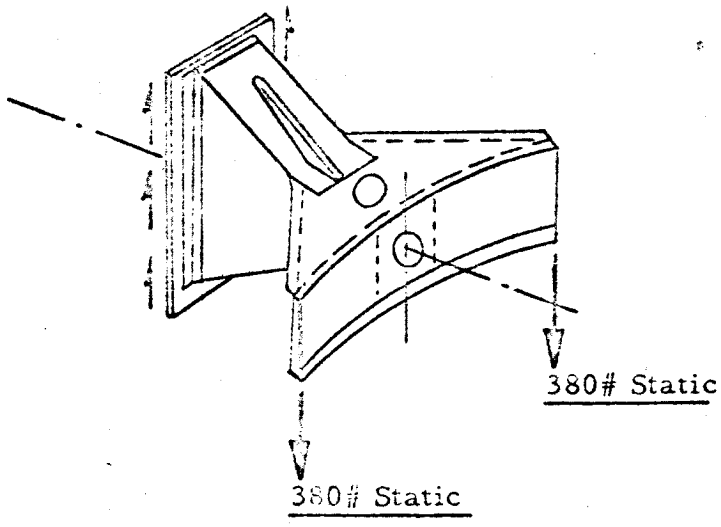

The V = 1/2 (35.6 + 15)(12 x 1.25) =380 lbs ult

Due to the shape of the structure, it will be considered as a cantilever beam of nonuniform cross section. By the Maxwell-Mohr solution, the beam is divided into n equal increments of Δ length and $f = \sum_{0}^{n} m\left(\frac{M}{EI}\right)\Delta$ where f is the deflection at the center of each increment. $\frac{M}{EI}$ is taken at the center of each increment, and 'm' represents the moment curve due to one pound placed at the deflection point in question. By the application of matrix

algebra, the equation for deflection at the center of any increment is,

$$\{\delta\} = |m|\ \left\{\frac{M}{EI}\right\}\Delta$$

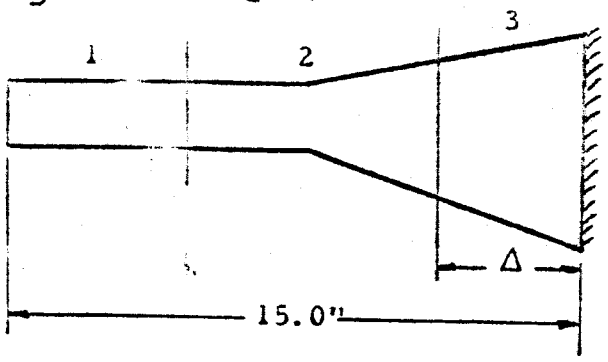

3 Equal Increments of 5" each

INCREMENTS → 1 2 3

$$\{\delta\} = \Delta \quad \begin{vmatrix} 0 & 1 & 2 \\ 0 & 0 & 1 \\ 0 & 0 & 0 \end{vmatrix} \quad \left\{\begin{matrix} .00005 \\ .00022 \\ .00008 \end{matrix}\right\} \Delta$$

Increment	δ
1.	.00038
2.	.00008
3.	0

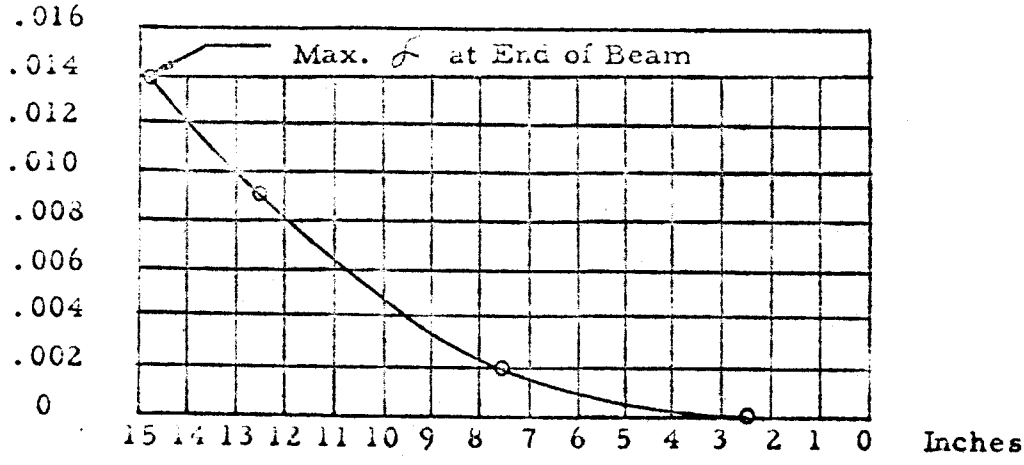

Then, $f_b = \frac{M}{I}$ at each point

$$f_{b(\text{point 1})} = \frac{(2)(380)(2.5)(1.7)}{3.62} = 892 \text{ psi ult}$$

$$f_{b(\text{point 2})} = \frac{(2)(380)(7.5)(1.7)}{2.44} = 3971 \text{ psi ult}$$

$$f_{b(\text{point 3})} = \frac{(2)(380)(12.5)(3.6)}{11.11} = 3078 \text{ psi ult}$$

And Buckling Allowance $= KE\left(\frac{t}{b}\right)^2$

$$= (8)(6.5 \times 10^6)\left(\frac{064}{5}\right)^2$$

$$= 8520 \text{ psi}$$

$$\text{M.S.} = \frac{8520}{3971} - 1 = +\underline{1.15}$$

If we consider a condition when the wrap drums are vibrating out of phase in a fundamental mode, then, torsional shear is considered at point 2. The torsional shear ,

$$S_s = \frac{T}{2bht} \quad \phi = \frac{\theta}{l} = \frac{bt \quad ht_1}{2tf_1 b^2 h^2} \times \frac{T}{G_s}$$

Where T = Torsional moment

ϕ = Angle of twist per unit of length

G_s = Shearing modulus of elasticity

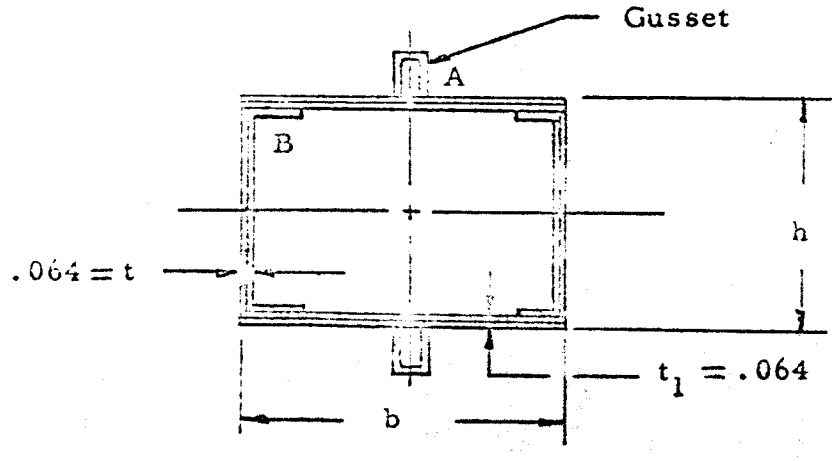

The total torsional load is taken as,

$V_2 + V_1 = 1/4\ (W)(g) = 1/4\ (31)(4 \times 12.5 \times 1.414 \times 1.25) = 685$ lbs ult

$V_2 = (W)(g) = (9.8)(1 \times 1.414 \times 1.25 \times 2) = 139$ lbs ult

and $V_1 + V_2 = V_{ult} = 685 + 139 = 824$ lbs ult

Then $T = (824)(16.625) = 13,699$ in.lbs ult

Then $S_{s(at\ A)} = \frac{13699}{(2)(5)(3.42)(.064)} = \frac{13699}{2.188} = 6,261$ psi ult

$S_{s(at\ B)} = \frac{13699}{(2)(5)(3.42)(.064)} = \frac{13699}{2.188} = 6,361$ psi ult

The buckling allowable $= K\Sigma \left(\frac{t}{b}\right)^2$ and K for torsional load $= 11.7$

Then at 'B' allowable $= (11.7)(6.5 \times 10^6) \left(\frac{.064}{5}\right)^2 = 12461$ psi ult

$$M.S. = \frac{12461}{6361} - 1 = +\underline{.96}$$

$$\phi_{avg} = \sum \varphi_1\ l_1 + \varphi_2\ l_2 + \varphi_3\ l_3$$

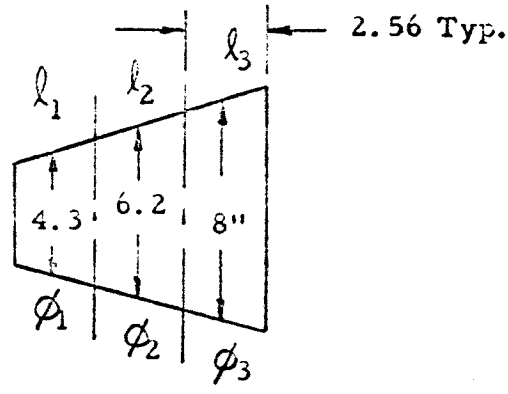

$$\phi_1 = \frac{(5)(.032)\quad (4.3)(.064)}{(2)(.032)(5)^2(4.3)^2} \times \left(\frac{13699}{2.4 \times 10^6}\right) = .8 \times 10^{-4} \text{ radians}$$

$$\phi_2 = \frac{(5)(.032)\quad (8)(.064)}{(2)(.032)(5)^2(6.2)^2} \times .00571 = 0.52 \times 10^{-4} \text{ radians}$$

$$\phi_3 = \frac{(5)(.032)\quad (8)(.064)}{(2)(.032)(5)^2(8)^2} \times .00571 = 0.37 \times 10^{-4} \text{ radians}$$

$$\phi_{avg} = (.8 \times 10^{-4})(2.56) + (.52 \times 10^{-4})(2.56) + (.37 \times 10^{-4})(2.56) = .00043 \text{ radians}$$

Then $\delta = (.00043)(10.73) = .0046$ in. which is the total at tip of structure.

5.10 Support Structure--Torsion Mode

This analysis is conducted to determine if the torsion mode frequency is sufficiently high to allow a reduction if magnesium were used in place of aluminum. An equal weight magnesium sheet structure would effect f_n as follows. Magnesium corrosion protection affects analysis negligibly since it amounts to less than 2% of the weight for the sheet thickness considered (See Figure 5-1).

$$\Delta f_n = \left(\frac{E_{Mag.}}{E_{AL.}} \times \frac{t_{Mag.}}{t_{AL.}} \times \frac{\rho_{AL.}}{\rho_{Mag.}} \right)^{1/2} - 1$$

if $t_{AL} = .040$ in, $t_{Mag.(\text{equal weight})} = .062$ in.

$$\Delta f_n = \left(\frac{6.5}{10} \times \frac{.062}{.040} \times \frac{.1}{.065} \right)^{1/2} - 1 = \underline{25\%} \text{ increase}$$

The minimum f_n to prevent modal coupling is $f_{n(\text{wrap drum})} \times \sqrt{2}$ which is 283 cps. The torsion mode frequency is calculated for the aluminum structure by application of the calculated torsion box section properties given in Section 5.0. Analysis is simplified by resolving the actual torque box into a torque box of constant cross-sections.

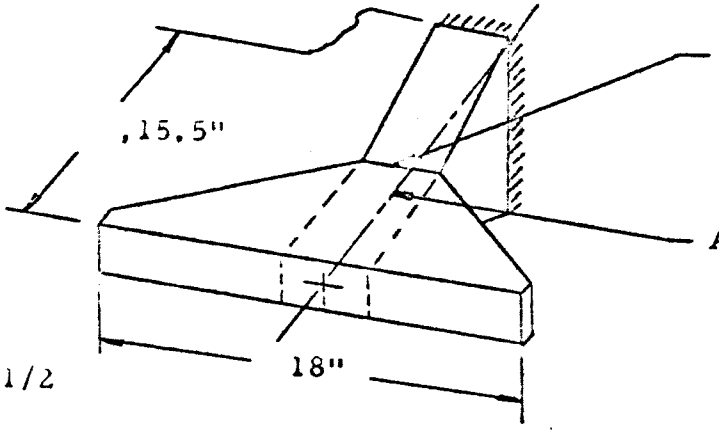

$$\omega = \frac{\pi}{2} \left(\frac{GJ}{\gamma_{polar} \ell^2} \right)^{1/2}$$

$$\gamma_{polar} = \left(\frac{W}{g} \right) \left(\frac{14.3}{\ell} \right) = \left(\frac{3.13}{386.4} \right) \left(\frac{14.3}{15.5} \right) = .0075 \text{ lbs-in.-sec}^2$$

$$\omega = \frac{\pi}{2} \left(\frac{4 \times 10^6 \times 5.0}{.0075 \times 15.5^2} \right)^{1/2} = 3.3 \times 10^3 \cdot \frac{\pi}{2}$$

$f_n = \frac{\omega}{2\pi} = 825$ cps, which is sufficiently high.

The load carrying capability is not critical as was shown in the stress section. If the actual f_n were 1/2 the calculated f_n, due to less than full fixity conditions at the spacecraft bus, the f_n is affected as follows by substituting the aluminum with magnesium,

$$f_n = \left(\frac{[illegible]}{2}\right)\left(\frac{6.5}{10} \times \frac{1}{.065}\right)^{1/2} = \left(\frac{825}{2}\right)(1) = \underline{412 \text{ cps}}$$

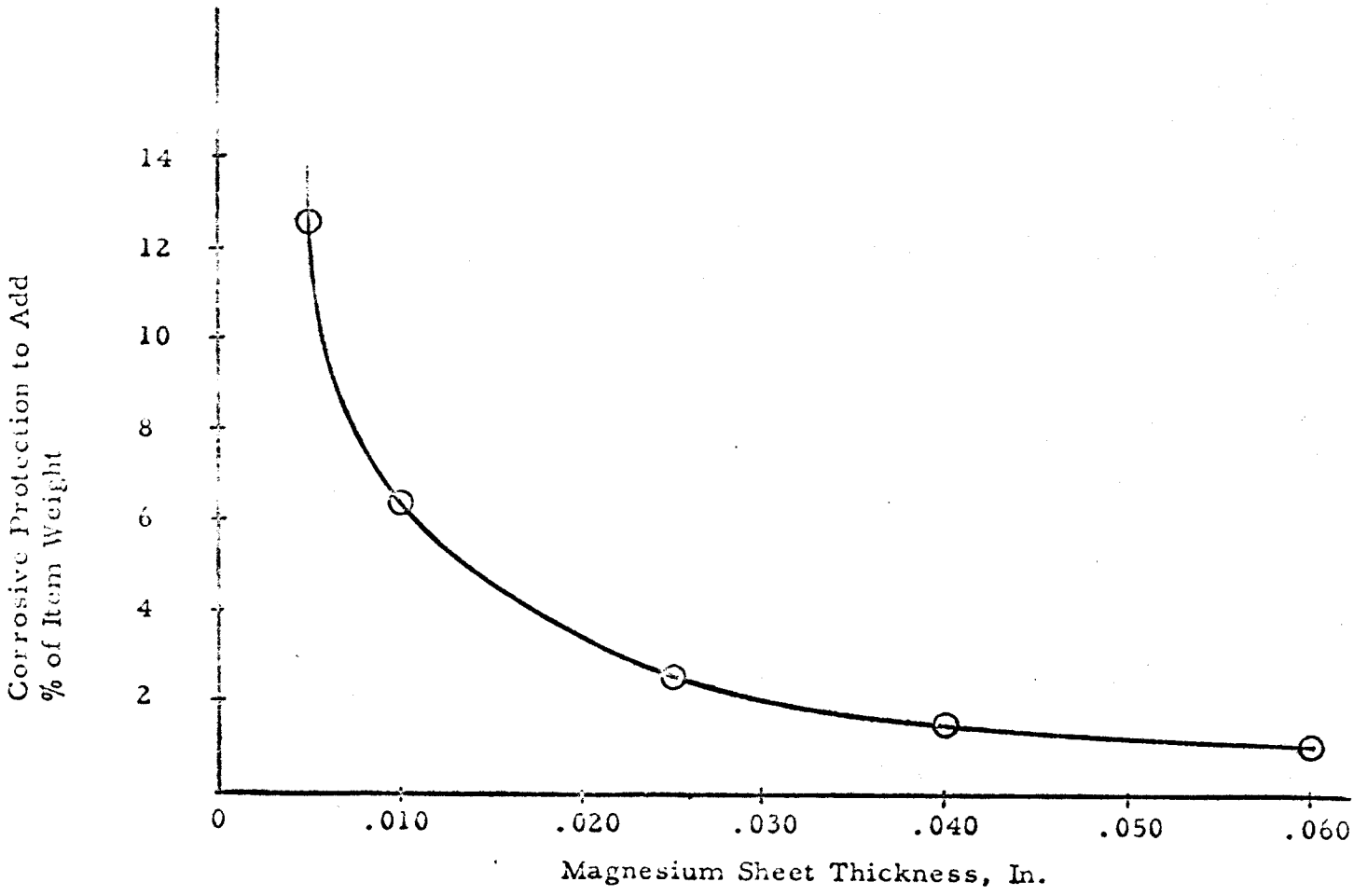

Figure 5-1 Added Weight of Magnesium Corrosion Protection

5.11 Lateral Beam Bending

This condition occurs during the .2g steady-state acceleration normal to the substrate plane during cruise maneuver between Earth and Mars. Beam temperatures are considered no greater than 250°F; substrate temperature is considered no greater than 150°F. The normal plane loading condition induces a lateral load in the beams with the substrate acting as a diaphragm. The magnitude of the lateral load decreases as lateral beam deflection increases. The point of equilibrium at which bending deflection energy equals the integrated lateral load components is calculated as follows:

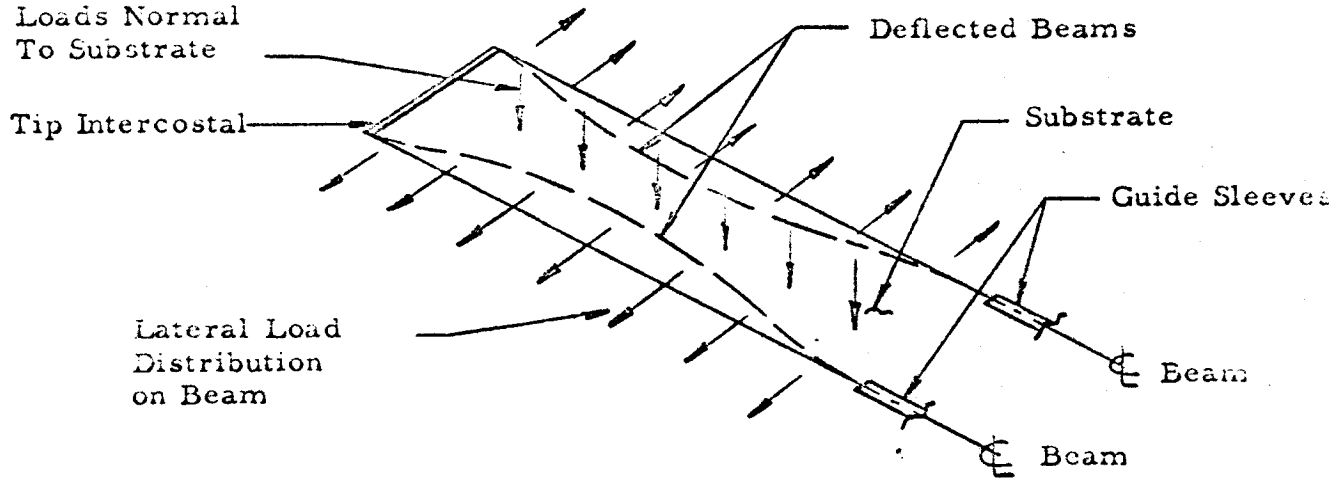

Variable lateral load, W_1 expressed as a function of maximum beam deflection,

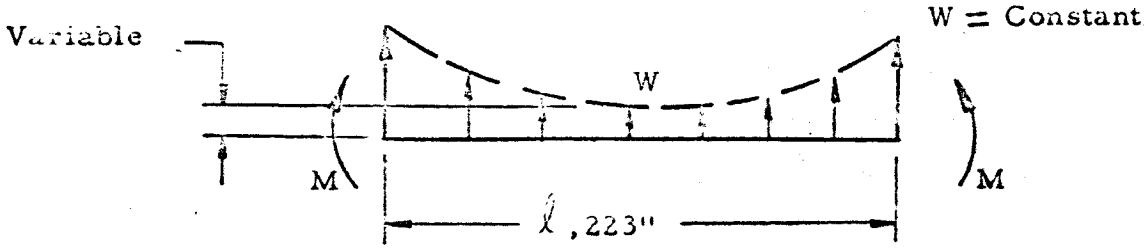

Load Distribution on Beam

At the points of no lateral beam deflection(Tip intercostal and guide sleeves), W is constant. W = 1.28 lbs/in. ult. is conservative (See Reference 8, page 101 corrected for $E = 3.5 \times 10^6$) due to the use of coefficients based on a substrate aspect ratio of 1.475. W is recalculated for an aspect ratio based on beam length, ℓ. Reference 14, Section A17.6, page A17.6 is used for analysis.

$$f_{t_{(membrane)}} = N_2 \left[E \left(\frac{qa}{t} \right)^2 \right]^{1/3}$$

Aspects Ratio $\frac{a}{b} = \frac{223}{36.7} = 6.04$

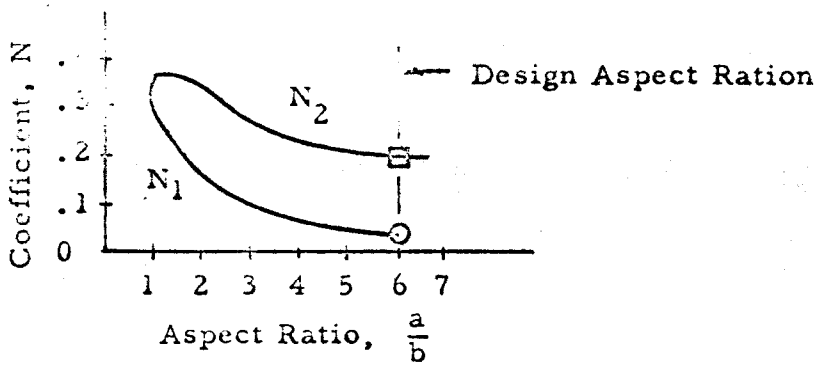

$E = 3.13 \times 10^6$ (Reference 9, page 9, Based on 112 Epoxy Impregnated Glass Cloth)

The effective modulus is increased somewhat due to the restraint against elongation with the solar cells attached to the substrate. The restraint is a function of the shear modulus of the solar cell bond adhesive, which is very low. Even if we consider a relatively large adhesive shear modulus, the comparative effect on $f_{t_{(membrane)}}$ is negligible.

q, load intensity $= .00061$ lbs/in.^{2} ult.

$t = .003$ in.

$$f_{t_{(membrane)}} = .2 \left[3.13 \times 10^6 \left(\frac{.00061 \times 223}{.003} \right)^2 \right]^{1/3} = 370 \text{ psi ult}$$

Lateral Load, $w = f_t \times t = 370 \times .003 = 1.11$ lbs/in. ult.

if t is increased effectively to .006,

$$W \quad 1.1 = \left(\frac{.006}{.003} \right) \quad \left(\frac{.003}{.006} \right)^{2/3} = 1.78 \text{ lbs/in.ult}$$

This does not indicate that lateral loads continue to increase as substrate thickness increases. When substrate deflection decreases to $\leq t/2$, lateral load will be reduced by beam

bending stiffness of the substrate. It is obvious that beam bending analysis is possible only when effective t is relatively large. For $t = .006$ in.,

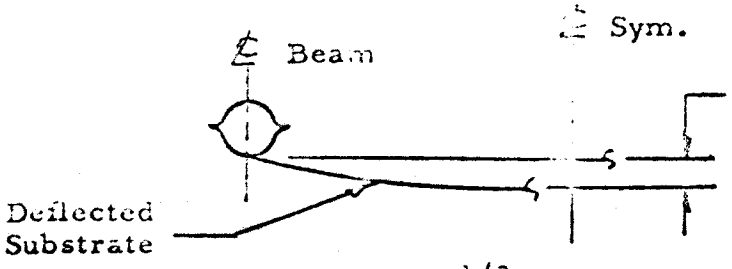

$$f = N_1 a \left(\frac{qa}{Et}\right)^{1/3}$$

$$= .04 \times 223 \left(\frac{.00061 \times 223}{3.13 \times 10^6 \times .006}\right)^{1/3}$$

$$f = .17 \text{ in.}$$

For $t = .003$ in.,

$$f = .04 \times 223 \left(\frac{.00061 \times 223}{3.13 \times 10^6 \times .003}\right)^{1/3}$$

$$f = .22 \text{ in.}$$

A .003 inch thick substrate is considered the practical minimum and will be considered for further analysis.

The beam moment of inertia for bending in the lateral plane is calculated as follows:

Mid-Span Area:

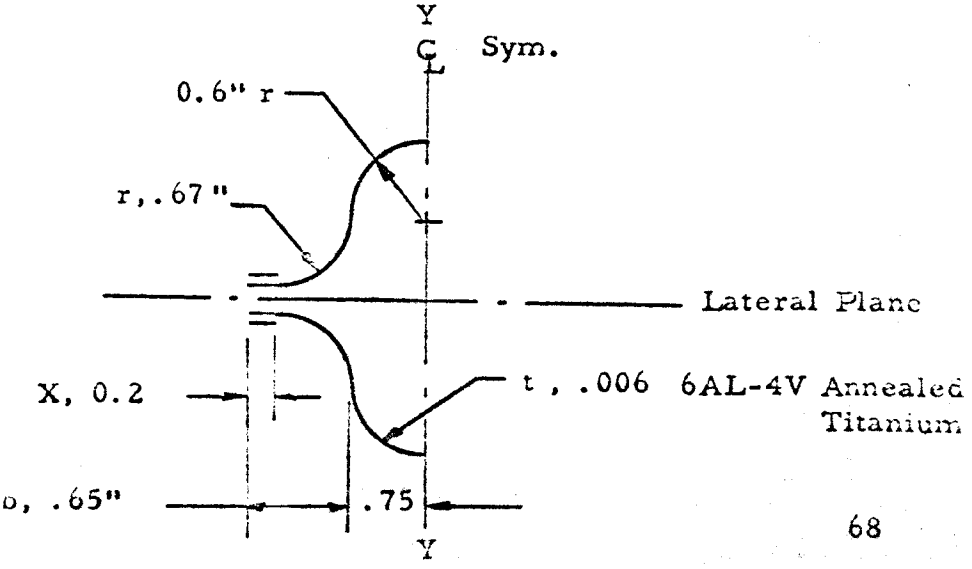

$$I_{y-y} = \pi r^3 t + 2\left[\frac{2t \times b^3}{12} + 2t \times b\left(.75 + \frac{b}{2}\right)^2\right]$$

$$+2\left[\frac{2t \cdot x^3}{12} + 2t \cdot x\left(.75 + b - \frac{x}{2}\right)^2\right]$$

$$= \pi \times .6^3 \times .006 + 2\left[\frac{2 \times .006 \times .65^3}{12} + 2 \times .006 \times .65 \times \left(.75 + \frac{.65}{2}\right)^2\right]$$

$$+2\left[\frac{2 \times .006 \times .2^3}{12} + 2 \times .006 \times .2\left(.75 + .65 - \frac{.2}{2}\right)^2\right]$$

$$= 40.72 \times 10^{-4} + 2\left[2.75 \times 10^{-4} + 90.09 \times 10^{-4}\right] + 2 \times \left[.08 \times 10^{-4} + 54.0 \times 10^{-4}\right]$$

$$I_{y-y} = \underline{\underline{.0335}} \text{ in.}^4$$

The compression stress capability of the free-edged lip is:

$$F_c = KE\left(\frac{4t}{x}\right)^2 \qquad K = 1.2 \text{ for a free, clamped condition at } \ell/x \longrightarrow \infty$$

$$F_c = 1.2 \times 16.0 \times 10^6 \left(\frac{4 \times .006}{.2}\right)^2 > F_{c_y}$$

Therefore the assumption that the full cross-section is 100% effective in bending is valid.

The bending capability of the above cross-section is calculated as follows:

By applying the equation given in Section 11.2 to the applicable element with r = .6 in.,

$$F_{c_{r_1}} = .25\, E\, \frac{t}{r}$$

To compensate for beam shear (2% reduction) and cruise manuever temperature (6% reduction) the above equation becomes,

$$F_{c_{r_1}} = (1-.08) \times .25\, E_c\, \frac{t}{r} = .23\, E_c\, \frac{t}{r}$$

$$F_{c_{r_1}} = .23 \times 16 \times 10^6 \left(\frac{.006}{.6}\right) = 36800 \text{ psi}$$

By applying the same equation to the applicable element with r = .67 in.,

$$F_{c_{r_2}} = .23 \times 16 \times 10^6 \left(\frac{.006}{.67}\right) = 32936 \text{ psi}$$

Since the unsupported edges are not critical,

F_{c_r} = 32936 will be used.

Then,

$$F_{c_r} = \frac{MC}{I}$$

$$M = \frac{F_{c_r} \times I}{C} \quad C = .75 + \frac{b - x}{2} = .75 + \frac{.65 - .2}{2} = .975 \text{ in.}$$

$$M = \frac{32936 \times .0335}{.975} = \underline{\underline{1132}} \text{ in.-lbs. ult}$$

Beam Ends -----

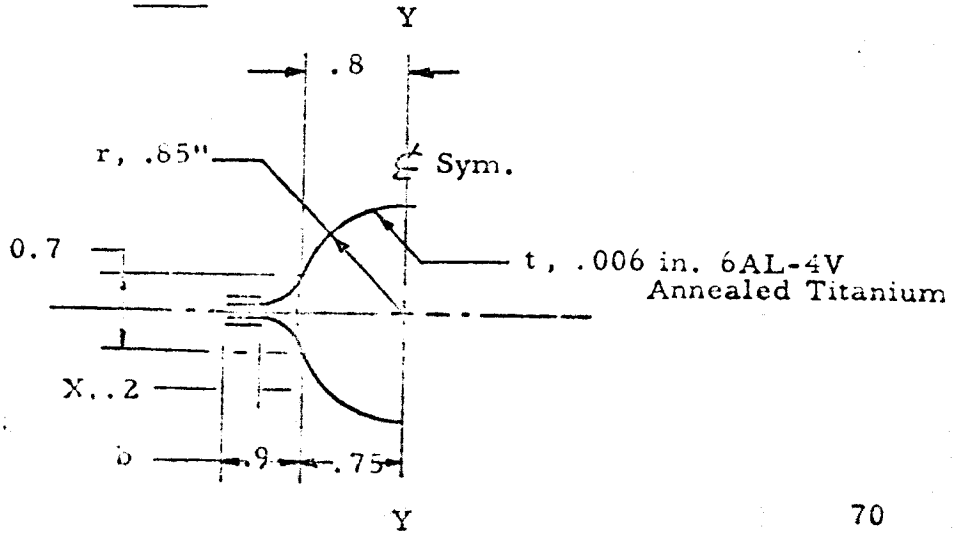

$$I_{y-y} = \pi r^3 t - 2\left[.7t \times .6^2\right] + 2\left[\frac{2tb^3}{12} + 2tb\left(.75+\frac{b}{2}\right)^2\right]$$

$$+ 2\left[\frac{2t\chi^3}{12} + 2t\chi\left(.75+b-\frac{\chi}{2}\right)^2\right]$$

$$= \pi \times .85^3 \times .006 - 2\left[.7 \times .006 \times .8^2\right] + 2$$

$$\left[\frac{2 \times .006 \times .9^3}{12} + 2 \times .006 \times .9\left(.75+\frac{.9}{2}\right)^2\right]$$

$$+ 2\left[\frac{2 \times .006 \times .2^3}{12} + 2 \times .006 \times .2\left(.75+.9-\frac{.2}{2}\right)^2\right]$$

$$= 115.76 \times 10^{-4} - 53.76 \times 10^{-4} + 325 \times 10^{-4} + 115.48 \times 10^{-4}$$

$$I_{y-y} = \underline{.0503} \text{ in.}^4$$

The bending capability of the above cross-section is calculated using the buckling equation given in Section 11.2. Applied to the critical element, r = .85 in.,

$$F_{c_r} = .23 \times 16 \times 10^6 \left(\frac{.006}{.85}\right) = 25944 \text{ psi}$$

$$M = \frac{F_{c_r} \times I}{C} \quad C = .75 \text{ in.} \quad = \frac{25944 \times .0503}{.75} = \underline{1740} \text{ in.-lbs.}$$

When variable load, W, is maximum (using Reference 2, page 108, case 33),

For conditions A plus B---

$$M_{(ends)} = \frac{wl^2}{12} \quad \frac{1.11\,(223)^2}{12} = 4600 \text{ in.-lbs ult}$$

$$M_{(center)} = \frac{4600}{2} = 2300 \text{ in.-lbs. ult.}$$

$$\delta_{(center} = \frac{w\ell^4}{384EI} = \frac{1.11\ (223)^4}{384 \times 15.4 \times 10^6 \times .0335} = 13.7 \text{ in.}$$

When variable load, W, is minimum $\delta_{(center)}$ is determined for the integrated conditions as follows:

M is maximum at the ends and is determined by letting the sum of the areas under the M/EI curves for the following conditions be equal to the change in slope between the beams ends.

Condition A,

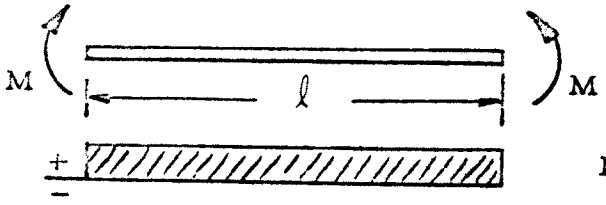

M/EI Curve

Condition B,

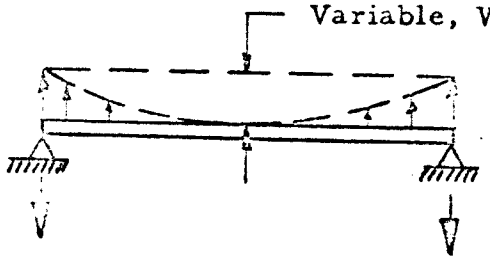

1.11 lbs/in. ult.

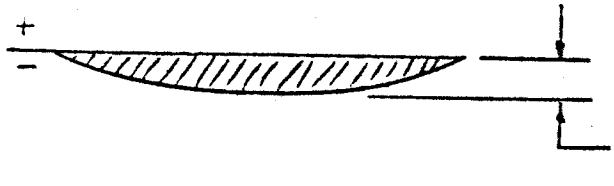

M/EI Curve

$\frac{W\ell^2}{48\ EI}$

$$\int_0^{\ell} \frac{M}{EI} = \text{slope} = 0$$

EI is cancelled for the uniform beam. Then,

$$\text{Slope} = 0 = \left(\frac{W\ell^2}{48}\right)\left(\frac{2}{3} \times \ell\right) - M\ell$$

$$M_{(ends)} = \frac{W \ell^2}{72}$$

$$M_{(center)} = \frac{W \ell^2}{48} - \frac{W \ell^2}{72} = \frac{W \ell^2}{144}$$

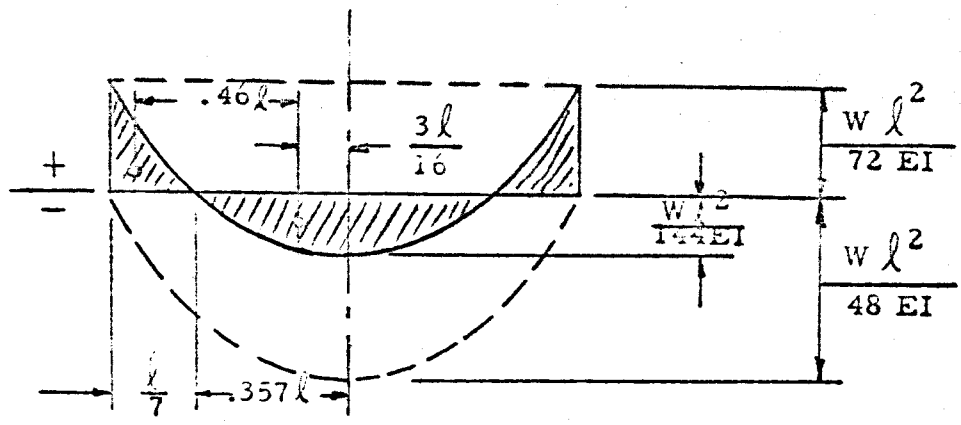

Integrated M/EI Distribution

Then, $\mathcal{f}_{(center)}$ when variable load W is minimum is,

$$2 \times \sum_{0}^{\ell/2} \cdot \frac{M}{EI} \times \Delta X \times X:$$

$$\mathcal{f} = \frac{2}{EI} \left[\left(\frac{1}{3} \times \frac{W \ell^2}{72} \times \frac{\ell}{7} \right) (.46 \ell) - \left(\frac{2}{3} \times \frac{W \ell^2}{144} \times .357 \ell \right) \left(\frac{3 \ell}{16} \right) \right]$$

$$\mathcal{f} = \frac{2}{EI} \left[3.04 \times 10^{-4} \, W \ell^4 - 3.09 \times 10^{-4} \, W \ell^4 \right] \cong 0$$

Which shows that $\mathcal{f}$ is effected critically by the exactness of shape of the $\frac{M}{EI}$ curve.

When variable load, W, is between minimum and maximum, say .02 lbs/ in. ult.,

Condition A,

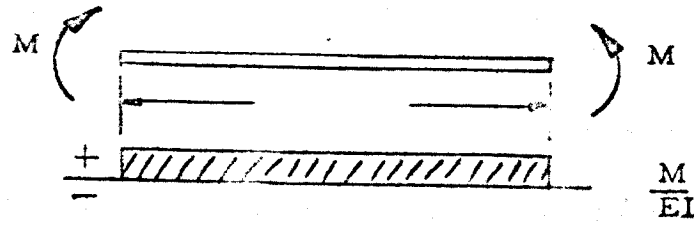

Condition B,

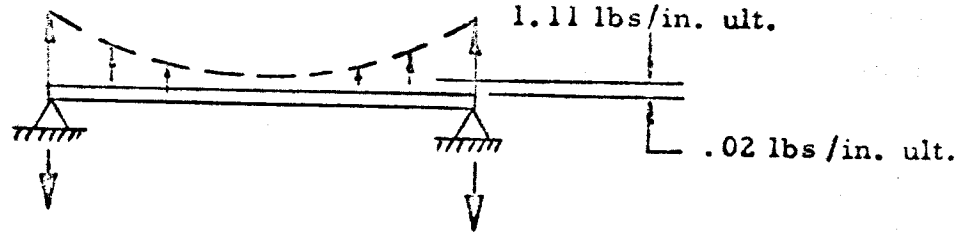

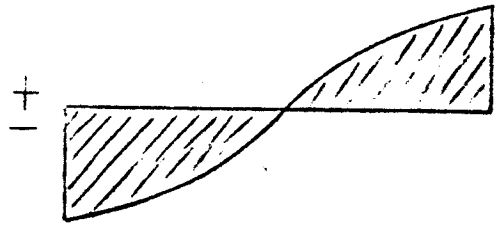

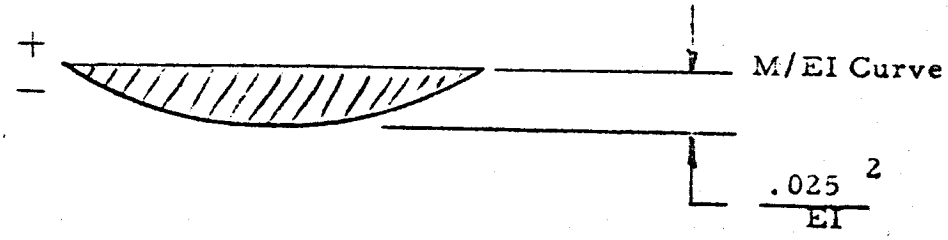

$$\frac{M}{EI} = \text{Slope} = 0$$

EI is cancelled for the uniform beam. Then,

$$\text{Slope} = 0 = \left(\frac{.025\,\ell^2}{EI}\right)\left(\frac{2}{3} \times \ell\right) - \frac{M \cdot \ell}{EI}$$

$$M_{(ends)} = .017\,^2$$

$$M_{(center)} = .025\ell^2 - .017\ell^2 = .008\ell^2$$

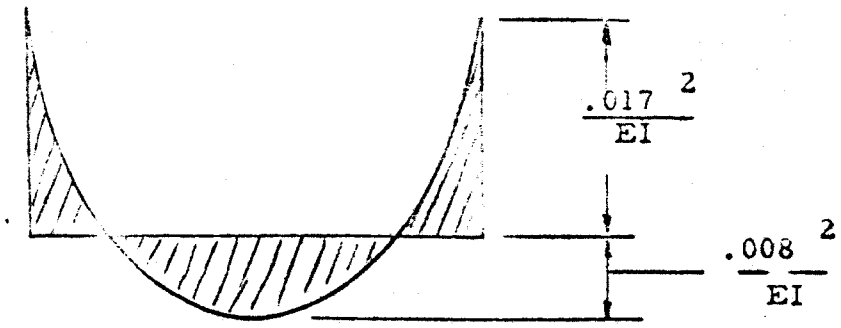

Integrated M/EI Distribution

Then $\delta_{(center)}$, when variable load is .02 lbs-in. ult., is calculated as,

$$\delta = 2\left[\left(\frac{1}{3} \times \frac{.017\,\ell^2}{EI} \times \frac{1}{7}\right)(.46\ell) - \left(\frac{2}{3} \times \frac{.008\,\ell^2}{EI} \times .357\ell\right)\left(\frac{3\ell}{16}\right)\right]$$

$$= 2\left[\frac{3.72 \times 10^{-4}\,\ell^4}{EI} - \frac{3.57 \times 10^{-4}\,\ell^4}{EI}\right] = \frac{2}{EI}\left[.15 \times 10^{-4}\ell^4\right]$$

$$\delta = \frac{2}{15.4 \times 10^{6} \times .0335}\left[.15 \times 10^{-4}(223)^4\right] = \underline{0.14}\text{ in.}$$

Variable load, W, expressed as a function of lateral substrate deflection:

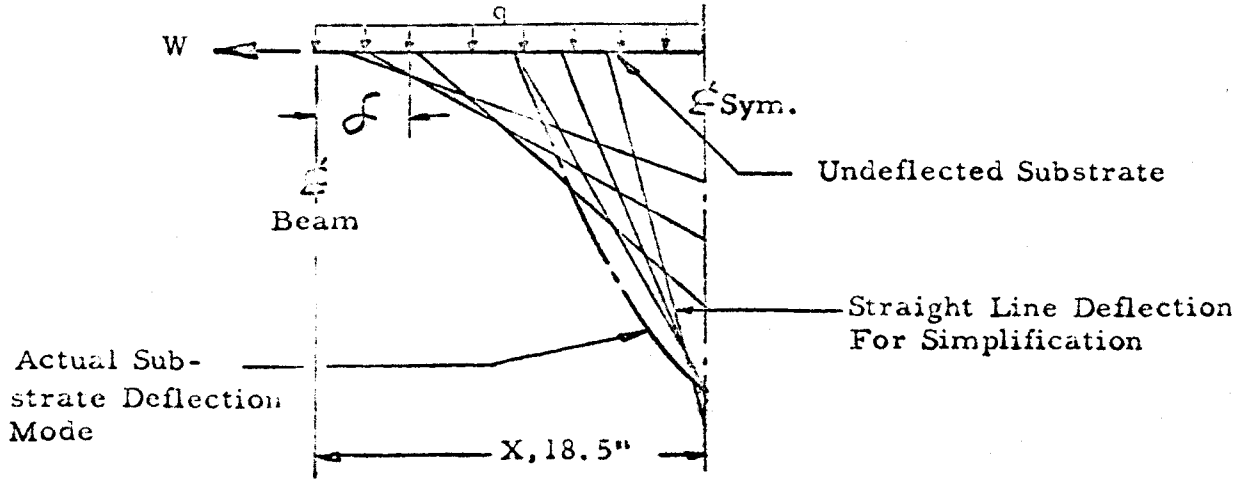

$$\text{at } \delta = \frac{X}{4}, \quad W = (q \cdot X)\left(\frac{X - \delta}{.65X}\right) = (q \cdot X)\left(\frac{.75X}{.65X}\right) = (1.15)(q \cdot X)$$

$$\text{at } \delta = \frac{X}{2}, \quad W = (q \cdot X)\left(\frac{X - \delta}{.86X}\right) = (q \cdot X)\left(\frac{.5X}{.86X}\right) = (.58)(q \cdot X)$$

$$\text{at } \delta = \frac{3}{4}\ X, \quad W = (q \cdot X)\left(\frac{X - \delta}{.96X}\right) = (q \cdot X)\left(\frac{.25X}{.96X}\right) = (.26)(q \cdot X)$$

Plotting the expressions for the conditions analyzed above gives.

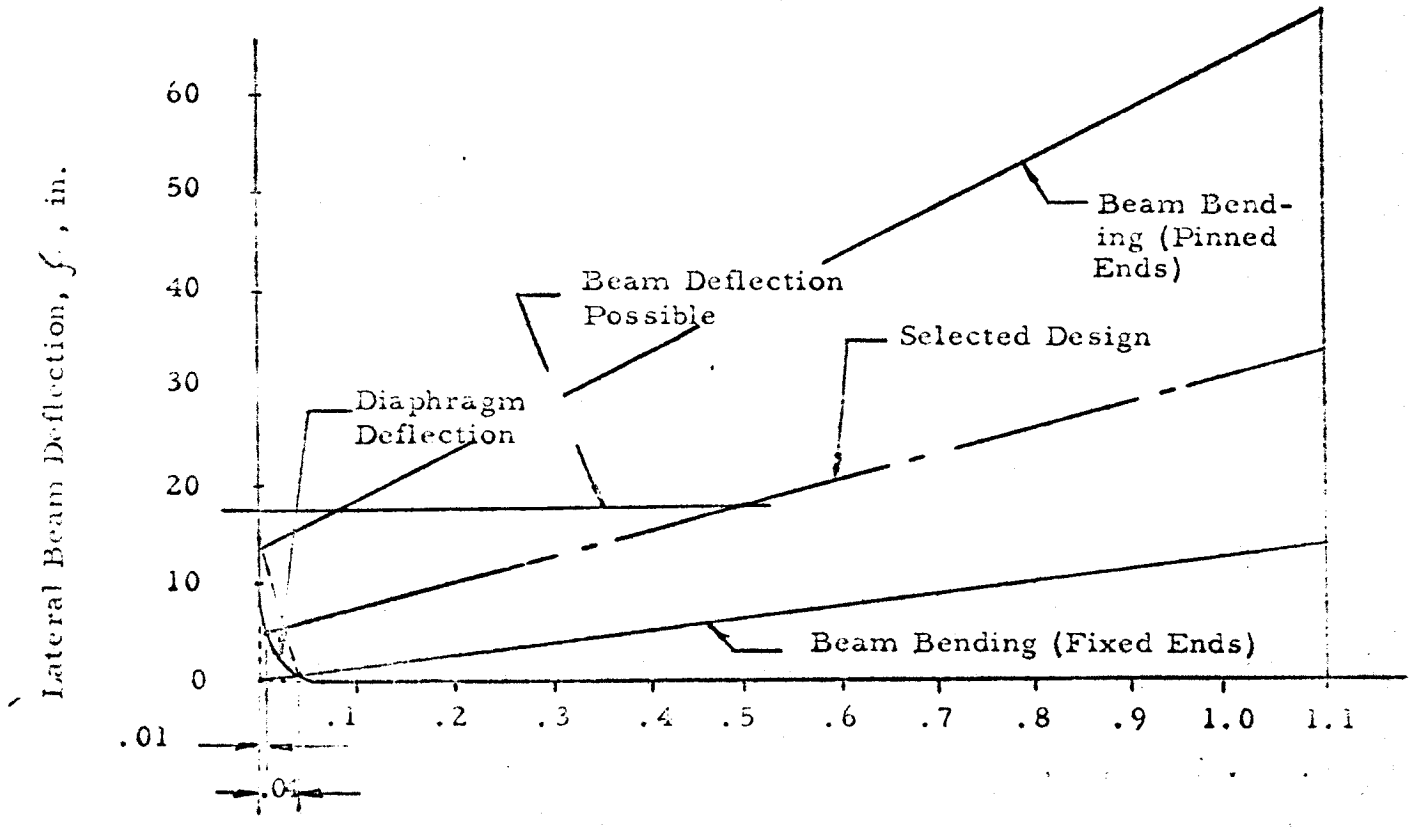

Figure 5-2 Lateral Beam Deflection at Mid-Span

The bending moments for the pinned and fixed end conditions are calculated as follows:

Fixed Ends--

Lateral Load at Mid-Span .04 lbs/in. ult.

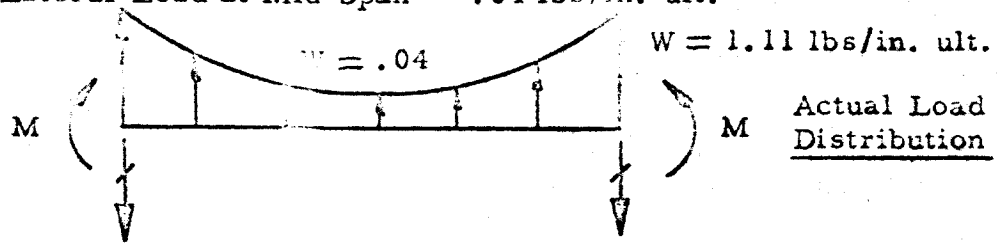

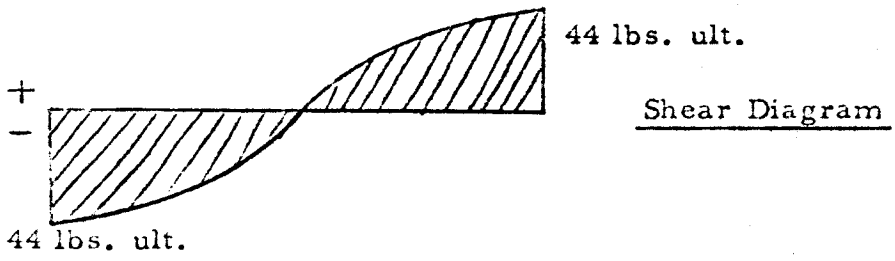

Condition A,

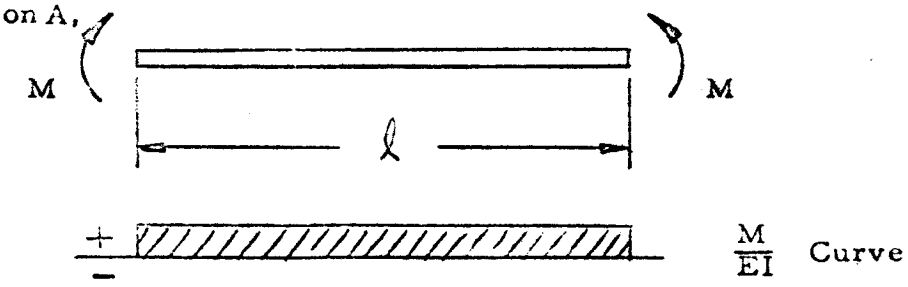

Condition B,

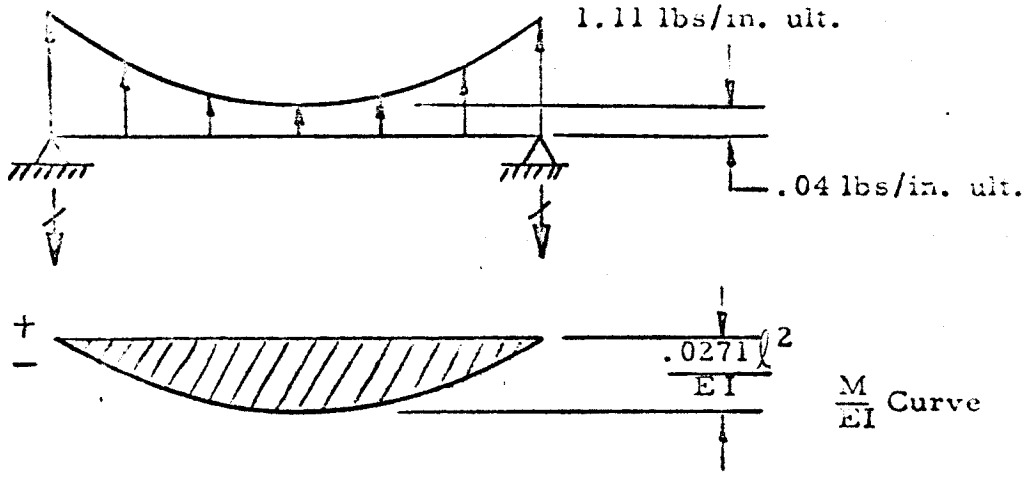

Then,

$$\text{Slope} = 0 = (.0271\ \ell^2)\left(\tfrac{2}{3} \cdot \ell\right) - M \cdot \ell$$

$$M_{(ends)} = .01807\ \ell^2 = .01807\ (223)^2 = \underline{899}\ \text{in.-lbs. ult.}$$

$$M_{(center)} = .0271\ \ell^2 - .01807\ \ell^2 = .00903\ \ell^2 = \underline{499}\ \text{in.-lbs. ult.}$$

Fixed Ends

Lateral load at mid-span = 1.11 lbs-in. ult.

$M_{(ends)}$ = 4600 in.-lbs. ult.

$M_{(center)}$ = 2300 in.-lbs. ult.

Pinned Ends

Lateral load at mid-span = 0

$M_{(ends)}$ = 0

$M_{(center)}$ = 1140 in.-lbs. ult.

Pinned Ends

Lateral load at mid-span = 1.11 lbs-in. ult.

$M_{(ends)}$ = 0

$M_{(center)}$ = 6838 in.-lbs. ult.

Figure 5-2 shows that the lateral beam load at beam mid-span is near 0 lbs-in. (See intersection of expressions for beam bending and diaphragm deflection) for either extreme of the beam end fixity range. The applicable extreme bending moments, then, are:

Fixed Ends (lateral deflection = 1 in.)

Actual Moment	Allowable Moment
$M_{(ends)}$ = 899 in.-lbs. ult.	$M_{(ends)}$ = 1740 in.-lbs
$M_{(center)}$ = 449 in.-lbs. ult	$M_{(center)}$ = 1132 in.-lbs

Pinned Ends (lateral deflection = 13.7)

Actual Moment	Allowable Moment
$M_{(ends)}$ = 0	$M_{(ends)}$ = 1740 in.-lbs
$M_{(center)}$ = 1140 in.-lbs. ult.	$M_{(center)}$ = 1132 in.-lbs

The beam bending capability exceeds the actual moment for fixed end conditions, but provisions at the beam ends to obtain a fixed condition would result in unnessary weight addition. The beam bending capability for a pin-ended beam nearly matches the corresponding moment requirement, however, lateral beam deflection would be excessive (13.7 inchs each beam) for the following reasons:

1. Solar cell and solar cell module interconnect damage could result from induced biaxial stresses in substrate due to the double curvature effects.

2. Excessive vertical plane beam bending could result with the substrate forced into a normal-to-plane accelleration as the beams relaxed in the lateral plane.

Therefore, beam end fixity will be relaxed. This shall be no more than to result in a reasonable tradeoff of lateral beam deflection vs. induced weight for fixity provisions. A lateral beam deflection of 5 inches shall be considered for further analysis. A linear extrapolation of actual bending moment corresponding to a lateral beam deflection of 5 inches is slightly conservative since the lateral load at mid-span is .01 lbs-in. ult. rather than .03 lbs-in. ult. (See Figure 5-2).

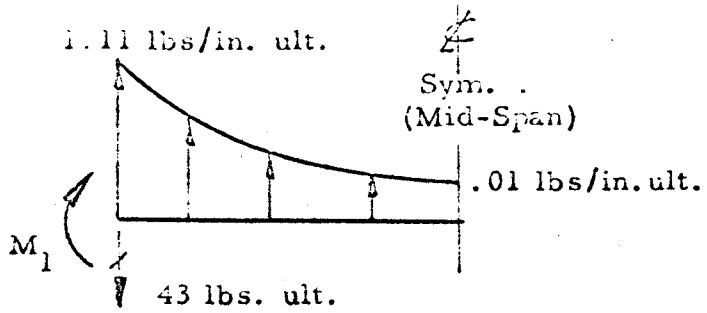

Actual Load Distribution Corresponding to 5 in. Deflection

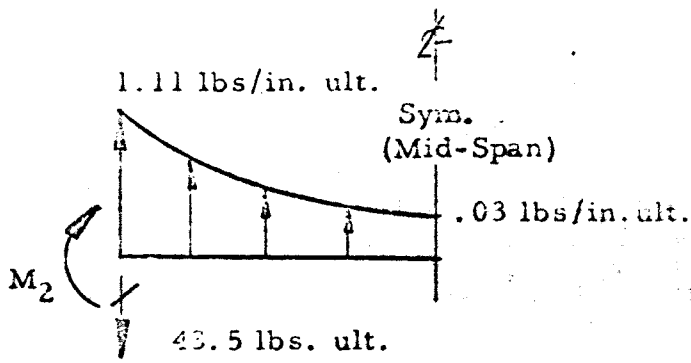

Load Distribution if Diaphragm Deflection Expression were Linear

Based on the conservative approach, required beam bending reaction at beam ends is extrapolated for the relaxed fixity condition as,

$$M_{(ends)} = \left(1 - \left(\frac{5}{13.7}\right)\right) \times 899 = 571 \text{ in-lbs. ult.}$$

and, the required degree of angular rotation ϕ at the beam ends corresponding to this fixity condition is calculated by linear extrapolation as,

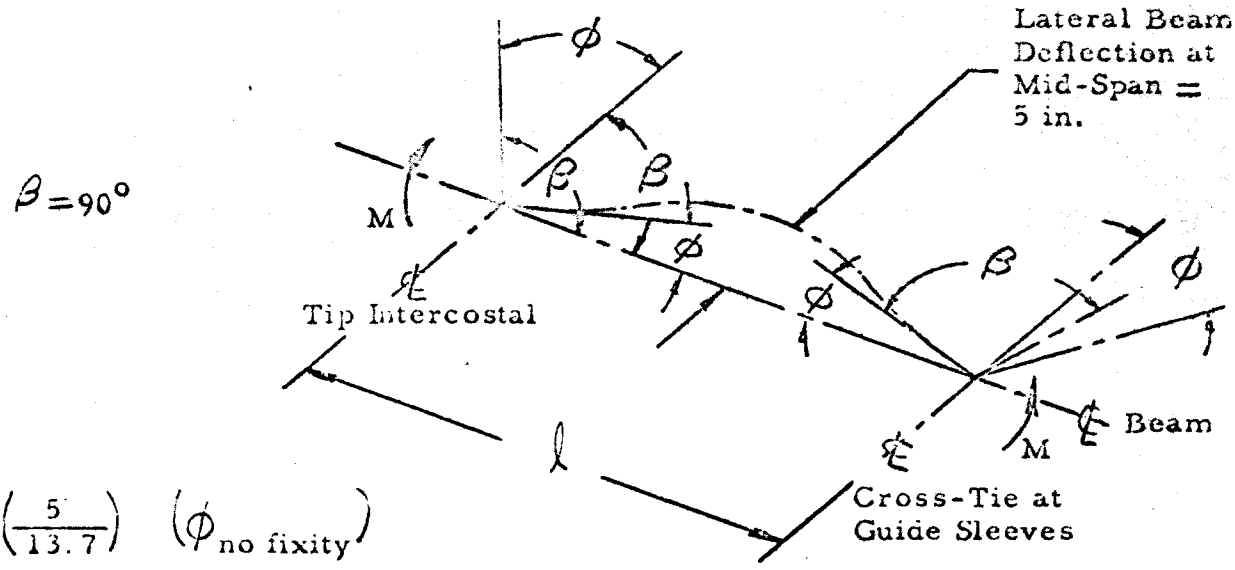

$$\phi = \left(\frac{5}{13.7}\right) \left(\phi_{\text{no fixity}}\right)$$

For $\phi_{\text{no fixity}}$,

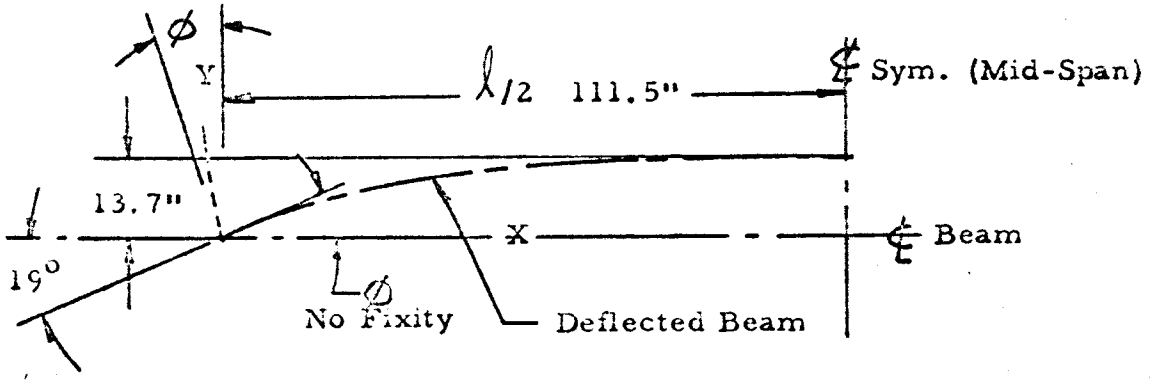

$$\phi = \left(\frac{5}{13.7}\right) (19^\circ) = 6.9^\circ = \frac{6.9\pi}{180} = 0 \cdot \underline{120} \text{ radians}$$

Then, the required cross-sectional moment of inertia of the tip intercostal is calculated as,

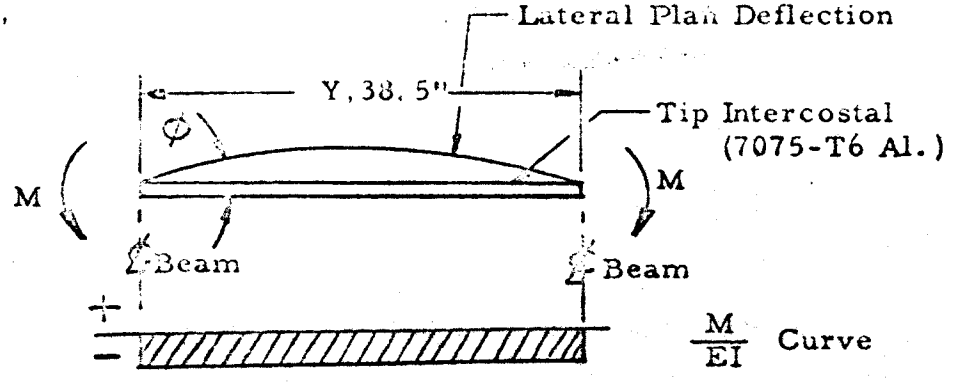

$$\phi = \int_0^{\frac{Y}{2}} \frac{M}{EI} \cdot d_y = \frac{M \cdot \frac{Y}{2}}{EI} = .120 \text{ Radians}$$

E is considered $\leq 75^{\circ}F = 10.3 \times 10^6$ (Reference 3) for 7075-T6 Alclad

$$I = \left| \frac{M \cdot Y}{2E \cdot \phi} \right| = \frac{571 \times 38.5}{2 \times 10.3 \times 10^6 \times .120} = \underline{.0089} \text{ in.}^4$$

7075-T6 alclad was chosen to provide the bending compression stress capability required.

5.12 Analysis of Tip Intercostal

The tip intercostal is analyzed for induced loads which occur during the .2 g cruise maneuver between Earth and Mars (See Section 5.11). Temperature is not considered to exceed 75°F with the tip intercostal shielded from solar radiation by the substrate. The induced distributed loads parallel to the ℄ beam at the substrate attachment are negligible with the substrate aspect ratio of 5.8. The induced distributed load in the vertical plane at the substrate attachment is approximately .0061 x 38.5 = .24lbs. ult., M = .55 x .24 = .13 in.- lbs and therefore considered negligible.

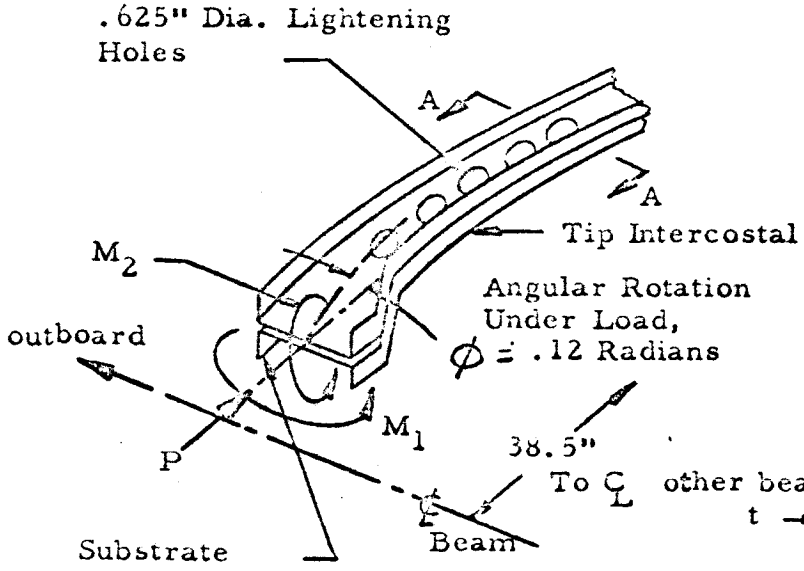

P = 43.5 lbs ult.
M_1 = 571 in.-lbs. ult.
M_2 = 43.5 x .85 = 37 in.-lbs. ult.

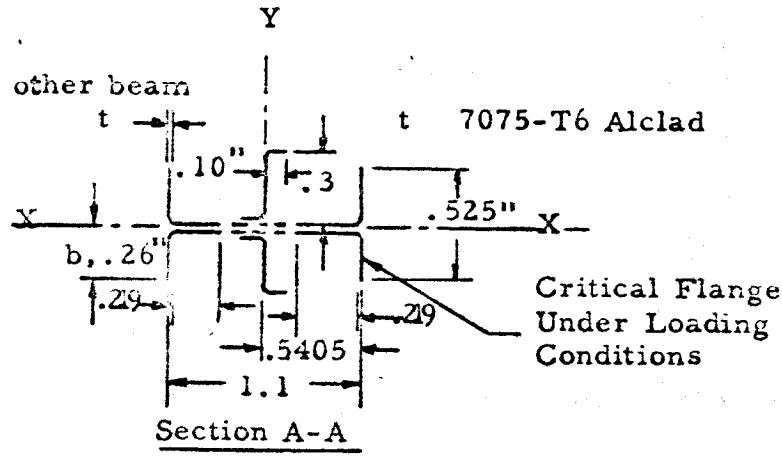

Section A-A

The bending stiffness requirement about the y-y axis (I_{y-y}) compatible with ϕ = .12 radians was calculated in Section 5.11 as .0089 in.^{4}. The above Section stiffness matches the requirement with a calculated I_{y-y} = .0088 in.^{4}.

Section A-A is now analyzed for the composite loading condition.

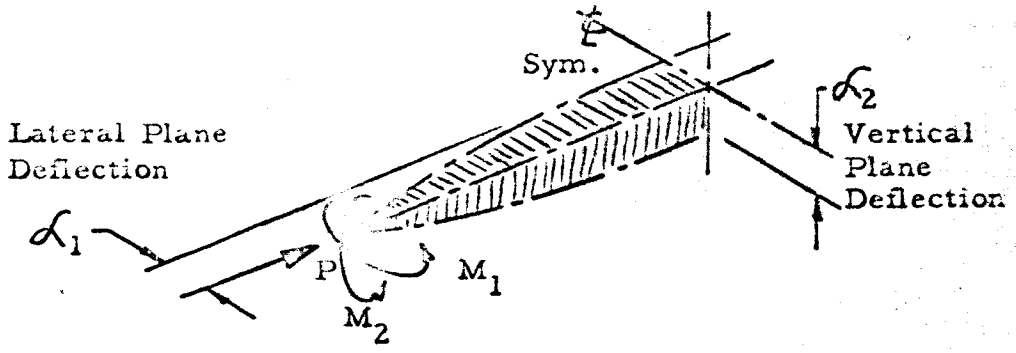

$$f_{c_{(\text{critical flange})}} = \frac{P}{A} + \frac{(P \cdot f_1)(.5405)}{I_{y-y}} + \frac{(P \cdot f_2)(.26)}{I_{x-x}} + \frac{(M_2)(.26)}{I_{x-x}} + \frac{(M_1)(.5405)}{I_{y-y}}$$

$$f_1 = \frac{M_1 (38.5)^2}{8\, EI_{y-y}} = \frac{571\ (38.5)^2}{8 \times 10.3 \times 10^6 \times .0088} = \underline{1.17}\ \text{in.}$$

$$f_2 = \frac{M_2 (38.5)^2}{8\, EI_{x-x}} = \frac{37\ (38.5)^2}{8 \times 10.3 \times 10^6 \times 1.23 \times 10^{-3}} = \underline{.54}\ \text{in.}$$

$$f_c = \frac{43.5}{.056} + \frac{(43.5 \times 1.17)(.5405)}{.0088} + \frac{(43.5 \times .54)(.26)}{1.23 \times 10^{-3}} + \frac{(37)(.26)}{1.23 \times 10^{-3}} + \frac{(571)(.5405)}{.0088}$$

$$f_c = 777 + 3126 + 4965 + 7821 + 35071 = 51760 \text{ psi ult.}$$

$$F_{c_r} = KE_c \left(\frac{t}{b}\right)^2$$

K = 1.2 for free, clamped condition (Reference 11)

$$= 1.2 \times 10.5 \times 10^6 \left(\frac{.019}{.26}\right)^2 = 67292 \text{ psi}$$

$$M.S. = \frac{F_{c_r}}{f_c} - 1 = \frac{67292}{51760} - 1 = \underline{+.30}$$

The attachment of the tip intercostal to the beam is not critical with the combination adhesive, rivet, spotweld attachment provided.

5.13 Analysis of Cross-Tie at Guide Sleeves

The cross-tie between the wrap drum end caps is analyzed for induced loads which occur during the .2g cruise maneuver between Earth and Mars (See Sections 5.11 and 11.2). Cross-tie temperature is considered equal to beam temperature (250°F) since no solar radiation shielding is provided by substrate in this area.

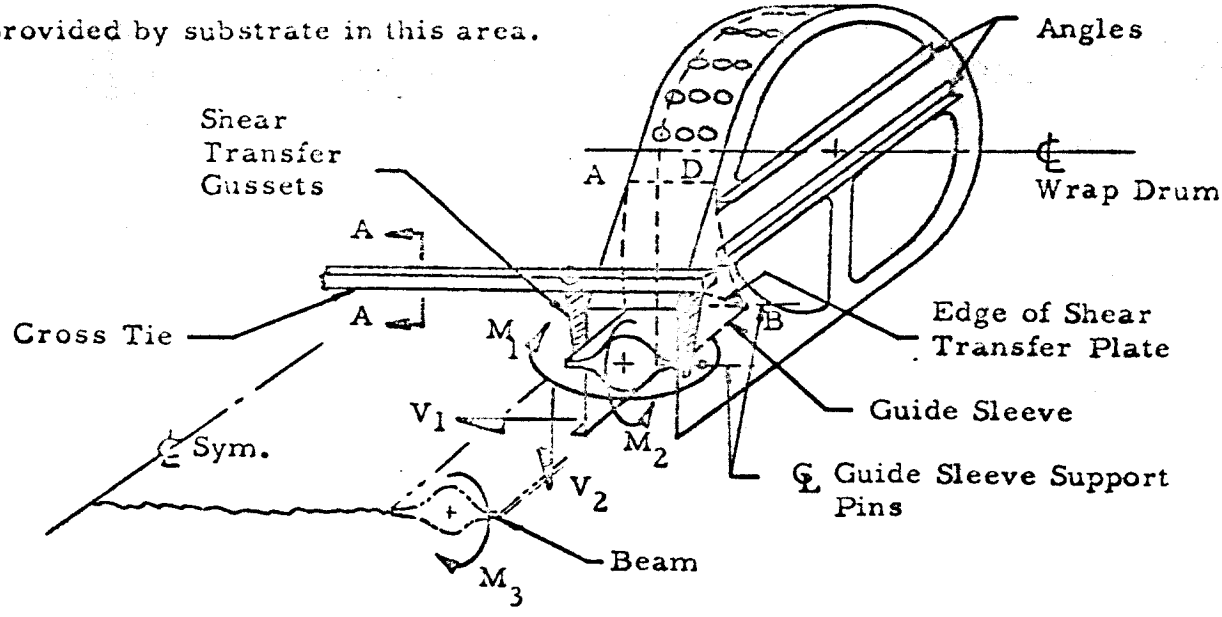

The composite loads with the exception of moment M_2, are transferred from the guide sleeve to the cross-tie by means of shear and bending in the shear transfer gussets and by means of shear in the shear transfer plate. Shear V_2 is 3.36 lbs. ult. which is relatively small and therefore neglected. Analysis is now conducted to determine the degree of angular beam rotation in the lateral plane due to load transfer between the beam and cross-tie.

The lateral angular rotation due to fabrication tolerance between the beam and guide sleeve is calculated as,

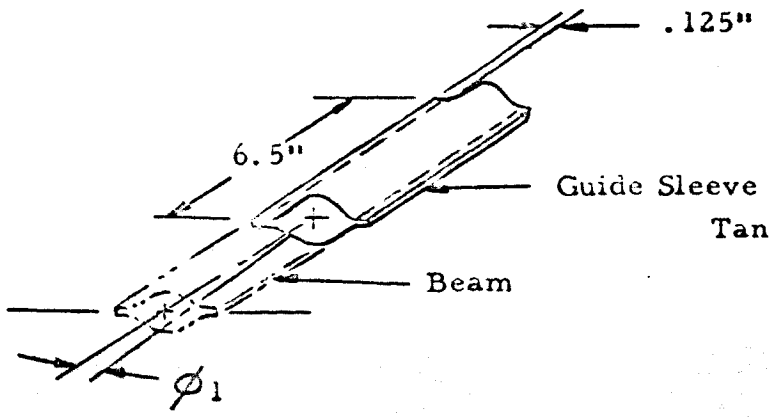

$$\text{Tan } \phi_1 = \frac{.125}{6.5} = .0192$$

$$\phi_1 = 1°6' = .0192 \text{ Radians}$$

Shear V_1 is reacted at the forward edge of the guide sleeve and transferred to the cross-tie by shear and bending in the shear transfer gussets. Lateral movement restraint of the guide sleeve support pins in both directions is considered equal at both ends of the pin and therefore both shear transfer gussets are loaded equally. The shear in each gusset is $V_{1/2}$ = 21.8 lbs. ult. Since there is no lateral plane component, no lateral angular rotation results.

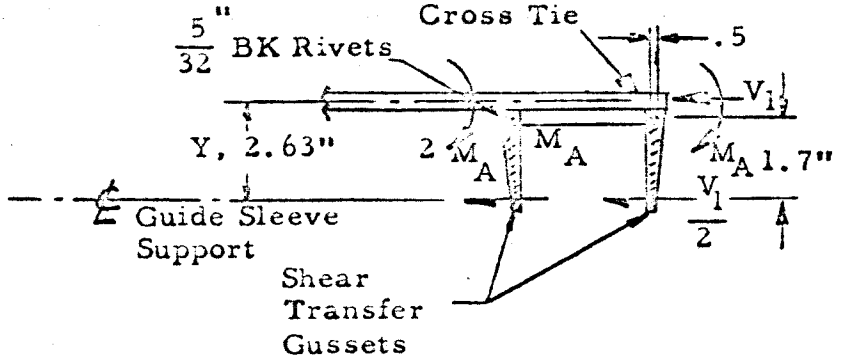

V_1 = 43.5 lbs. ult.

$2M_A = 2\left(\frac{V_1}{2}\right) = Y$

$2M_A = 2(21.8 \times 2.63)$

$= 114.4$ in-lbs. ult.

Moment M_1 is reacted as a couple between the guide sleeve support pins. If the transfer shear plate is elastically stable, then the degree of lateral angular rotation of the beam in transferring the moment M_1 to the cross-tie is a function of the cantilevered bending of the shear transfer gussets.

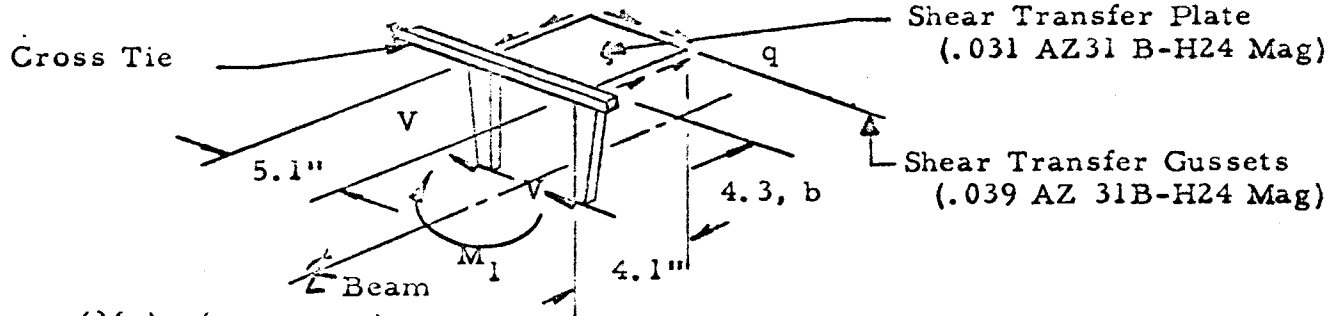

$$f_s = \left(\frac{M_1}{4.1}\right)\left(\frac{1}{5.1 \times .031}\right) = \left(\frac{571}{4.1}\right)\left(\frac{1}{5.1 \times .031}\right) = 881 \text{ psi ult}$$

$$q_{cr} = KE_c \left(\frac{t}{b}\right)^2 \cdot \frac{\pi^2}{12\left(1-\mu^2\right)}$$

K = 12.7 for clamped edges (Ref. 11)

$E_c = 6.5 \times 10^6$ psi (room temp) because of solar radiation shielding by guide sleeve.

$$q_{cr} = 12.7 \times 6.5 \times 10^6 \left(\frac{.031}{4.3}\right)^2 \cdot \frac{\pi^2}{12\left(1-.35^2\right)} = 4011 \text{ psi}$$

Therefore the shear transfer plate is elastically shear stable.

The cantilevered bending of the shear transfer gussets due to moment M_1 is calculated by resolving the shear transfer gusset into a straight section.

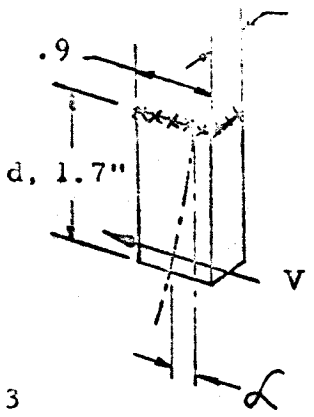

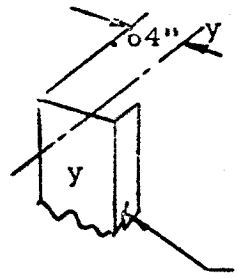

$I_{y-y} = .0053 \text{ in}^4$

.039 Sheet
AZ31 B-H24
Magnesium

$$\delta = \frac{Vd^3}{3EI_{y-y}}$$

$$V = \frac{1}{2} \cdot \left(\frac{M_1}{4.1}\right) = \frac{1}{2} \cdot \left(\frac{571}{4.1}\right) = 69.6 \text{ lbs. ult.}$$

$E = 6.3 \times 10^6$ psi (250°F) because of no solar radiation shielding

$$\delta = \frac{69.6\ (1.7)^3}{3 \times 6.3 \times 10^6 \times .0053} = \underline{.0034 \text{ in.}}$$

$$f_{b_c} = \frac{[M]\,(C)}{I_{y-y}} = \frac{\left[\left(V + \frac{V_1}{2}\right) \cdot 1.7\right] \cdot \left(\frac{2}{3} \quad .64\right)}{.0053} = \frac{\left[(69.6 + 21.8) \times 1.7\right]\ (.43)}{.0053}$$

$f_{b_c} = 12606$ psi ult.

$K = 1.2$ for clamped, free condition (Ref. 11)

$$F_{cr} = KE_c \left(\frac{t}{b}\right)^2$$

$$F_{cr} = 1.2 \times 6.3 \times 10^6 \left(\frac{.039}{.9}\right)^2 = 14194 \text{ psi}$$

$$\text{M.S.} = \frac{14194}{12606} - 1 = +\underline{.13}$$

Then the degree of lateral angular rotation in transferring moment M_1 to the cross-tie is calculated as,

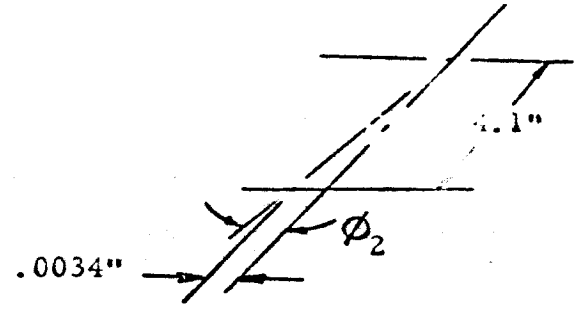

$$\text{Tan } \phi_2 = \frac{.0034}{4.1} = .000038$$

$\phi_2 < 0^\circ 1'$, Therefore neglect

Shear in rivets attaching shear transfer gussets,

$$= \left(\frac{V_1}{2} + V\right) \times 1.7 \left(\frac{1}{.5}\right) = (21.8 + 69.6) \times 1.7 \left(\frac{1}{.5}\right) = 311 \text{ lbs. ult.}$$

Rivet shear allowable = 432 lbs. (Reference 16)

$$\text{M.S.} = \frac{432}{311} - 1 = +\underline{.39}$$

Moment M_2 is reacted as a couple between the guide sleeve support pins. The couple is transferred into the outboard facing of the end cap as shear.

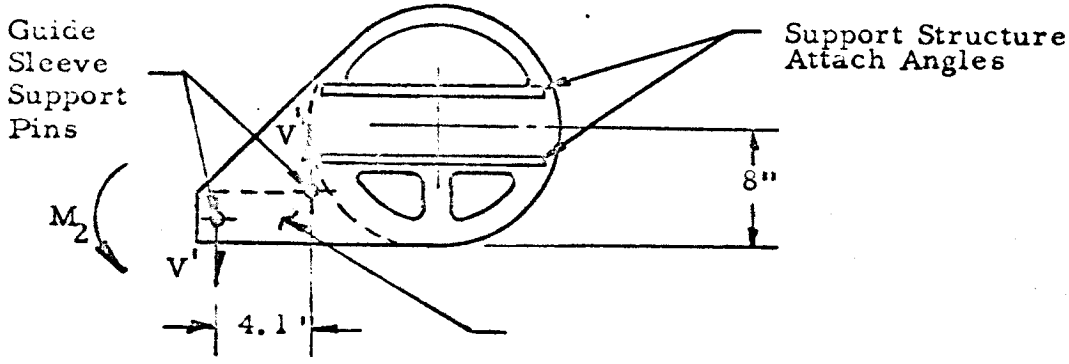

$$V' = \frac{M_2}{4.1} = \frac{371}{4.1} = 90.5 \text{ lbs. ult.}$$

Shear stress in the doubled area is based on a panel 4" x 4":

$$f_s = \left(\frac{V'}{4}\right) \left(\frac{1}{t}\right) = \left(\frac{90.5}{4}\right) \left(\frac{1}{.038}\right) = 595 \text{ psi ult.}$$

$$q_{cr} = KE_c \left(\frac{t}{b}\right)^2$$ K = 10 for simply supported edges (Reference 11)

$$q_{cr} = 10 \times 6.3 \times 10^6 \left(\frac{.038}{4}\right)^2 = 5686 \text{ psi.}$$

M.S. ⟶ HIGH

The elastically shear stable face sheet transfers the moment into the support structure as a couple in the face sheet. The lower couple load is carried in the face sheet truss A, B, C.

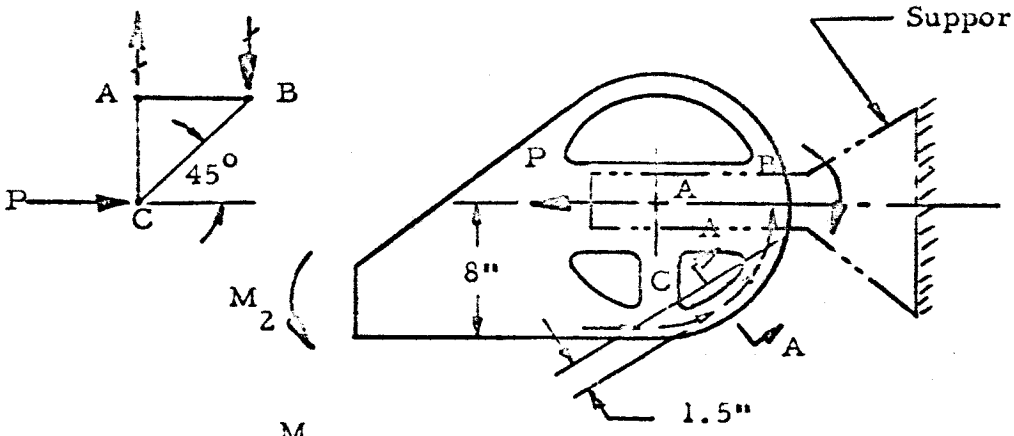

$$P = \frac{M_2}{8} = \frac{371}{8} = 46 \text{ lbs. ult.}$$

I_{x-x} 1.76×10^{-3} in.^{4}

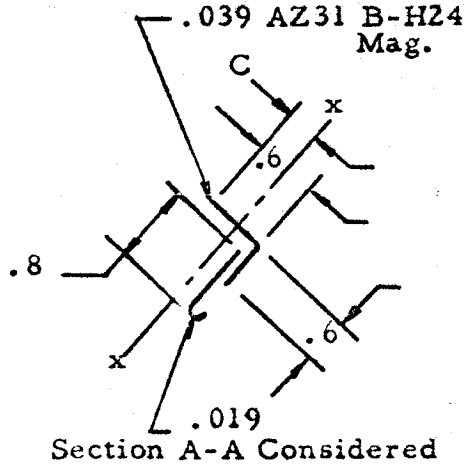

Section A-A Considered Effective

$$f_{b_c\text{(Section A-A)}} = \frac{1.414\,P}{\text{Area}} + \frac{(8P)(C)}{I_{x-x}}$$

$$f_{b_c\text{(Section A-A)}} = \frac{1.414 \times 46}{.062} + \frac{(1.5 \times 46)(.467)}{1.76 \times 10^{-3}} = 1049 + 18309 = 19358 \text{ psi ult}$$

$= 15486$ psi yield

$F_{cy} = 19200$ psi. for AZ31B-H24 Magnesium at 250°F (Reference 3)

$$\text{M.S.} = \frac{192000}{15486} - 1 = +.24$$

The degree of lateral angular beam rotation is calculated as,

$$\phi = \phi_{(total)} - \phi_1 = .12 - .0192 = \underline{.10} \text{ Radians}$$

The lateral beam rotation is expressed as a function of cross-tie deflection between end caps as,

$$\phi = \left[f_{\left(\begin{matrix}\text{vertical}\\ \text{plane}\\ \text{loads}\end{matrix}\right)} + f_{\left(\begin{matrix}\text{lateral}\\ \text{plane}\\ \text{loads}\end{matrix}\right)} \right]$$

$$\phi = \frac{\ell}{2E} \left[\frac{\left(M^{1} \times \frac{2.63}{4.1} \right)}{I_{x-x}} + \left(\frac{M_1}{I_{y-y}} \right) \right]$$

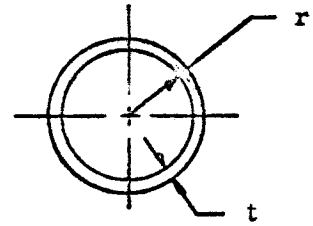

Cross-Tie
Cross-Section

For the tube section shown and t = .040 2024-T3 Al Tubing

$$\phi = \frac{33.5}{2 \times 10.2 \times 10^{6}} \left[\left(\frac{366 \times \frac{2.63}{4.1}}{.0139} \right) + \left(\frac{571}{.0139} \right) \right] = \underline{.095} \text{ Radians}$$

The loads for strength analysis are summarized as,

Lateral Plane:

$V_1 = 43.5$ lbs. ult.

$M_1 = 571$ in-lbs. ult.

$M''' = V_1 \cdot f_{(M_1)}$

Vertical Plane:

$^{2}M_A = 114.4$ in-lbs. ult.

$V_1 = 43.5$ lbs. ult.

$M' = 2V \times 2.63 = 2 \times 69.6 \times 2.63 = 366$ in-lbs. ult.

$M'' = V_1 \times f_{(2 M_A + M')}$

$$f_{b_{\left(\text{lateral plane}\right)}} = \frac{M_1 r}{I_{Y-Y}} + \frac{V_1}{\text{Area}} + V_1 \left[\frac{M_1^{\,2}}{8EI_{Y-Y}}\right]\left(\frac{r}{I_{Y-Y}}\right)$$

$$= \frac{571 \times .48}{.0139} + \frac{43.5}{.1206} + 43.5 \left[\frac{571 \times 33.5^2}{8 \times 9.5 \times 10^6 \times .0139}\right] \times \left(\frac{.48}{.0139}\right)$$

$$f_{b_{\left(\text{lateral plane}\right)}} = 19716 + 361 + 911 = 20990 \text{ psi ult.}$$

$$f_{b_{\left(\text{vertical plane}\right)}} = \frac{2\ M_A \cdot r}{I_{x-x}} + \frac{V_1}{\text{Area}} + \frac{M' \cdot r}{I_{x-x}} + V_1 \left[\frac{(M'+2M_A)^{\,2}}{8EI_{x-x}}\right]\left(\frac{r}{I_{x-x}}\right)$$

$$= \frac{114.4 \times .48}{.0139} + 361 + \frac{366 \times .48}{.0139} + 43.5 \left[\frac{(366\ \ 114.4)33.5^2}{8 \times 9.5 \times 10^6 \times .0139}\right]\left(\frac{.48}{.0139}\right)$$

$$f_{b_{\left(\text{vertical plane}\right)}} = 3951 + 361 + 12639 + 767 = 17718 \text{ psi ult.}$$

The resultant stress, $f_b = \left[(17718)^2 + (20990)^2\right]^{1/2} = \underline{27460}$ psi. ult.
or 21968 psi yield.

$F_{cr} > F_{t_y} = 38220$ psi (Reference 3) at 250°F

$$\text{M.S.} = \frac{38220}{21968} - - 1 = \underline{+.74}$$

5.14 Compression of Beam on Wrap Drum

The critical condition occurs locally on the wrap drum in the area at which the beam is transformed from a full cross-section to the wrapped, flattened shape. Since the beam is flattened at the inboard end prior to assembly to the wrap drum, the local radial forces exerted on the wrap drum have been lessened. The critical condition occurs during retraction prior to retro-rocket firing. Beam and wrap drum temperatures are considered at 150°F. The torque which induces the radial force is calculated, using analysis given in Section 11.1, assuming beam sheet thickness is .0065 in.

$$M_{(beam)} = Torque_{(retract)} - Torque_{(System\ Friction)}$$

$$= \frac{142}{2} - 50.5 = \underline{20.5}\ \text{in.-lbs. limit or yield}$$

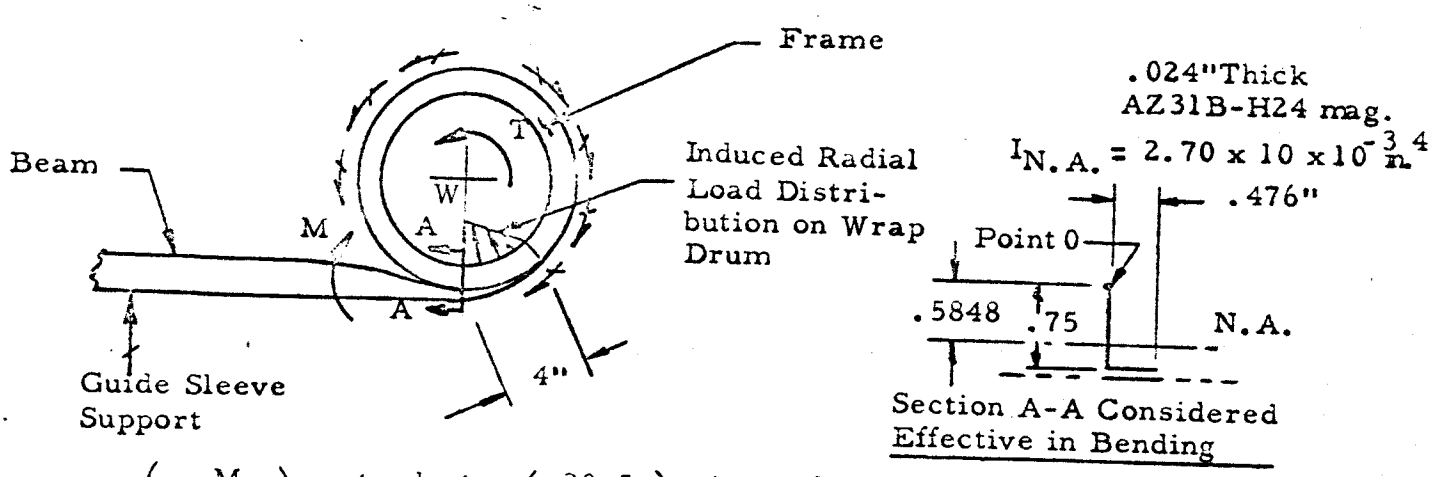

$$W = \left(\frac{M}{.67 \times 4}\right)\left(\frac{1}{.5 \times 4}\right) = \left(\frac{20.5}{.67 \times 4}\right)\left(\frac{1}{.5 \times 4}\right) = 3.8\ \text{lbs/in. yield}$$

$$\sum \text{Radial load} = 3.8\ (.5 \times 4) = 7.6\ \text{lbs yield}$$

It can be shown by integration that a concentrated radial force equal to the integrated load distribution may be applied at the point of peak radial load distribution, resulting in an equivalent maximum radial bending moment in the wrap drum.

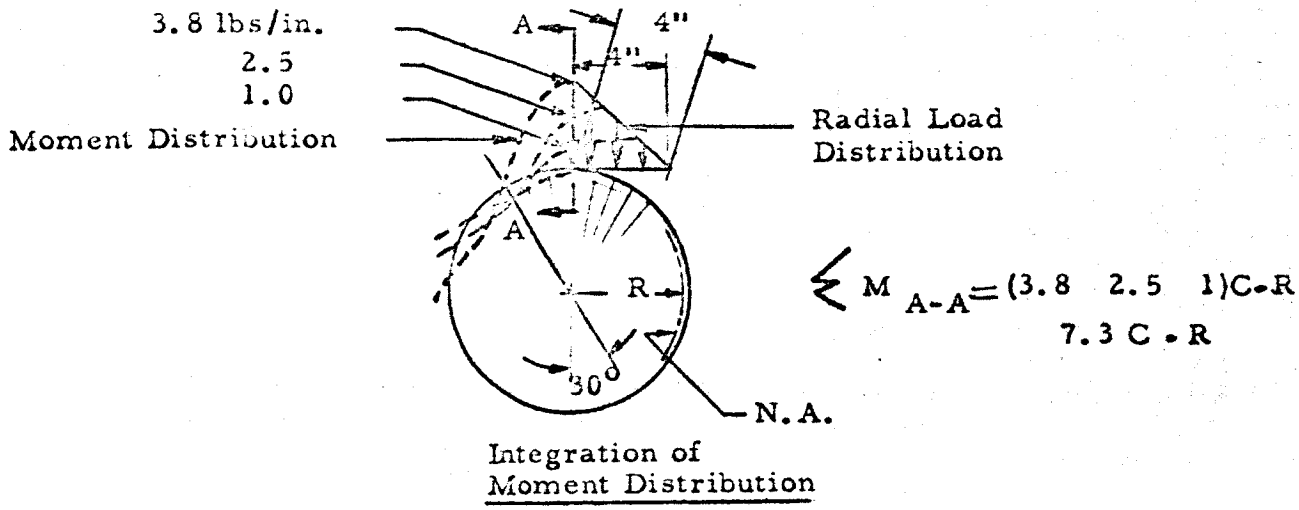

Integration of
Moment Distribution

Using page .03.06.08 of Reference 15, the radial moment in Section **A-A** is calculated conservatively assuming the frame as a rigid ring,

$$M_{A-A} = 7.3\ C \cdot R = 7.3 \times .24 \times 5.81 = 10.2 \text{ in.-lbs yield}$$

$$f_{b_t}\ (\text{point 0 of Section A-A}) = \frac{M \times .5848}{2.7 \times 10^{-3}} = \frac{10.2 \times .5848}{2.7 \times 10^{-3}} = 2209 \text{ psi yield}$$

$F_{t_y} = 24940$ psi. (Reference 3)

M.S. $\longrightarrow$ HIGH

5.15 Bending in Lower Plate of End Cap

The beam radial restraint rollers transfer a normal load to the lower plate which cannot be reacted as hoop tension in this area due to the flatness of the sheet. Temperature is considered equal to beam temperature (250°F).

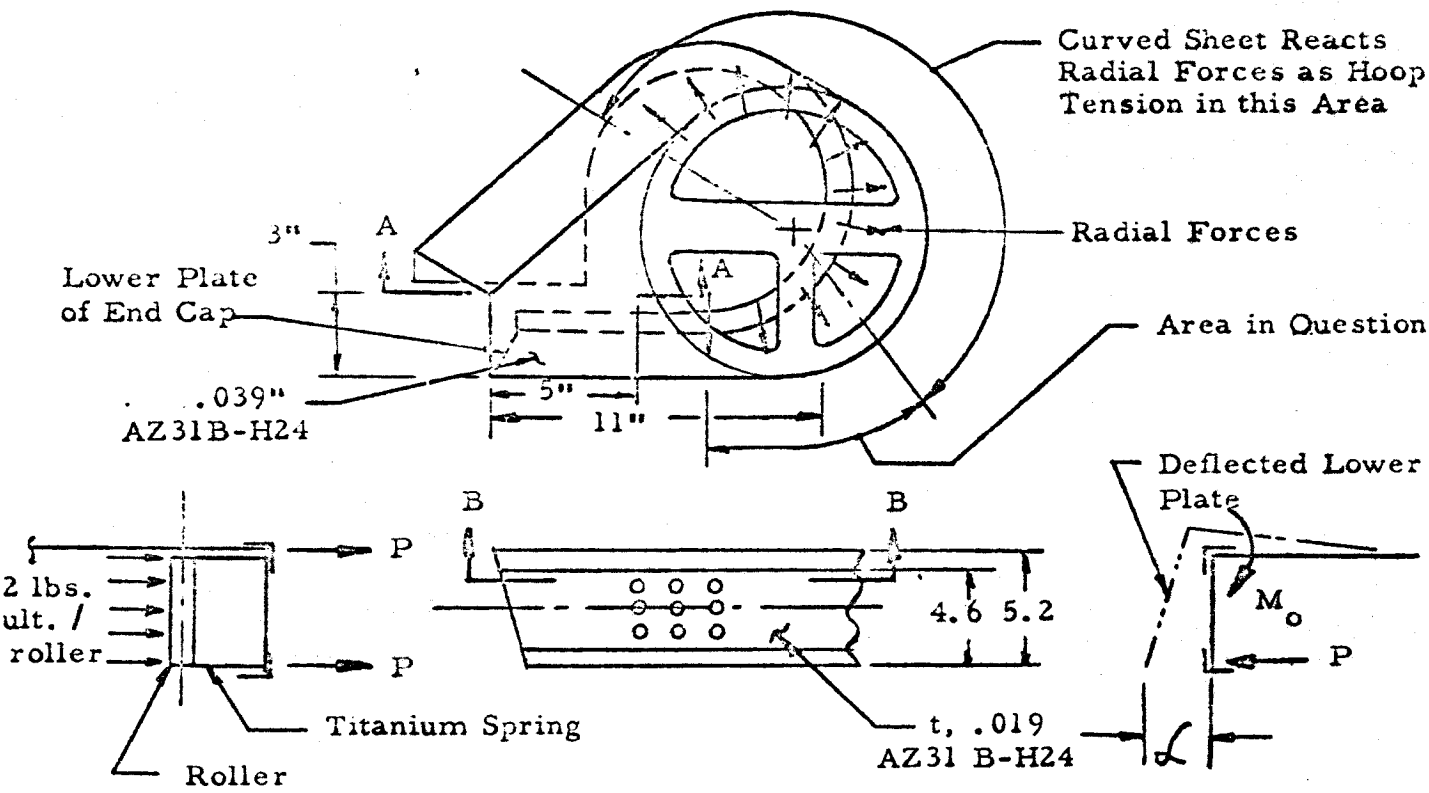

The bending deflection, δ, of the lower plate is a function of bending stiffness at Sections A-A and B-B.

$$\delta = \left(\frac{f_{b\ (B-B)}}{E}\right)\left(\frac{4.6}{t_{1/2}}\right) + \frac{(M_o)(3)^2}{2EI_{A-A}} \cdot \left(\frac{5.2}{3}\right)$$

$$f_{b(B-B)} = \frac{(P \times \text{No. of rollers forces} \times 4.6) \times \left(\frac{t}{2}\right)}{I_{B-B}}$$

$$f_{b(B-B)} = \frac{(1 \times 4 \times 4.6)\left(\frac{.019}{2}\right)}{6.27 \times 10^{-6}} = 27870 \text{ psi ult.}$$

$$f_{v(B-B)_y} = \frac{27870}{1.25 \times 1.5} = 14864 \text{ psi yield effective}$$

$$\text{M.S.} = \frac{F_{cy}}{f_{b(B-B)_y}} - 1 = \frac{19440}{14864} - 1 = +.31$$

$$\delta = \left(\frac{27870}{6.3 \times 10^6}\right)\left(\frac{4.6}{.0095}\right) + \frac{(P \times \text{no. of rollers} \times 5.2)}{2 \times 6.3 \times 10^6 \times 2.47 \times 10^{-5}} \cdot \left(\frac{5.2}{3}\right)$$

$$\delta = 2.1 + \frac{(1 \times 4 \times 5.2)}{2 \times 6.3 \times 10^6 \times 2.47 \times 10^{-5}} \left(\frac{5.2}{3}\right) = 2.1 + .35 = \underline{2.45} \text{ in.}$$

The above deflection is hypothetical because the spring rate of the titanium spring is not constant, thereby relieving the radial force as the lower plate deflects. However, the result is to transfer the radial force to the outboard edge of the roller.

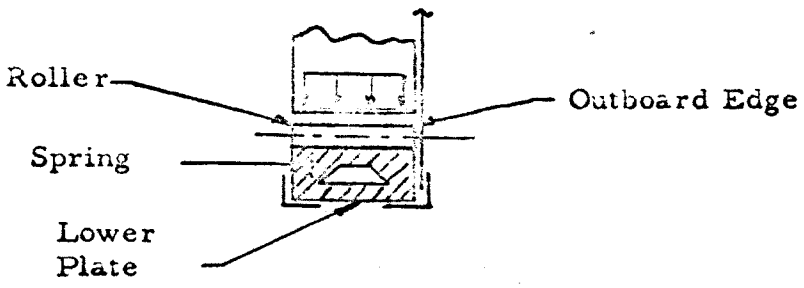

Radial Force Distribution
with No Lower Plate Deflection

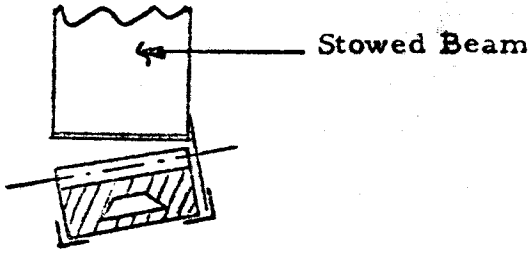

Radial Force Distribution
with Lower Plate Deflection

Since the stowed beam is restrained against rotation by the guide sleeve and at the attachment to wrap drum, it does not appear that the beam would rotate. The radial force would be transmitted by a smaller cross-section of the spring and therefore result in less stowed beam radial force restraint. It is suggested that the problem be eliminated with a corner bracket as shown.

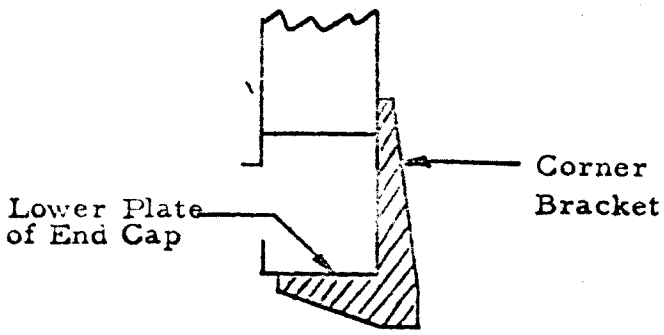

5.16 Vertical Plane Beam Bending

This analysis is conducted to determine the amount of beam tip deflection during cruise maneuver between Earth and Mars. The extended array is subjected to a .2g steady-state acceleration normal-to-substrate. Beam temperature is considered at 250°F. Analysis is slightly conservative by neglecting moment arm shortening effects (ΔL) as the beam deflects. Thermal deflection is not considered in this analysis which will reduce the calculated load deflection.

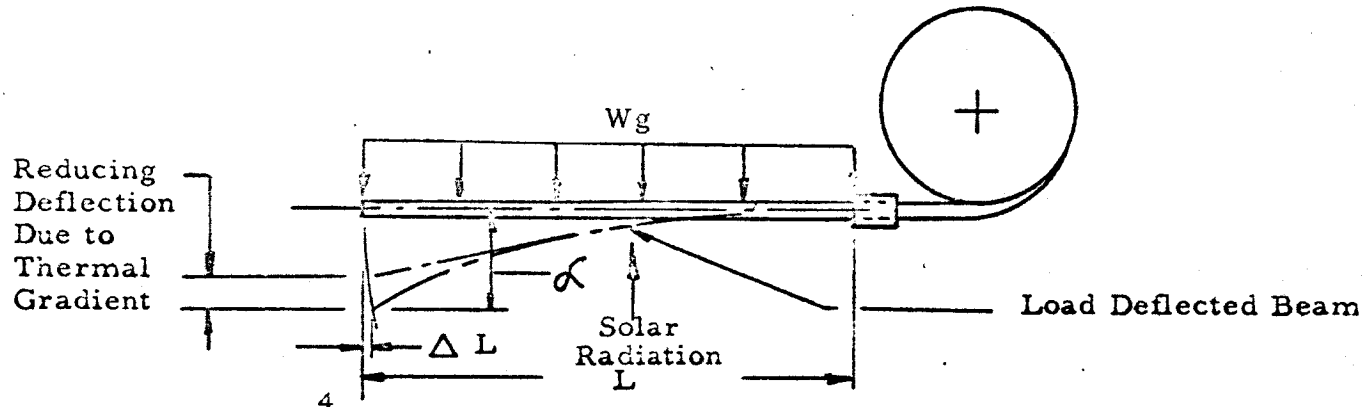

$$\delta = \frac{(Wg)(L)^4}{8EI}$$ (Reference 2, page 100, case 3)

$$\delta = \frac{(.058 \times .2)\,(223)^4}{8 \times 14.5 \times 10^6 \times .01459} = \underline{17} \text{ in.}$$

5.17 Thermal Stress at Substrate Edge Attachment

For the adhesive bonded edge, the maximum temperature gradient will occur in Earth vicinity when the predicted substrate temperature $T_F = 129^\circ F$ and the titanium edge $T_T = 210^\circ F$ (See Section 7.0).

The relative displacement induced by the thermal difference is,

$$\Delta \ell = \alpha_T (T_T - 75) - \alpha_F (T_F - 75)$$

when α_F = coefficient of thermal expansion of fiberglass

$\alpha_F = 6.7 \times 10^{-6} / ^\circ F$

α_T = coefficient of thermal expansion of titanium

$\alpha_T = 5.2 \times 10^{-6} / ^\circ F$

$$\Delta \ell = 135 \times 5.2 \times 10^{-6} - 54 \times 6.7 \times 10^{-6}$$

$$= (702 - 362) \times 10^{-6}$$

$$= 0.340 \times 10^{-3} \text{ in/in.}$$

The thermal shear stress in the joint is

$$f_s = G_a \times \text{Strain}$$

$$= \text{where } G_a = \text{Shear modulus of adhesive} = 0.5 \times 10^6 \text{ psi}$$

$$f_s = 0.5 \times 10^6 \times 0.34 \times 10^{-3} = 170 \text{ psi}$$

The allowable shear strength for the adhesive is 2000 psi at $200^\circ F$.

$$\text{M. S.} = \frac{2000}{170} - 1 \longrightarrow \underline{\text{HIGH}}$$

For the aluminum connector edge attachment, maximum thermal gradients are predicted in Earth vicinity where substrate temperature $T_F = 129^\circ F$, aluminum connector $T_A = 140^\circ F$, and the titanium edge $T_T = 210^\circ F$ (See Section 7.0).

The relative displacement in the fiberglass to aluminum joint is

$$\Delta \ell_{F-A} = \alpha_A \ (T_A - 75) - \alpha_F \ (T_F - 75)$$

where α_A = coefficient of linear thermal expansion of aluminum

$$\alpha_A = 12.5 \times 10^{-6} / ^\circ F$$

$$\Delta \ell_{F-A} = 65 \times 12.5 \times 10^{-6} - 54 \times 6.7 \times 10^{-6}$$

$$= (812 - 362) \times 10^{-6}$$

$$\Delta \ell_{F-A} = 0.45 \times 10^{-3} \text{ in/in.}$$

The shear stress developed in the joint is

$$f_s = G_F \times \text{Strain} \quad (G_F = 0.6 \times 10^6)$$

$$= 0.6 \times 10^6 \times .45 \times 10^{-3}$$

$$f_s = 270 \text{ psi}$$

Assuming no clearance between the edge of the connector and the fiberglass slot,

$$f_{br} = f_s \cdot \frac{0.6\, t_F}{A}$$

$$= 270 \left(\frac{.6 \times .012}{.005 \times .012} \right)$$

$$f_{br} = 32,400 \text{ psi}$$

Based on the edge attachment tests of Section 11.3, the bearing strength of the substrate at 200°F is F_{br} = 28,000 psi. Therefore, the substrate will shear at the edge of the connector until the thermal stress is relieved. After the slot length has adjusted to the bearing loads, the edge attachment will continue to carry load and have the same strength as reported in Section 11.3.

The relative displacement in the aluminum to titanium joint is

$$\Delta \ell_{A-T} = \mathcal{L}_A (T_A - 75) - \mathcal{L}_T (T_T - 75)$$

$$= 65 \times 12.5 \times 10^{-6} - 135 \times 5.2 \times 10^{-6}$$

$$= (812 - 703) \times 10^{-6}$$

$$\Delta \ell_{A-T} = .109 \times 10^{-3}$$

The shear strength developed is,

$$f_s = G_A \times \text{Strain}$$

$$G_A = 4.0 \times 10^6$$

$$f_s = 4.0 \times 10^6 \times .109 \times 10^{-3}$$

$$= 436 \text{ psi}$$

$$f_{br} = 436 \text{ psi}$$

$$f_{br} = 436 \left(\frac{0.6 \times .006}{.005 \times .006}\right)$$

$$= 52,300 \text{ psi}$$

For F_{br} = 25,000 psi, the aluminum connector will deflect at the edge until the thermal stresses are relieved, then continue to carry load as reported in Section 11.3.

The design provides a clearance of .005 at each slot, which is sufficient to allow for the relative elongation predicted. The analysis above is conservative in assuming that no clearance exists, which may occur at random locations in the assembly.

6.0 STRUCTURAL DYNAMICS

6.1 Substrate -- Stowed Position

Summary

The following analysis is for a radial "Breathing Mode" with substrate spacer strips at 4 in. apart. The response of the stowed array to specification inputs was calculated for the fundamental mode in a non-linear Rayleigh analysis. The array was treated as a multi-layer cylindrical membrane, the outer layer being critical. Membrane support flexibility (the separating strips) was considered. The calculated fundamental frequency is 285 cps, the maximum deflection is 0.009 in., the maximum slope between support strips is 0.4° and the maximum curvature between support strips is 0.3°/inch. It is noted that the calculated maximum curvature is well within the allowable maximum value per specification, 1.0°/inch.

Introduction

In a Rayleigh analysis, the fundamental natural frequency which meets the boundary conditions is calculated by assuming a fundamental mode shape and computing the maximum potential and kinetic energies of the system based on the assumed mode shape. The maximum potential energy is equaled to the maximum kinetic energy, which contains this unknown frequency term (this equality is equivalent to specifying conservation of mechanical energy) and the equation of $KE_{max} = PE_{max}$ is solved for this frequency. One of the main features of the method is its relative insensitivity to modal inaccuracy; Δt is also fairly easy to apply.

However, in a membrane that is statically unstressed, the edge tension forces, the restoring forces, are not proportional to the out-of-plane deflection of the membrane. It is a characteristic of the general non-linear system that frequency is displacement dependent and such was the case found herein. The displacement was worked out from the specification input (which itself is stepwise frequency dependent), and from a value of transmissibility based on an assumed value of 0.04 for the damping coefficient of the fiberglass stowed array.

The maximum displacement, slope and curvature calculated herein must be considered as roughly approximate since they are based on the assumed fundamental mode only. Higher modes, as well as an accurate fundamental mode, are required for good response information. Such exacting work, especially considering the non-linear nature of this problem, is beyond the scope of the present treatment.

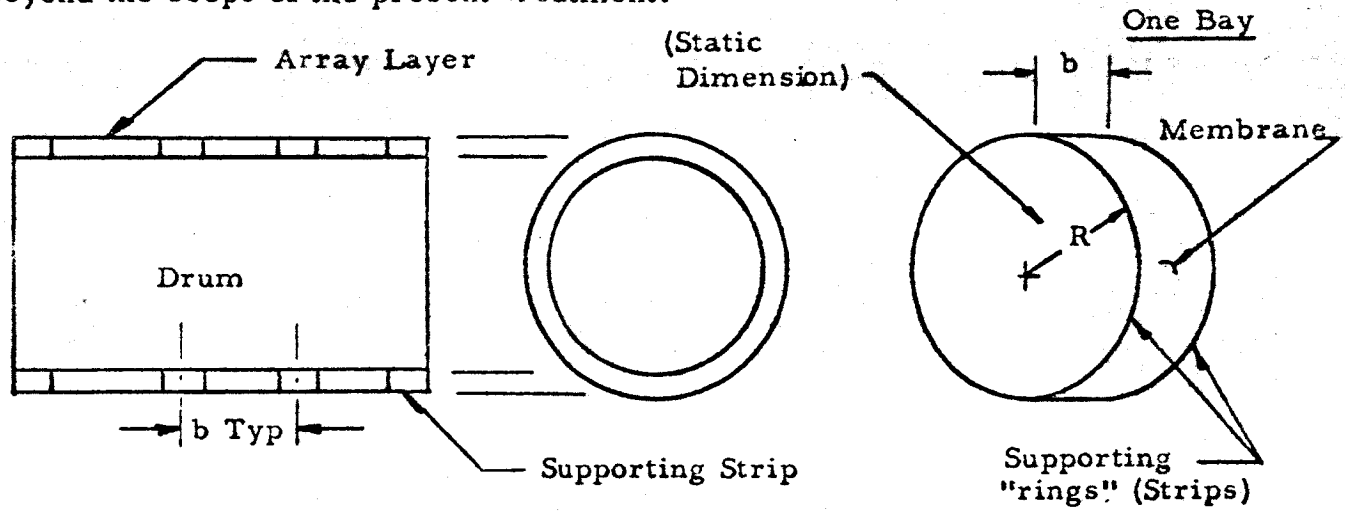

The wrapped array is viewed as a multi-layered membrane, capable of developing tensile loads only. The outer layer is critical since it has the minimum static curvature. A typical bay is treated; a bay being between adjacent supporting strips. Simple supports at the center of the supporting strips are assumed (thus the supports are considered as rings), and the rings are initially assumed rigid. Later we consider their radial flexibility.

Assumed Fundamental Mode Shape,

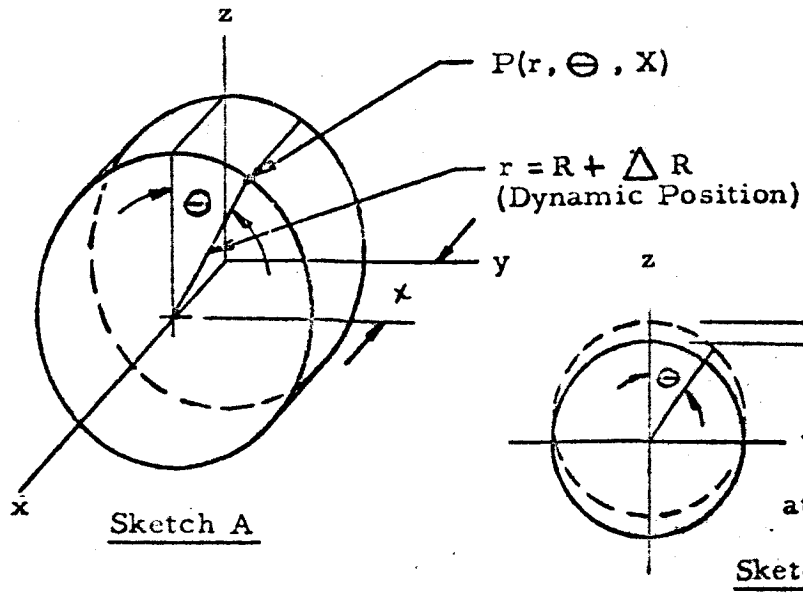

Sketch A

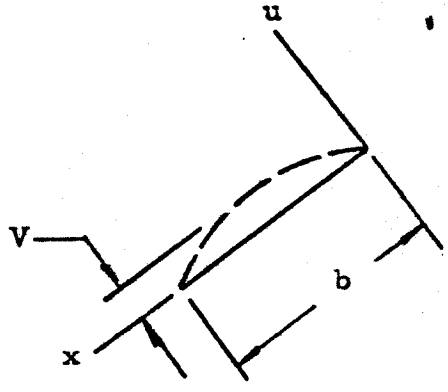

Sketch B

Sketch C

We used, for simplicity, cylindrical coordinates to describe the position of a point on the membrane surface, i.e. $P = P(r, \Theta, x)$. See Sketch A. Now $r = R + \Delta R$ where R is the static radius of the membrane and ΔR is the change in R during motion. It is this ΔR in which we are primarily interested and we give its amplitude, i.e. (ΔR_{max}), the symbol u, for brevity.

Referring to Sketch B, the fundamental mode shape in the x direction is assumed to be,

$$u = \gamma \sin \frac{\pi x}{b}$$

Note that $u = 0$ at $x = 0$ and b (the support rings are initially assumed rigid) and $u = \gamma$ at $x = \frac{b}{2}$

Referring to Sketch C, the fundamental mode shape in the Θ direction (around the central circumference of the membrane, i.e. at $x = \frac{b}{2}$) is assumed to be

$$v = u_o \cos \Theta$$

Note that $\gamma = u_o$ at $\Theta = 0$, $\gamma = 0$ at $\Theta = \frac{\pi}{2}$ and at $\Theta = \frac{3\pi}{2}$

and $\gamma = -u_o$ at $\Theta = \pi$, which seem reasonable. u_o may be regarded as the maximum dynamic radial deformation.

The complete assumed mode shape is thus,

$$u = u_o \cos \Theta \sin \frac{\pi x}{b}$$

Kinetic Energy

An element of mass d_m has kinetic energy $dKE = \frac{1}{2} \dot{r}^2 d_m$ where $r = R + \Delta R$, ΔR is assumed harmonic with time and is of amplitude u, i.e. $r = R + ue^{i\omega t}$, where ω is the circular frequency of the motion

(rad/sec). Thus $\dot{r} = ui\omega e^{i\omega t} = i\omega\Delta R$ or $|\dot{r}| = \dot{r}_{max} = \omega\gamma$.

Thus the differential of KE_{max} (we are going to call KE_{max} just KE from this point on) is $dKE = \frac{1}{2}\omega^2 u^2 d_m$.

We have $d_m = r\,Rd\,\Theta.\ dx$ where r = mass/in^2 of membrane surface area (units lb-sec^2-in^{-3}), R d Θ = width of the membrane element in the Θ direction (actually the width is $rd\Theta = (R+u)\,d\Theta \cong Rd\Theta$ for $u < R$, which is assumed, and dx = width of the membrane element in x direction. Thus,

$$dKE = \frac{1}{2}\ \omega^2\ u^2\ rRd\,\Theta\,dx$$

or upon substitution of $u = u_o \cos\Theta \sin\frac{\pi x}{b}$,

$$dKE = \frac{1}{2}\ \omega^2\ rRu_o^2 \cos^2\Theta \sin^2\frac{\pi x}{b}\ d\Theta \cdot dx$$

let $K = \frac{1}{2}\omega^2\ \rho Ru_o^2$ for brevity. Then

$$KE = K \int_0^b \int_0^{2\pi} \cos^2 \sin^2 \frac{\pi x}{b}\ d\,\Theta\,dx$$

Integration gives $KE = \frac{K\pi b}{2}$

So $KE = \frac{\pi}{4}\ \omega^2\ \rho Rbu_o^2$

Potential Energy

The potential energy of a membrane, in xy coordinates (Reference 18, page 431), is,

$$PE = \frac{S}{2} \int\int \left[\left(\frac{dx}{dx}\right)^2 + \left(\frac{dx}{dy}\right)^2 \right] \quad dx \cdot dy$$

where r is displacement of any point of the membrane normal to this xy plane during vibration, and S is the uniform tension per unit length of the boundary (S is assumed large enough so that it remains constant during deformation).

In the present case, we have a few changes:

1. Instead of dy, we have $Rd\Theta$
2. Instead of r, we have u
3. Instead of S being uniform, we have S varying with x, and also S is not constant, but raises from zero (where $\dot{r}$ is maximum) to some maximum value (where $\dot{r}$ is zero). We take S at its maximum value since PE_{max} (which we call just PE) is of primary interest. Also we have a tangetial tension S_Θ per unit length, and a lateral tension S_x per unit length. They are related by $S_x = \mu S_\Theta$ where μ = Poisson's ratio. Both S_x and S_Θ are functions of x, but are constant with Θ.

Putting S_x and S_Θ under the integral sign, making the indicated changes of variables and intorducting the limits of integration in the Timoshenko equation,

$$PE = \frac{\mu}{2} \int_0^{2\pi} \int_0^b S_\Theta (x) \left(\frac{du}{dx}\right)^2 \cdot dx \cdot Rd\Theta + \frac{1}{2}$$

$$\int_0^{2\pi} \int_0^b S_\Theta (x) \left(\frac{1}{R} \frac{du}{d}\right)^2 dxRd\Theta$$

or, upon rearranging,

$$PE = \frac{\mu R}{2} \int_0^{2\pi} \int_0^b S_\theta(x) \left(\frac{du}{dx}\right)^2 \cdot dx d\theta + \frac{1}{2R} \int_0^{2\pi} \int_0^b S_\theta(x) \left(\frac{du}{dx}\right)^2 dx d\theta$$

In order to evaluate these integrals, we need to determine $S_\theta(x)$. This work follows. The arc length (circumference) of a ring-like element of width dx in a deflected position is

$$\ell = \int_0^2 \sqrt{r^2 + \left(\frac{dr}{d}\right)^2} \cdot d\theta$$

(Reference 19, page 53).

We have, as discussed previously,

$r = R + u$

or $r^2 = R^2 + 2Ru + u^2 \cong R^2 + 2Ru$ for $u < R$

and $\frac{dr}{d\theta} = R + \frac{du}{d\theta}$

or $\left(\frac{dr}{d\theta}\right)^2 = R^2 + 2R\left(\frac{du}{d\theta}\right) + \left(\frac{du}{d\theta}\right)^2 \cong R^2 + 2R\left(\frac{du}{d\theta}\right)$ for small $\left(\frac{du}{d\theta}\right)$

so $\ell = \int_0^{2\pi} \sqrt{2R^2 + 2Ru + 2R\frac{du}{d\theta}} \cdot d\theta$

$$= \sqrt{2} \int_0^{2\pi} \sqrt{1 + \frac{u}{R} + \frac{1}{R} \cdot \frac{du}{d\theta}} \cdot Rd$$

for small u and $\frac{du}{d\theta}$

$$\ell = \sqrt{2} \int_0^{2\pi} \left[1 + \frac{1}{2}\left(\frac{u}{R}\right)^2 + \frac{1}{2}\left(\frac{1}{R}\frac{du}{d\theta}\right)^2\right] \cdot Rd\theta$$

The change in arc length $\Delta \ell = \ell - \int_0^{2\pi} R\,d\theta$ is

$$\Delta \ell = \sqrt{\frac{2}{2R}} \int_0^{2\pi} \left[u^2 + \left(\frac{du}{d\theta}\right)^2 \right] d\theta$$

The strain $\epsilon = \frac{\Delta \ell}{2\pi R}$ and the stress $\sigma = \frac{S_\theta}{t}$ were t = thickness of membrane. Also $\frac{\sigma}{\epsilon} = E$ where E = modulus of elasticity of the membrane material.

Thus $\frac{S_\theta}{t} \cdot \frac{2\pi R}{\Delta \ell} = E$ or $S_\theta = \frac{t \cdot E}{2\pi R} \cdot \Delta \ell$

and $S_\theta (x) = \sqrt{\frac{2}{4\pi R^2}}\, t\, E \int_0^{2\pi} \left[u^2 + \left(\frac{du}{d\theta}\right)^2 \right] d\theta$

For the particular case, letting $\sqrt{\frac{2\, t\, E}{4\pi R^2}} = \sigma$, for brevity

$$S_\theta (x) = \sigma \int_0^{2\pi} \left(u_o^2 \cos^2\theta \sin^2 \frac{\pi x}{b} + u_o^2 \sin^2\theta \sin^2 \frac{\pi x}{b} \right) d\theta$$

$$= \sigma\, u_o^2 \sin^2 \frac{\pi x}{b} \int_0^{2\pi} \overbrace{(\cos^2\theta + \sin^2\theta)}^{1}\, d\theta$$

$$= 2\pi\sigma\, u_o^2 \sin^2 \frac{\pi x}{b}$$

$$= \sqrt{\frac{2}{2}}\, \frac{tE}{R^2}\, u_o^2 \sin^2 \frac{\pi x}{b}$$

letting $\beta = \sqrt{\frac{2}{2}} \cdot \frac{tE}{R^2}$

$$S_\theta (x) = \beta \cdot u_o^2 \sin^2 \pi\, x/b$$

substitution in the PE equation gives

$$PE = \frac{\mu R}{2} \int_0^{2\pi} \int_0^b \beta\, u_o^2 \sin^2 \frac{\pi x}{b} \left(\frac{dy}{dx}\right)^2 dx d\theta$$

$$+ \frac{1}{2R} \int_0^{2\pi} \int_0^b \beta\, u_o^2 \sin^2 \frac{\pi x}{b} \left(\frac{dy}{d\theta}\right)^2 dx d\theta$$

$$= \frac{\mu R}{2} \beta\, u_o^2 \int_0^{2\pi} \int_0^b \sin^2 \frac{\pi x}{b} \left(\frac{\pi}{b} u_o \cos\theta \cos \frac{\pi x}{b}\right)^2 dx d\theta$$

$$+ \frac{1}{2R} \beta\, u_o^2 \int_0^{2\pi} \int_0^b \sin^2 \frac{\pi x}{b} \left(- u_o \sin\theta \sin \frac{\pi x}{b}\right)^2 dx d\theta$$

$$= \frac{\mu R}{2} \cdot \frac{\pi^2}{b^2} \beta\, u_o^4 \int_0^{2\pi} \int_0^b \cos^2\theta \left(\sin^2 \frac{\pi x}{b} \cos^2 \frac{\pi x}{b} dx\right) d\theta$$

$$+ \frac{1}{2R} \beta\, u_o^4 \int_0^{2\pi} \int_0^b \sin^2\theta \left(\sin^4 \frac{\pi x}{b} dx\right) d\theta$$

$$PE = \frac{\pi}{16} \beta\, u_o^4 R \left[3 \left(\frac{b}{R}\right)^2 + \mu \pi^2\right]$$

Substitutions $\beta = \sqrt{\frac{2}{2}} \frac{tE}{R^2}$

$$PE = \sqrt{\frac{2}{2}} \cdot \frac{\pi}{16} \frac{tEu_o^4}{bR} \left[3 \left(\frac{b}{R}\right)^2 + \mu \pi^2\right]$$

Frequency Equation

Equating KE to PE,

$$\frac{\pi}{4} \omega^2 \gamma R b u_o^2 = \sqrt{\frac{2}{2}} \frac{\pi}{g} \frac{tEu_o^4}{bR} \left[3 \left(\frac{b}{R}\right)^2 + \pi^2 \mu\right]$$

$$\text{or } \omega^2 = \frac{u_o^2}{b^2 R^2} \quad \sqrt{\frac{2}{\gamma}} \quad \frac{tE}{\gamma} \quad \left[3 \left(\frac{b}{R}\right)^2 + \pi^2 \mu \right]$$

Note that ω is proportional to u_o, a characteristic of the non-linear nature of the tensile forces S_θ vs. u_o.

We next make a correction for ω^2 associated with the deflection of the supporting strips. We reason as follows:

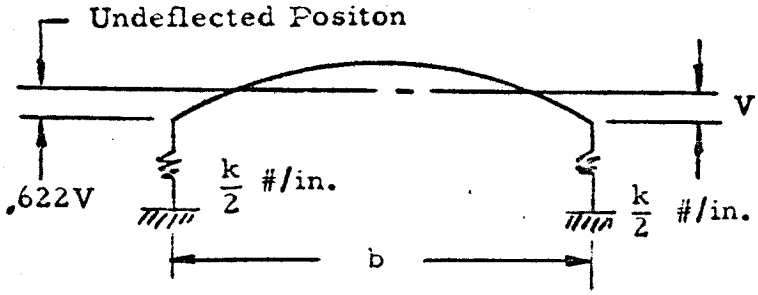

For a strip of width $Rd\theta$ and length b with center deflection $u = \underbrace{u_o \cos\theta}_{\gamma} \sin \frac{\pi x}{b}$, we assume a free-free configuration for the moment, so that, for an extremely low value of K (soft support strips), the spring deflection would be approximated by $u_{\text{spring}} = 0.622\gamma$ and the change in potential energy is

$$\Delta PE = \frac{1}{2} K u_{\text{springs}}^2 = \frac{1}{2} K (.622\, u_o \cos\theta)^2 = .1934\, K u_o^2 \cos^2\theta$$

This Δ PE is for a strip of width $Rd\theta$. for the entire supporting ring.

$$\Delta PE = .1934\, K u_o^2 \int_0^2 \cos^2\theta \, d\theta$$

$$\Delta PE = .1934\, \pi K u_o^2 \quad \text{(for small K)}$$

For large K (hard supporting strips), the spring deflection is zero and the Δ PE is zero. We bracket our results between the two extremes of $\Delta PE \cdot \Delta KE$ is assumed zero.

The change in ω^2 is given by equating ΔPE to KE:

$$\frac{\pi}{4} \Delta(\omega)^2 \gamma R b u_o^2 = .1934\, \pi K u_o^2$$

or $\Delta(\omega)^2 = .7736 \frac{K}{\gamma Rb}$ for small K

$= 0$ for large K

Spring Constant K

Two load-deflection points are available for the support strips:

1) 0.7 psi pressure causes a $\frac{1}{32}$" deflection

2) 2.5 psi pressure causes a $\frac{1}{16}$" deflection

The relationship (1) is the critical one since it gives the lower value of K. The strips are 1" wide and $\frac{1}{8}$" thick

For a strip $Rd\theta$ wide and 1" long, $dK = \frac{0.7R\, d\, \theta\, (1)}{\frac{1}{32}} = 22.4\ Rd\theta$

For the entire support strip, $K = 22.4\ (2)\ \pi R = 140.7R$

Response Characteristic

We now investigate μ_o as a function of ω from an input-output viewpoint. The critical input acceleration spectrum (sinusoidal) per specification is:

1.6 g rms, 2-20 cps
4.0 g rms, 2-200 cps

For a sinusoidal function, maximum (peak) amplitude $= \frac{\sqrt{2}}{2}$ rms value also circular frequency ω (rad/sec) $= 2\pi \cdot$ frequency f (cps).

Thus the input acceleration spectrum is:

2.26 g peak, 12.56 — 125.6 rad/sec
5.66 g peak, 125.6 — 1256 rad/sec

We have $\ddot{q}_o = \omega^2 q_o$ for harmonic motion, where q_o = peak input amplitude (inches) and $\ddot{q}_o$ = peak input acceleration (in/sec^2). In g units

$$\ddot{q}_o = \frac{\omega^2 q_o}{y} \qquad \text{or} \qquad q_o = \frac{y\,\ddot{q}_o}{\omega^2}$$

We also assume a damping ratio $\zeta = \frac{C}{C_c} = 0.04$ for the fiberglass substrate with cemented cells attached. Further, we assume that the single degree of freedom equation for the transmissibility at resonance applies, i.e.

$$TR = \frac{1}{2\zeta}\sqrt{1 + (2\zeta)^2}$$

(Reference 20, page 91 with $\zeta = \frac{C}{C_c}$ and $\frac{\omega}{\omega_n} = 1$)

Substitution of $\zeta = .04$ gives TR = 12.54 at resonance.

Thus, the response displacement u_o is

$$u_o = \frac{12.54 \times 386.04\,\ddot{q}_o}{\omega^2} = 4841\,\frac{\ddot{q}_o}{\omega^2} \qquad \text{(Response)}$$

where $\ddot{q}_o$ is the maximum input acceleration in q's

For $12.56 \leq \omega \leq 125.6$, $\ddot{q}_o$ = 2.26 g's peak, and

$$u_o = \frac{10940}{\omega^2} \qquad \text{(Response)}$$

For $125.6 < \omega \leq 1256$, $\ddot{q}_o$ = 5.66 g's peak and

$$u_o = \frac{27400}{\omega^2} \qquad \text{(Response}$$

i.e. $u_o = \frac{B}{\omega^2}$ where B = 10,940; 27,400 (two values) with units in Sec -2.

From which 1129.6 rad/sec which is inconsistent with the assumption that $12.56 \leq \omega \leq 125.6$ rad/sec.

For $125.6 \leq \omega \leq 1256$ (B = 27,400) ratioing according to the square root of the B's,

$$\omega = 1129.6 \sqrt{\frac{27,400}{10,940}} = 1787.7 \text{ rad/sec}$$

This value is still outside the range of B validity, but is fairly close to it. We assume B = 27,400 in sec -2 is valid. Thus

$$f = \frac{\omega}{2\pi} = \frac{1787.7}{2\pi} = 285 \text{ cps}$$

This is the fundamental membrane frequency.

Response Values

The maximum deflection (response) is:

$$u_o = \frac{B}{\omega^2} = \frac{27,400}{(1787.7)^2} = .0085735 \text{ in.}, \quad \text{Say } 0.009 \text{ in.}$$

The maximum slope in the x direction comes from

$$\frac{du}{dx} = u_o \cos\theta \frac{\pi}{b} \cos\frac{\pi x}{b}$$

$$\left(\frac{du}{dx}\right)_{max} = \frac{\pi}{b} u_o = \frac{\pi}{4.0} .0085735 = .0067336 \text{ rad}$$

$$= .38581^o, \text{ say } 0.4$$

Technical Evaluation of the Fundamental Membrane Frequency

Substitution of $u_o = \frac{B}{\omega^2}$ in the frequency equation gives

$$\omega^4 = \frac{B^2}{b^2 R^2} \cdot \frac{\sqrt{2}}{8} \frac{tE}{\gamma} \left[3\left(\frac{b}{R}\right)^2 + \mu\pi^2\right]$$

The value of ω obtained from this equation is uncorrected for support flexibility.

We now put in numbers:

$B = 10,940;\ 27,400$ in. sec^{-2}

$b = 4.00$ in.

$R = 6.80$ in. (To $\mathbb{C}$ of outer layer)

$t = 0.006$ in.

$E = 3.0 \times 10^{6}$ #/in.^{2} (Fiberglass)

$\gamma = .300$ for cells $+ .056$ for substrate $= .356$ #/ft^2

$= .002472$ #/in.^{2} $= 6.403 \times 10^{-6}$ # sec^2 - in.^{-3} (mass/in^2)

$\mu = 0.1$ (Poisson's ratio for fiberglass)

$k = 140.7\ R$ #/in. (k is the spring constant of the supporting strips. It is so high as to be of negligible effect).

Thus, for $12.56 \leq \omega \leq 125.6$ rad/sec ($B = 10,940$)

$$\omega^4 = \left(\frac{10,940}{4 \cdot 6.80}\right)^2 \cdot \frac{1.4142}{8} \cdot \frac{.006 \cdot 3.0 \cdot 10^6}{6.403 \cdot 10^{-6}} \left[3\left(\frac{4.00}{6.80}\right)^2 + 0.1 \cdot 9.8696\right]$$

$$= 162.80 \cdot 10^{12}$$

The maximum curvature in the x direction is derived from

$$\frac{d^2u}{dx^2} = u_o \cos\theta \cdot \frac{\pi^2}{b^2}\left(-\sin\frac{\pi x}{b}\right)$$

$$\left(\frac{d^2u}{dx^2}\right)_{max} = \frac{\pi^2}{b^2} u_o = \frac{\pi}{b}\left(\frac{du}{dx}\right)_{max} = .78539 \cdot .38581 = .30°/\text{in.}$$

6.2 Substrate -- Deployed Position

Summary

Bending Frequencies

1st Bending	0.60 cps
2nd Bending	3.78 cps
3rd Bending	10.57 cps

Torsional Frequencies

1st Torsion	10.24 cps
2nd Torsion	17.06 cps
3rd Torsion	23.89 cps

It is noted that the required minimum fundamental bending frequency of 0.5 cps has been exceeded. Analysis was conducted for room temperature conditions. A reduced modulus of elasticity at cruise maneuver temperature (250°F) will reduce the above frequencies by 3%. The actual beam length is 223 inches rather than 216 inches which results in a further reduction of 6%. This reduces the first bending f_n to 0.55 cps.

Introduction

Structural changes in the array require recalculation of the bending and torsional natural frequencies relative to those used in the preliminary report. The primary goal was to determine whether this specified fundamental bending frequency of 0.5 cps was exceeded or if further redesign was required.

Changes made, relative to the preliminary design array structure were:

1. The titanium tubes were reduced in width at the root (the depth remains the same).
2. The titanium tube constant section extending from 100 inches outboard of the root to the tip (216 inches outboard of the root) is narrower but deeper.

3. Doubler strips have been added to the titanium tubes on the top and on the bottom, further increasing the bending stiffness.
4. Improved information regarding weights of substrate and cells.

The re-analysis contained herein follows closely that made originally. The general method is the same. Allowance for taper effects and new numbers are the only substantial changes.

Stiffness EI and GJ

Root Section

Arc length and enclosed area of titanium tube

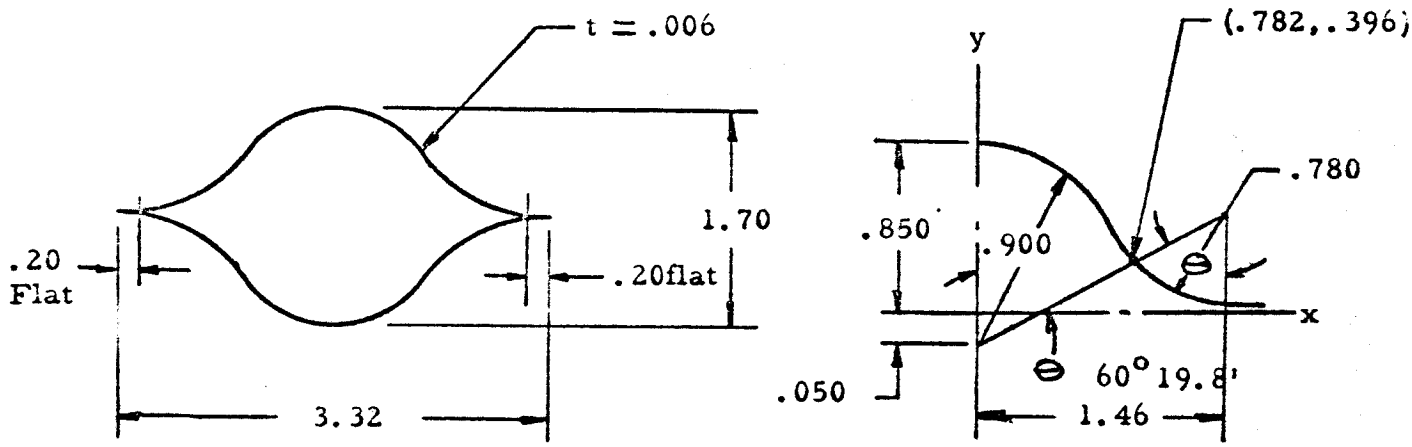

The basic dimensions for the quarter section, less flats, were obtained from a large scale plot of the quarter section calculated as the sum of two circular arcs is:

$$S\ \frac{1}{4} = S_1 + S_2 = .9477 + .8213 = 1.7690 \text{ inches (Root, less flats)}$$

The enclosed area of the quarter section, (i.e. the area bounded by the x axis, the y axis and the contour arc) calculated as the sum of areas of circular sectors, triangles and trapezoids, is:

$$A_{\frac{1}{4}} = 0.6401 \text{ in}^2 \text{(Root)}$$

Thus, for the entire tube section (one tube), the arc length and enclosed area are:

$$\left.\begin{aligned} S &= 4 \times 1.7690 = 7.076 \text{ in (omits flats)} \\ A &= 4 \times 0.6401 = 2.560 \text{ in}^2 \end{aligned}\right\} \text{ Root}$$

For comparison purposes, the original values were:

$$S = 7.518 \text{ in. and } A = 2.688 \text{ in}^2$$

Bending Stiffness EI (Root)

The moment of inertia $I_{x\,\frac{1}{4}}$ of the quarter section is calculated as the sum of moments of inertia of the two arc portions about the x axis, one of radius r = 0.900 in. and the other of radius r=0.780 in. The formulas used in calculating $I_{\frac{1}{4}}$ were taken from Roark's Formulas for Stress and Strain, 1st Edition, page 64, and are identical to those used in the original analysis.

They are repeated here:

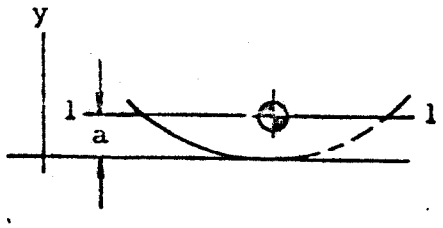

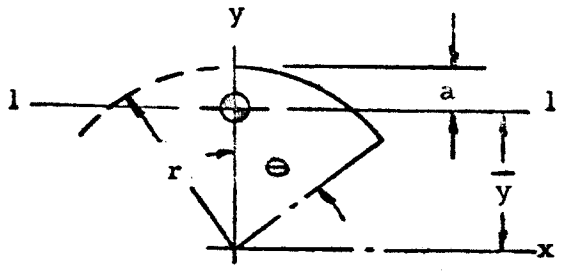

$$I_{1\text{-}1} = \frac{1}{2} r^3 t \left(\theta + \sin\theta\cos\theta - \frac{2\sin^2\theta}{\theta}\right)$$

$$a = r \left(1 - \frac{\sin\theta}{\theta}\right)$$

additionally, by the arc's transfer theorem, for the upper arc:

$$I_{x1} = I_{1\text{-}1} + S_1 \cdot t \; y^{-2}$$

and for the lower arc

$$I_{x_2} = I_{1\text{-}1} + S_2 \; t \cdot a^2$$

Then $I_{x\,\frac{1}{4}} = I_{x_1} + I_{x_2}$

Putting in numerical values for r and θ

$$I_{x1} = 0.4725\ t + 0.0270\ t = 0.4995\ t$$

At the root there are two 0.3 wide doubler strips of thickness t, one at the top and the other at the bottom of the section so the section moment of inertia, for thickness t=0.006 in., is:

$$I \quad 4\ I_{x1} + 2 \cdot .300\ t \cdot (.850)^2 = 2.4315t$$

$$= 2.4315 \cdot .006 = 0.01459\ \text{in.}^4 \text{ (one tube)}$$

The modulus of elasticity E for 6AL4V Titanium Alloy, used for the tubes, is: (Reference 3)

$$E = 16.4 \cdot 10^6\ \#/\text{in.}^2$$

and for the two tubes, the total EI is:

$$EI = 16.4 \cdot 10^6\ (2 \cdot 0.01459) = 4.786 \cdot 10^5\ \#\text{in.}^2 \text{ (Array Root)}$$

For comparison purposes, this original value was $3.962 \cdot 10^5\ \#\text{in.}^2$

Torsional Stiffness GJ(Root)
For one tube

$$J = \frac{4A_o^2}{\int \frac{ds}{t}} = \frac{4A^2t}{S} = \frac{4(2.560)^2 \cdot 0.006}{7.076} = 0.02223\ \text{in.}^4$$

The shear modulus G for the tube material is: $G = 6.2 \cdot 10^6\ \#/\text{in.}^2$

and for the two tubes, the GJ is: $GJ = 6.2 \cdot 10^6 \cdot 2 \cdot 0.02223 = 2.757 \cdot 10^5\ \#/\text{in.}^2$

(Root, uncorrected for differential bending stiffness)
For comparison purposes, the original value was $2.870 \cdot 10^5\ \#/\text{in.}^2$

Tip Section

Arc length and enclosed area of titanium tube,

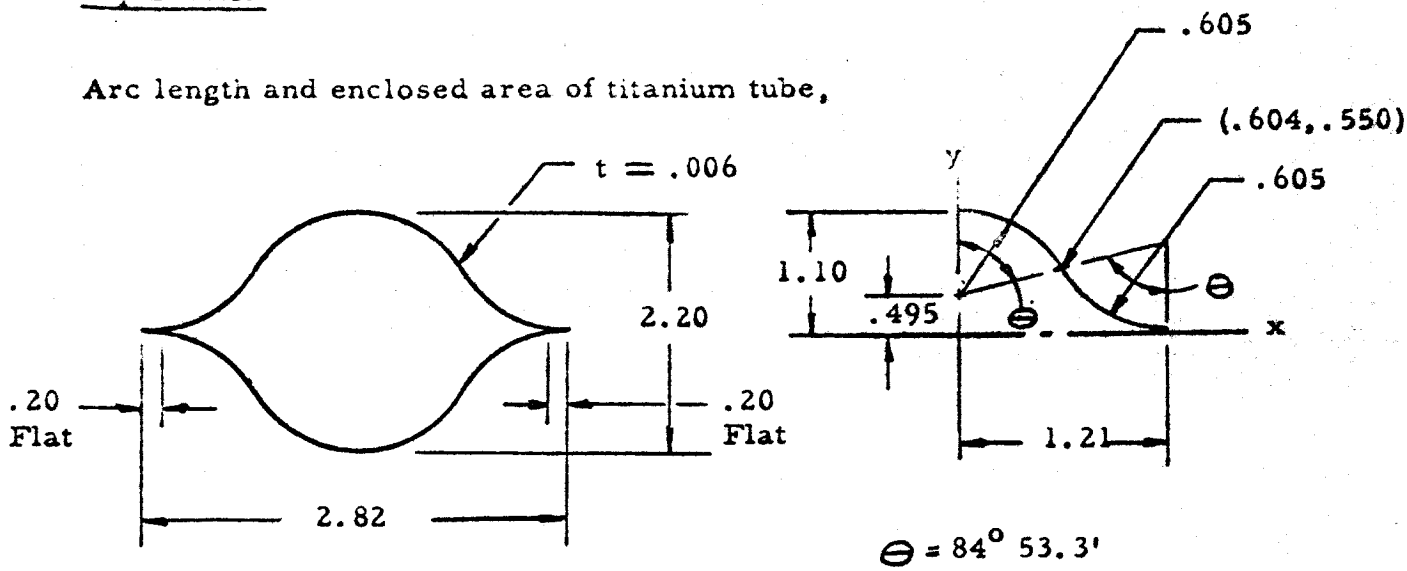

The basic dimensions for the quarter section, less flats, again were obtained from a large scale plot of the quarter section. The arc length of the quarter section, calculated again as the sum of two circular arcs, is:

$$S_{\frac{1}{4}} = S_1 + S_2 = .8962 + .8962 = 1.7974 \text{ (Tip, less flats)}$$

The enclosed area of the quarter section, i.e. they are bounded by the x axis, the y axis, and the contour arc, calculated as the sum of areas of sectors and trapezoids, similar to the procedure used for the root section, is:

$$A_{\frac{1}{4}} = 0.6656 \text{ in}^2 \quad \text{(Tip)}$$

Thus, for the entire tube section (one tube), the arc length and enclosed area are:

$$\left.\begin{aligned} S &= 4 \cdot 1.7924 = 7.170 \text{ in. (omits flats)} \\ A &= 4 \cdot 0.6656 = 2.662 \text{ in.}^2 \end{aligned}\right\} \text{ Tip}$$

For comparison purposes, the root values herin are $S = 7.076$ in. and $A = 2.560$ in.^{2}. The original values (constant over this span) were $S = 7.518$ in. and $A = 2.688$ in.^{2}.

Bending Stiffness EI (Tip)

Following the procedure used before for the root section, but with $r = 0.605$ and $\Theta = 84^{\circ}\ 53.3'$, for both upper and lower arcs of the tip quarter section, the I for one tube, less flats and spotwelded strip is:

$$I_x = 0.01956 \text{ in.}^4 \text{ (tip)}$$

The I for one tube including flats and the spotwelded strips is calculated in the following table:

Item	A	y	Ay	Ay^2	I_o
Basic Tube (A=7.170 x .006=.0432)	.04320	0	0	0	.01956
Flats (A=4 x .20 x .006=.0048)	.00480	0	0	0	-
Strip (A=.30 x .006=.0018)	.00180	1.103	.001985	.00219	-
Total:	.04980		.001985	.00219	.01956
					.00219
					-.00008
					.02167

$$\bar{y} = \frac{.001985}{.04980} = .03986$$

$$A\bar{y} = .001985 \times .03986 = .00008$$

$$I_x = 0.02167 \text{ in.}^4$$

For the two tubes, the total EI is:

$$EI = 16.4 \times 10^6 \ (2 \times 0.02167) = 7.108 \times 10^5 \ \#\text{in.}^2 \text{ (Array, tip)}$$

For comparison purposes, the root value herein in EI 4.786×10^5 $\#\text{in.}^2$ and the original value (constant over this span) was 3.962×10^5 $\#\text{in.}^2$.

Torsional Stiffness GJ (Tip) -- for one tube:

$$J = \frac{4 A_o^2}{\int \frac{ds}{t}} = \frac{4 A^2 t}{S} = \frac{4 (2.662)^2 \times .006}{7.170} = 0.02372 \text{ in.}^4$$

and for two tubes, the GJ is:

$$GJ = 6.2 \times 10^6 (2 \times 0.02372) = 2.941 \times 10^5 \text{ \#in.}^2 \text{ (Tip,}$$

uncorrected for differential bending stiffness).

For comparison purposes, the root value herein is:

$GJ = 2.757 \times 10^5$ #in.^{2} and the original value (constant over the span) was $GJ = 2.870 \times 10^5$ #in.^{2}.

Correction of GJ for Differential Bending

Due to a unit torque, T, applied to the array at the tip, the twist Θ_T (radians) at the tip, is the torsion-in-the-tubes alone system (which we call the torque box system) is:

$$\Theta_T = T \int_0^L \frac{dx}{GJ}$$

where x is measured outboard from the root. Note that the presence of the intercostal at the tip of the array ensures transmitting both torsion and differential bending loads (moments) to the tubes. The GJ distribution is as follows:

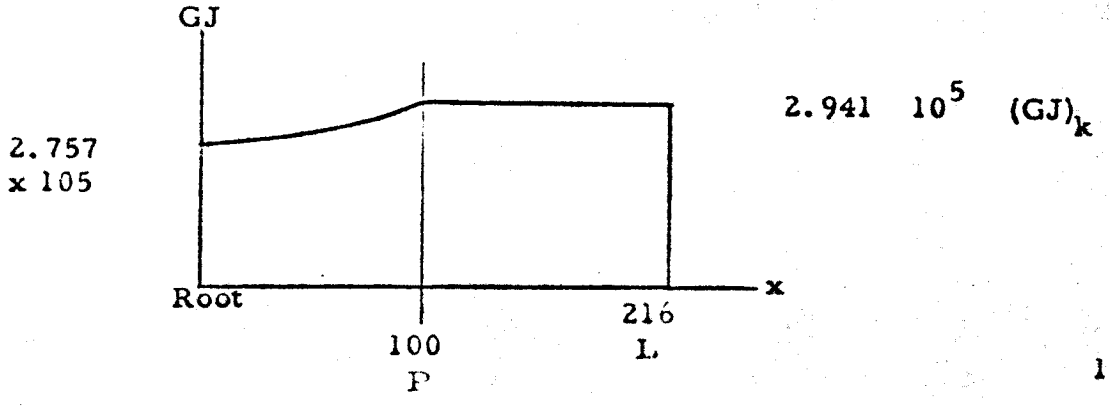

For $0 \leq x \leq p$, the cross section dimensions of the tubes are assumed to vary linearly, i.e. the effective radius of the torque box = a + bx. Noting that GJ is propostional to $A_o^2 / \int \frac{ds}{t}$ where A_o is proportional to r^2 and $\int ds$ to r (t is constant), it is concluded that GJ varies as $r^4 / r = r^3$. Thus we set $GJ = (a + bx)^3$ and solve for a and b:

$$\text{At } x = 0, \quad 2.757 \times 10^5 = (a + b \times 0)^3 = a^3$$

$$\text{or} \quad a = 65.085$$

$$\text{At } x = 100, \quad 2.941 \times 10^5 = (65.085 + b \times 100)^3$$

$$\text{from which } b = 0.01417$$

Thus, $GJ = (65.085 + 0.01417\,x)^3$ #in.^{2}, $0 \leq x \leq 100$

2.941×10^5 #in.^{2} $\quad 100 \leq x \leq 216$

Returning to the twist equation given previously, with T = 1 in.#

$$\Theta_T = \int_0^p \frac{dx}{GJ} + \left(\frac{1}{GJ}\right)_k \int_p^L dx$$

$$= \int_0^p (a + bx)^{-3} \, dx + \frac{L - p}{(GJ)_k}$$

$$\text{or } \Theta_T = \frac{1}{2b(a + bx)^2} \Bigg|_0^p + \frac{L - p}{(GJ)_k}$$

Putting in numbers for a, b, p, L and $(GJ)_k$,

$$\Theta_T = 0.0003512 + 0.0003944 = 0.0007456 \text{ rad.}$$

Due to a unit-torque T applied to the array at the tip, the twist Θ_B (radians) at the tip, in the differential bending system, is:

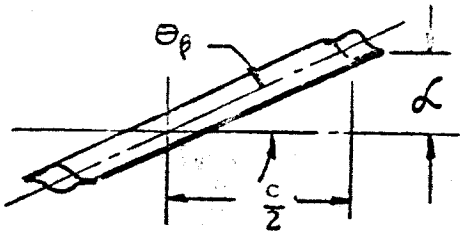

C = 41.60 t(for small β)

View looking Inboard from tip.

$\Theta_B \quad \frac{2\beta}{c}$

where $\beta = y_x \quad L$ and is small compared to c.

Also $\frac{d^2y}{d_x^2} = \frac{M}{EI}$

Where $M = P(L - x)$ and P = Tip load = $\frac{1}{c}$ for 1 in.# of torque applied at the tip.

For $0 \leq x \leq p$, EI varies as r^3, t being constant, as was found to be the case with GJ. Thus, again, but with different a & b, $EI = (a + bx)^3$. with $EI = 4.786 \times 10^5$ # $in.^2$ at $x = 0$ and 7.108×10^5 # $in.^2$ at $x = 100$, $a = 78.221$ and $b = 0.11024$. The values are for the entire array (two tubes).

Thus, $EI = (78.226 + .111024)^3$ # $in.^2$, $0 \leq x \leq 100$

7.108×10^5 # $in.^2$ $\quad 100 \leq x \leq 216$

Numerical integration of $\frac{d^2y}{d_x^2} = \frac{M}{EI}$ (Two Integrations)

from $0 \leq x \leq 100$ for unit P gives $y_{x=100} = 0.61956$ and $y = 0.61956$ in. at $x = 100$

and $\frac{dy}{dx} = 0.0091698$ in/in. at $x = 100$

For the constant part of the array ($100 \leq x \leq 216$), from cantilever beam theory, still with unit P,

$$\Delta_y = \frac{P^1 (L - p)^3}{3EI} + \left(\frac{dy}{dx}\right)_{x = p} (L - p)$$

$$= \frac{1(116)^3}{3 \times 7.1081 \times 10^5} + 0.0091698 \times 116$$

$$= 1.79568$$

and for unit P, $\delta = y_{x\ L} = 0.61956 + 1.79568 = 2.4152$ in. (at tip).

For $P = \frac{1}{c}$ (unit torque at tip), and EI for one tube only,

$$\delta = \frac{2 \times 2.4152}{41.60} = 0.116115 \text{ in.}$$

$$\Theta_B = \frac{2\delta}{c} = \frac{2 \times .116115}{41.60} = 0.0055825 \text{ rad.}$$

Thus, the ratio of twist angles for the same loadings, is:

$$\frac{\Theta_T}{\Theta_B} = \frac{0.0007456}{0.0055825} = 0.13356$$

i.e., the differential bending system is 13.356 % as stiff as the torque box system. The total torsional stiffness of the array is thus 1.13356 times the torsional stiffness of the torque box system alone. For comparison purposes, the orginal correction factor was 1.04865. Thus,

$$GJ = 1.3356 (65.085 + 0.01417 x)^3 \ \#\text{in.}^2, \quad 0 \leq x \leq 100 \text{ in.}$$
$$= 3.334 \times 10^5 \ \#\text{in.}^2 \qquad 100 \leq x \leq 216 \text{ in.}$$

(at $x = 0$, $GJ = 3.125 \times 10^5 \ \#\text{in.}^2$)

The bending stiffness of the array is given again here, for convenience

$$EI = (78.221 + .11024x)^3 \qquad 0 \leq x \leq 100 \text{ in.}$$
$$= 7.108 \times 10^5 \ \#\text{in.}^2 \qquad 100 \leq x \leq 216 \text{ in.}$$

(at $x = 0$, $EI = 4.786 \times 10^5 \ \#\text{in.}^2$)

Effective EI and GJ

For simplicity of the frequency analysis, we assume single effective (average) EI and GJ values, constant over the entire span. Let y = either EI or GJ. Either can be expressed as $\phi\ (a + bx)^3$, where ϕ is the correction constant (1.13356 for GJ and 1.0 for EI). We assume $\bar{y}$ to be the arithmetic avarage value of y over the span, i.e.

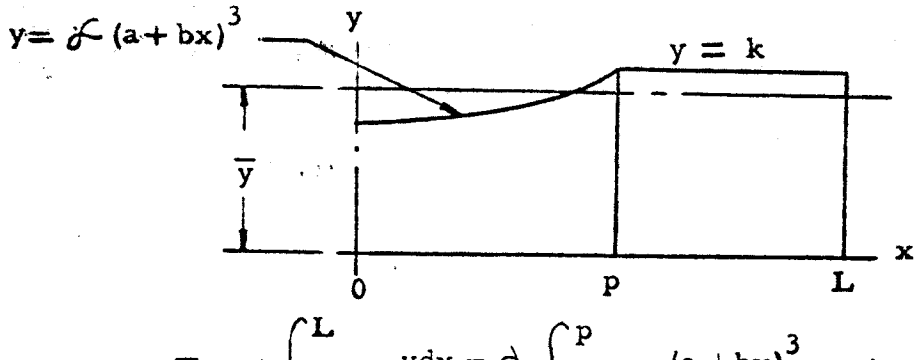

$$L\ \bar{y} = \phi \int_0^L ydx = \phi \int_0^p (a+bx)^3\ dx + k\ (L - p)$$

From which, upon integration, $\bar{y} = \frac{\phi}{4bL}\left[(a + bp)^4 - a^4\right] + k\ (1 - \frac{P}{L})$

Putting in numbers for the a's, b's, k's, ϕ's, p and L

$$\overline{EI} = 6.547 \times 10^5\ \#\ in.^2$$

and $$\overline{GJ} = 3.285 \times 10^5\ \#\ in.^2$$

There are the values of EI and GJ used in the frequency analysis of the solar array. For comparison purposes the original values were EI = 3.962 x 10^5 # $in.^2$ and GJ = 3.010 x 10^5 # $in.^2$ (constantly).

Mass per Unit Span Length,

Substrate

Surface density $\sigma_1 = 0.056\#/ft^2$

$$= \frac{.056}{144} = 0.0003889\ \#/in.^2$$

$$\omega_1 = \sigma_1 \ell_1 = .0003889 \times 36.7 = 0.01427 \text{ \#/in.}$$

Cells

Surface density $\sigma_2 = 0.300 \text{ \#/ft}^2$

$$= \frac{.300}{144} = 0.002083 \text{ \#/in.}^2$$

$$\omega_2 = \sigma_2 \ell_2 = .002083 \times 32.8 = 0.06833 \text{ \#/in.}$$

Tube and Strips (One Tube)

Material weight density ρ, Titanium Alloy $= 0.160 \text{ \#/in.}^3$

$$\omega_3 = t\rho \left(S_{\text{tube}} + S_{\text{flats}} + S_{\text{connecting strip}} + S_{\text{bottom strip}}\right)$$

$= .006 \times .160 \ (7.076 + .800 + 1.125 + .300) = 0.00893$ #/in. „

Root (x = 0)

$\omega_3 = .006 \times .160 \ (7.170 + .800 + 1.125 + 0) = 0.00873$ #/in. for constant section ($100 \leq x \leq 216$)

Over the tapered region of the tube section ($0 \leq x \leq 100$), ω_3 is linear with respect to the effective radius r, which in turn is linear with respect to x. Thus, the average ω_3 is:

$$\bar{\omega}_3 = \left(\frac{.00893 + .00873}{2} \times 100 + .00873 \times 116\right) \frac{1}{216}$$

$= 0.008776$ #/in. (one tube).

Total (array) weight per inch of span

$$\bar{\omega} = \omega_1 + \omega_2 + 2 \bar{\omega}_3 = .01427 + .06833 + 2 \times .008776$$

$= 0.10015$ #/in.

and the required mass per inch of span, μ, for the array, assumed constant over the span, is:

$$\mu = \frac{\bar{\omega}}{y} = \frac{.0015}{386.04} = 0.0002594 \text{ \# sec}^2 \text{ in.}^{-2}$$

For comparison purposes, the original value was 0.0003041 # sec^2 in.^{-2}

Mass Moment of Inertia Per Unit Span Length, r

Substrate

$$I_1 = \frac{1}{12} \omega_1 \ell_1^2 = \frac{1}{12} \times .01427 (36.7)^2 = 1.602 \text{ \# in.}^2/\text{in.}$$

cells

$$I_2 = \frac{1}{12} \omega_2 \ell_2^2 = \frac{1}{12} \times 0.06833 (32.8)^2 = 6.126 \text{ \#in.}^2/\text{in.}$$

Tubes and Strips (Two Tubes)

$$I_3 = 2 \omega_3 d^2 = 2I_o = 2 \omega_3 (d^2 + \bar{r}^2)$$

where d = Distance, array ℓ to ℓ of tube = 19.75 in.,

$I_o = \omega_3 \bar{r}^2$ and $\bar{r}$ = radius of circle with same enclosed area as tube. $\bar{r}$ is an effective radius of the tube for purposes of approximating the I_o of the tube.

$$\bar{r}^2 = \frac{2.560}{\pi} = 0.8147, \text{ Root } (x = 0)$$

$$\bar{r}^2 = \frac{2.662}{\pi} = 0.84734, \text{ constant section } (100 < x \leq 216)$$

$I_3 = 2 \times .00893 \left[(19.75)^2 + (.81487)^2 \right] = 6.978 \text{ \#in.}^2/\text{in., Root } (x = 0)$

$I_3 = 2 \times .00873 \left[(19.75)^2 + (.84734)^2 \right] = 6.823 \text{ \#in.}^2/\text{in., constant section } (100 < x \leq 216).$

Over tapered region of the tube section, I_3 varies linearly with respect to the weight/inch, ω_3 very nearly (the effect of I_o variation is minor), and ω_3 in turn varies linearly with x, as mentioned previously.

Thus the effective I_3 is :

$$\bar{I}_3 = \left(\frac{6.978 \quad 6.823}{2} \times 100 + 6.823 \times 116\right) \frac{1}{216} = 6.859 \#in.^2/in.$$

(two tubes)

Total (array weight moment of inertia per inch of span:

$$\bar{I} = I_1 + I_2 + I_3 = 1.602 + 6.126 + 6.859 = 14.587 \#in.^2/in.$$

and the required mass moment of inertia per inch of span, γ , for the array, assumed constant over the span, is:

$$\gamma = \frac{\bar{I}}{g} = \frac{14.587}{386.04} = 0.03779 \#sec^2 in./in.$$

Natural Frequencies

The natural frequencies are calculated from formulas in Reference 20, pages 458 and 459.

Bending Frequencies (Cantilever Beam)

$$\omega_n = a_n \sqrt{\frac{EI}{\mu L^4}}$$

where $a_1 = 3.52$, $a_2 = 22.04$ (Den Hartog gives $a_2 = 22.4$, but this value is a mis-print as an independent check will verify), $a_3 = 61.7$, $EI = 6.547 \times 10^5 \#in.^2$, $\mu = 0.0002594 \#\ sec^2 in.^{-2}$, and $L = 216.0$ in. ($L^4 = 2.177 \times 10^9$ in.^{4}). The parameter $\sqrt{\frac{EI}{\mu L^4}}$ is:

$$\sqrt{\frac{EI}{\mu_L^4}} = \sqrt{\frac{6.547 \times 10^5}{2.594 \times 10^{-4} \times 2.177 \times 10^9}} = 1.0767 \text{ Sec}^{-1}$$

The original value was 0.7736. Thus, the new bending frequencies reflect a 39.2% increase. Using the values given above, and $f \frac{\omega}{2\pi}$, we find the bending frequencies are:

Mode	ω rad/sec	f cps	
1	3.79	0.60	(was 0.43)
2	23.73	3.78	(was 2.71)
3	66.43	10.57	(was 7.60)

Torsional Frequencies (Torsional Cantilever)

$$\omega_n = a_n \sqrt{\frac{GJ}{\gamma L^2}}$$

where $a_1 = 4.712$, $a_2 = 7.854$, $a_3 = 10.996$, $GJ = 3.285 \times 10^5 \#in.^2$ and $\gamma = 0.03779 \#sec^2 in./in.$ L remains 216.0 in ($L^2 = 46.656$ in.^{2}).

The parameter:

$$\sqrt{\frac{GJ}{\gamma L^2}} = \sqrt{\frac{3.285 \times 10^5}{.03779 \times 46.656}} = 13.65 \text{ sec}^{-1}$$

The original value was 11.70. Thus, the new torsional frequencies reflect a 16.7% increase. Using the a values given above, and $f = \frac{\omega}{2\pi}$, we find the torsional frequencies are:

Mode	ω rad/sec	f cps	
1	64.32	10.24	(was 8.77)
2	107.21	17.06	(was 14.62)
3	150.10	23.89	(was 20.42)

7.0 THERMAL ANALYSIS

The thermal analysis is based on the design criteria given in Section 4.0 and the detail design configuration presented in this report. For the purpose of this analysis a Mars' mission is assumed.

The analysis is limited to consideration of the solar array structure in the deployed position. Thermodynamic behavior during launch and prior to deployment depends upon the relationship of the deployable solar array to other vehicle systems which is not defined for this program.

The work presented in this section includes:

1. Basic physical measurements of the thermal radiative properties for design associated materials.

2. Detailed computer results of a thermal mathematical model developed for a specific design configuration and using the radiative property date of 1.

3. Design verification tests conducted in a thermal vacuum chamber of the array model.

Finally, the results of this thermal design are discussed as they relate to the design criteria of Section 4.0.

7.1 Radiative Surface Properties of Materials

Monochromatic room temperature reflectance data is presented for several of the materials associated with the deployable solar cell array. The data is integrated against various source temperature Planckian blackbody functions to yield a curve of total normal emittance as a function of source temperature.

The Johnson 1954 solar radiation curve is used to obtain value of solar absorptance. (Reference 31), (Figure 7-1).

7.1.1 Purpose of Measurements

The temperatures of objects in space are determined by internal conductive paths within the object, by the surface radiative properties of the object and by the external radiative environment which the surfaces see. The radiative properties of concern are the absorptance for solar radiation and the thermal (I.R.) emittance which governs the radiation rate of heat flow away from the object. The purpose of Section 7.1 of this report is to define these properties accurately, so that a thermal model of the array and beam may be created. This model which may be used to compute temperatures for various conditions of environment is discussed in Section 7.2.

7.1.2 Definition of Terms

Definition of terms used in this report are given below:

Normal Monochromatic Reflectance:

ρ_λ: The ratio of the reflected radiant intensity from a body to that incident upon it at a particular wavelength, when the incident radiation is directed normal to the surface.

α_λ: Monochromatic Absorptance:

The ratio of the absorbed radiant intensity by body to that incident upon it at a particular wavelength.

ϵ_η: Total Normal Emittance:

The ratio of the emitted radiant intensity, integrated over all wavelengths) in a normal direction to that of a blackbody at the same temperature.

ϵ: Total Emittance:

The ratio of the emitted radiant intensity, integrated over all

wavelengths, emitted by a planar body into a solid angle of 2 π steradian to that of a blackbody at the same temperature.

ϵ_λ: Monochromatic Emittance:

The ratio of the emitted radiant intensity to that of a blackbody at the same temperature at a particular wavelength.

α_S: Total Solar Absorptance:

The ratio of the radiant intensity absorbed by a body to that incident upon it from the sun as defined by the F.S. Johnson curve of Reference 1. (Figure 7-1).

H_λ: Monochromatic solar intensity (Watts/ μ - cm^2) as defined by the Johnson curve. (Figure 7-1).

J_λ: Monochromatic blackbody intensity distribution (Watts/μ - cm^2), a function of temperature given by Planck's function.

The use of emittance, reflectance and absorptance in these definitions rather than emissivity, reflectivity and absorptivity indicates that the values given are for real surfaces and include the effects of application technique, substrate, and environmental degradation. In this report where the terms having the suffix "ity" are used a theoretical value, or a laboratory measurement of a chemically pure substance on a completely flat substrate, is intended.

7.1.3 Apparatus and Procedure

All measurements were made in the Space Science Laboratory of GD/ Astronautics using the same apparatus and procedures as were used in the AIA Round Robin Program. These are described in Reference 32. This apparatus includes a Cary Model 14 Spectrometer and associated integrating sphere, a Perkin Elmer Model 13 Spectrometer with an associated hohlraum.

7.1.4 Results

The materials measured during the subject phase were:

1. The epoxy fiberglass substrate

2. The teflon coating of the cushion material used on the rear of the solar array (side away from cells)

3. Various preparations of the same titanium alloy Ti-6AL-4V used in the construction of the beam. These include:
   a. Polished material
   b. Blue oxidized coating (1000°F) from test section.
   c. Blue oxidized coating (1000°F) from lab flat material.
   d. Green oxidized coating (1200°F).
   e. Brown oxidized coating (1300°F).
   f. Dust blasted-brown oxidized coating (1300°F).

The oxidation process attempts to raise the value of the thermal emittance of the surface. For interior surfaces a high emittance tends to lower front to back temperature gradients on the beam. A high value of emittance also lowers the α_s/ϵ ratio, lowering beam temperatures in the full sun. The low emittance value of the polished titanium is useful on the beam side away from the sun. This lowers the heat loss rate to space and also improves the front-to-back temperature gradient. It should be noted that the thermal emittance is a function of temperature. This data is given in Section 11.5.

The data used in the analysis for space stable white coatings were not measured since this information is already well covered in the literature. Some pertinent results of the measurements are tabulated below, detailed results are given in Section 11.5.

Surface	α_s	ϵ_n@ 80°F	ϵ_n@260°F
1. Epoxy fiberglass	.881	---*	
2. Teflon	.851	.902	.908

Surface		ϵ_n@80°F	ϵ_n@260°F
3.	Titanium Ti-6AL-4V		
a.	Polished	.532	.134	.153
b.	Blue oxidized coating (1000°F) from test section.	.749	.127	.151
c.	Blue oxidized coating (1000°F) from lab flat material.	.776	.159	.185
d.	Green oxidized coating (1200°F)	.707	.189	.228
e.	Brown oxidized coating (1300°F)	.769	.302	.355
f.	Dust blasted-brown oxidized coating (1300°F)	.882	.544	.596

* Not measured because of temperature effects in the blackbody cavity on the fiberglass (darkening) calorimetric data indicates $\epsilon > .9$.

7.1.5 Computations

The spectral data of Section 11.5 was processed using an IBM digital computer to produce the values of total normal emittance ϵ_n, and solar absorptance, α_s, given in the tables of the same section.

ϵ_n was determined using the relation

$$\epsilon_n (T°K) = \frac{\sum_{\lambda=.3}^{\lambda=32} \left[(1-\rho_\lambda)\, J_\lambda\, \Delta\lambda\right] + (1-\rho)_{32\mu} \sum_{\lambda=32}^{\infty} J_\lambda \Delta\lambda}{\int_0^\infty J_\lambda\, d\lambda}$$

where J_λ is the plackian blackbody function corresponding to T°K.

α_s was determined using the relation

$$\alpha_s = \frac{\sum_{\lambda=.3}^{\lambda=.7} (1-\rho_\lambda)\, H\lambda\, \Delta\lambda}{\sum_{\lambda=.3}^{\lambda=.7} H_\lambda \Delta_\lambda}$$

The results are given as a function of blackbody temperature for each surface coating.

The value of solar absorptance is also plotted, a solar temperature (10,400°R), for purposes of comparison. Values of total normal emittance, ϵ_η, were used to obtain values of total emittance, ϵ, from Figure 7-2.

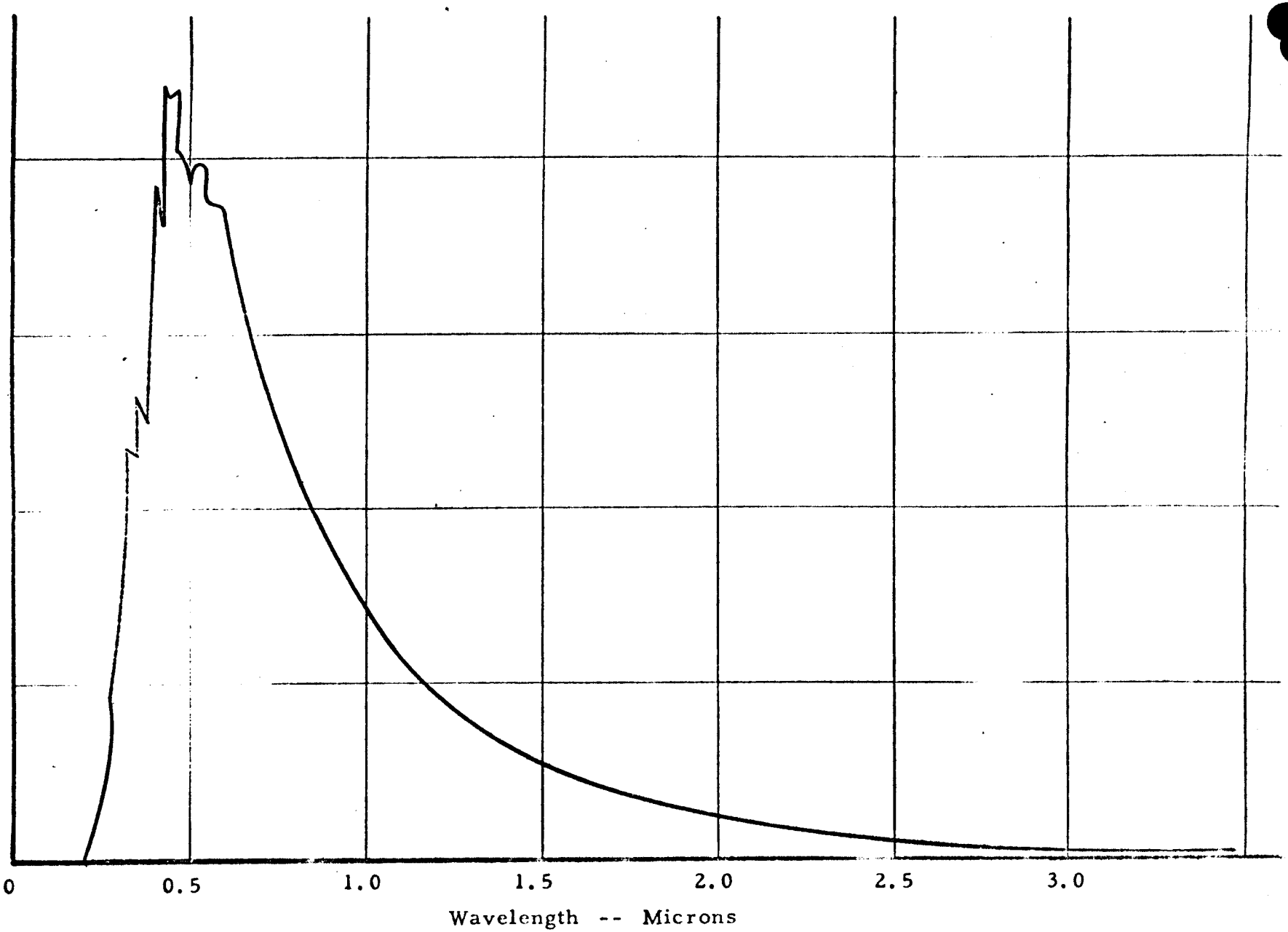

Figure 7-1

Solar Spectral Irradiance Above Atmosphere at Earth Mean Distance From the Sun (Johnson, 1954)

Figure 7 - 1

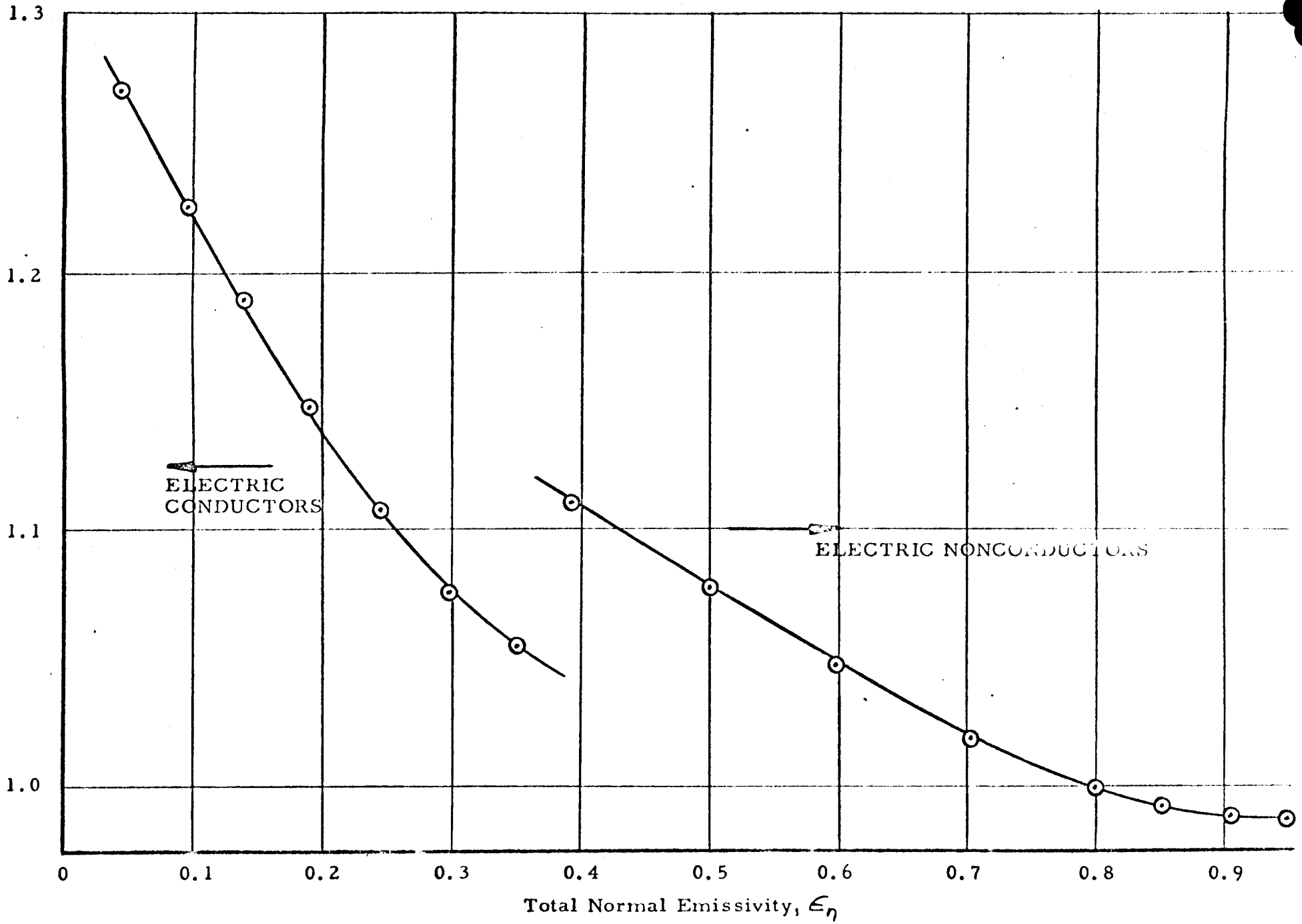

Figure 7 - 2

Theoretical Values For the Ratio of Hemispherical to Normal Emissivity

Figure 7-2

7.2 Analysis of Design Configurations

In order to determine representative temperatures for the array and beam in the environment of space, a thermal mathematical model was created for use on the 704 computer. The configuration is shown in cross-section in Figure 7-3. A section 10 inches in length was considered long enough to properly represent the internal radiation network. This section was divided into 23 nodes on the basis of near isothermality. The nodes are shown in Figure 7-3 by the circled numbers. All internal and external view factors and conduction paths were computed for the model. The path length and heat flow cross-sectional area for each conductive path was determined using the physical properties of .006 in. thick titanium alloy Ti-6AL-4V. The model includes 24 nodes, 22 conductive paths, 168 radiative paths where seven of the nodes are subject to 442 BTU/HR-FT^2 of solar radiation. The performance of this system is examined in this section for various coatings applied to the titanium as discussed in Section 7.1.

7.2.1 Beam Analysis for Blue Oxidized (1000°F) Titanium Alloy With a Polished Rear Face

The beam of Figure 7-3 was analyzed for the blue oxide and polished titanium coatings of Section 7.1.6. Nodes 1 through 10 and 23 had this blue coating both sides. Nodes 11 through 20 were polished outside, blue inside. Node22 was considered fiberglass both sides which is representative of the array. An internal and external radiosity network was computed and program runs were made to evaluate steady-state temperature distributions for the system. This is shown in Figure 7-4.

7.2.2 Beam Analysis for Blue Oxidized Titanium Alloy With a Polished Rear Face and White Paint Front Face

The same beam model was evaluated for the blue oxide and polished titanium coatings of 7.1.6 as in 7.2.1. However, the outside of nodes 1 through 5 was considered painted with a U.V. stable white coating such as S 13, having a solar absorptance of $\alpha = .2$ and $\epsilon = .85$. After computing the internal and external radiosity networks, the temperature distribu-
of Figure 7-5 were computed.

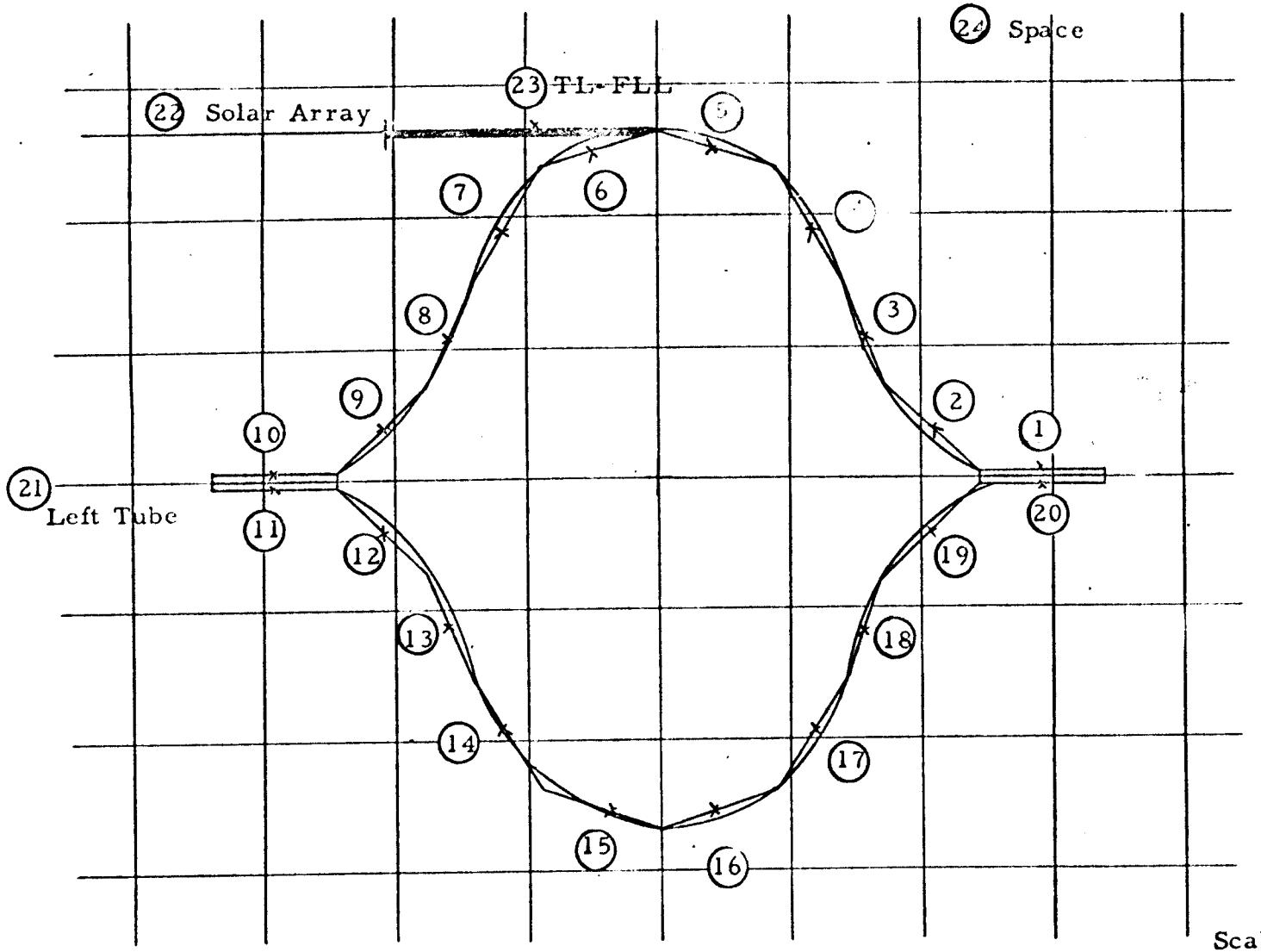

Schematic Thermal Model of Deployable Solar Array Support Beam

Figure 7 - 3

Figure 7 - 3

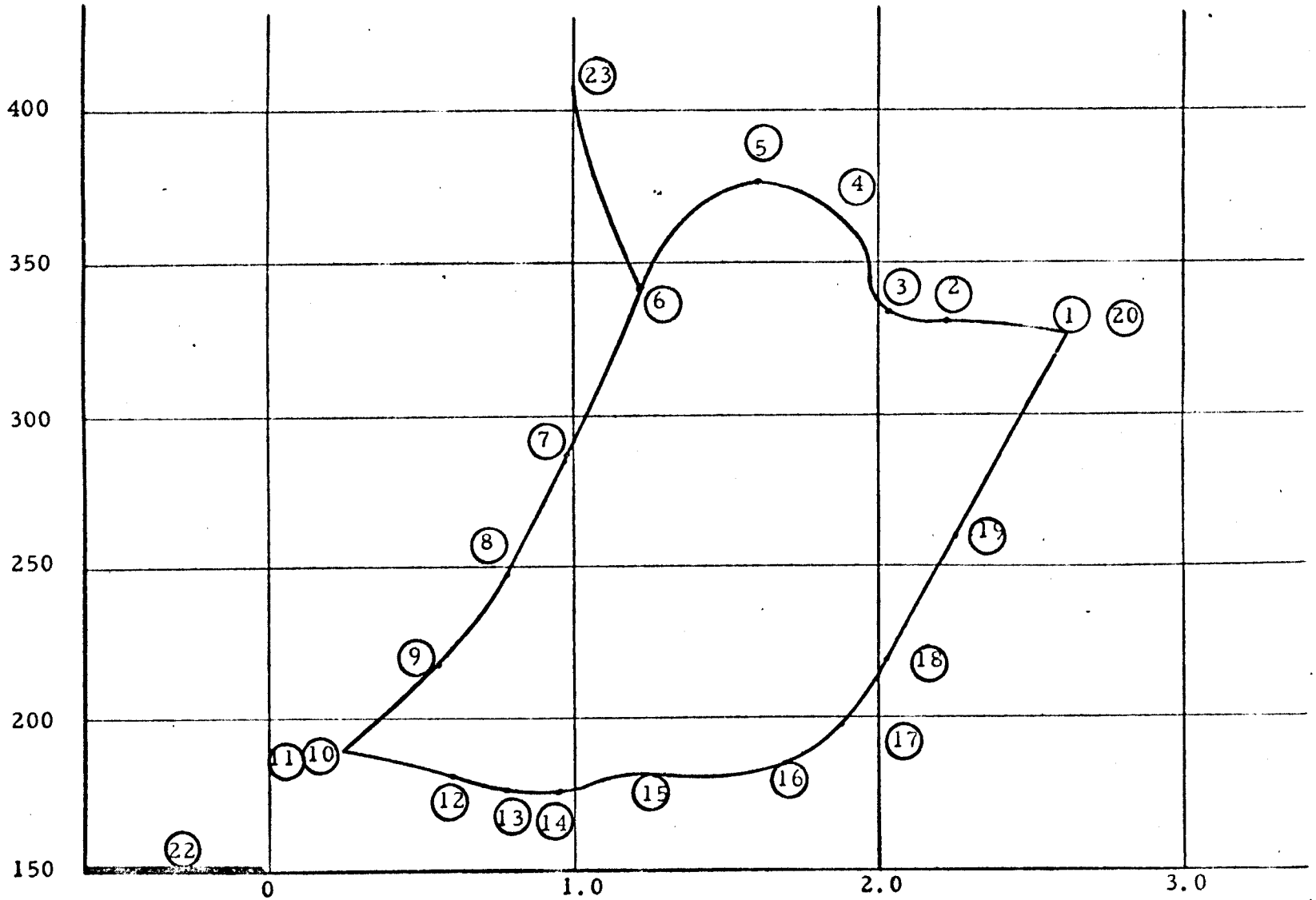

Beam Position (inches) From Arbitrary Origin

Beam Temperature Distribution Oxidized Titanium

Figure 7 - 4

Figure 7 - 4

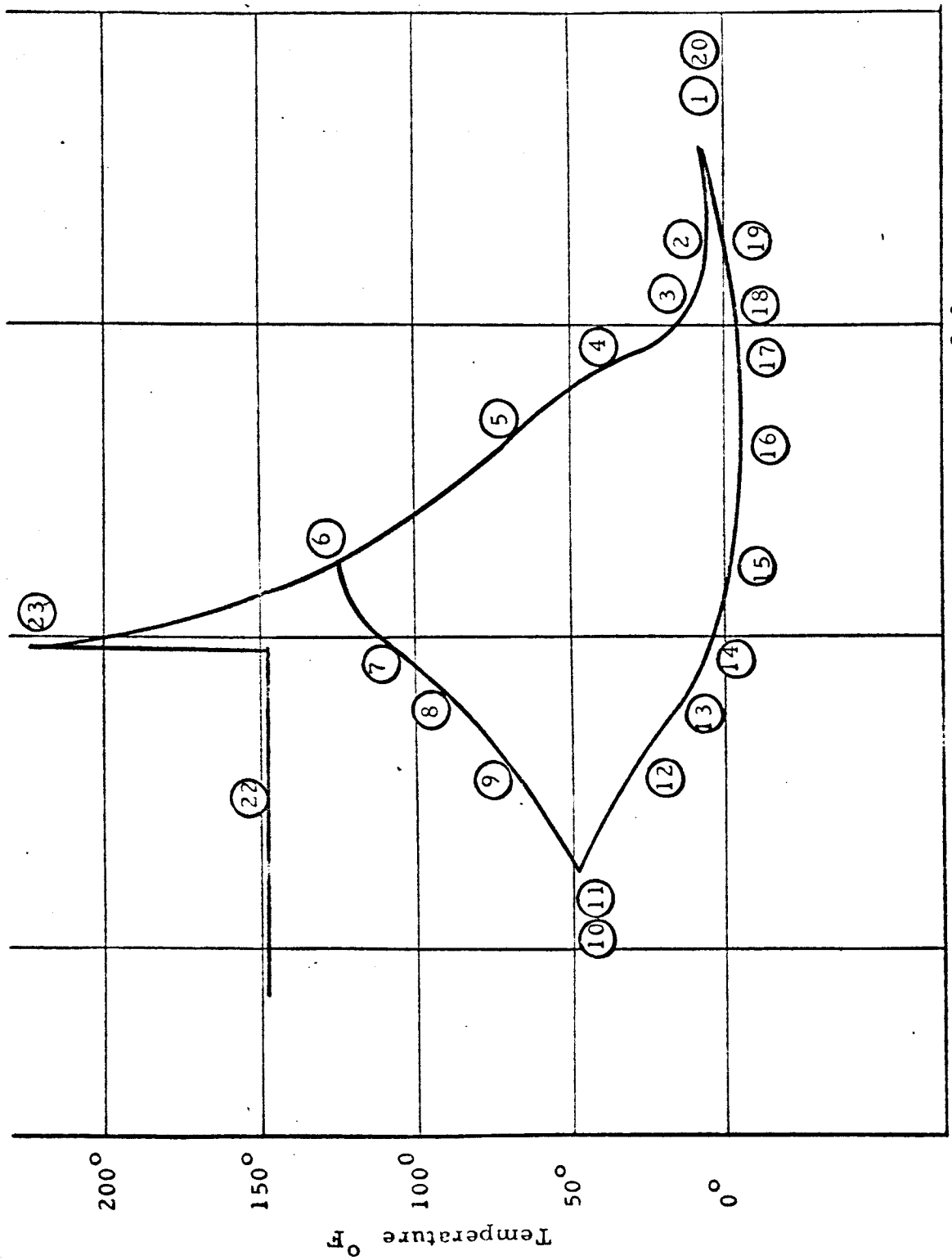

Beam Temperature Distribution -- White Paint

Figure 7 - 5

Figure 7 - 5

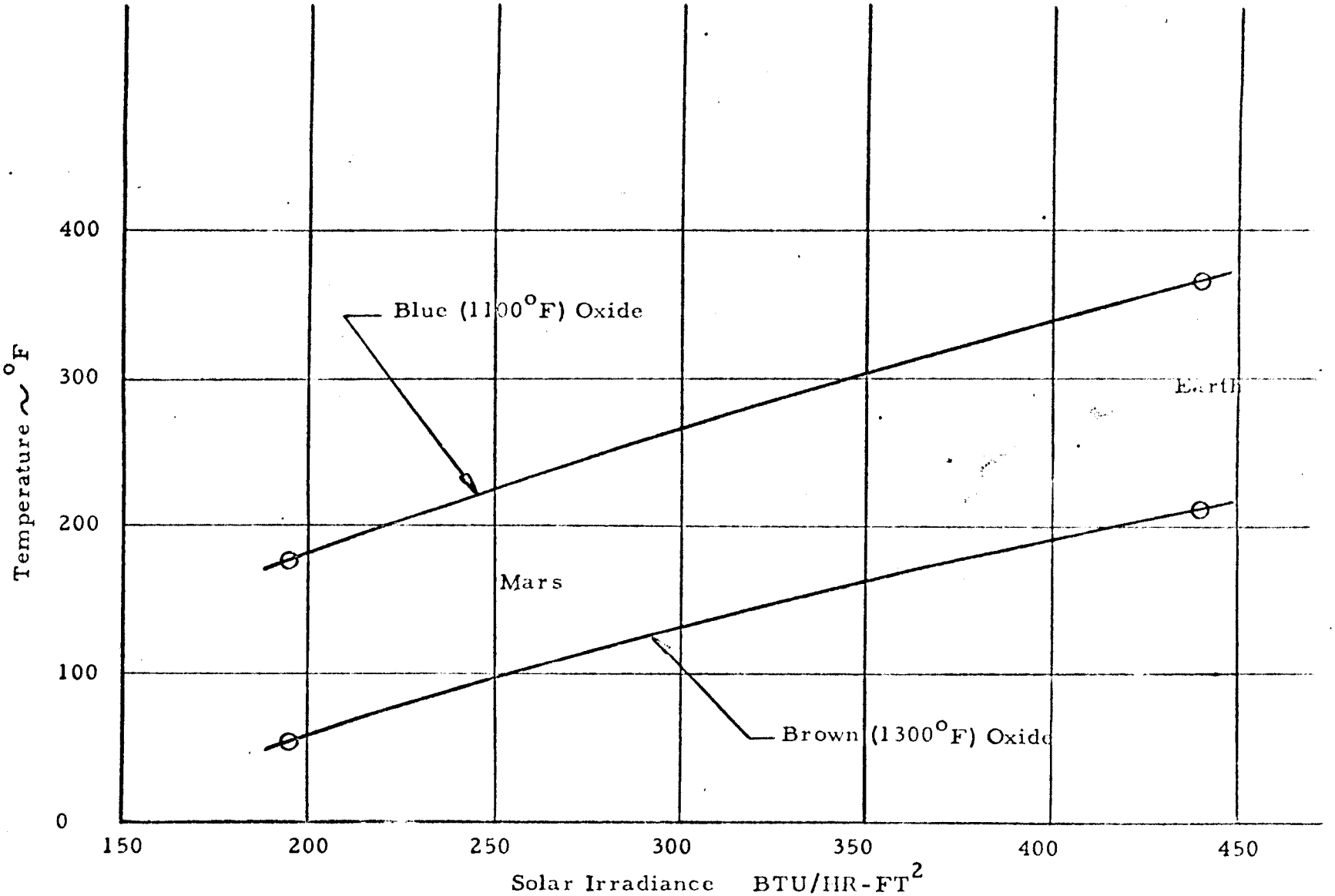

Figure 7 - 6

Maximum Beam Temperature of Blue and Brown Oxide Surface as a Function of Solar Irradiance

Figure 7 - 6

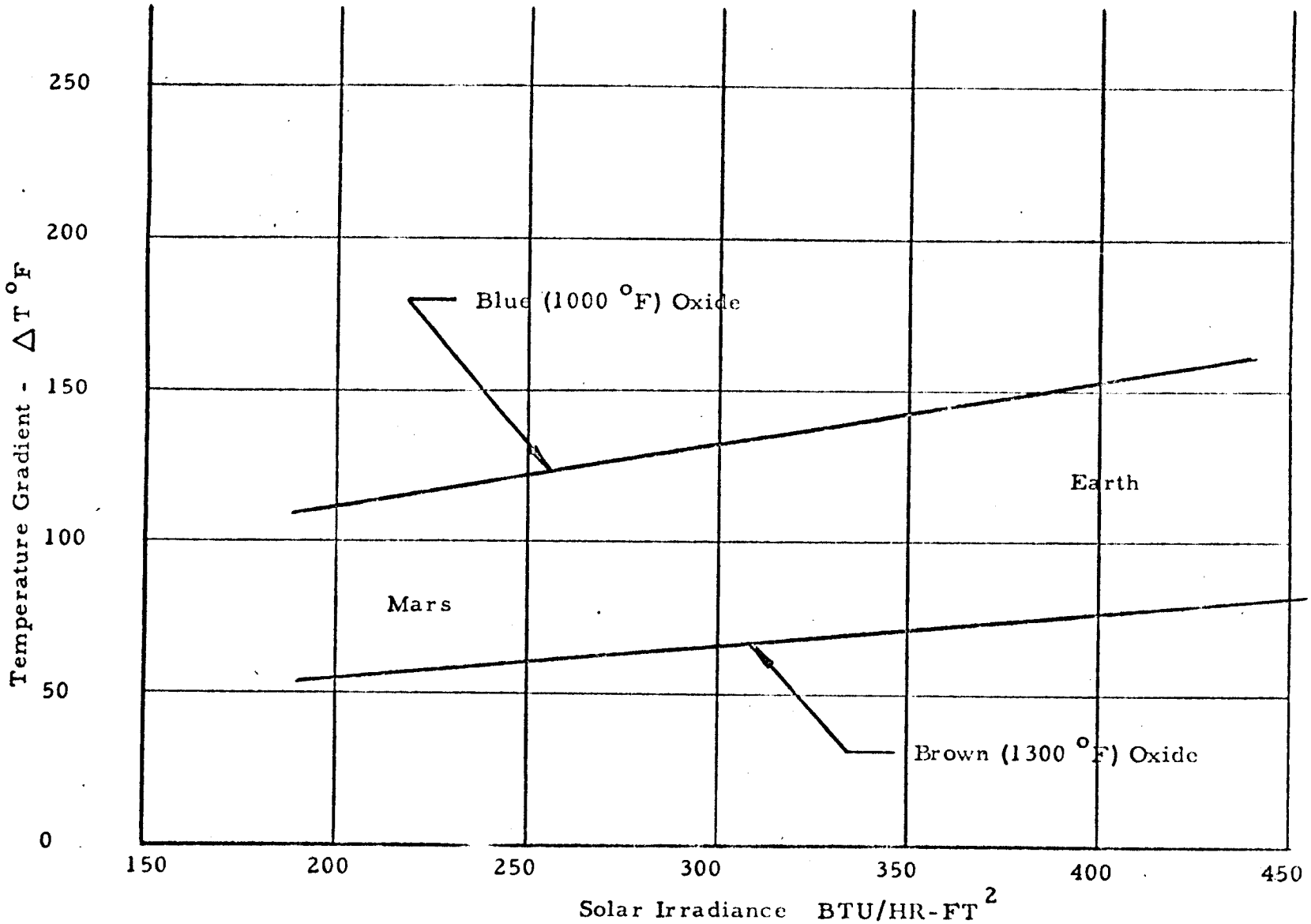

Figure 7 - 7

Beam Temperature Gradient for Blue and Brown Oxide Surface as a Function of Solar Irradiance

Figure 7 - 7

7.2.3 Effect of Brown Oxidized (1300° F) Titanium Surface on Beam Temperature

To supplement the precise analysis performed on the blue oxidized beams, a simplified mathematical model was constructed including 4 nodes, 2 conductive paths and 5 radiative paths. This model was used to predict the maximum temperatures and temperature gradients for brown oxidized beams in both Earth and Mars vicinity.

Figure 7-6 shows the maximum temperatures predicted for blue oxidized and brown oxidized titanium beams as a function of solar flux. Figure 7-7 shows the change of temperature gradient.

7.2.4 Simplified Solar Array Analysis

Using the measured thermal radiative properties for the fiberglass substrate and the teflon - RTV damping pad material, a simplified thermal analysis was performed of the solar array. This analysis assumes the following properties for solar cells with cover glass:

$$\alpha_s = .782$$

$$\epsilon = .82$$

The analysis accounts for front to back temperature gradients due to the generally poor conductive properties of the glass, fiberglass, RTV and bonding agents. Assuming the following physical properties:

backside damping pad area	3.0%	
backside fiberglass area	97.0%	
conductivity damping pad	.026	$\frac{BTU}{HR\ FT^{\circ}\ F}$
" fiberglass	.17	"
" glass	.3	"
thickness fiberglass	.006 in.	
" glass	.025 in.	
" damping pad	.12 in.	

Considering a space environment and solar orientation at 1 A.U. where the solar constant $\cong$ 440 $\frac{BTU}{HR\ FT^2}$ the following temperatures are realized.

Solar cells	131°F
Rear Fiberglass	129°F
Rear Damping Pad	80°F

7.2.5 Substrate Edge Connector Analysis

The substrate edge connector is coated with Cat-A-Lac 463-1-8 epoxy black paint. The temperature of this connector, assuming no conduction to adjacent materials can be calculated from the relationship

$$SA\alpha = 2\epsilon A \sigma \left(\frac{T^4}{100}\right)$$

$$\left(\frac{S\alpha}{2\epsilon\sigma}\right)^{1/4} = \left(\frac{T}{100}\right)$$

For a solar constant = 400 $\frac{BTU}{HR\ FT^2}$ and $\alpha/\epsilon = 1$ the connector temperature is calculated to be 140°F.

7.3 Design Verification Test

In order to verify the beam temperature distribution of 7.2.1, a thermal vacuum chamber test was devised. Since a solar simulator was not available for this test, it was determined that the test could only check the thermal model for conduction paths within the titanium and welded joints and the radiosity network corresponding to the internal surface oxide coating. Assuming that the temperature predicted for the front face for colimated solar energy is accurate, the test should then produce corresponding backside temperatures to that of the model.

7.3.1 Test Outline

The beam test section with a blue oxide coating on the front face and a

polished rear face was suspended within a thermal vacuum test chamber as shown in Figure 7-8. The front face and associated fiberglass panel and heat shield were mounted opposite to a blanket heater and radiating on the backside to the chamber cold wall which was maintained at -285°F. The backside of the heater was insulated (multiple reflective shields) to prevent heat loss and electrical energy was dissipated within the heater blanket until the front face attained 350°F. Thermocouple instrumentation is shown in Figure 7-9.

7.3.2 Test Results and Correlation of Analysis

The temperature distribution on the test article are shown as a function of beam position in Figure 7-10. For the test article with the front face set at 350°F, the back face (thermocouple 8) reached 176°F. This value compares to 180° F for the analytic model. Several deviations in the shape of the temperature curves may be noted. The fiberglass panel runs at a higher temperature than the analytic model. This is explained by its inability to reject heat in the direction of the heater blanket--as it would in space under sunlight. The elevated fiberglass panel temperature tends to elevate the beam temperature at the location of thermocouples 12 and 13. Thermocouples 10 and 11 are at lower temperatures than the model because of the action of the shield. The most significant deviations in test results from analysis are to be found in the temperature differences between nodes 12 and 13 and 10 and 11. The temperature difference at the weld joint between upper and lower halves of the beam indicates that the assumptions made with regard to conductance at the welded joint were incorrect in the analytic model. This will be corrected for future runs. A tabulation of significant test data is given in Table 7-1.

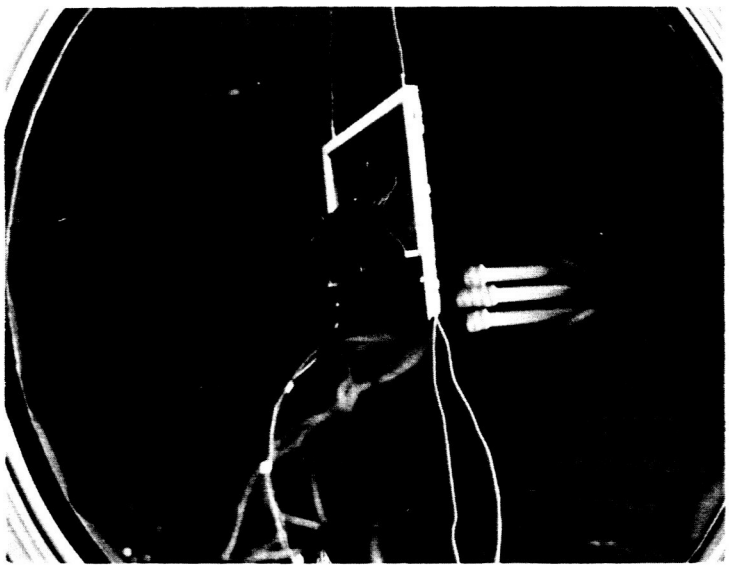

Figure 7 - 8 b Beam Section in Thermal-Vacuum Test Chamber

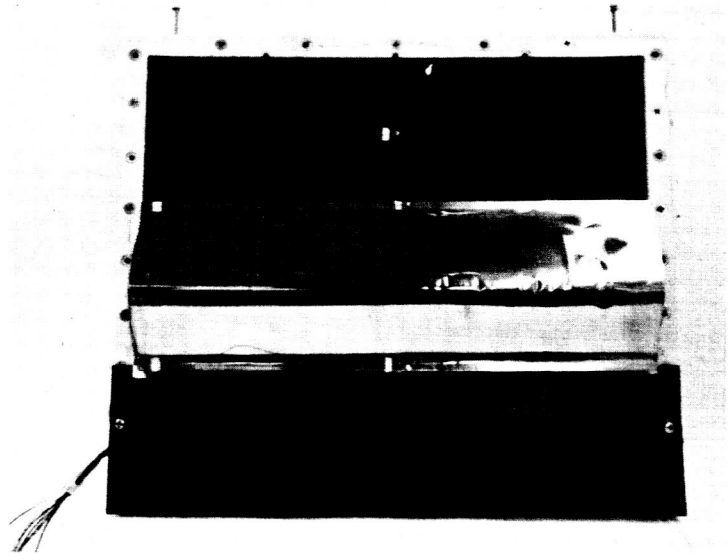

Figure 7 - 8 a Polished Rear Surface of Test Beam Section

Test Data of 1-11-66

Blue oxidized beam with polished rear face
Steady-state temperatures, Pressure 4 x 10^{-7} Torr, Heater power 108 watts, Heater Area 117 sq. inches

Thermocouple	Position	Temp °F
1	Beam	350
2	"	346
3	"	268
4	"	324
5	"	342
6	"	255
7	"	214
8	"	177
9	"	229
10	"	264
11	"	251
12	"	221
13	"	241
14	Titanium flange	399
15	Fiberglass	362
16	"	270
17	Heater	392*
18	"	394*
19	Cold Wall	-285
20	"	-287

* Heater temperatures low probably due to poor t/c attachment to rubber blanket

Table 7-1

7.4 Relation of Thermal Design to Design Criteria

7.4.1 Substrate Design

The substrate configuration and materials are compatible with the thermal requirements of Section 4. The total hemispherical emissivity has been measured for the fiberglass-epoxy sheet and the teflon damper pad surface. The test data indicate $\epsilon > 0.9$ for each material. The solar cell temperatures predicted are below the maximum state in Figure 4-2.

The distribution of damper pads on the rear surface of the substrate provides a minimum effect on front surface temperature.

7.4.2 Beam Design

The beam has been designed to control temperature and temperature gradients within limits necessary to meet design requirements. The brown oxide surface has been selected to maintain temperatures below $300^{\circ}F$ throughout the mission. Predicted gradients are below $80^{\circ}F$. Lower temperatures and gradients are attainable using white paint, however, this method of control requires additional weight.

The temperature distribution through the beam has been analyzed precisely for the blue oxide coating. Temperature distribution for the brown oxide coating will have a similar shape but translated to the lower range predicted.

The beam temperature distribution analysis is based on solid titanium attach strip connecting to the substrate. The effect of lightening holes in the edge attach strip will be to make the temperature distribution more symmetrical.

7.4.3 Effect of Thermal Gradient on Beam Deflection

The temperature difference between the beam surfaces will cause the beam to deform into a circular arc. The amount of deflection $\ominus$, can be calculated as a function of beam height and thermal coefficient of expansion of

the beam material.

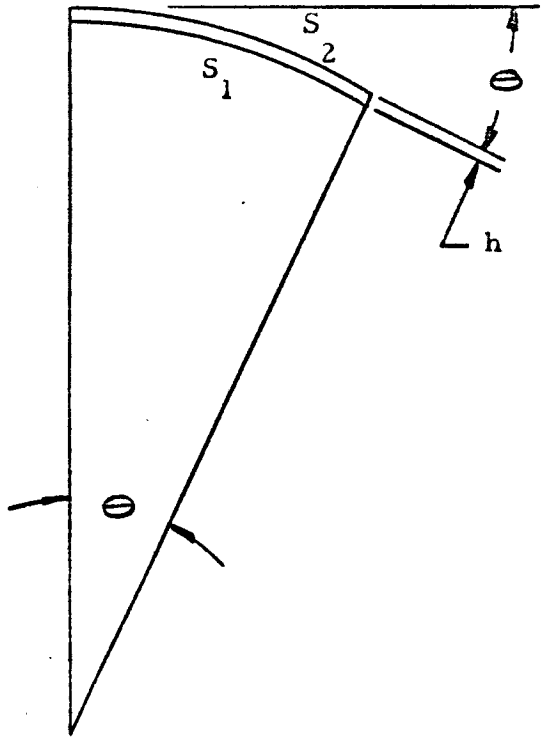

The relationship between the length of the upper and lower beam surface is given by

$$S_2 = S_1 \quad (1 + \alpha \Delta T)$$

where α = coefficient of thermal expansion, $5.2 \times 10^{-6}/^{\circ}F$

also $S_1 = r\theta$ and $S_2 = (r + h)\theta$

where h = height of beam

It follows that $S_2 = r\theta + h\theta = S_1 + h\theta$

$$\text{and } \theta = \frac{S_2 - S_1}{h} = \frac{S_1 (1 + \alpha \Delta T) - S_1}{h}$$

$$= \frac{S_1 \alpha}{h} \Delta T$$

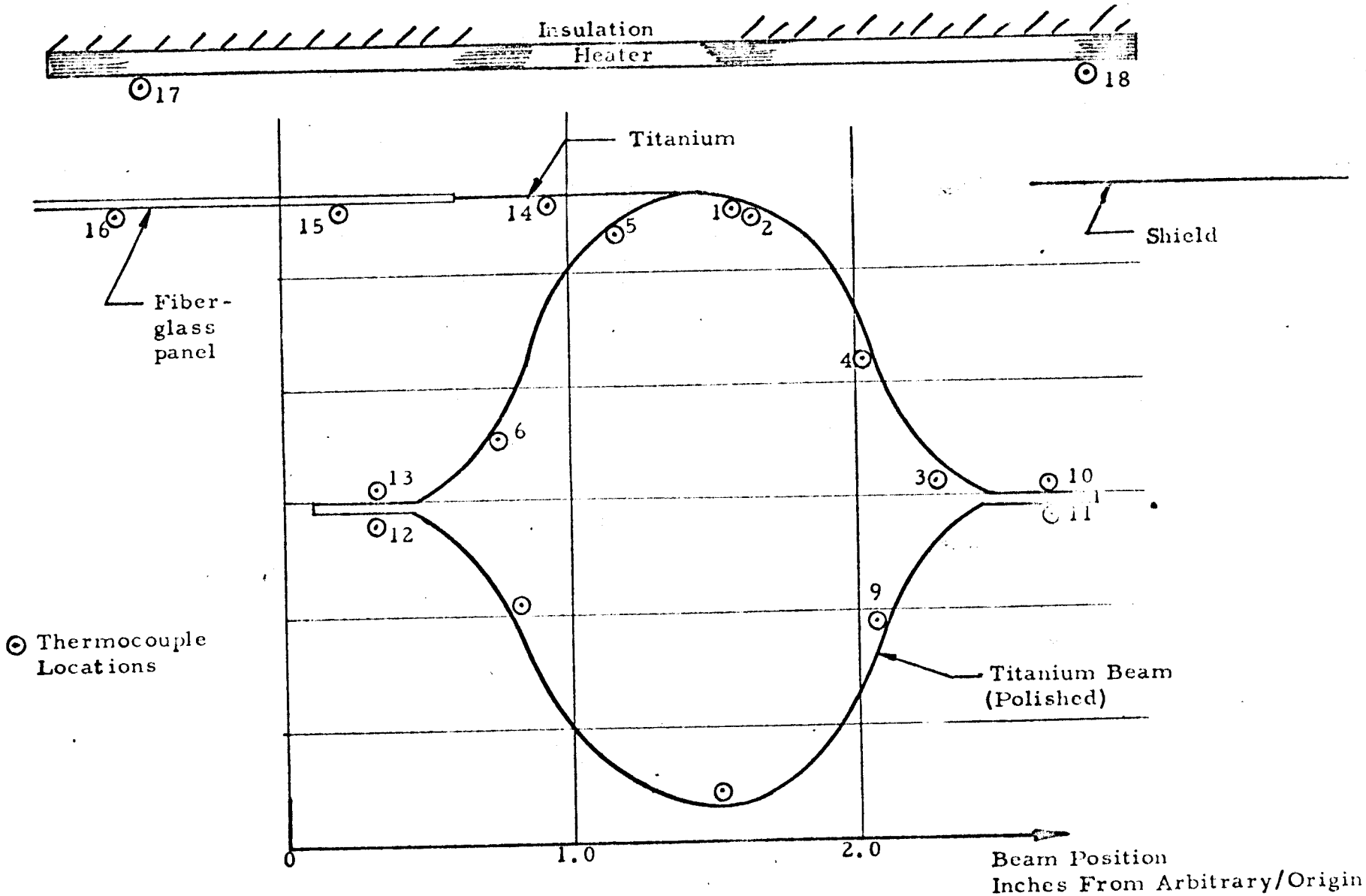

Figure 7 - 9

Schematic Test Assembly Showing Thermocouple Locations

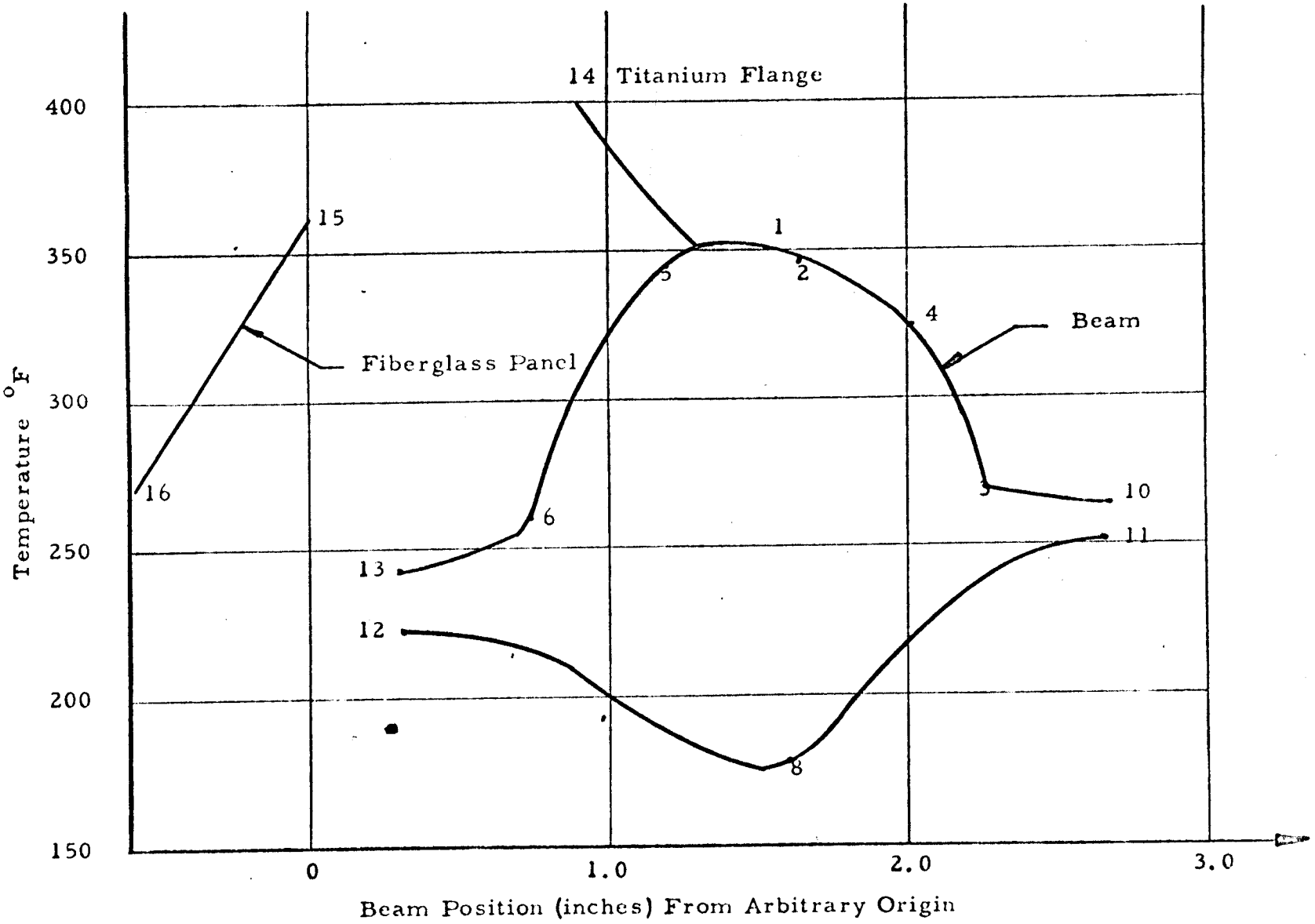

Figure 7 - 10

Beam Temperature Distribution Test

Figure 7 - 10

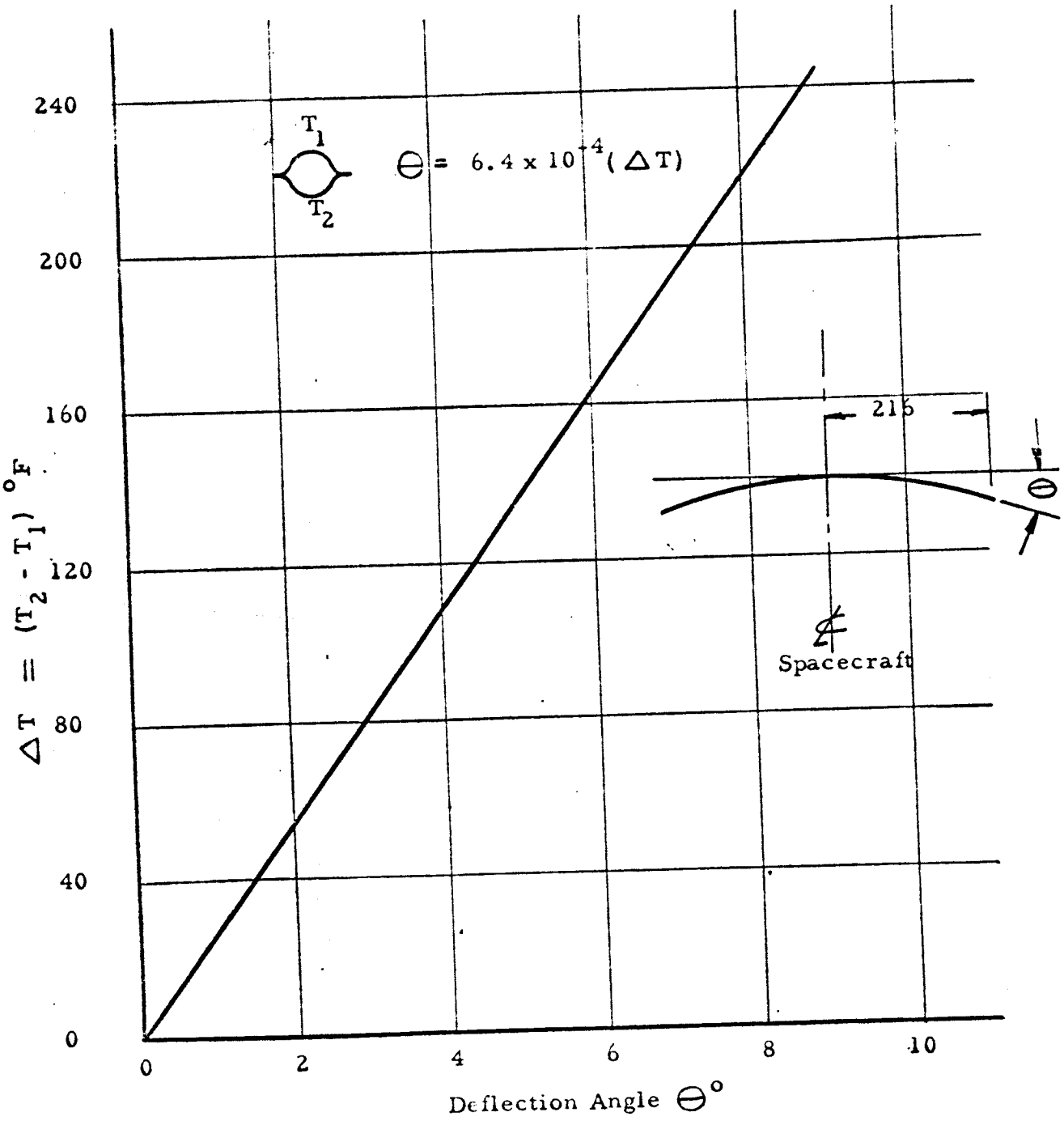

Beam Deflection as a Function of Thermal Gradient

Figure 7 - 11

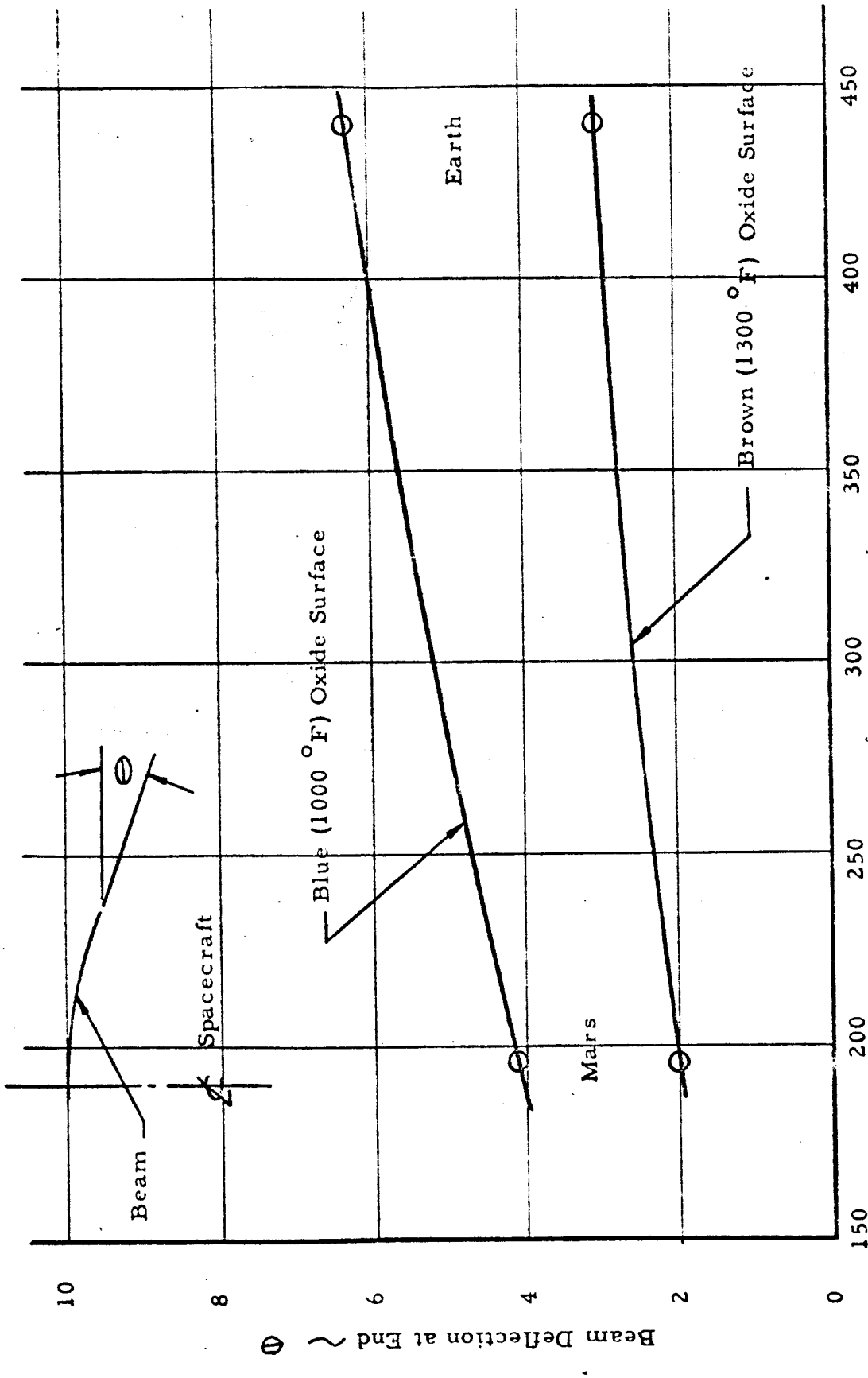

Beam Tip Deflection as a Function of Solar Irradiance

Figure 7 - 12

Figure 7 - 12

For $S_1 = 216$

$\alpha = 5.2 \times 10^{-6}$

$h = 1.75$

We have $\Theta = \frac{216 \times 5.2 \times 10^{-6}}{1.75} \Delta T$

$= 6.42 \times 10^{-4} \Delta T$

This relationship is plotted in Figure 7-11. Figure 7-12 shows the relationship of beam deflection to solar irradiance.

7.4.4 Effect of Beam Distortion on Solar Power

The beam curvature will cause the angle of incidence of solar radiation to vary along the length of the solar array. Assuming a cosine law variation, the total power available to the curved array can be expressed as:

$$W_c = w \int_0^s I_o \cos \Theta \, ds$$

where w = panel width

I_o = normal power intensity

s = length of array

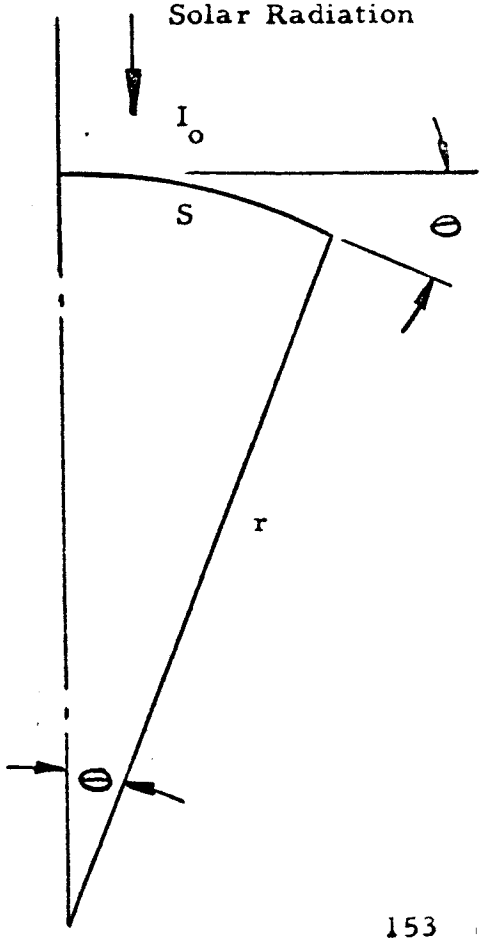

The total power available at normal incidence to a flat panel of the same size is

$$W_f = wsI_o$$

The effect of curvature on power conversion can be shown as the ratio of curved panel available power to flat panel available power

$$\text{efficiency} = \frac{W_c}{W_f} = \frac{W \int_0^s I_o \cos \Theta \, ds}{Ws \, I_o}$$

$$\frac{1}{s} \int_0^s \cos \Theta \, ds$$

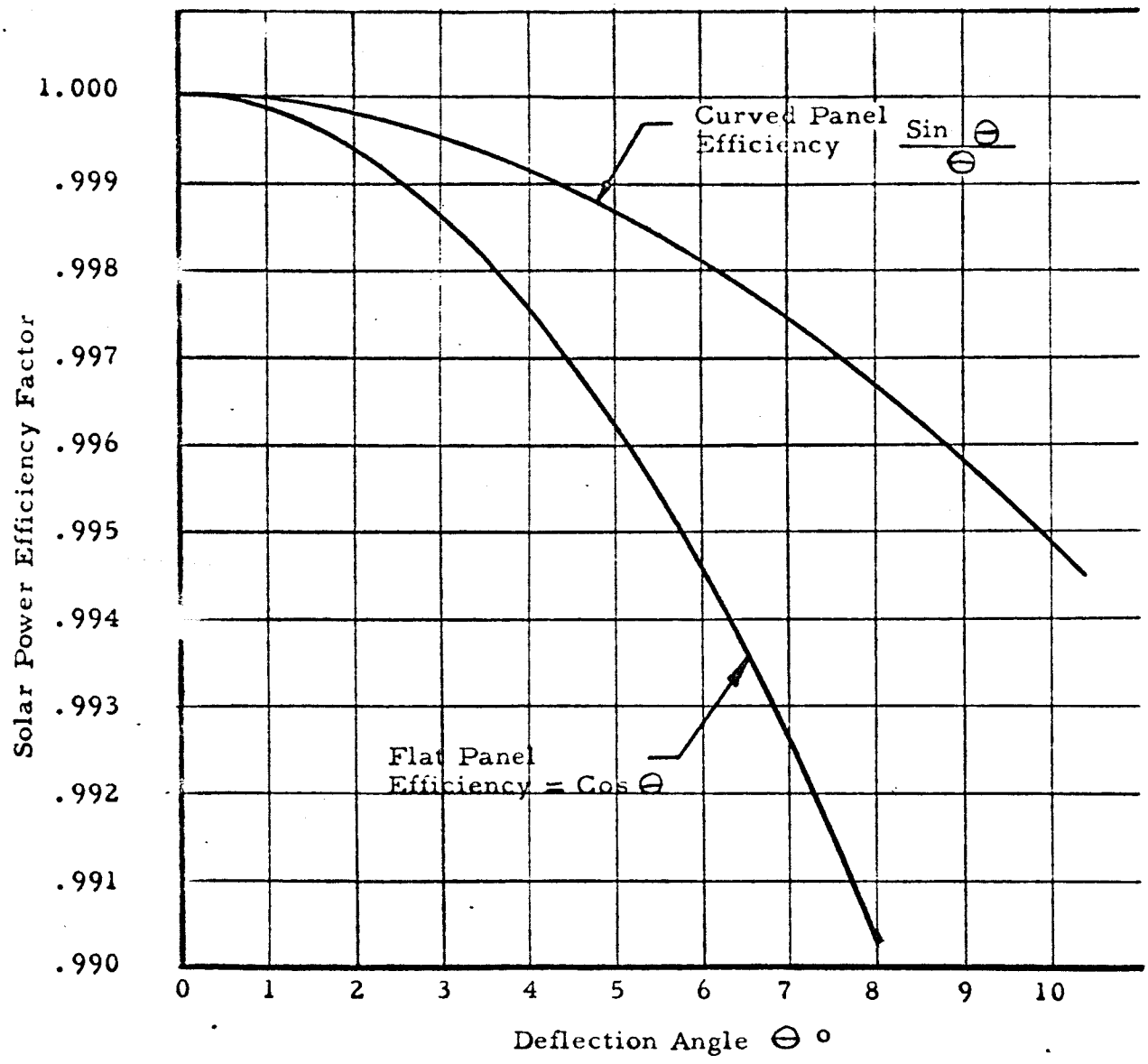

Solar Power Efficiency

vs

Beam Tip Deflection Angle

Figure 7 - 13

substituting $s = r\,\theta$ gives

$$\frac{W_c}{W_f} = \frac{1}{\theta} \int_0^{\theta} \cos\theta \; d\,\theta = \frac{\sin\,\theta}{\theta}$$

This efficiency function is plotted in Figure 7-13. A curved panel with a deflection angle of 8.7° at the tip would have an efficiency of .996. This would correspond to a flat panel whose angle of incidence was arc cos. 966 or 5°.

8.0 WEIGHT ANALYSIS, DEPLOYABLE PANEL ASSEMBLY

Weight variations are calculated assuming that all sheet thicknesses are maximum or minimum, based on design tolerance allowables. Where sheet thickness tolerances are not specified on drawings, commercial mill tolerances apply. Weight variations are calculated for use in satisfying the design criteria requirements as follows:

A. The first mass moment shall vary less than 5% as measured about the spacecraft thrust axis during powered flight. For the design presented, the requirement pertains to the array and support structure in the stowed position.

B. Cantilevered stiffness to mass shall vary less than 10%. This requirement pertains to the substrate support beams with substrate in the deployed position.

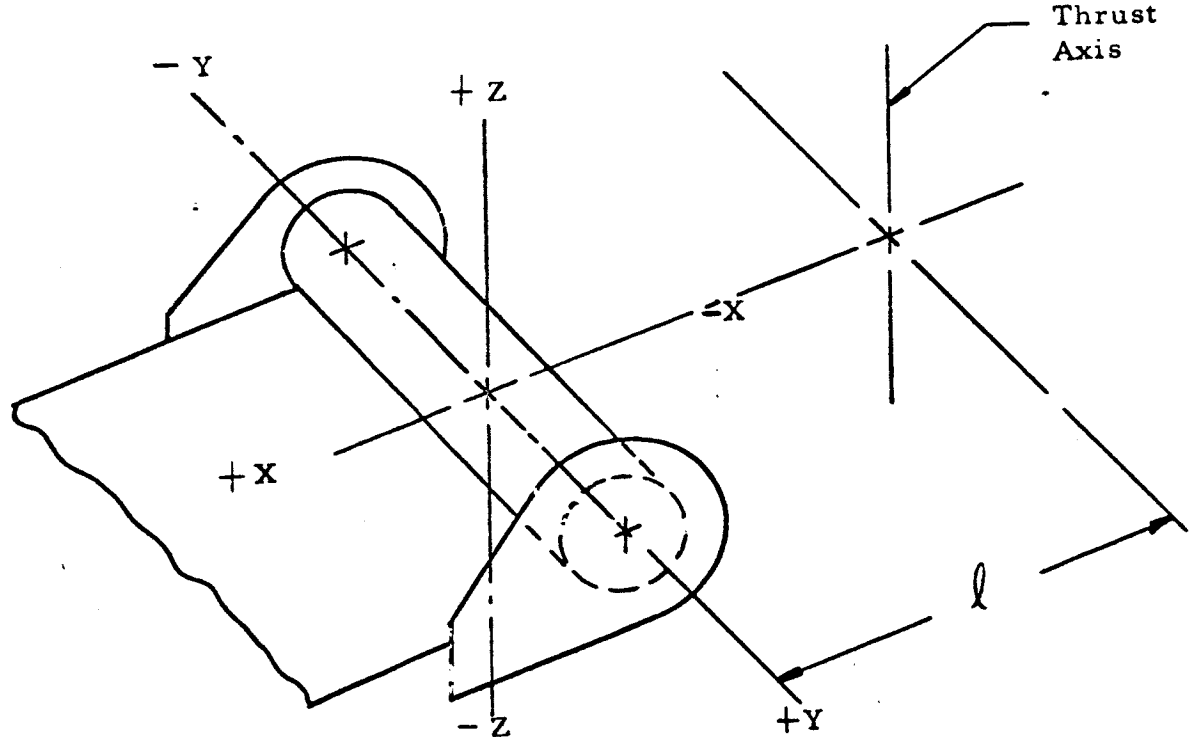

DEPLOYABLE SOLAR PANEL -- WEIGHT SUMMARY, TOTAL PER PANEL

Assembly Name	Dwg.No.	No. Req	Total Weight #		. Weight • $(\bar{X})$		WT_{avg} x $\bar{Z}avg$	Unit WT # Ft^2	
			Max	Min	Max	Min		Max	Min
Beam Guide	208V004	2	1.537	1.408	10.150	9.318	8.79	.031	.028
Drum Assembly	208V003	1	4.837	4.438	-.189	-.174	.171	.097	.089
Harness Assembly *	208V008	1	.387	.367	.159	.150	-.131	.0077	.0073
Panel Assembly	208V001	1	2.076	2.004	45.49	40.076	3.973	.042	.040
Substrate Assembly	208V005	1	2.3035	1.8753	0	0	0	.046	.038
End Cap	208V006	2	4.254	3.732	2.960	2.488	1.382	.085	.075
Support Structure *	208V002	1	2.078	1.965	-19.39	-18.301	0	.042	.039
Beam Installation	208V007	1	5.550	5.104	7.057	6.405	2.382	.111	.101
Total			23.02	20.89	46.237	39.962	-13.934	.462	.417
Total Less *			20.34	18.34				.413	.371
Total less items req'd for substrate modularization			22.41	20.33				.454	.411

$$\bar{Z} = \frac{\sum WT_{avg}(Z)}{WT_{avg}} = \frac{-13.934}{21.96} = \underline{-.635}$$

$$\bar{X}_{max} = \frac{\sum WT_{max}(X)}{WT_{max}} = \frac{46.237}{23.02} = \underline{2.009}$$

$$\bar{X}_{min} = \frac{\sum WT_{min}(X)}{WT_{min}} = \frac{39.962}{20.89} = \underline{1.913}$$

TABLE 8-1

The hypothetical variation in the first mass moment about the spacecraft thrust axis for the stowed array assuming all sheet thicknesses maximum or all minimum is calculated as follows:

Based on Weight $_{(min)}$,

$$I_{(mass)} = \frac{Wt_{(min)}}{g} \left(\ell + \bar{X}_{min} \right)^2$$

$$= \frac{20.89}{386.4} \quad (32 + 1.913)^2 = 62.17 \text{ lb-in-sec}^2$$

Based on Weight $_{(max)}$,

$$I_{(mass)} = \frac{Wt_{(max)}}{g} \left(\ell + \bar{X}_{max} \right)^2$$

$$= \frac{23.02}{386.4} \quad (32 + 2.009)^2 = 68.91 \text{ lbs-in-sec}^2$$

The variation, then, is,

$$\frac{68.91 - \frac{1}{2}(68.91 + 62.17)}{\frac{1}{2}(68.91 + 62.17)} = \frac{3.37}{65.54} = \pm \underline{5.1}\ \%$$

Based on Ryan's experience with solar panel fabrication, a variation of $\pm$ 2.5 % is reasonable.

The hypothetical variation in the cantileverd stiffness to mass ratio of the deployed substrate structure is calculated as follows:

Based on maximum stiff beams and minimum weight substrate,

$$\frac{K}{W/g} = \frac{.02596}{7.56/386.4} = 1.33 \quad \frac{\text{in.}^5}{\text{lbs-sec}^2}$$

Based on minimum stiff beams and maximum weight substrate,

$$\frac{K}{W/g} = \frac{.02398}{7.57/386.4} = 1.22 \ \frac{\text{in.}^5}{\text{lbs.-sec}^2}$$

The variation, then, is

$$\frac{1.33 - \frac{1}{2}(1.33 + 1.22)}{\frac{1}{2}(1.33 + 1.22)} = \frac{.005}{1.275} = \pm \underline{\underline{4.3}}\ \%$$

WEIGHT AND CG DATA

Drawing No. 208V004

Drawing Title: Beam Guide Installation - Deployable Panel

Dash No	Req. No.	Unit Weight lbs. Max	Unit Weight lbs. Min	X, in	Z, in.	Weight (X) Max	Weight (X) Min	$Wt_{avg}(Z_{avg})$
-21	1	.019	.018	+10.6	-5.447	.201	.191	-.101
-23	1	.0035	.0033	-10.6	-6.705	.037	.035	-.023
-25	1	.0111	.0106	+10.6	-6.839	.118	.112	-.074
-27	1	.0089	.0085	+10.6	-6.280	.094	.090	-.055
-29	2	.0370	.0350	- 6.6	-6.03	.488	.462	-.434
-31	4	.0030	.0028	+ 6.425	-6.28	.077	.072	-.073
-33	1	.0071	.0067	+ 6.30	-5.68	.045	.042	-.039
-34	1	.0071	.0067	+ 6.30	-5.68	.045	.042	-.039
-35	1	.0071	.0067	+ 8.79	-5.77	.062	.059	-.040
-37	1	.0089	.0085	+ 8.79	-6.155	.078	.075	-.054
-39	1	.0095	.0090	+ 6.77	-5.72	.064	.061	-.053
-41	1	.0101	.0096	+ 6.77	-6.120	.068	.065	-.060
-43	1	.0104	.0099	+ 5.83	-6.09	.061	.058	-.062
-45	1	.0089	.0085	+ 5.83	-5.845	.052	.050	-.051
-47	1	.0126	.0120	+ 4.07	-5.88	.051	.049	-.072
-49	1	.0160	.0152	+ 4.07	-6.11	.065	.062	-.095
-51	1	.0082	.0078	+ 2.65	-6.68	.022	.021	-.053
-53	1	.0066	.0063	+10.6	-5.83	.070	.067	-.038
-54	1	.0066	.0063	+10.6	-5.83	.070	.067	-.038
-55	2	.0040	.0038	+10.6	-6.28	.085	.081	-.049
-57	2	.00225	.00214	+ 6.4	-4.34	.029	.027	-.019
-59	1	.0356	.0338	+ 5.705	-5.27	.203	.193	-.183
-60	1	.0356	.0338	+ 5.705	-5.27	.203	.193	-.183
-61	1	.0378	.0342	+ 6.3	-5.08	.238	.215	-.183
-63	1	.0023	.0021	+ 6.3	-5.08	.014	.013	-.011
-65	1	.0112	.0102	+ 6.3	-5.085	.071	.064	-.054
-67	1	.0080	.0072	+ 6.3	-5.08	.050	.045	-.039
-69	1	.0024	.0022	+ 6.3	-5.08	.015	.014	-.012
-71	1	.0092	.0084	+ 6.3	-5.08	.058	.053	-.045
-73	1	.0053	.0048	+ 6.3	-5.08	.033	.030	-.026
-75	2	.0086	.0086	+ 6.3	-5.34	.108	.103	-.090
-7	1	.0470	.0423	+ 6.425	-6.83	.302	.272	-.305

WEIGHT AND CG DATA

Drawing No. 208V004 Continued

Dash No	Req. No.	Unit Weight lbs. Max	Unit Weight lbs. Min	X, in.	Z, in.	Weight (X) Max	Weight (X) Min	$Wt_{avg}(Z_{avg})$
-9	1	.0429	.0386	+ 6.425	-6.83	.276	.248	-.278
-11	1	.0838	.0754	+ 6.425	-5.447	.538	.484	-.434
-13	2	.0138	.0113	+ 6.425	-6.38	.177	.145	-.160
-15	1	.1039	.0940	+ 6.425	-6.28	.668	.604	-.621
-17	1	.0185	.0151	+ 5.9	-7.28	.109	.089	-.122
-19	1	.0202	.0165	+ 6.425	-6.90	.130	.106	-.127
Sub Total		.7686	.7041			5.075	4.659	-4.395

$$\bar{Z} = \frac{\sum Wt_{avg} \cdot (Z_{avg})}{\sum Wt_{avg}} = \frac{4.395}{.7364} = \underline{5.968"}$$

$$\bar{X}_{(max)} = \frac{\sum Wt. \cdot (X)_{max}}{\sum Wt._{max}} = \frac{5.075}{.7686} = \underline{6.603"}$$

$$\bar{X}_{(min)} = \frac{\sum Wt. \cdot (X)_{min}}{\sum Wt._{min}} = \frac{4.659}{.7041} = \underline{6.617"}$$

WEIGHT AND CG DATA

Drawing No. 208V003

Drawing Title: Drum Assembly, Deployable Solar Panel (1 required per panel assembly)

Dash No.	Req. No.	Unit Weight lbs. Max	Unit Weight lbs. Min	X, in	Z, in	Weight (X) Max	Weight (X) Min	$Wt_{avg}(Z_{avg})$
208V009	1 (Gear)	.2741	.2479	0	0	0	0	0
-15	1	2.093	1.936	0	0	0	0	0
-17	2	.0063	.0057	0	0	0	0	0
-19	2	.0126	.0113	0	0	0	0	0
-23	1	.0820	.0759	0	0	0	0	0
-25	1	.0287	.0265	0	0	0	0	0
-27	2	.0031	.0028	0	0	0	0	0
-29	2	.0026	.0024	-4	-4	-.021	-.019	-.010
-31	1	.0154	.0142	-4	-4	-.062	-.057	-.059
-33	1	.0266	.0246	-4	-4	-.106	-.098	-.102
-37	1	.1374	.1271	0	0	0	0	0
-39	1	.0557	.0469	0	0	0	0	0
-41	2	.006	.0054	0	0	0	0	0
-45	2	.6143	.5528	0	0	0	0	0
-47	2	.0180	.0171	0	0	0	0	0
-49	2	.3990	.3718	0	0	0	0	0
Sub Total		4.837	4.438			-.189	-.174	-.171

$$\bar{Z} = \frac{\sum Wt_{avg}\ (Z_{avg})}{\sum Wt_{avg}} = \frac{.171}{4.638} = \underline{-.037"}$$

$$\bar{X}_{(max)} = \frac{\sum Wt\ (X)_{max}}{\sum Wt_{max}} = \frac{-.189}{4.837} = \underline{-.039"}$$

$$\bar{X}_{(min)} = \frac{\sum Wt\ (x)_{Min}}{\sum Wt_{min}} = \frac{-.174}{4.438} = \underline{.039"}$$

WEIGHT AND CG DATA

Drawing No. 208V008

Drawing Title Harness Assembly, Deployable Panel (1 required per panel assembly)

Dash No.	Req. No.	Unit Weight lbs Max	Unit Weight lbs Min	X, in	Z, in	Weight (X) Max	Weight (X) Min	$Wt_{avg}(Z_{avg})$
-9	1	.0183	.0146	0	0	0	0	0
-11	2	.00145	.00135	+1.0	0	.0029	.0027	0
-13	1	.0018	.0017	+ .9	0	.0016	.0015	0
-15	1	.0071	.0066	+4.6	-1.3	.0327	.0304	-.009
-17	1	.0630	.0600	+ .7	+1.2	.0441	.0420	-.074
-19	1	.0620	.0590	+1.2	.8	.0744	.0708	-.048
-21	2	.00063	.00051	0	0	0	0	0
-23	20	.00007	.000068	0	0	0	0	0
-5	1	.0562	.0505	0	0	0	0	0
-7	1	.0327	.0294	0	0	0	0	0
Misc.		.1400	.1400	0	0	0	0	0
Sub Total		.387	.367			.159	.150	-.131

$$\bar{Z} = \frac{\sum Wt_{avg}\ (Z_{avg})}{\sum Wt_{avg}} = \frac{.131}{.377} = \underline{-.347"}$$

$$\bar{X}_{(max)} = \frac{\sum Wt\ (X)_{max}}{\sum Wt_{max}} = \frac{.159}{.387} = \underline{.411"}$$

$$\bar{X}_{(min)} = \frac{\sum Wt\ (X)_{min}}{\sum Wt_{min}} = \frac{.150}{.367} = \underline{.409"}$$

WEIGHT AND CG DATA

Drawing No. 208V001

Drawing Title: Deployable Solar Panel Assembly

Dash No.	Req. No.	Unit Weight lbs. Max	Unit Weight lbs. Min	X, in	Z, in.	Weight (X) Max	Weight (X) Min	$Wt_{avg}(Z_{avg})$
-3	1	.0362	.0344	5.4	0	.1955	.1858	0
208V012	76	.0022	.0018	117.5	-7.18	19.646	16.074	-1.091
Bearing	2	.130	.130	0	0	0	0	0
-13	1	.0103	.0093	5.4	0	.0556	.0502	0
Motor	1	.750	.750	5.4	0	4.05	4.05	0
Misc.	1 set	.177	.177	-	-	-	-	-
-11	5	.026	.0234	117.5	-7.18	15.275	13.747	-.887
-9	1	.545	.519	11.5	-3.75	6.268	5.969	-1.995
Sub Total		2.076	2.004			45.49	40.076	-3.973

$$\bar{Z} = \frac{Wt_{avg}(Z_{avg})}{Wt_{avg}} = \frac{3.973}{2.04} = \underline{1.948}$$

$$\bar{X}_{(max)} = \frac{Wt\ (X)_{max}}{Wt_{max}} = \frac{45.49}{2.076} = \underline{21.912}$$

$$\bar{X}_{(min)} = \frac{Wt\ (X)_{min}}{Wt_{min}} = \frac{40.076}{2.004} = \underline{19.998}$$

WEIGHT AND CG DATA

Drawing No. 208V007

Drawing Title: Beam Installation - Deployable Solar Panel

Dash No.	Req. No.	Unit Weight lbs. Max	Unit Weight lbs. Min	X, in	Z, in	Weight (X) Max	Weight (X) Min	$Wt_{avg}(Z_{avg})$
-7	4	1.011	.934	.259	-.259	1.047	.971	1.009
-9	2	.167	.154	.250	-.250	.084	..077	.080
-11	2	.015	.014	0	0	0	0	0
-15	2	..032	..030	12.135	0	.777	.728	0
-17	2	.147	.132	12.2	-6.28	3.587	3.221	-.876
-19	2	.052	.047	12.51	-6.28	1.301	1.176	-.311
-21	4	.051	.047	.259	-.259	.053	.05	.005
-23	4	..006	.005	0	0	0	0	0
-25	2	.213	.192	0	0	0	0	0
-27	1	.016	.014	13.01	-6.78	.208	.182	.101
Misc	1	.010	.008	0	0	0	0	0
Sub Total		5.550	5.104			7.057	6.405	-2.382

$$\bar{Z} = \frac{\sum Wt_{avg}(Z_{avg})}{\sum Wt_{avg}} = -.\underline{447}$$

$$\bar{X}_{(max)} = \frac{\sum Wt \cdot (X)_{Max}}{\sum Wt_{max}} = \frac{7.057}{5.55} = \underline{1.272}$$

$$\bar{X}_{(min)} = \frac{\sum Wt \cdot (X)_{Min}}{\sum Wt_{min}} = \frac{6.405}{5.104} = \underline{1.255}$$

WEIGHT AND CG DATA

Drawing No. 208V013

Drawing Title: Substrate Assembly - Deployable Solar Panel (1 required per panel assembly or 208V005)

Dash No.	Req. No.	Unit Weight lbs. Max	Unit Weight lbs. Min	X, in	Z, in	Weight (X) Max	Weight (X) Min	$Wt_{avg}(Z_{avg})$
-5	1	1.7794	1.4559	0.	0	0	0	0
-7	672 Total wt.	.1134	.0906	^	^	^	^	^
-9	672 Total wt.	.0229	.0183	|	|	|	|	|
-11	1	.0180	.0164	v	v	v	v	v
-13	1	.0075	.0069					
Bond	AR	.080	.054	0	0	0	0	0
Sub Total		2.0212	1.6421					

$$\bar{Z} = \frac{\sum Wt_{avg}(Z_{avg})}{\sum Wt_{avg}} = 0$$

$$\bar{X}_{max} = \frac{\sum Wt \cdot (X)_{max}}{\sum Wt_{max}} = 0$$

$$\bar{X}_{min} = \frac{\sum Wt \cdot (X)_{min}}{\sum Wt_{min}} = 0$$

WEIGHT AND CG DATA

Drawing No. 208V005

Drawing Title: Substrate Assembly - Deployable Solar Panel (1 required per panel assembly or 208V0013)

Dash No.	Req. No.	Unit Weight lbs. Max	Unit Weight lbs. Min	X, in	Z, in	Weight (X) Max	Weight (X) Min	$Wt_{avg}(Z_{avg})$
-7	4	.4897	.4025	0	0	0	0	0
-9	4	.0130	.0102	↑	↑	↑	↑	↑
-11	3	.0130	.0102					
-13	1	.0158	.0130					
-15	1	.0309	.0253					
-23	655 total wt.	.0222	.0178					
-25	655 total wt.	.1048	.0838	↓	↓	↓	↓	↓
Misc.Bond	AR	.080	.054	0	0	0	0	0
Sub Total		2.3035	1.8753					

$$\bar{Z} = \frac{\sum Wt_{avg}(Z_{avg})}{\sum Wt_{avg}} = 0$$

$$\bar{X}_{max} = \frac{\sum Wt \cdot (X)_{max}}{\sum Wt_{max}} = 0$$

$$\bar{X}_{min} = \frac{\sum Wt \cdot (X)_{min}}{\sum Wt_{min}} = 0$$

WEIGHT AND CG DATA

Drawing No. 208V006-1

Drawing Title: End Cap Assembly - Deployable Solar Panel (One -1 & one -2 required(-1 = -2 less item 41)

Dash No.	Req. No.	Unit Weight lbs. Max	Unit Weight lbs. Min	X, in	Z, in	Weight (X) Max	Weight (X) Min	$Wt_{avg}(Z_{avg})$
-3	22	.0372	.0295	- 1.2	+1.2	-.982	-.779	+ .880
-6	1	.066	.060	+ 2.62	-2.2	+.173	-.157	- .139
-8	1	.0523	.0487	0	-1.5	0	0	- .076
-10	1	.0543	.0507	+ .30	+1.5	+.016	+.015	+ .079
-11	1	.096	.090	+ 7.375	+1.0	+.708	+.664	+ .093
-13	1	.0585	.0548	+ 8.5	-3.8	+.497	+.466	- .215
-15	1	.0468	.0421	+7.5	-4.9	+.351	+.315	- .218
-17	1	.0310	.0290	+2.3	0	+.071	+.067	0
-20	1	.167	.158	- .5	+1.4	-.084	-.079	+ .228
-22	1	.211	.202	- 1.0	+ .7	-.211	-.202	+.145
-24	1	.0122	.0115	+10.5	-6.20	+.128	+.121	- .073
-26	1	.0055	.0052	+11.00	-5.75	+.061	+.057	- .031
-28	1	.015	.014	+11.3	-3.15	+.170	+.158	- .046
-29	1	.018	.017	+11.3	-4.3	+.203	+.192	- .075
-31	1	.0097	.0091	+ 2.0	0	+.019	+.018	0
-34	1	.0075	.0069	+ 8.15	-8.1	+.061	+.056	- .058
-36	1	.284	.263	- .5	+1.4	-.142	-.132	+ .383
-38	1	.0916	.0824	0	0	0	0	0.
-39	2	.0074	.0067	+10.6	-6.28	-.157	+.142	- .088
-41	1	.0348	.0314	0	0	0	0	0
Misc.		.05	.05	0	0	0	0	0
Sub Total	-1 Ass'y	2.144	1.882			+1.480	+1.244	+.691
Sub Total	-2 Ass'y	2.110	1.850			+1.480	+1.244	+.691
Sub Total	-1 & -2	4.254	3.732			+2.960	+2.488	+1.382

$$\bar{Z} = \frac{\sum Wt_{avg}(Z_{avg})}{\sum Wt_{avg}} = \frac{1.382}{3.993} = +\underline{.346}$$

$$\bar{X}_{max} = \frac{\sum Wt_{max}(X)_{max}}{\sum Wt_{max}} = \frac{2.96}{4.254} = +\underline{.696"} \quad , \quad \bar{X}_{min} = \frac{\sum Wt_{min}(X)_{min}}{\sum Wt_{min}} = \frac{2.488}{3.732} = +\underline{.666"}$$

WEIGHT AND CG DATA

Drawing No. 208V002

Drawing Title: Solar Array Installation, Support Structure

Dash No.	Req. No.	Unit Weight lbs. Max	Unit Weight lbs. Min	X, in	Z, in	Weight (X) Max	Weight (X) Min	$Wt_{avg}(Z_{avg})$
-5	2	.170	.159	- 8.5	0	-2.890	-2.703	0
-7	2	.219	.206	-10.6	0	-4.643	-4.367	0
-9	1	.209	.196	- 5.0	0	-1.045	- .980	0
-11	2	.126	.118	- 6.12	0	-1.542	-1.444	0
-13	1	.036	.034	- 9.00	0	- .324	- .306	0
-15	2	.172	.164	-14.5	0	-4.988	-4.756	0
-17	2	.081	.077	-14.5	0	-2.349	-2.233	0
-19	2	.007	.0065	- 5.0	0	- .07	- .065	0
-21	2	.0097	.009	- 5.0	0	- .097	- .090	0
-23	2	.068	.064	-10.6	0	-1.442	-1.357	0
Misc	AR	.128	.128	0	0	0	0	0
Sub Total		2.078	1.965			-19.39	-18.301	

$$\bar{X}_{(min)} = \frac{\sum Wt_{min}(X_{min})}{\sum Wt_{min}} = \frac{18.301}{1.965} = \underline{9.313"}$$

$$\bar{X}_{(max)} = \frac{\sum Wt_{max}(X_{max})}{\sum Wt_{max}} = \frac{19.39}{2.078} = \underline{9.331"}$$

9.0 MATERIALS

9.1 Introduction

Materials used in the design have been chosen with regard to the functional and environmental requirements stated in Section 4.0. The selection of materials has been based on their ability to withstand deep space environment. Resistance to solar radiation, penetrating radiation, hard vacuum, high and low temperatures and other factors have been considered. Although a large number of materials can meet these environmental conditions, the special requirements of the deployable array concept have largely dictated specific materials choices.

One significant factor affecting material selection is the sterilization requirement of 108 hours at 145°C. During this procedure, the array structure will be in the stowed position in which many components will be deformed from their natural shape. The process precludes the use of many otherwise acceptable polymeric materials which would be expected to creep during sterilization. However, all materials which have been designated are heat resistant and capable of withstanding the sterilization procedure. It can also be noted that as a rule, the higher heat resistant polymers are more stable in the deep space environment than those of lower heat stability (Reference 21 and 30).

Non-magnetic materials are used throughout the structure assembly except for the drive motor. Metals used in the structure are magnesium, aluminum, titanium, corrosion resistant steel, beryllium-copper and brass. The non-metallic materials can be classified as epoxy, teflon or silicone. A summary list of materials is given in Paragraph 9.7.

Materials have been selected whose properties are well known and which can be processed within the state-of-the-art. Materials whose implementation would require research programs have been avoided.

Limited materials testing and process development have been conducted as needed to establish properties or processes peculiar to the design

requirements. This work has been previously described in the preliminary development report No. 20869-1 (Reference 8) and is summarized herein as it pertains to the selected design.

9.2 Beam

Both metallic and non-metallic beam materials were considered. Titanium was selected as the preferred beam material because of its superior wrapping properties and its stability while wrapped during the heat-sterilization process. Several glass fiber reinforced plastics were also found satisfactory, but are inferior to titanium.

Titanium (6AL-4V) was selected because of its high mechanical properties in the annealed state, weldability, and good fatigue properties. During the development forming program, the preferred process was to seam weld the two sheets before forming. Forming of annealed titanium can be accomplished at up to 1350° F without affecting mechanical properties. Beams were developed at 1000°F forming temperature. However, in order to increase emittance of the surface, a forming temperature of 1300°F is to be used to obtain a darker oxide coating. Results of radiative properties tests on titanium are discussed in Section 7.0.

9.3 Substrate

The substrate material is a glass fiber reinforced epoxy resin system employing EPON 828 resin with DION RP-7A aromatic amine hardener. The glass reinforcement is type 113 woven fabric. This system has good stability in vacuum over a temperature range from -400 to 350°F (Reference 21 and 28). Substrate thickness is the factor controlling wrapping ability. The stiffness of the glass fiber laminate will increase only about 25% over a 250°F temperature drop (Reference 22). Typical properties of the laminate material are shown in Table 9-1 (Reference 28 and 34). In general, the laminate meets the requirement of MIL-P-25421 type I.

Special edge attachment tests were conducted to measure the strength of the thin clip type substrate-edge attachment. These tests are

described in detail in Section 11. The tests were conducted at 75°F and 300°F loading a typical edge section in shear and tension. The tests indicated the design loads could be met by increasing the substrate thickness in the attach area.

For an adhesive bonded edge attachment, shear strength values will be the same as the shear properties of the adhesive system used. These values for EPON 934 are shown in Figure 9-1 (Reference 10).

Table 9-1

Mechanical Properties of Glass Fabric-Epoxy Resin Laminates Using DION RP-7A and EPON 828

Property	Test Value
Tensile Strength at 75°F, psi	64,000
Compressive Strength at 75°F, psi	50,500
Flexural Strength at 75°F, psi	85,300
Flexural Modulus of Elasticity at 75°F, psi	3.87×10^6
Flexural Strength at 160°F, psi	74,100
Flexural Modulus of Elasticity at 160°F, psi	3.79×10^6
Flexural Strength at 300°F, psi	33,400
Flexural Modulus at 300°F, psi	3.0×10^6

9.4 Cushioning Materials

In order to protect the solar cells during launch, a cushion arrangement is provided on the reverse side of the substrate. Because the cushion surface contacts the cells directly, teflon (TFE) film is selected to provide an inert, low friction bearing surface. The cushion is silicone rubber foam which is specified for its resistance to penetrating radiation and uniform properties from -100°F to 400°F (Reference 21 and 23).

The physical properties and vacuum stability of three foam rubbers were compared. Materials considered were Silastic RTV S-5370, G.E. RTV-7 and Hadbar 404. Physical properties of these foams are summarized in Table 9-2. Silastic RTV S-5370 was selected because of its superior stability when exposed to 10^{-6} torr at 350°F. Results of vacuum stability tests are shown in Figure 9-3 and Section 11.4.

The foam cushion is prepared by casting the foam in place against a primed-etched teflon film. By means of this process, no additional adhesive is required between the teflon and the foam rubber. The Hadbar 404 foam cannot be processed in this manner and was not selected.

Silicone rubbers have been found to outgas when heated at pressures less than 10^{-5} torr and may deposit oily films by condensation on cooler surfaces. These condensible products can be removed by use of a prior thermal-vacuum cleaning treatment (Reference 30). In the solar array design, the silicone rubber materials will be directly adjacent to solar cell surfaces while retracted. When deployed, the Silicone materials will be on the reverse side of the substrate from the cells. In every case the solar cell temperature will exceed or be equal to the Silicone rubber temperature; therefore, no condensation will occur on the solar cells and thermal-vacuum cleaning will not be required.

The spacer strip along the deployable beam surface is AMS 3304 Silicone rubber. This stock is chosen for low compression set and negligible change in hardness in space-thermal environment (Reference 30).

9.5 Adhesives

Both epoxy and silicone adhesives are used in the array structure depending upon material types to be joined and design requirements. Silastic 140 adhesive has been selected for its versatility of application and uniform properties over the design environment (Reference 21 and 26). All flexible bonds are designed with Silastic 140 and A-4094 primer.

Rigid joints are designed with Shell Chemical Company EPON 934, EPON 956 (EPON 934 unfilled) or American Cyanamid-Bloom FM-1000. These adhesives meet the requirements of MIL-A-5090 or MIL-A-25463. Principle reason for selection of EPON 934 is its good mechanical properties at 300°F needed to resist sterilization environment and to withstand deep space environment (Reference 10 and 21). See Figures 9-1 and 9-2 for properties (Reference 10 and 33).

FM-1000 is used in honeycomb sandwich because of its light weight, high-peel strength and acceptability in the space environment (Reference 21).

9.6 Surfaces Finishes

Consideration of surface finishes has dealt primarily with thermal control coatings and corrosion protection. In order to provide minimum weight, the use of paints to control temperature has been avoided. The titanium beam, for example, is allowed to oxidize sufficiently during forming to produce acceptable thermal radiative properties.

Thermal control paints which have been considered include IIT S-13 methyl silicone-zinc oxide white, Fuller 517-W-1 white and Cat-A-Lac 443-1 epoxy white and Cat-A-Lac 463-1-8 epoxy black. The 480°F cure temperature of the Fuller 517-W-1 restricts its use, but if required, this material can be applied to the titanium beam to provide a stable, glossy paint which will slide through the teflon support guide.

The S-13 paint is stable and preferred for critical control requirements. However, the material is very soft and would not be preferred on sliding surfaces. (Reference 24)

The aluminum substrate edge connector is coated with Cat-A-Lac 463-1-8 epoxy. The α / ϵ ratio of this paint is similar to the fiberglass substrate and will maintain connector temperature within the same range. The paint will satisfactorily control the clip temperature as shown in Section 7.0. Cat-A-Lac 463-1-8 is selected because of its good adhesion and resistance to damage during assembly.

Magnesium requires a protective coating to prevent corrosion in the pre-launch environment. Dow 17 anodize treatment is used throughout the design except in special cases where Dow 19 is employed.

Bonded joints develop superior strength on Dow 19 finished surfaces (Reference 25). Therefore, this treatment is specified where adhesive bonding is required. Also in locations where other metals contact the magnesium surface, Dow 19 finish is coated with a film of Cat-A-Lac 473-1 resin to prevent galvanic corrosion.

Electrofilm 4396 (MoS_2 - Graphite) dry film lubricant is used in the gear drive assembly to give additional protection and separation between the aluminum and magnesium surfaces. The drive motor bearings and gear box are lubricated with Versilube G-300 Silicone grease--selected for its stability in space environment (Reference 21).

9.7 Summary of Materials Used

Material Designation	Manufacturer
Aluminum Alloy 6061, 2024, 5050, 5056	-
Titanium Ti-6AL-4V, Ti (C.P.)	-
Magnesium Alloy AZ-31B, HK-31A	-
EPON 828 - DION RP-7A, Epoxy resin	Shell Chemical Co. & Diamond Alkali Co.
EPON 934 Adhesive - epoxy	Shell Chemical Co.
EPON 956 Adhesive - epoxy	" " "
FM-1000 Adhesive-epoxy-nylon	American Cyanamid
Silastic S-5370, Silicone Foam	Dow Corning
A-4094 Silicone Primer	" "
Teflon (TFE) Polymer	DuPont
Type 181 Glass Cloth	-
Type 113 Glass Cloth	-
EPON 1031-Methyl NADIC Anhydride, Epoxy resin	Shell Chemical Co.
Cat-A-Lac 473-1-500 resin, epoxy	Finch Paint & Chem. Co.
Electrofilm 4396, Dry film lubricant	Electrofilm, Inc.
AMS 3304 Silicone Rubber	-
Beryllium Copper	-
Brass	-
Cat-A-Lac 443-1, epoxy	Finch Paint & Chem.Co.
Corrosion Resistant Steel	-
Versilube G-300	General Electric. Co.

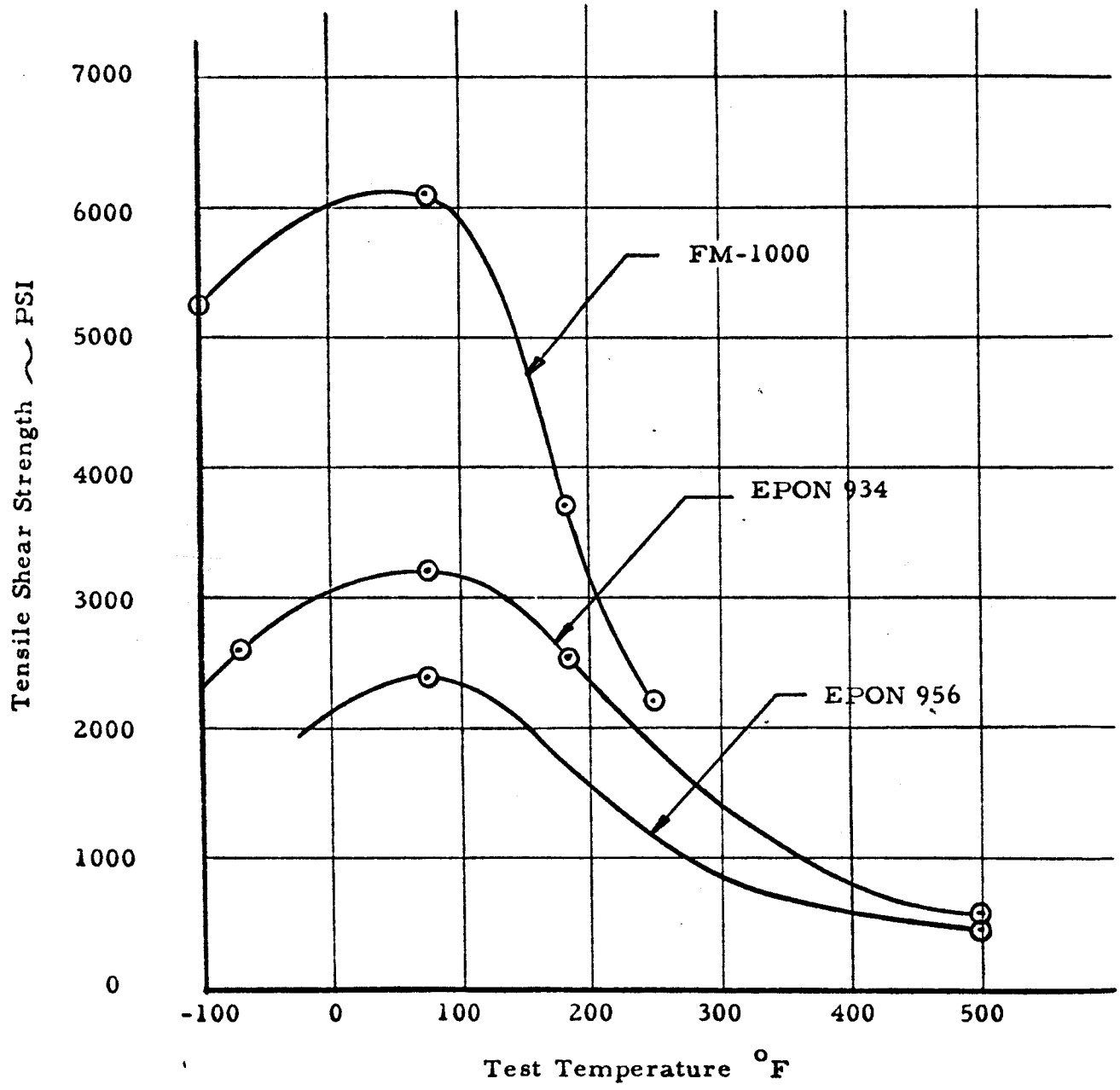

Shear Strength vs. Temperature for Several Adhesives

Figure 9 - 1

EPON(R) ADHESIVE 934

Trend of Tensile Shear Strength Vs. Exposure at 300° & 400°F

(Substrate: Chromate Etched 2024-T3 Alclad. Cure: 7 days at 75°F)

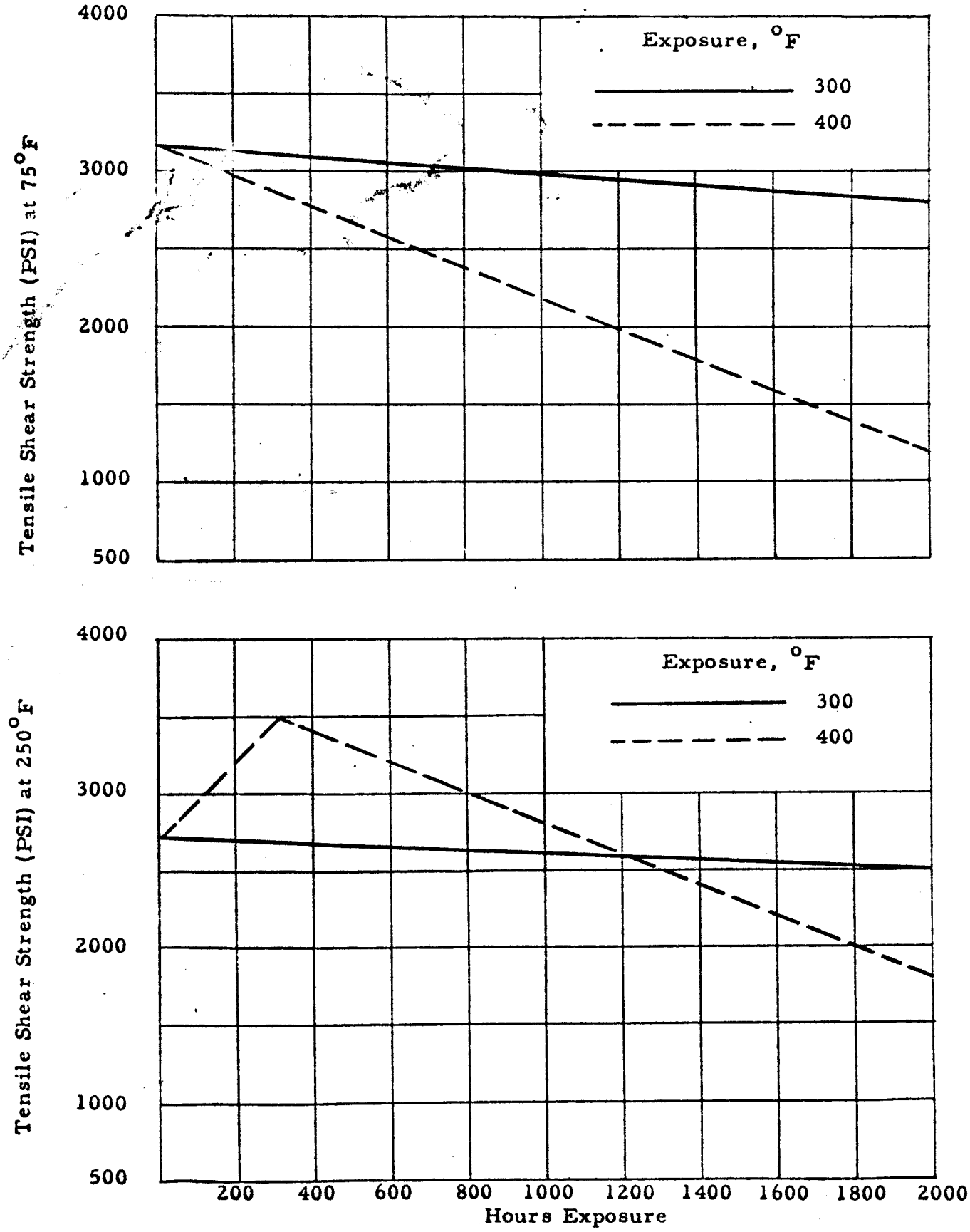

Figure 9-2

Table 9-2

Properties of Silicone Rubber Foams

Material	Description	Density lb/cu.ft.	Compression Deflection 25 % psi	Compression Deflection 50 % psi
RTV-7	1/8" molded with .002 teflon surface	15.6	.7	2.5
S-5370	1/8" molded with .002 teflon surface	20.1	1	3
S-5370	1/8" molded with smooth surface	18.5	1	3
Hadbar 404	1/2" extruded strip	12-16	.7	2.5
RTV-7	1/8" molded with smooth surface	13.2	.7	2.5

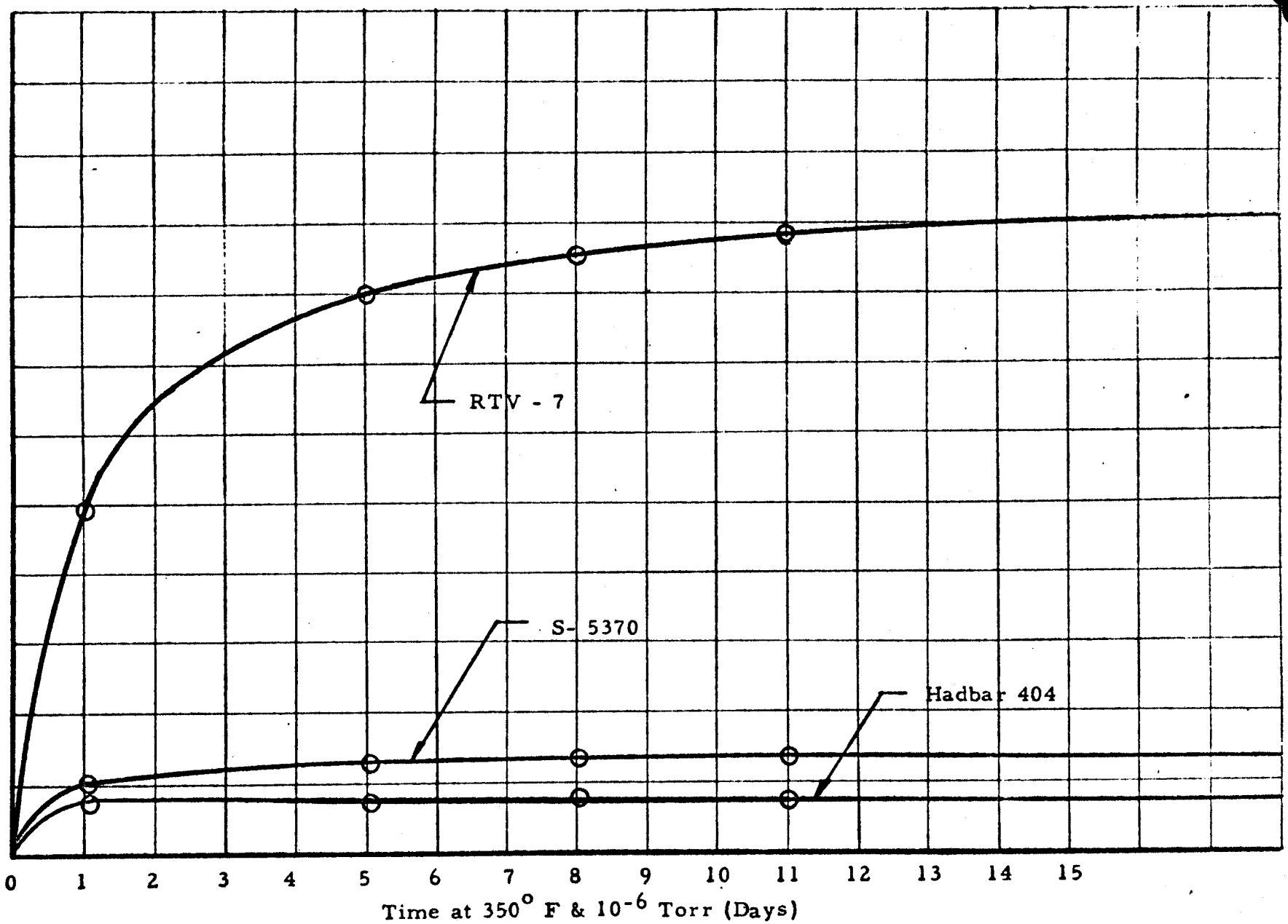

Figure 9-3

Weight Loss of Silicone Foams in Vacuum at 350°F

Figure 9 - 3

10.0 RELIABILITY CONSIDERATIONS

Due to the nature of the program and the number of elements that have been employed in a unique manner and fashion, obtaining specific reliability numbers and data for use in summarizing as a numerical rating would be largely a matter of opinion. Therefore, at this stage, before tests could be conducted to accumulate reliability numbers for the components, the problem of reliability was handled in the following manner.

The overall design was first divided into five basic design areas. These areas, namely the array support beams, substrate, wrap drum, deployment mechanism and electrical provisions, were investigated in detail by the designers. Layouts were made to investigate the problem areas. As these layouts gradually solidified the design, alternate approaches were investigated to collect a number of ideas from which to evaluate and choose a design most reliably compatible with thermal, dynamic and space environment. As the layouts proceeded, functional reliability problems were uncovered which could only be solved by testing models of representative areas. This approach was followed in the design of the beams, beam guides, substrate attachments, damping pads, electrical harness leads, solar cell substrate and the determination of deployment torque requirements and beam bending capabilities.

As data and operating characteristics were obtained form the test samples, these inputs were incorporated into design layouts. In addition to the information which was obtained from these tests, other information was supplied by the technical section in areas of thermodynamics, dynamics, loads, stress and weights as the design investigation required.

For example, thermal characteristics of the beam could effect its load carrying and extension and retraction abilities. A technical thermal investigation was conducted to determine beam operating temperatures. The effects of these temperatures were studied in design layouts and structural analysis.

Another example of the use of technical analysis to provide information in a questionable reliability area was in dynamic analysis of the beam

and substrate assemblies in retracted and extended positions. The analysis was conducted for the purpose of discovering any possible excess deflections which might occur that could affect functional reliability.

As the combined data from sample tests and technical analysis was accumulated, the design layouts were evaluated. Design approaches which best fulfilled the criteria were selected for further analysis.

11.0 SUPPORTING TESTS

This section includes data and tests which are conducted to support analysis where theoretical predictions were questionable or design allowables were unobtainable.

11.1 Actuation Torque Requirements

This test was conducted to determine the minimum extension and retraction torques required with the beam held radially against the wrap drum. The minimum torques required were determined when the radial forces were such that the wrapped beam was held against the wrap drum with no deformation from the wrap drum curvature between the radial force points. The radial forces were provided by 3/8 in. dia. rollers held against the flattened beam by a tension spring each side of the beam. The number of rollers and relative positions are shown in the following sketch.

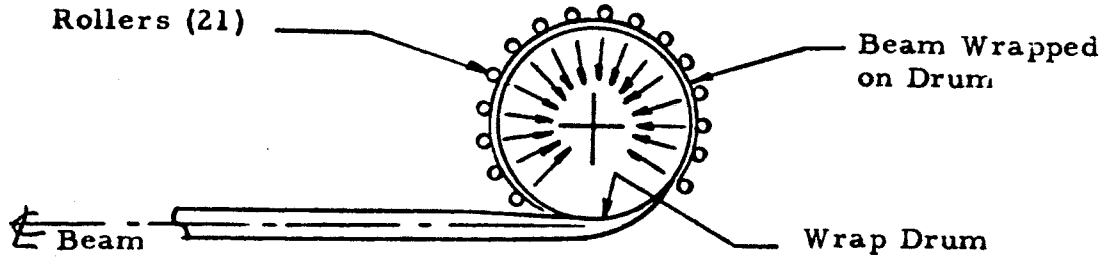

One beam of full-scale cross-section (.0060 in. thick sheet, 6AL-4V annealed titanium) less beam caps (required for additional bending strength) was used in the test model (See Figure 11-1). The torque requirements of the drive motor for the two beam systems should be little greater than twice test values justified as follows:

1) Stress analysis shows the wrap drum twist to be only 5.6×10^{-4} in. (See Section 5.2) measured on the wrap drum surface when transmitting the drive torque from the drum gear to the beam at the opposite end of the wrap drum.

2) The torque required to wrap the substrate is relatively negligible (approximately 0.3%) compared to wrapping the beam and overcoming friction in the radial force mechanisms.

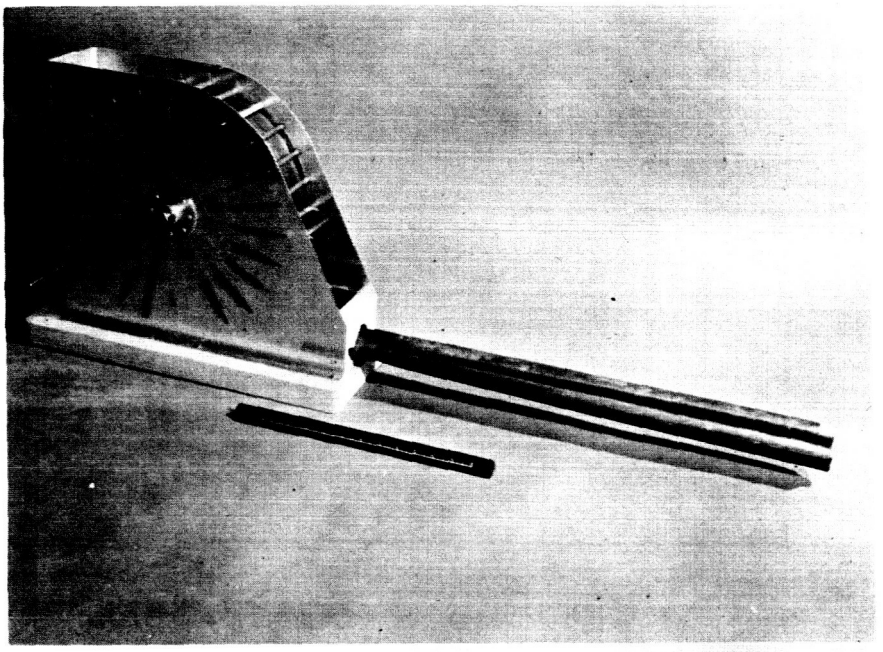

Figure 11-1 Mockup of Rollout Drum

The test was conducted by recording the force, at a given crank arm (torque), to extend and to retract the beam. Test results for the radial force springs at 5 tension settings are shown in Figure 11-2. The extension and retraction torques were not equal for the radial force spring settings chosen. If the system were frictionless and no tangential restraint forces existed at the beam-roller contact points, the assumption is made that the retraction torque and torque to prevent extension would be equal.

Since the friction and tangential restraint forces would have been difficult to obtain, miniature beam models requiring no radial force restraints (See Figure 11-3) were employed to justify the above theory assumption.

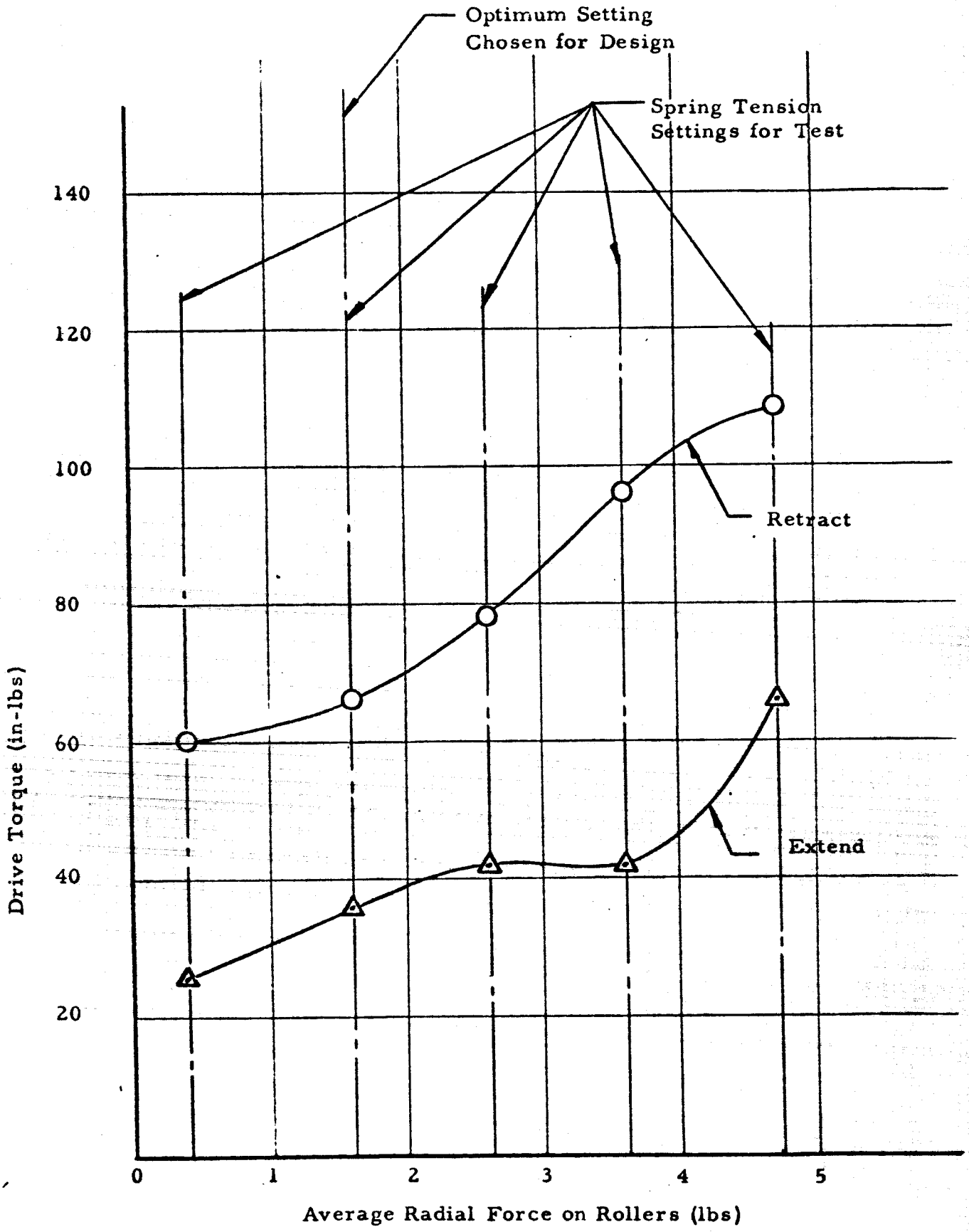

Peak Torque Actuation Requirements Per Beam

Figure 11 - 2

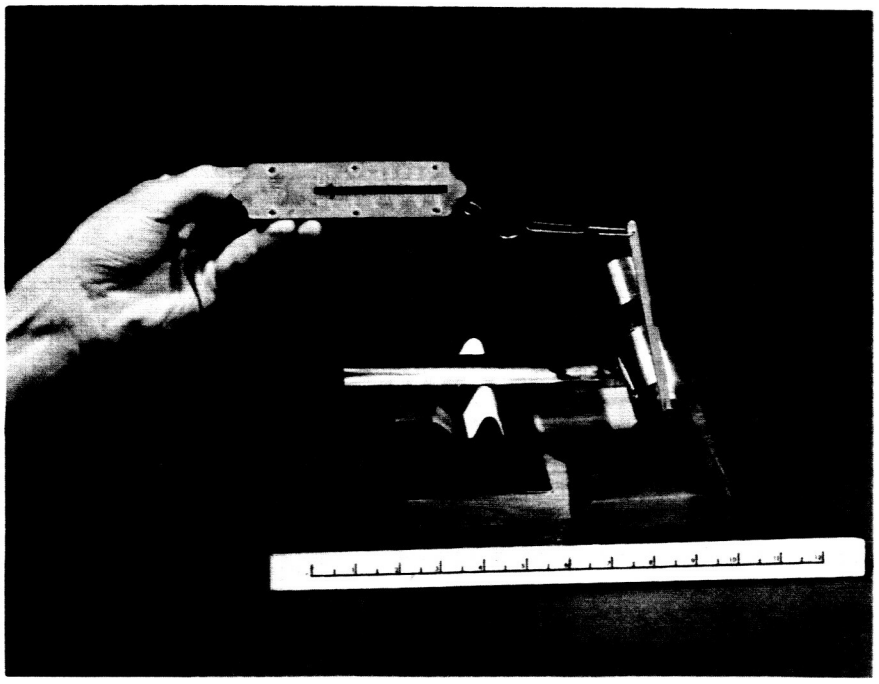

Figure 11-3 Miniature Beam Test Model

Due to the complexity in determining the effective area over which the beam flattening load is applied, the torque required is determined experimentally and from this an effective cross-sectional beam stiffness may be computed using the equation,

$$M = T = f \times r = \frac{EI_{(eff)}}{r}$$

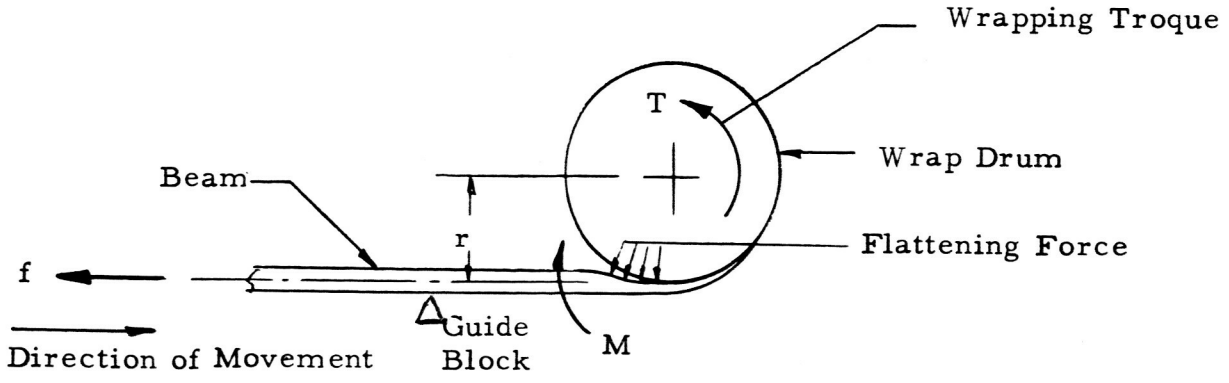

For miniature beam model A,

$b_1 = .67$ in.

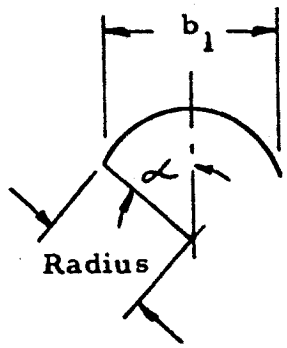

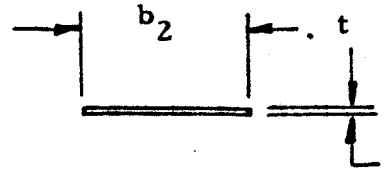

Beam After Flattening

$I = .25 \times 10^{-7}$ in.^{4}

Beam Before Flattening

b_2 = .71 in.
= .499 radians
t = .0075 in.
radius = .7 in.
r = .75 in.
Material - Stainless Steel

$$T_{(extend)} = \frac{EI_{(flat)}}{r} = \frac{29 \times 10^6 \ (.25 \times 10^{-7})}{.75} = \underline{.97} \text{ in.- lbs}$$

The test torque, after correction for torque resistance of .094 in.-lbs due to system friction,

$T_{test_{(extend)}} = 1.13 + .094 = 1.22$ in.-lbs.

$T_{test_{(retract)}} = 1.32 - .094 = 1.22$ in.-lbs.

This correlates with the theoretical assumption. Theoretical torque calculations were within 20% of test data by using bending stiffness of the flattened beam rather than an effective stiffness of the partially flattened beam.

A second miniature beam of a closed cross-section also showed test correlation with theoretical assumption. Theoretical torque calculations were within 14% of test data by using bending stiffness of the flattened beam rather than an effective stiffness of the partially flattened beam.

The retraction torque and the torque to prevent extension is now calculated for the beam of full scale cross-section by compensating for torque due to system friction:

EQN 1) $T_{(friction)} = T_{(test)} - T_{(retract)} = 66 - T_{(retract)}$

EQN 2) $T_{(friction)} = T_{(test)} + T_{(extend)} = 35 + T_{(extend)}$

$T_{(extend)} = T_{(friction)} - 35$

since $T_{(retract)} = T_{(extend)}$, EQN 2) is substituted in EQN 1),

$$T_{(friction)} = T_{(test)} - \left[T_{(friction)} - 35\right]$$

$$T_{(friction)} = \frac{T_{(test)} + 35}{2} = \frac{66 + 35}{2} = \underline{50.5} \text{ in.-lbs.}$$

and substituting in EQN 2),

$$T_{(extend)} = T_{(retract)} = 50.5 - 35 = \underline{15.5} \text{ in.-lbs.}$$

By analysis, using stiffness properties of the flattened beam,

$$T = \frac{(E)(I)}{r} = \frac{(15.4 \times 10^{6})(5.76 \times 10^{-7})}{6} = 1.5 \text{ in.-lbs.}$$

which is $\frac{1.5}{15.5} = 9.7\%$ of $T_{(extend \text{ or } retract)}$

Since the tests were conducted at room temperature, the retraction torque data for the full-scale cross-section beam is conservative by the affect of the percent reduction in modulus of the 6AL-4V titanium beam material at the temperature expected when retraction occurs (approximately 150°F in the vicinity of Mars). This modulus reduction is 3% using Reference 3. In addition, the presence of the beam caps will increase the retraction torque requirement (i.e. test data to be unconservative) to bend the flattened beam by the affect of the percent increase in bending stiffness of the flattened beam.

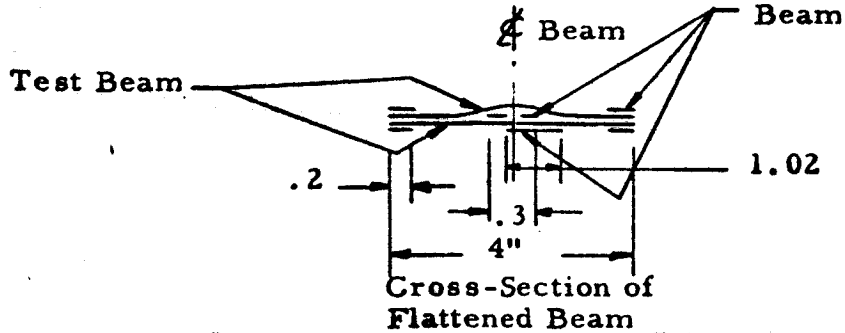

Cross-Section of Flattened Beam

Material ~ .0060" thick 6AL-4V Annealed Titanium.

$$\Delta I = \frac{I_{(beam\ caps)}}{I_{(test\ beam)}} = \frac{5.62 \times 10^{-7}}{4.77 \times 10^{-7}} = 97.6\%$$

which affects the system torque by $97.6 \times 9.7\% \left(\frac{15.5}{66}\right) = 2.2\%$

The retraction torque test data is therefore, unconservative by $2.2\% - 3\% \left(\frac{15.5}{66}\right)$ $= 1.5\%$. Retraction torgue requirements of the system are calculated as $(66 \times 2)(1.015) = 134$ in.-lbs. The available torque for the drive motor and gear box selected is 219 in.-lbs.

The test beam was fabricated of .0060 in. thick sheets. If the sheet thicknesses are increased to a maximum .0065 in., the retraction torque requirement of the system is increased by an additional percentage calculated as follows:

$$\Delta T = \frac{15.5 \left(\frac{.0065}{.006}\right)^3 - 15.5}{66} = \underline{\underline{6.4\%}}$$

The retraction torque requirement of the system would then increase to $(66 \times 2)(1 + .064 + .015) = 142$ in.-lbs.

Extension torque data is conservative by a negligible amount. The expected beam temperature during extension could be less than 75°F, resulting in an increased modulus value and a reduced extension torque requirement.

11.2 Beam Bending

This test was conducted to determine the vertical plane bending capability of the cantilevered deployable beam. The test model used (See Figure 11-1) had a full-scale cross-section beam (less beam caps) fabricated of 6AL-4V annealed titanium .0060 in thick sheets. If the sheet thicknesses are increased to a maximum .0065 in., the test data is conservative by 8.3%.

The test was conducted at various deployed length positions of the beam. A steady-state load was applied at the end of the beam. The beam is considered as if it were extended one-half length further to simulate relative load C.G. position for the actual loading condition which is a 0.2 g steady-state load during cruise maneuver between Earth and Mars. The test was conducted in each of two directions until beam buckling occured. The test results are shown in Figure 11-4. Since the beam was tested at room temperature, the design requirement is increased by the 6% reduction in modulus (Reference 3) for the 250° temperature expected. Calculation is made as follows:

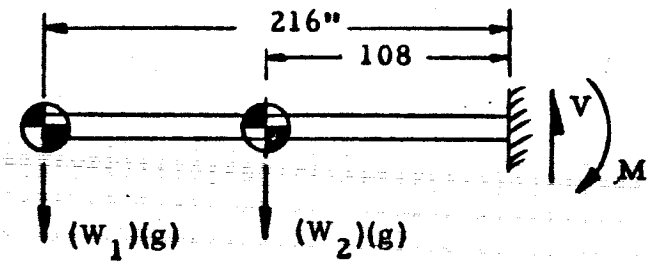

$(W_1)(g) = (.275)(.2 \times 1.25) \times 1.06 = .073$ lbs. ult.

$M_1 = .073 \times 216 = 15.8$ in.lbs. ult.

$(W_2)(g) = (13.167)(.2 \times 1.25) = 1.06 = 3.489$ lbs. ult.

$M_2 = 3.489 \times 108 \quad 376.8$ in. lbs. ult.

$V = .073 + 3.489 = 3.56$ lbs. ult.

$M = 15.8 + 376.8 = \underline{393}$ in-lbs. ult.

This calculation does not compensate for reduction in bending allowable due to the presence of shear and torsion in the beam. It does not include shear and moment effects in the lateral plane which will be considered later.

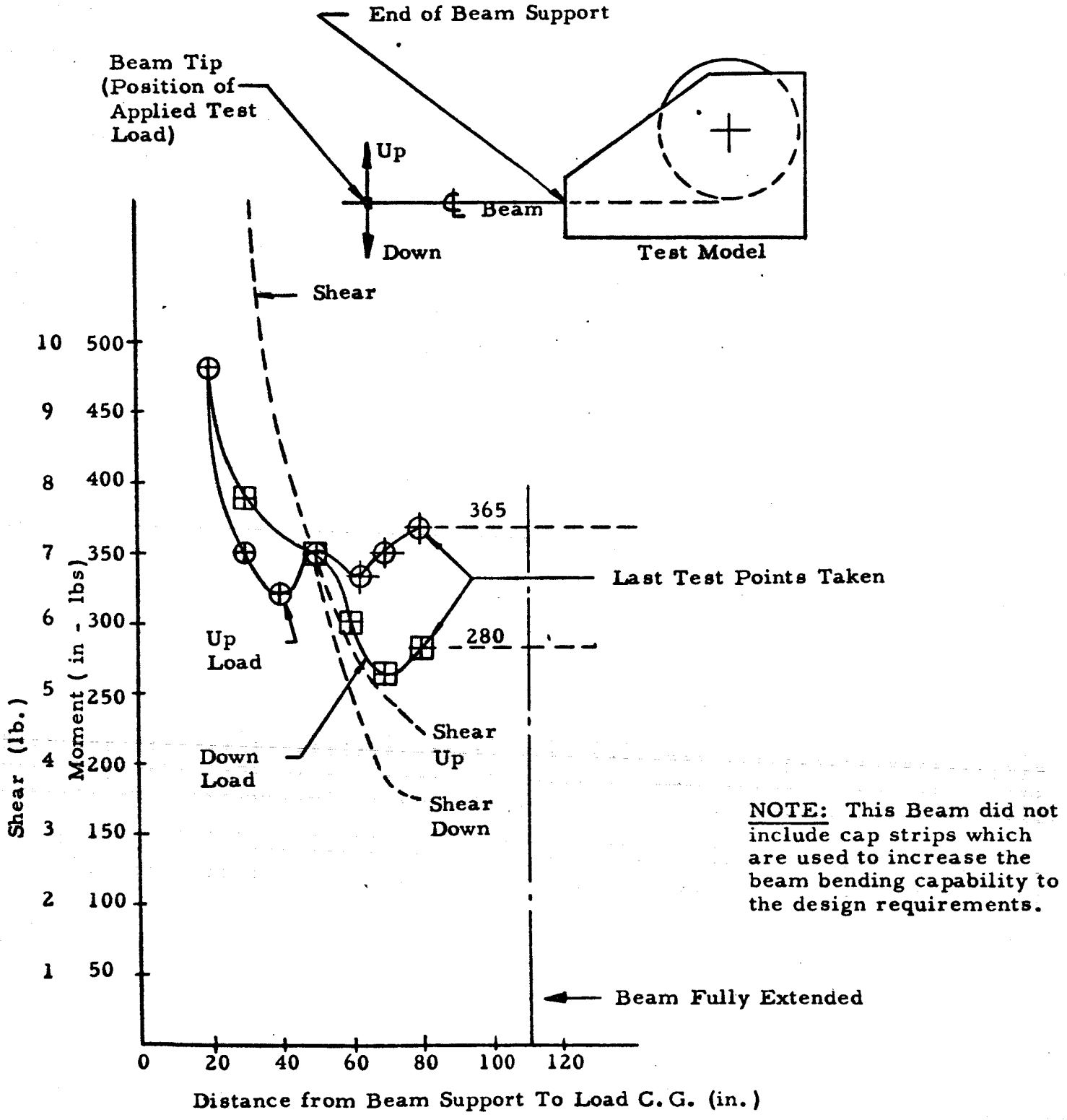

Longitudinal Bending Capability of Deployable Beam

Figure 11 - 4

The beam support provided in the test model resulted in a difference between the allowable bending moments due to loads in the up direction vs. loads in the down direction. The difference is explained by examining the shear and moment diagrams for the two conditions. The critical shear moment interaction occurs in an area of the beam with reduced cross-section for the down-load condition; for the up-load condition it occurs in an area of the beam with full cross section.. The relative shear and moment magnitudes are shown for the load C.G. 80 in. from the beam support which is near full deployment.

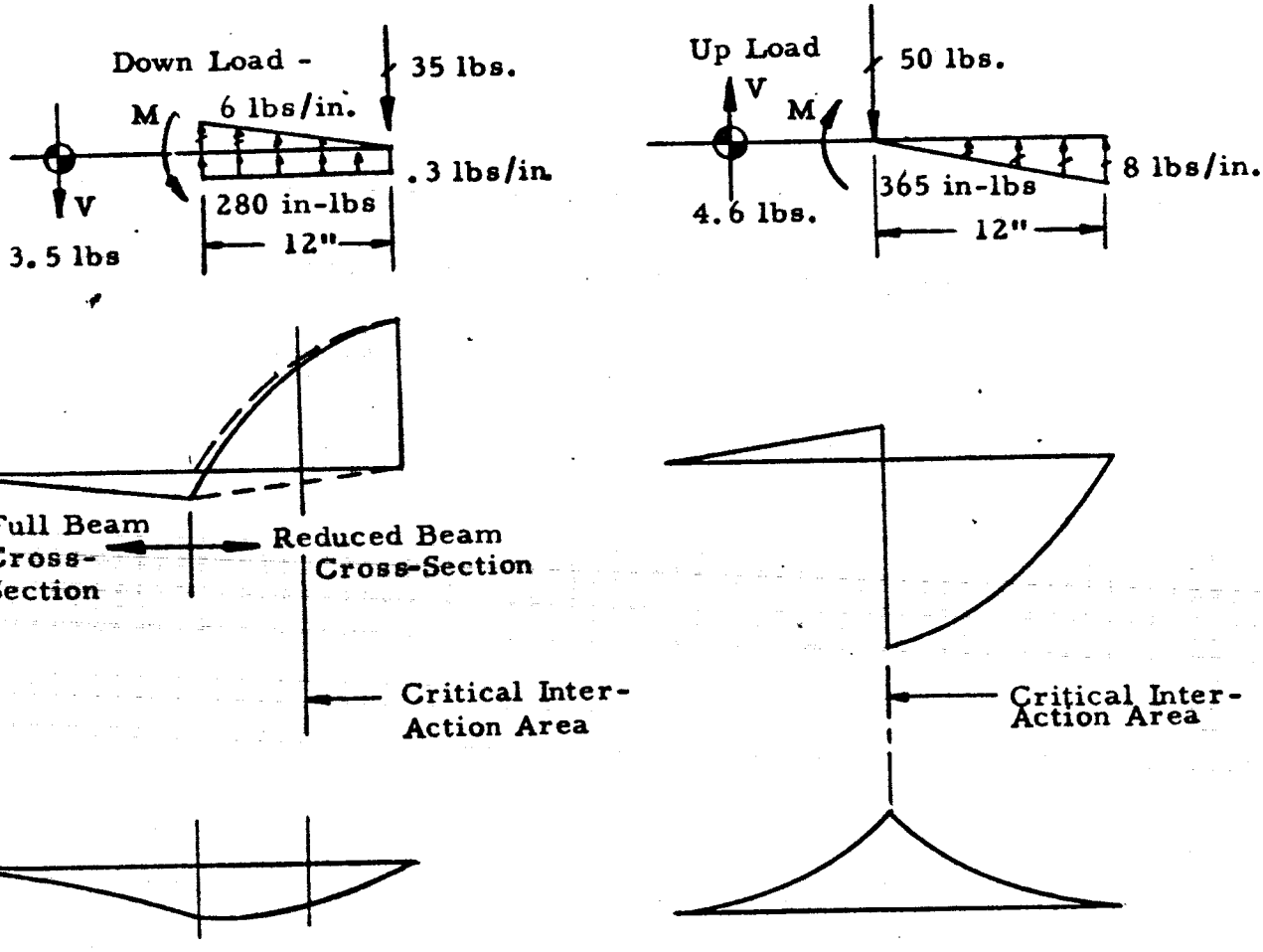

Since the point of buckling is obvious for the up-load condition when referring to the shear and moment diagrams, the effect of the presence of this respective shear on the calculated bending allowable is compared to the test bending allowable.

From the shear-moment interaction EQN, Reference 7, Page 8.2:

$$\left(\frac{f_b}{F_{cr_b}}\right)^2 + \left(\frac{f_s}{F_{cr_s}}\right)^2 = 1$$

$$f_b = \left[1 - \left(\frac{f_s}{F_{cr_s}}\right)^2\right]^{1/2} \cdot F_{cr_b}$$

$$F_{cr_b} = \frac{.36\,Et}{r} \quad \text{for } r/t < 720, \text{ Reference 29}$$

$$= \frac{.36 \times 16 \times 10^6 \times .006}{.9} = 38400 \text{ psi.}$$

$$f_s = \frac{V}{2ht} = \frac{4.5}{2 \times 1.7 \times .006} = 2206 \text{ psi}$$

F_{cr_s} = 11012 psi, Calculated in the Preliminary Development Report, Reference 8, page 107

$$f_b = \left[1 - \left(\frac{2206}{11012}\right)^2\right]^{1/2} \times 38400 = .98 \times 38400 = 37632 \text{ psi}$$

Therefore, the shear magnitude of 45 lbs. reduced the bending moment capability by only 2% at full-beam cross-section. The calculated allowable bending moment is:

$$M = (.98\,F_{cr_b}) \times \frac{I}{r} = (37632) \times \frac{.01199}{.90} = 501 \text{ in-lbs.}$$

This bending moment is greater than test. The coefficient, K, in the EQN for F_{cr_b} is therefore corrected to K = .25, rather than .36, as suggested in the preliminary development report, Reference 8, page 98.

$$M = 501 \left(\frac{.25}{.36}\right) = 348 \text{ in-lbs which is 4.7\%}$$

conservative with respect to the test result and therefore good correlation.

By examining the shear and moment diagrams for the final design support condition, it is difficult to assume the critical shear-moment interaction area.

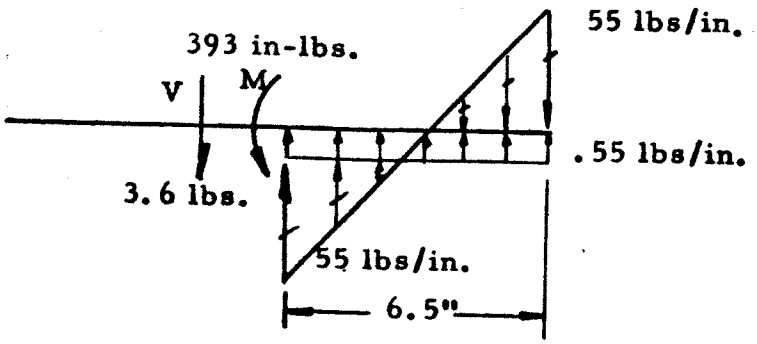

Loads May be in Direction Shown or Opposite

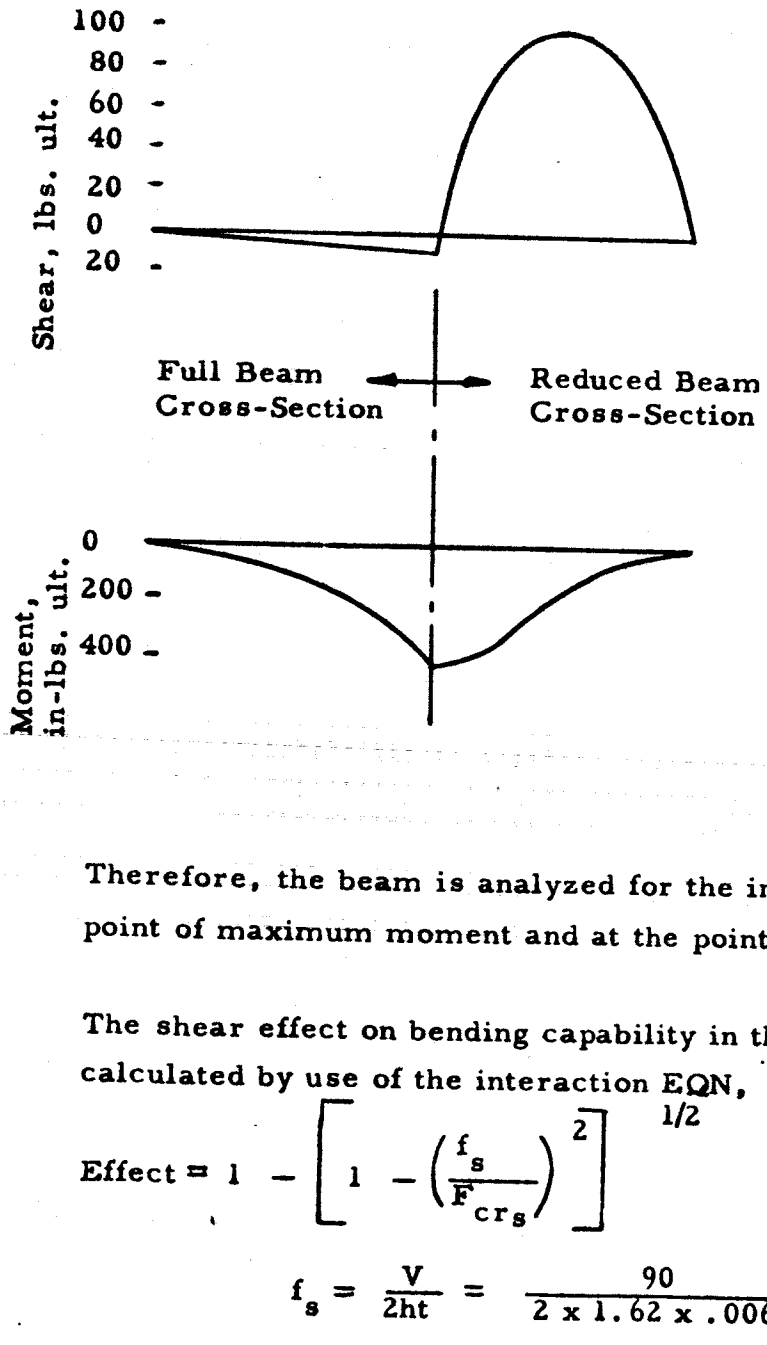

Therefore, the beam is analyzed for the interaction conditions at both the point of maximum moment and at the point of maximum shear.

The shear effect on bending capability in the area of maximum shear is calculated by use of the interaction EQN,

$$\text{Effect} = 1 - \left[1 - \left(\frac{f_s}{F_{cr_s}} \right)^2 \right]^{1/2}$$

$$f_s = \frac{V}{2ht} = \frac{90}{2 \times 1.62 \times .006} = 4630 \text{ psi}$$

$$F_{cr_s} = K_s E_c \left(\frac{t}{b} \right)^2 \cdot \frac{\pi^2}{12 (1 - \mu^2)}$$

Ref 7, page 6.9
K = 55 for clamped edge conditions

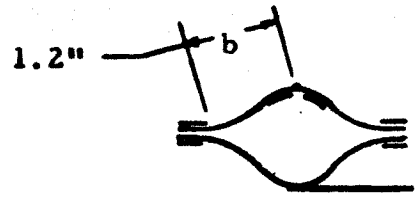

Beam Cross-Section

$$F_{cr_s} = 55 \times 16\ 10^6 \left(\frac{.006}{1.2}\right)^2 \cdot \frac{\pi^2}{12\ (1 - .24^2)} = 19199 \text{ psi}$$

$$\text{Effect} = 1 \left[1 - 1 - \left(\frac{4630}{19199}\right)^2\right]^{1/2} = 3\% \text{ reduction in bending capability}$$

The 3% reduction is not great enough to change the critical area from that at full beam cross-section. This reduction is based on vertical plane load conditions only. The effect on vertical plane bending due to the presence of torsion and shear induced by lateral plane substrate tension (See Section 5.11) is calculated as follows.

The effect of torsion outside the guide sleeve at full beam cross-section is calculated as,

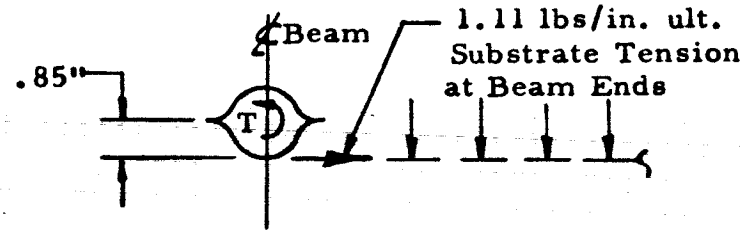

Loads Inducing Torsion in Beam

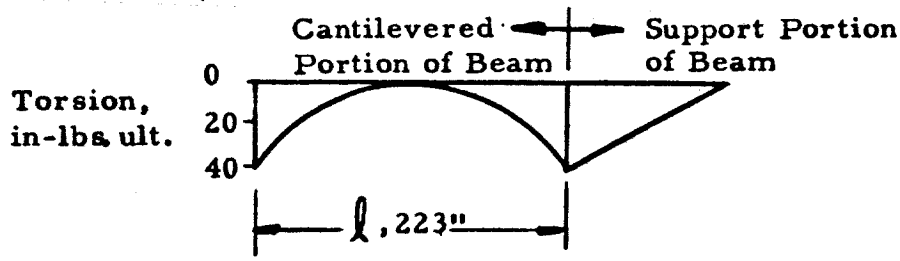

$$f_s = \frac{T}{2At} = \frac{43.5 \times .85}{2 \times 2.56 \times .006} = 1204 \text{ psi ult.}$$

$$F_{cr_s} = K_s\ E \left(\frac{t}{\ell_1}\right)^2 \times \frac{\pi^2}{12\ (1 - \mu^2)}, \text{ Reference 7, page 6.7.}$$

for the load distribution, ℓ' is considered = .25 x $\frac{\ell}{2}$ = 28 in.

$$F_{cr_s} = 8 \times 10^3 \times 15.4 \times 10^6 \left(\frac{.006}{28}\right)^2 \times \frac{\pi^2}{12(1-.24^2)} = 4936 \text{ psi}$$

From the bending-torsion interaction EQN, Reference 7, Page 8.2:

$$\text{Effect} = \left(\frac{f_s}{F_{cr_s}}\right)^2 = \left(\frac{1204}{4936}\right)^2 = 5.9\% \text{ Reduction in bending capability}$$

The torsion effect in the area of the guide sleeve is considerably less and therefore no calculation is shown.

The effect of lateral plane shear in the area of the guide sleeve compared to vertical or lateral plane bending is calculated as follows (this calculation is made considering the presence of the beam caps as acting to reduce the effective shear panel width, b).

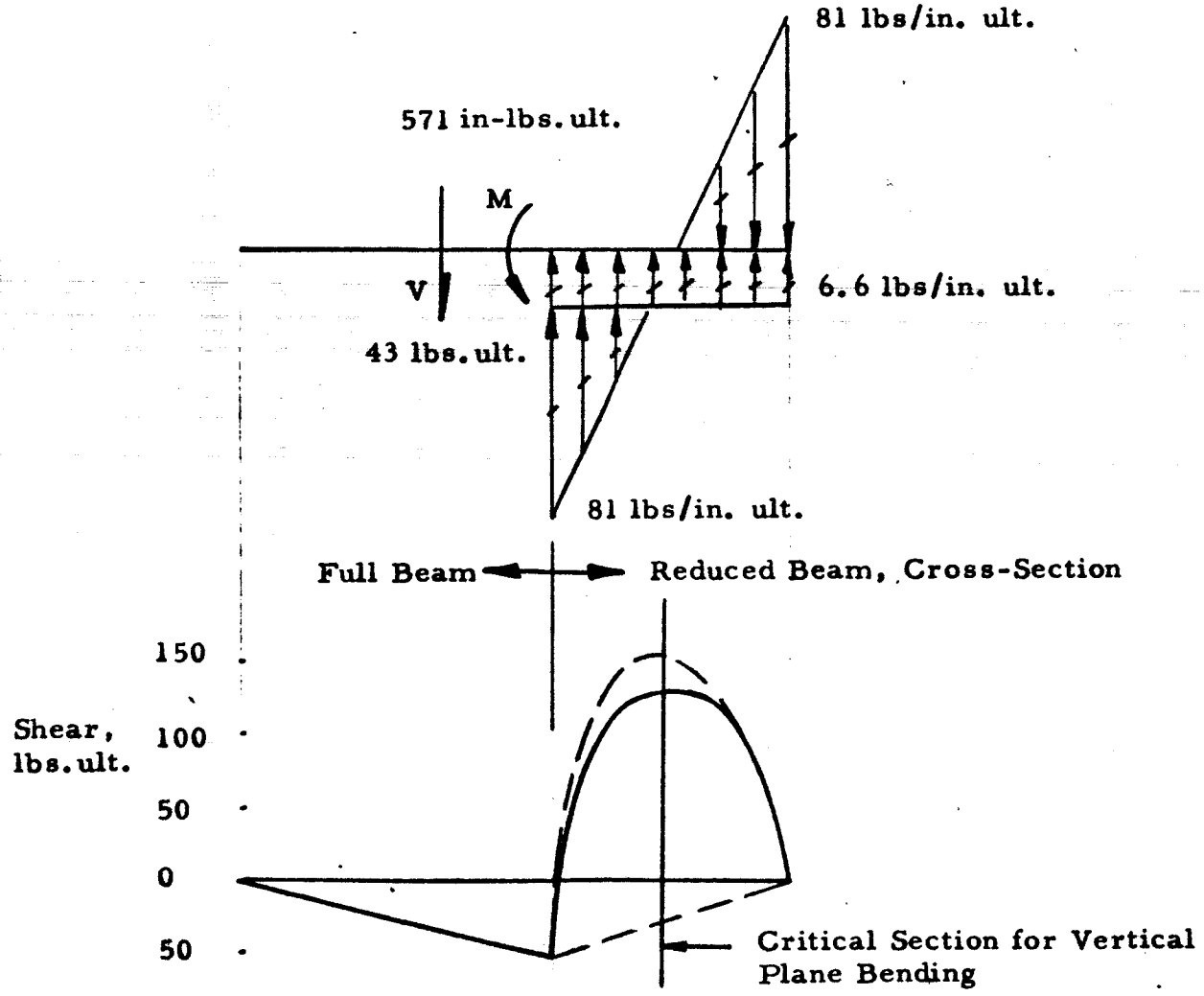

$$\text{Effect} = 1 - \left[1 - \left(\frac{f_s}{F_{cr_s}}\right)^2\right]^{1/2}$$

$$f_s = \frac{V'}{2ht} = \frac{106 + 90}{2 \times 1.62 \times .006} = 10082 \text{ psi}$$

$$F_{cr_s} = K_s E \left(\frac{t}{b}\right)^2 \cdot \frac{\pi^2}{12(1 - \mu^2)}$$

Reference 7, page 6.9

$K_s = 55$ assum.

$$F_{cr_s} = 55 \times 16 \times 10^6 \left(\frac{.006}{1.2}\right)^2 \cdot \frac{\pi^2}{12(1 - .24^2)} = 19199 \text{ psi}$$

$$\text{Effect} = 1 - \left[1 - \left(\frac{10082}{19199}\right)^2\right]^{1/2} = 15\% \text{ reduction in beam bending capability}$$

This 15% reduction is not great enough to change the critical area from that at full beam cross-section. Therefore the beam is critical in elastic compression buckling at the outboard edge of the guide sleeve. The reduction in vertical plane beam bending capability is summarized as,

Reduction due to shear	2.0%
Reduction due to torsion	5.9%
Reduction due to temperature	6.0%
Total Reduction	= 13.9%

This means that the calculated room temperature vertical plane beam bending requirement must be increased by 13.9%

$$M = \left(\frac{393}{1.06}\right) (1.139) = \underline{422} \text{ in.-lbs. ult required}$$

Since $M_{(\text{test beam})} = 365$ in.lbs ult, the vertical plane beam bending stiffness (I_{x-x}) must increase by $\frac{422-365}{365} = \underline{16\%}$

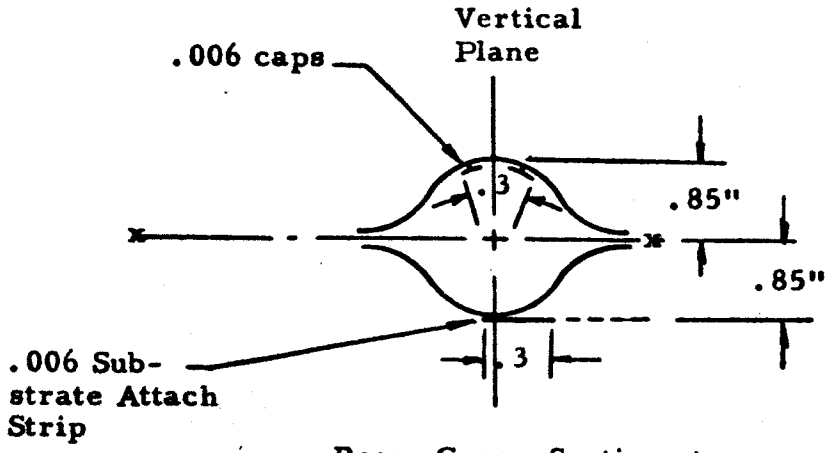

Beam Cross-Section at
Guide Sleeve Edge

If we consider the effective portion ($F_{cr} \geq F_{cy}$) of the titanium substrate attach strip (.3 in.) and add caps effectively .3 x .006, the increase in vertical plane bending stiffness is calculated as,

$$\text{increase} = \frac{\left[I_{\binom{\text{with caps}}{\text{and strip}}}\right] - I_{\binom{\text{less caps}}{\text{and strip}}}}{I_{\binom{\text{less caps}}{\text{and strip}}}}$$

$$= \frac{\left[.01199 + 2\ (.3 \times .006)(.86)^2\right] - .01199}{.01199}$$

$$\text{increase} = \frac{.01459 - .01199}{.01199} = 22\% \text{ which is sufficient}$$

11.3 Substrate Edge Attachment Tests

11.3.1 Test Procedure

Test specimens typical of the aluminum clip-substrate to beam edge attachment configuration were prepared using .006 inch and .012 inch thick fiberglass substrate, .005 inch thick 5050 aluminum alloy clips, and .006 inch thick 6AL-4V titanium. A specimen width of 2.7 inches was chosen to provide four tabs in the joint. The samples were tested in tension and shear at 75°F and 300°F to determine mechanical properties. The elongation was autographically recorded to aid in determining yield strength.

Tests were conducted in a Tinius-Olsen stress machine. Load rate was adjusted to cause failure between one and three minutes after loading. The specimens tested at 300°F were conditioned 30 minutes at temperatures before testing. Figures 11-5 and 11-6 show a shear and tension specimen in the test machine.

11.3.2 Test Results

The test results are summarized in Table 11-1. Values reported are an average of three specimens tested. In the tests conducted at 75°F, the failure mode shifted from the fiberglass substrate to the aluminum clip when the thickness of the fiberglass was increased from .006 inch to .012 inch. In the tests conducted at 300°F, the failure was always in the fiberglass. Tension yield strengths reported correspond to initial deformation of aluminum clip. Ultimate strengths represent either failure of the fiberglass or complete deformation of aluminum clip. Examples of 75°F tension failures are shown in Figures 11-7 and 11-8. Figure 11-9 shows a tension failure at 300°F.

Shear failures occurred when either the fiberglass or aluminum material sheared. Figure 11-10 shows the failure of a shear specimen tested at 75°F. In this case the substrate is .012 inch thick and the aluminum clip has failed.

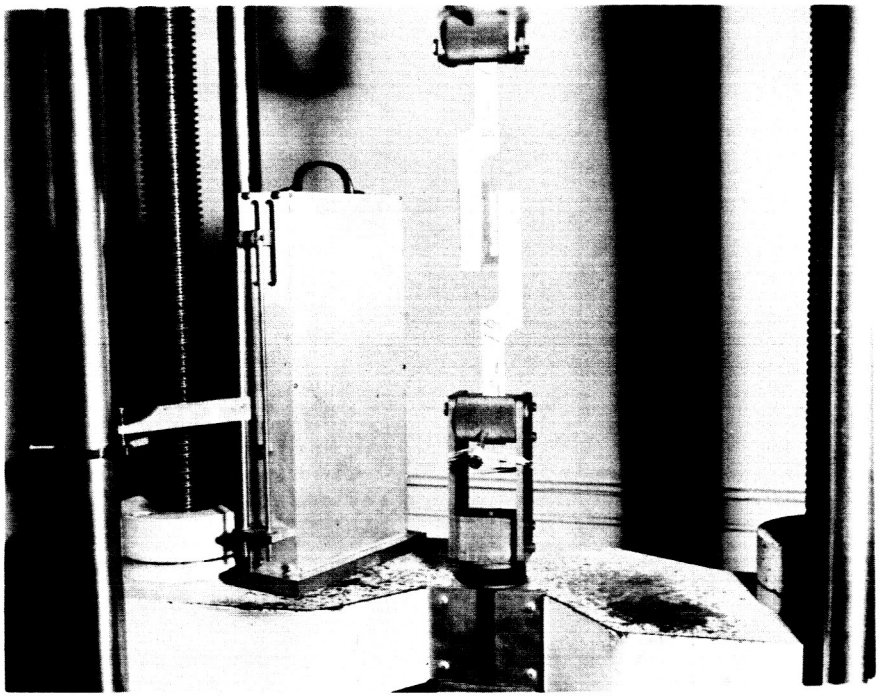

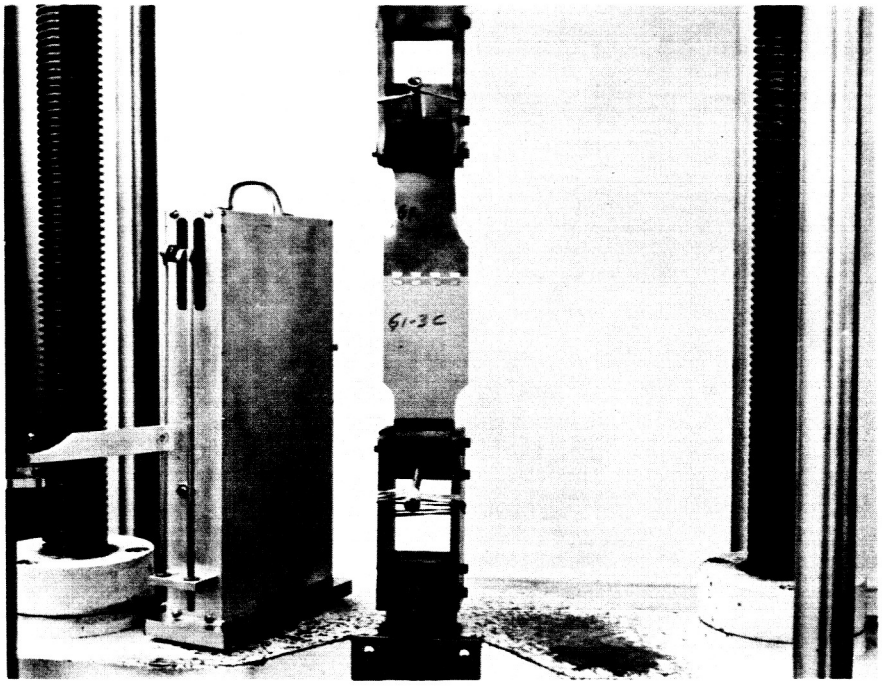
61-3C

TABLE 11-1

Summary of Substrate Edge Attachment Tests

Specimen Type	Substrate Thickness in.	Temp. °F	Ult. Strength lbs/lin. in.	Yield Strength lbs/lin. in.	Failure Mode
-1 (Tension	.006	75	7.6	5.5	Fiberglass Tore
-3 (Tension)	.012	75	14.3	10.3	Alum. Clip Bent
-1 (Tension)	.006	300	6.3	4.6	Fiberglass Tore
-3 (Tension)	.012	300	9.6	6.2	Alum. Clip Bent
-5 (Shear)	.006	75	-	2.4	Fiberglass Sheared
-7 (Shear)	.012	75	--	6.0	Aluminum Sheared
-5 (Shear)	.006	300	-	1.1	Fiberglass Sheared
-7 (Shear)	.012	300	-	2.1	Fiberglass & Alum. Sheared

1. Test results are based on average of three specimens tested
2. Test sample configuration per SK 8714

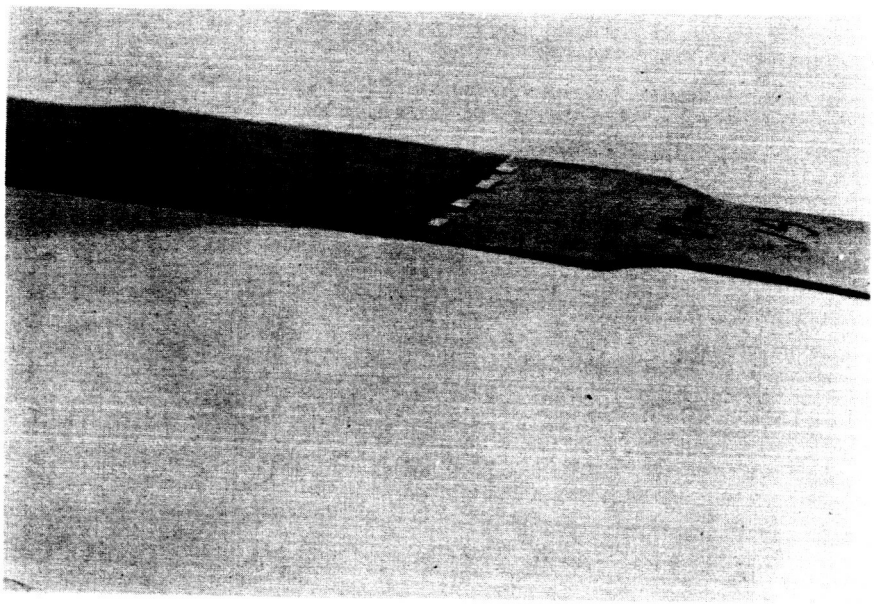

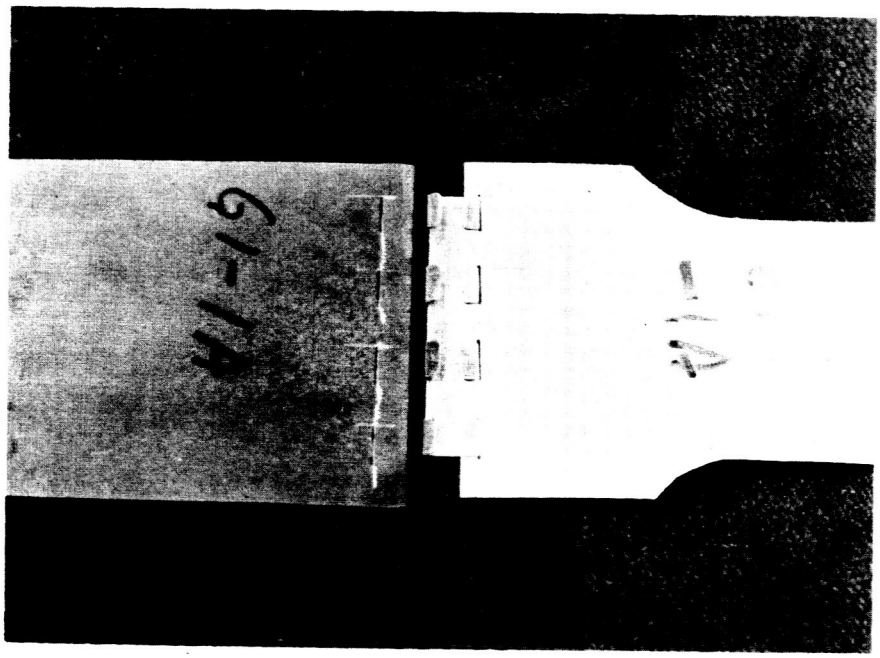
61-1A

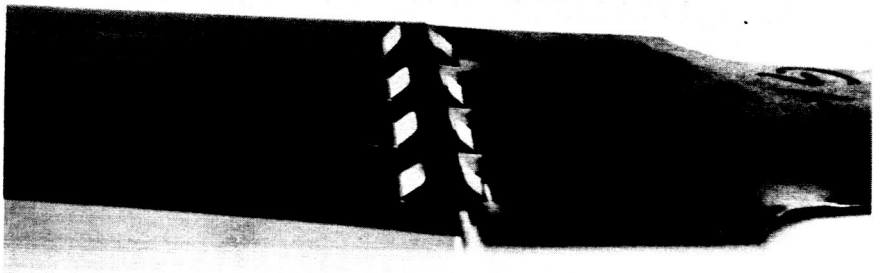

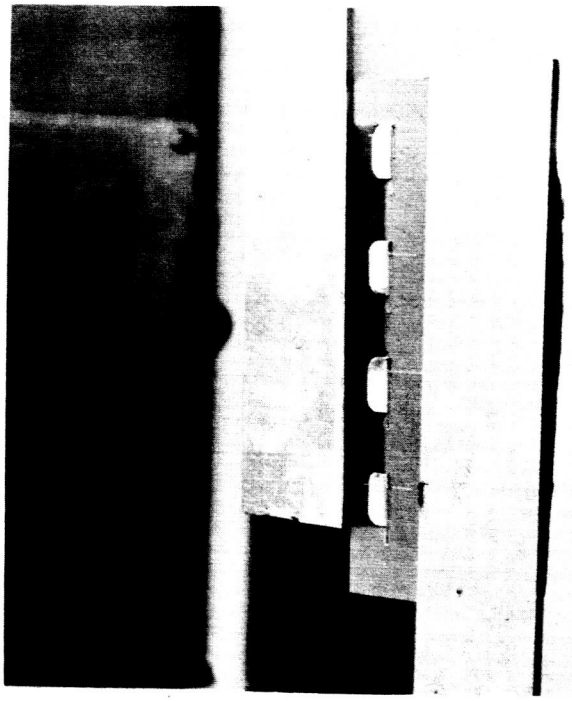

11.4 Weight Loss of Silicone Rubber Foams in Thermal Vacuum

11.4.1 Test Procedure

Three silicone foams were submitted to a thermal vacuum environment to determine weight loss. Test specimens were as follows:

1. General Electric RTV-7 -- 2.8" x 2.9" x 1/8" Sheet-black
2. Dow Corning RTV S-5370--2.9" x 2.9" x 1/8" Sheet-salmon
3. Hadbar 404 -- 1.0" x 1.5" x 1/2" block-buff

Sample material for items 1 and 2 was post-cured 4 hours at 300°F prior to testing. Sample of item 3 was tested as received from the vendor. After initial weighing, the specimens were placed in a vacuum chamber and the pressure was reduced to the 10^{-6} torr. range and the temperature was raised to 350°F. The specimens were removed from the chamber at intervals of 25 hours, 5 days, 8 days, and 11 days and weighed.

11.4.2 Test Results

A summary of test results is recorded in tabular form below.

Weighing	Time	RTV-7	S-5370	Hadbar 404
1	0(Ref.)	3.585	5.245	3.765
2	25 hr.	3.350	5.195	3.735
3	5 Day	3.300	5.188	3.740
4	8 Day	3.280	5.175	3.735
5	11 Day	3.270	5.175	3.740

(a) During weighings 2 and 3, oily deposits were noted under the RTV-7.
(b) During weighing 4, a one-inch crack was noticed in the S-5370.
(c) The Hadbar 404 specimen was shriveled when brought back to sea-level pressure. This observed during all weighings after the start of the test.
(d) Chamber environment was 350°F $\pm$ 10° and 1.2 – 6 x 10^{-6} torr.

11.5 Thermal Radiative Test Data

The thermal radiative data for all materials measured during the design phase are contained in this section. The measurements were made using the procedures discribed in Section 7.1.3.

The data are presented in the following figures and tables.

REFLECTIVITY DATA--EPOXY-FIBERGLASS SHEET

Wavelength	Reflectance	Wavelength	Reflectance	Wavelength	Reflectance	Wavelength	Reflectance
0.300E-00	0.510E-01	0.320E-00	0.520E-01	0.330E-00	0.600E-01	0.335E-00	0.600E-01
0.350E-00	0.600E-01	0.360E-00	0.610E-01	0.370E-00	0.630E-01	0.375E-00	0.660E-01
0.390E-00	0.730E-01	0.400E-00	0.750E-01	0.410E-00	0.760E-01	0.420E-00	0.800E-01
0.430E-00	0.810E-01	0.440E-00	0.830E-01	0.445E-00	0.830E-01	0.450E-00	0.840E-01
0.465E-00	0.880E-01	0.475E-00	0.890E-01	0.490E-00	0.900E-01	0.495E-00	0.910E-01
0.500E-00	0.900E-01	0.510E-00	0.920E-01	0.520E-00	0.930E-01	0.540E-00	0.950E-01
0.570E-00	0.100E-00	0.700E-00	0.150E-00	0.800E-00	0.149E-00	0.900E-00	0.130E-00
0.100E-01	0.140E-00	0.110E-01	0.150E-00	0.120E-01	0.151E-00	0.130E-01	0.160E-00
0.140E-01	0.131E-00	0.150E-01	0.155E-00	0.160E-01	0.168E-00	0.170E-01	0.162E-00
0.180E-01	0.162E-00	0.200E-01	0.165E-00	0.250E-01	0.800E-01	0.300E-01	0.600E-01
0.350E-01	0.550E-01	0.400E-01	0.600E-01	0.450E-01	0.900E-01	0.500E-01	0.700E-01
0.550E-01	-0.	0.600E-01	0.700E-01	0.650E-01	-0.	0.700E-01	0.700E-01
0.750E-01	-0.	0.800E-01	-0.	0.850E-01	-0.	0.900E-01	-0.
0.950E-01	-0.	0.100E-02	-0.	0.105E-02	-0.	0.110E-02	-0.
0.115E-02	-0.	0.120E-02	-0.	0.125E-02	-0.	0.130E-02	-0.
0.140E-02	-0.	0.150E-02	-0.	0.160E-02	-0.	0.170E-02	-0.
0.180E-02	-0.	0.190E-02	-0.	0.200E-02	-0.	0.210E-02	-0.
0.220E-02	-0.	0.230E-02	-0.	0.240E-02	-0.	0.250E-02	-0.
0.260E-02	-0.	0.270E-02	-0.	0.280E-02	-0.	0.250E-02	-0.
0.300E-02	-0.	0.310E-02	-0.	0.320E-02	-0.	-0.	-0.

Emissivity required 100 300 500 Solar absorptivity X other

200 400 Carbon Arc Absorptivity

Solar Absorptivity = 0.881302E-00 Summation Ratio = 0.881302E-00

TABLE 11-2

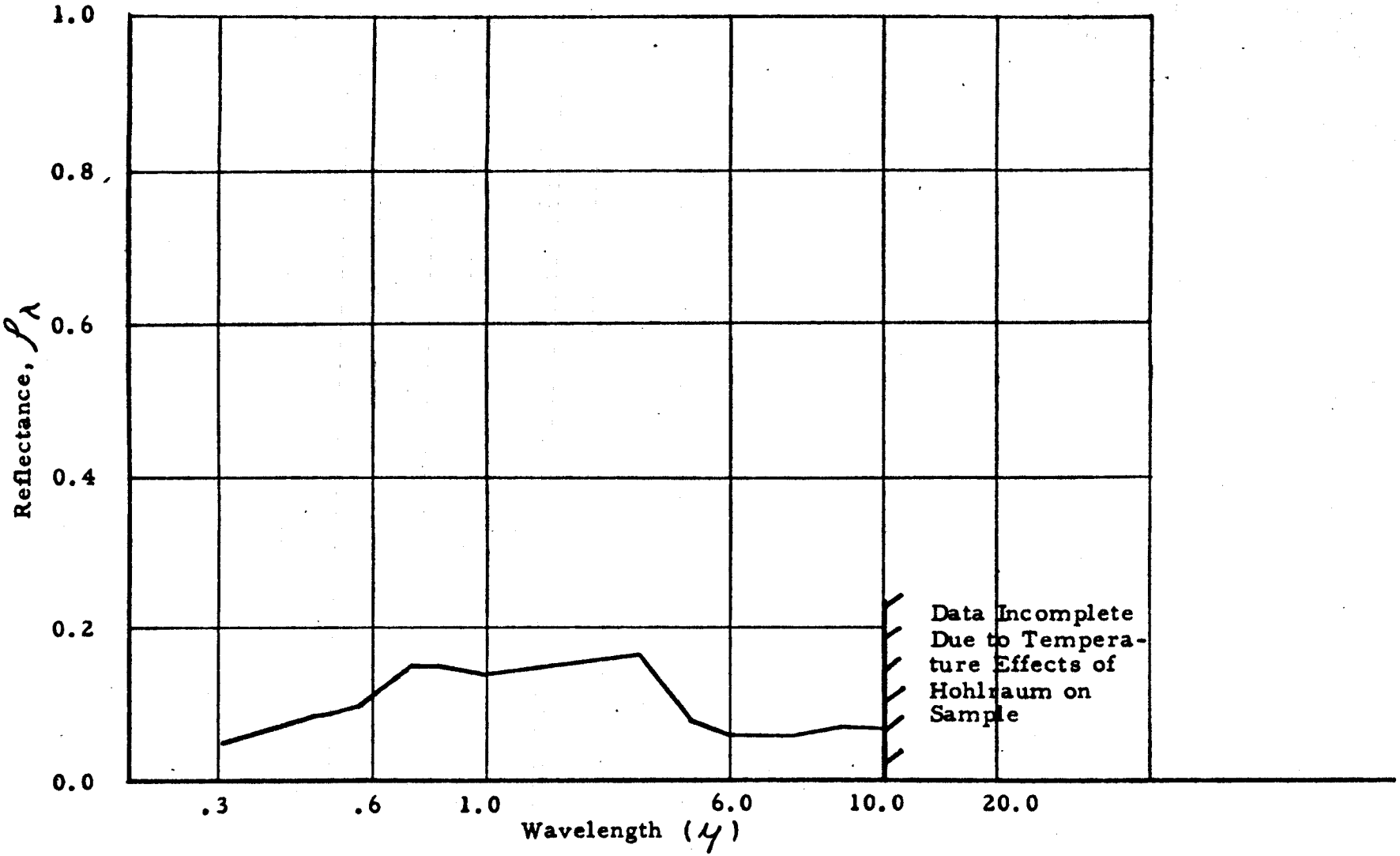

Figure 11 - 11

Normal Momochromatic Reflectance - Epoxy Fiberglass Sheet

Figure 11 - 11

REFLECTIVITY DATA--TEFLON (TFE) 0.002 INCH THICK

Wavelength	Reflectance	Wavelength	Reflectance	Wavelength	Reflectance	Wavelength	Reflectance
0.300E-00	0.113E-00	0.320E-00	0.111E-00	0.330E-00	0.110E-00	0.335E-00	0.110E-00
0.350E-00	0.105E-00	0.360E-00	0.100E-00	0.370E-00	0.980E-01	0.375E-00	0.970E-01
0.390E-00	0.930E-01	0.400E-00	0.920E-01	0.410E-00	0.890E-01	0.420E-00	0.970E-01
0.430E-00	0.860E-01	0.440E-00	0.830E-01	0.445E-00	0.820E-01	0.450E-00	0.810E-01
0.465E-00	0.800E-01	0.475E-00	0.800E-01	0.490E-00	0.800E-01	0.495E-00	0.800E-01
0.500E-00	0.800E-01	0.510E-00	0.800E-01	0.520E-00	0.830E-01	0.540E-00	0.850E-01
0.570E-00	0.920E-01	0.700E-00	0.152E-00	0.800E-00	0.170E-00	0.900E-00	0.170E-00
0.100E-01	0.198E-00	0.110E-01	0.213E-00	0.120E-01	0.222E-00	0.130E-01	0.250E-00
0.140E-01	0.230E-00	0.150E-01	0.277E-00	0.160E-01	0.288E-00	0.170E-01	0.255E-00
0.180E-01	0.278E-00	0.200E-01	0.290E-00	0.250E-01	0.130E-00	0.300E-01	0.500E-01
0.350E-01	0.400E-01	0.400E-01	0.900E-01	0.450E-01	0.135E-00	0.500E-01	0.900E-01
0.550E-01	0.650E-01	0.600E-01	0.450E-01	0.650E-01	0.500E-01	0.700E-01	0.500E-01
0.750E-01	0.600E-01	0.800E-01	0.750E-01	0.850E-01	0.850E-01	0.900E-01	0.110E-01
0.950E-01	0.900E-01	0.100E-02	0.800E-01	0.105E-02	0.800E-01	0.110E-02	0.800E-01
0.115E-02	0.800E-01	0.120E-02	0.650E-01	0.125E-02	0.750E-01	0.130E-02	0.800E-01
0.140E-02	0.850E-01	0.150E-02	0.100E-00	0.160E-02	0.105E-00	0.170E-02	0.100E-00
0.180E-02	0.110E-00	0.190E-02	0.120E-00	0.200E-02	0.150E-00	0.210E-02	0.160E-00
0.220E-02	0.130E-00	0.230E-02	0.150E-00	0.240E-02	0.115E-00	0.250E-02	0.150E-00
0.260E-02	0.140E-00	0.270E-02	0.160E-00	0.280E-02	0.120E-00	0.290E-02	0.100E-00
0.300E-02	0.125E-00	0.310E-02	0.130E-00	0.320E-02	0.150E-00	-0.	-0.

Emissivity Required 100 x 300 x 500 x Solar Absorptivity x other

200 x 400 x Carbon Arc Absorptivity

Emissivity (100 K) =	0.857352E-00	Summation Ratio =	0.287586E-00
Emissivity (300 K) =	0.901712E-00	Summation Ratio =	0.817824E-00
Emissivity (500 K) =	0.913571E-00	Summation Ratio =	0.872037E-00
Solar Absorptivity =	0.851143E-00	Summation Ratio =	0.851143E-00
Emissivity (200 K) =	0.876510E-00	Summation Ratio =	0.657590E-00
Emissivity (400 K) =	0.907731E-00	Summation Ratio =	0.837580E-00

TABLE 11-3

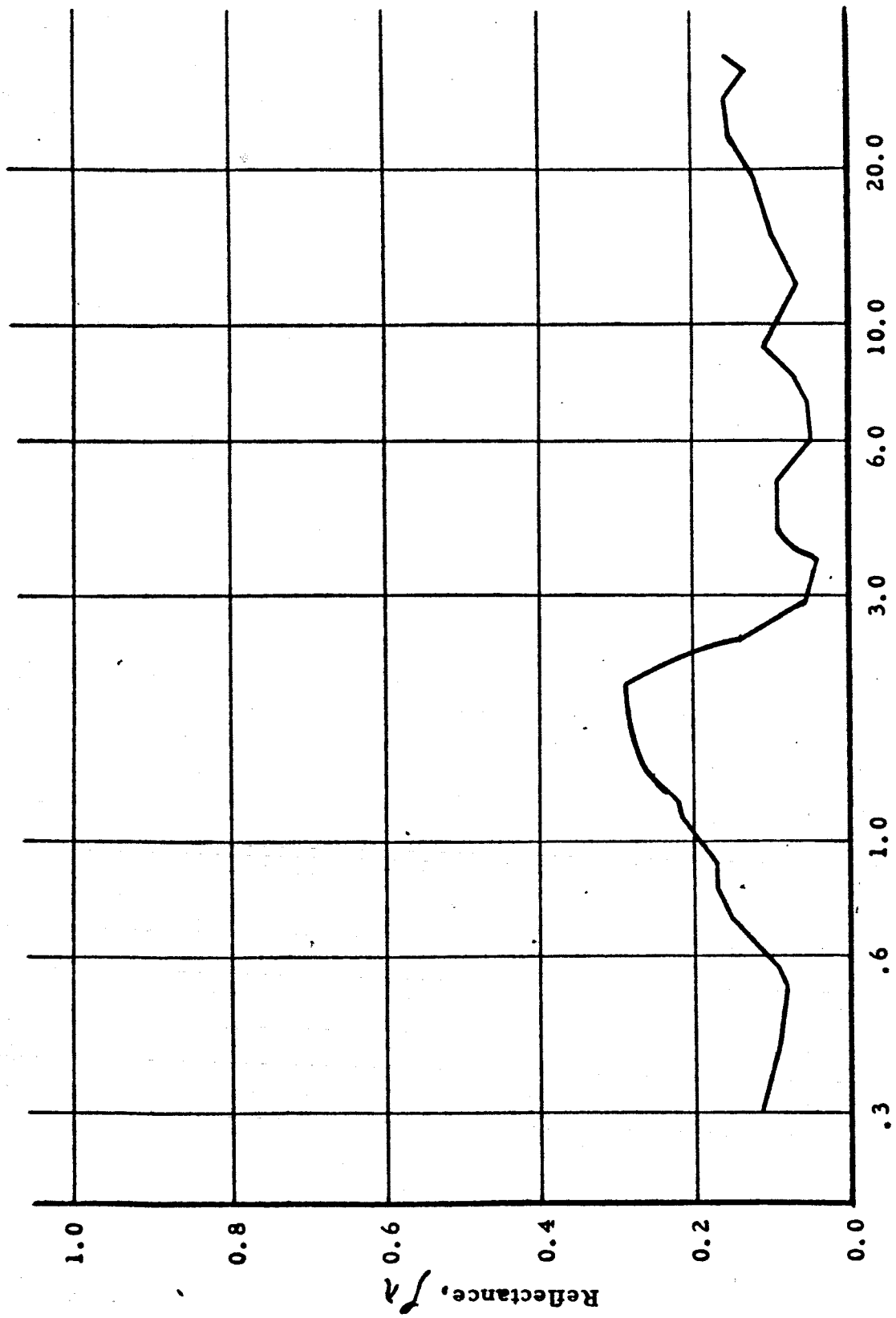

Normal Momochromatic Reflectance - Teflon (TFE)

Figure 11 - 12

Figure 11 - 12

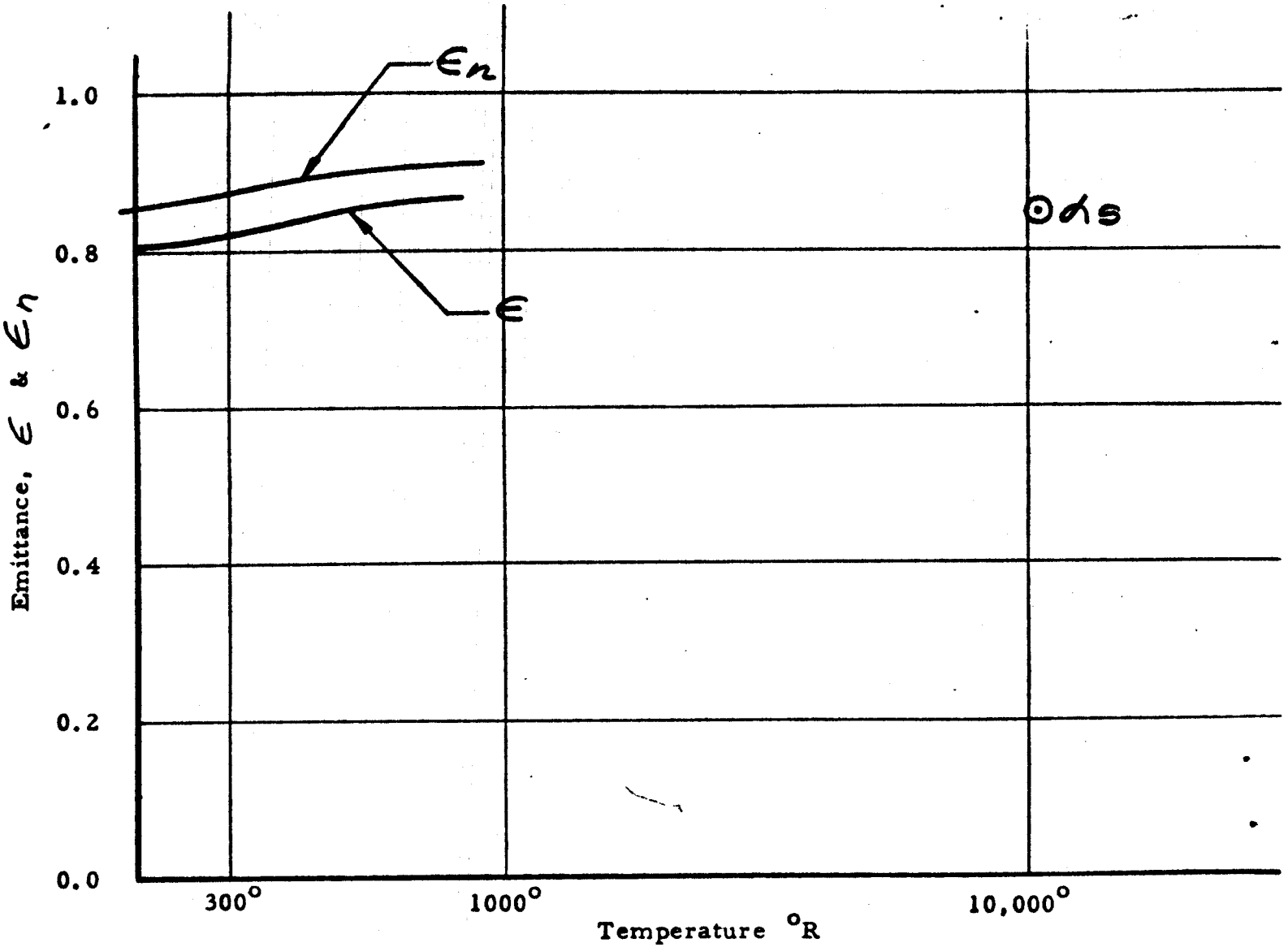

Figure 11 - 13

Total Normal & Total Emittance as a Function of Blackbody Temperature-Teflon (TFE)

REFLECTIVITY DATA--POLISHED TITANIUM

Wavelength	Reflectance	Wavelength	Reflectance	Wavelength	Reflectance	Wavelength	Reflectance
0.300E-00	0.218E-00	0.320E-00	0.240E-00	0.330E-00	0.280E-00	0.335E-00	0.285E-00
0.350E-00	0.290E-00	0.360E-00	0.320E-00	0.370E-00	0.330E-00	0.375E-00	0.330E-00
0.390E-00	0.335E-00	0.400E-00	0.335E-00	0.410E-00	0.345E-00	0.420E-00	0.345E-00
0.430E-00	0.345E-00	0.440E-00	0.395E-00	0.445E-00	0.390E-00	0.450E-00	0.400E-00
0.465E-00	0.405E-00	0.475E-00	0.410E-00	0.490E-00	0.405E-00	0.495E-00	0.410E-00
0.500E-00	0.410E-00	0.510E-00	0.405E-00	0.520E-00	0.410E-00	0.540E-00	0.415E-00
0.570E-00	0.415E-00	0.700E-00	0.480E-00	0.800E-00	0.490E-00	0.900E-00	0.490E-00
0.100E-01	0.500E-00	0.110E-01	0.515E-00	0.120E-01	0.545E-00	0.130E-01	0.550E-00
0.140E-01	0.562E-00	0.150E-01	0.570E-00	0.160E-01	0.580E-00	0.170E-01	0.596E-00
0.180E-01	0.600E-00	0.200E-01	0.635E-00	0.250E-01	0.660E-00	0.300E-01	0.685E-00
0.350E-01	0.720E-00	0.400E-01	0.735E-00	0.450E-01	0.745E-00	0.500E-01	0.770E-00
0.550E-01	0.780E-00	0.600E-01	0.795E-00	0.650E-01	0.810E-00	0.700E-01	0.810E-00
0.750E-01	0.825E-00	0.800E-01	0.835E-00	0.850E-01	0.835E-00	0.900E-01	0.840E-00
0.950E-01	0.840E-00	0.100E-02	0.845E-00	0.105E-02	0.850E-00	0.110E-02	0.860E-00
0.115E-02	0.860E-00	0.120E-02	0.860E-00	0.125E-02	0.865E-00	0.130E-02	0.870E-00
0.140E-02	0.870E-00	0.150E-02	0.875E-00	0.160E-02	0.875E-00	0.170E-02	0.885E-00
0.180E-02	0.890E-00	0.190E-02	0.890E-00	0.200E-02	0.895E-00	0.210E-02	0.895E-00
0.220E-02	0.900E-00	0.230E-02	0.900E-00	0.240E-02	0.910E-00	0.250E-02	0.910E-00
0.260E-02	0.910E-00	0.270E-02	0.915E-00	0.280E-02	0.905E-00	0.290E-02	0.9103-00
0.300E-02	0.915E-00	0.310E-02	0.915E-00	0.320E-02	0.915E-00	-0.	-0.

Emissivity Required 100 x 300 x 500 x Solar Absorptivity x other

200 x 400 x Carbon Arc Absorptivity

Emissivity (100 K) = 0.887989E-01	Summation Ratio = 0.318224E-01
Emissivity (300 K) = 0.133558E-00	Summation Ratio = 0.125169E-00
Emissivity (500 K) = 0.174790E-00	Summation Ratio = 0.170637E-00
Solar Absorptivity = 0.532280E-00	Summation Ratio = 0.532280E-00
Emissivity (200 K) = 0.107767E-00	Summation Ratio = 0.858754E-01
Emissivity (400 K) = 0.152749E-00	Summation Ratio = 0.145734E-00

TABLE 11-4

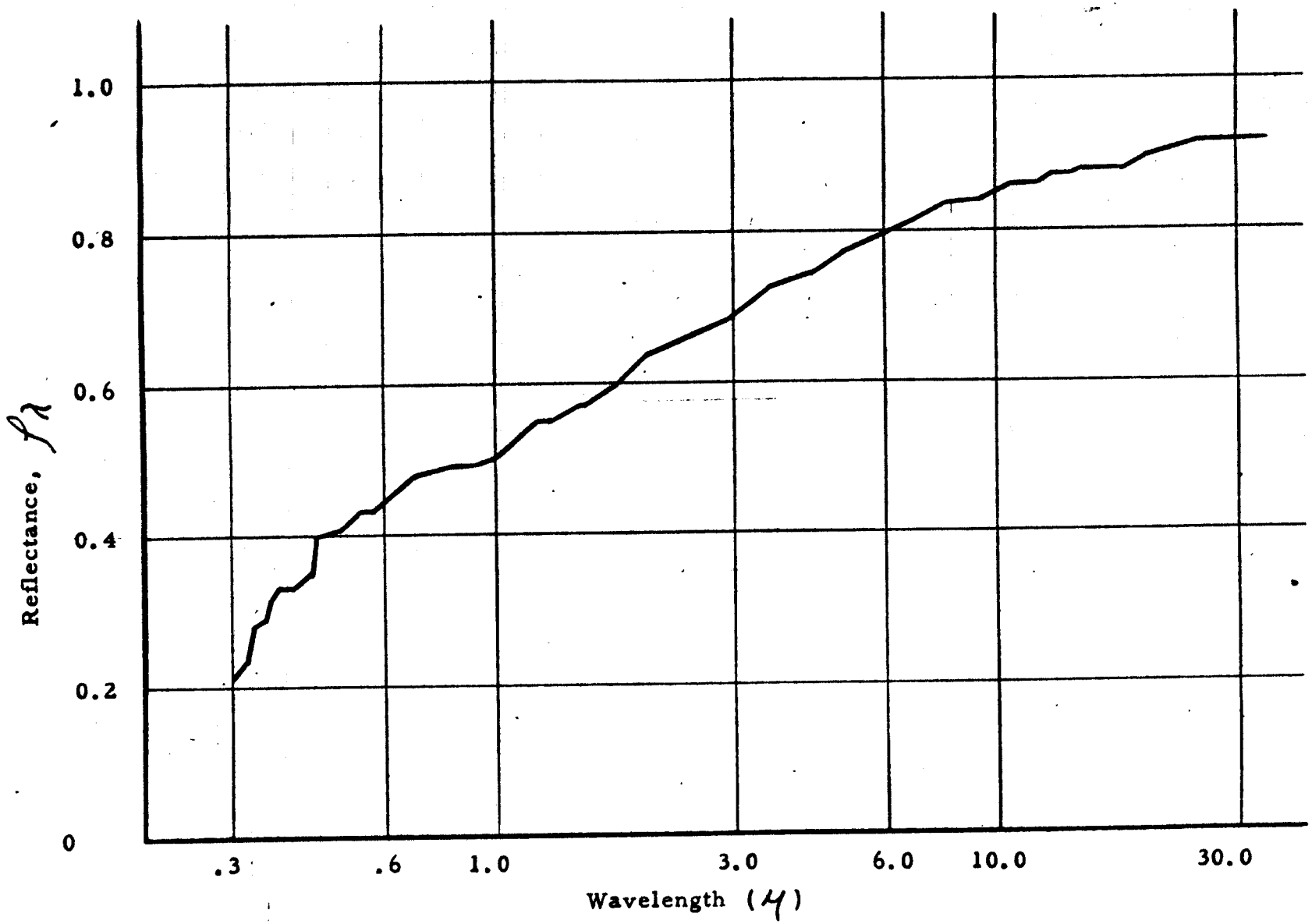

Figure 11 - 14

Normal Monochromatic Reflectance - Polished Titanium

Figure 11-14

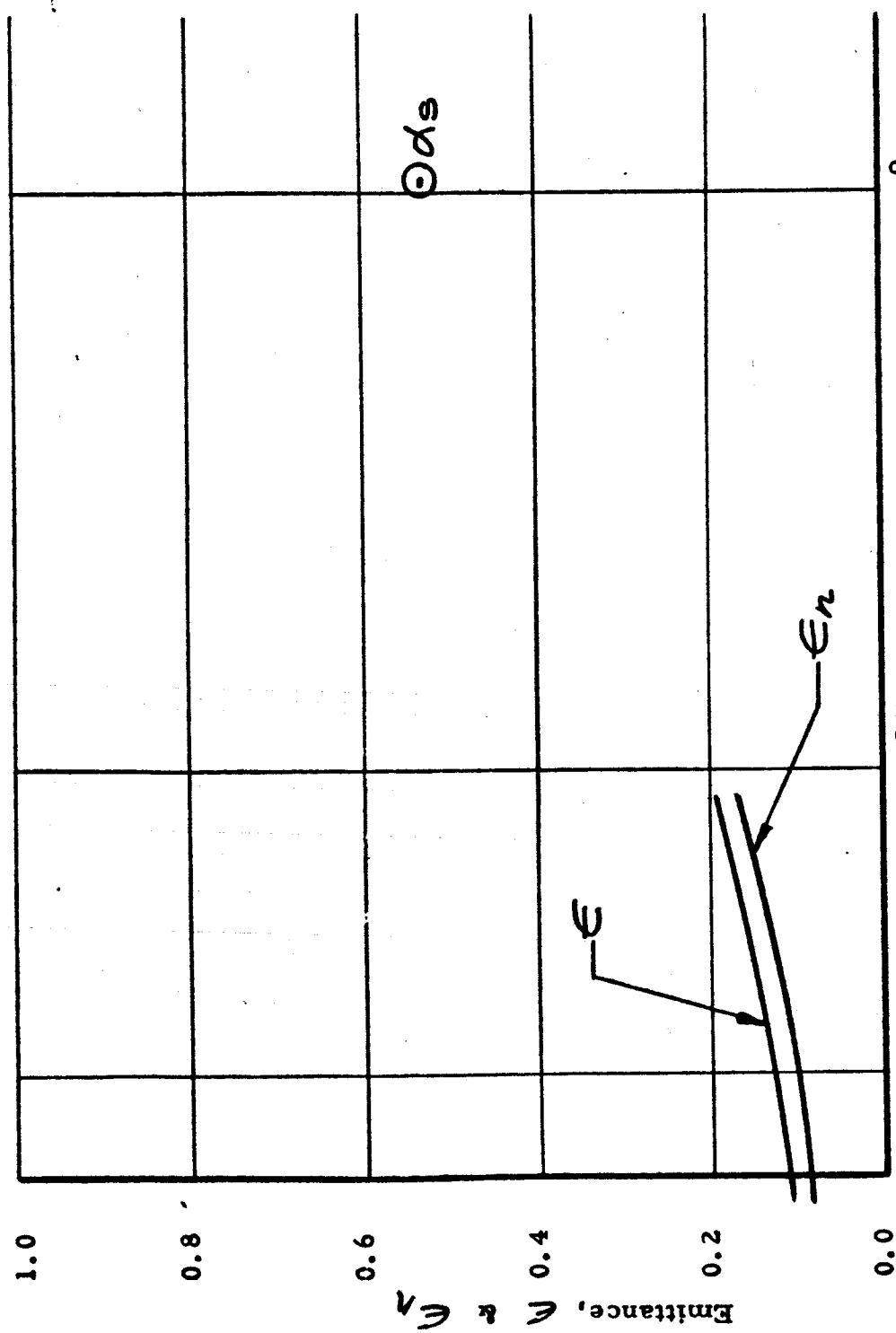

Total Normal & Total Emittance as a Function of Blackbody Temperature---

Polished Titanium

Figure 11 - 15

Figure 11 - 15

REFLECTIVITY DATA--OXIDIZED TITANIUM 1000 F LAB FLAT

Wavelength	Reflectance	Wavelength	Reflectance	Wavelength	Reflectance	Wavelength	Reflectance
0.300E-00	0.110E-00	0.320E-00	0.111E-00	0.330E-00	0.158E-00	0.335E-00	0.164E-00
0.350E-00	0.189E-00	0.360E-00	0.206E-00	0.370E-00	0.218E-00	0.375E-00	0.218E-00
0.390E-00	0.225E-00	0.400E-00	0.223E-00	0.410E-00	0.221E-00	0.420E-00	0.218E-00
0.430E-00	0.211E-00	0.440E-00	0.205E-00	0.445E-00	0.201E-00	0.450E-00	0.200E-00
0.465E-00	0.188E-00	0.475E-00	0.183E-00	0.490E-00	0.174E-00	0.495E-00	0.170E-00
0.500E-00	0.169E-00	0.510E-00	0.161E-00	0.520E-00	0.162E-00	0.540E-00	0.141E-00
0.570E-00	0.139E-00	0.700E-00	0.105E-00	0.800E-00	0.155E-00	0.900E-00	0.165E-00
0.100E-01	0.210E-00	0.110E-00	0.280E-00	0.120E-01	0.333E-00	0.130E-01	0.338E-00
0.140E-01	0.375E-00	0.150E-01	0.390E-00	0.160E-01	0.401E-00	0.170E-01	0.411E-00
0.180E-01	0.426E-00	0.200E-01	0.490E-00	0.250E-01	0.555E-00	0.300E-01	0.600E-00
0.350E-01	0.630E-00	0.400E-01	0.680E-00	0.450E-01	0.695E-00	0.500E-01	0.710E-00
0.550E-01	0.730E-00	0.600E-01	0.745E-00	0.650E-01	0.750E-00	0.700E-01	0.770E-00
0.750E-01	0.780E-00	0.800E-01	0.790E-00	0.850E-01	0.795E-00	0.900E-01	0.800E-00
0.950E-01	0.810E-00	0.100E-02	0.820E-00	0.105E-02	0.815E-00	0.110E-02	0.820E-00
0.115E-02	0.835E-00	0.120E-02	0.840E-00	0.125E-02	0.845E-00	0.130E-02	0.850E-00
0.140E-02	0.850E-00	0.150E-02	0.860E-00	0.160E-02	0.865E-00	0.170E-02	0.865E-00
0.180E-02	0.865E-00	0.190E-02	0.870E-00	0.200E-02	0.870E-00	0.210E-02	0.880E-00
0.220E-02	0.885E-00	0.230E-02	0.890E-00	0.240E-02	0.890E-00	0.250E-02	0.900E-00
0.260E-02	0.900E-00	0.270E-02	0.910E-00	0.280E-02	0.905E-00	0.290E-02	0.900E-00
0.300E-02	0.910E-00	0.310E-02	0.910E-00	0.320E-02	0.905E-00	-0.	-0.

Emissivity Required 100 x 300 x 500 x Solar Absorptivity x other

200 x 400 x Carbon Arc Absorptivity

Emissivity (100 K) =	0.995162E-01	Summation Ratio =	0.358365E-01
Emissivity (300 K) =	0.158566E-00	Summation Ratio =	0.149190E-00
Emissivity (500 K) =	0.214186E-00	Summation Ratio =	0.209544E-00
Solar Absorptivity =	0.775694E-00	Summation Ratio =	0.775694E-00
Emissivity (200 K) =	0.123676E-00	Summation Ratio =	0.992083E-01
Emissivity (400 K) =	0.184540E-00	Summation Ratio =	0.176699E-00

TABLE 11-5

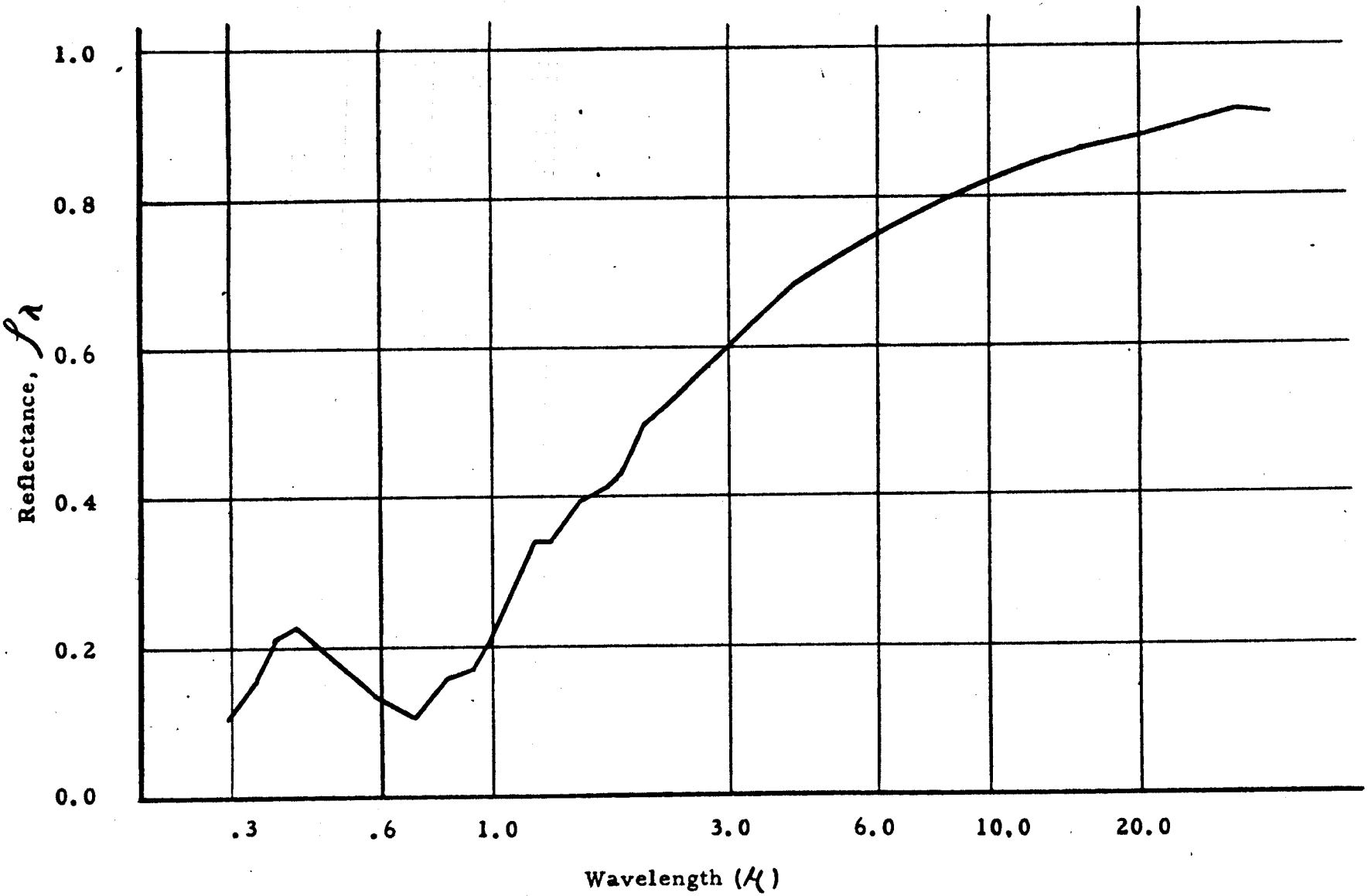

Normal Monochromatic Reflectance - Oxidized Titanium Lab. Flat Mat'l Oxid. @ 1000°F

Figure 11 - 16

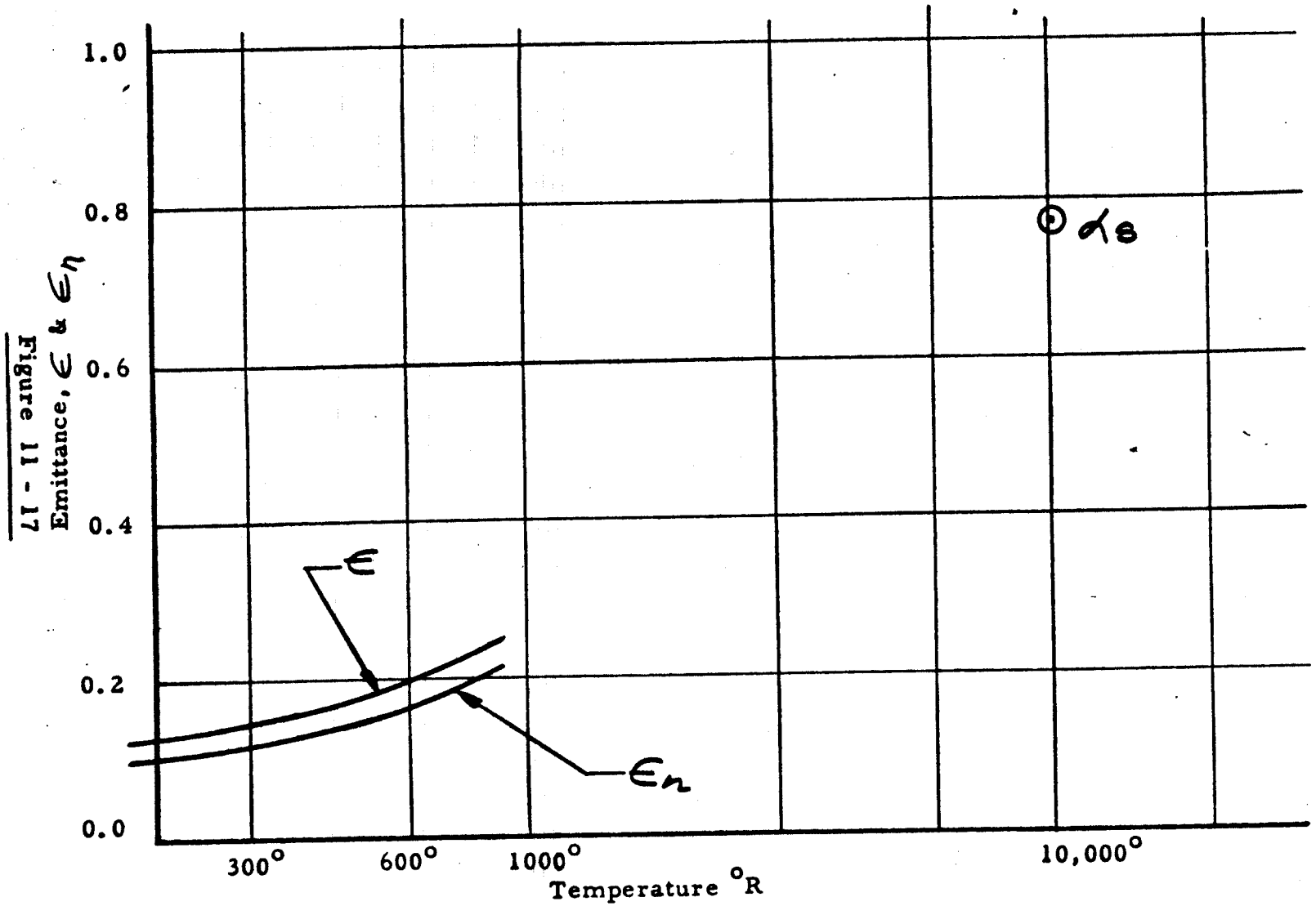

Figure 11 - 17

Total Normal & Total Emittance as a Function of Blackboy Temperature - Oxidized Titanium Lab. Flat Material

Figure 11 - 17

REFLECTIVITY DATA--OXIDIZED TITANIUM--BEAM TEST SECTION

Wavelength	Reflectance	Wavelength	Reflectance	Wavelength	Reflectance	Wavelength	Reflectance
0.300E-00	0.148E-00	0.320E-00	0.182E-00	0.330E-00	0.207E-00	0.335E-00	0.220E-00
0.350E-00	0.255E-00	0.360E-00	0.315E-00	0.370E-00	0.333E-00	0.375E-00	0.338E-00
0.390E-00	0.352E-00	0.400E-00	0.359E-00	0.410E-00	0.365E-00	0.420E-00	0.370E-00
0.430E-00	0.370E-00	0.440E-00	0.370E-00	0.445E-00	0.369E-00	0.450E-00	0.368E-00
0.465E-00	0.357E-00	0.475E-00	0.353E-00	0.490E-00	0.346E-00	0.495E-00	0.345E-00
0.500E-00	0.346E-00	0.510E-00	0.335E-00	0.520E-00	0.351E-00	0.540E-00	0.287E-00
0.570E-00	0.235E-00	0.700E-01	0.950E-00	0.800E-01	0.700E-00	0.900E-00	0.900E-01
0.100E-01	0.130E-00	0.110E-01	0.175E-00	0.120E-01	0.225E-00	0.130E-01	0.290E-00
0.140E-01	0.320E-00	0.150E-01	0.397E-00	0.160E-01	0.410E-00	0.170E-01	0.425E-00
0.180E-01	0.439E-00	0.200E-01	0.475E-00	0.250E-01	0.540E-00	0.300E-01	0.605E-00
0.350E-01	0.650E-00	0.400E-01	0.695E-00	0.450E-01	0.725E-00	0.500E-01	0.750E-00
0.550E-01	0.770E-00	0.600E-01	0.785E-00	0.650E-01	0.800E-00	0.700E-01	0.810E-00
0.750E-01	0.825E-00	0.800E-01	0.830E-00	0.850E-01	0.835E-00	0.900E-01	0.840E-00
0.950E-01	0.845E-00	0.100E-02	0.850E-00	0.105E-02	0.855E-00	0.110E-02	0.855E-00
0.115E-02	0.860E-00	0.120E-02	0.870E-00	0.125E-02	0.875E-00	0.130E-02	0.880E-00
0.140E-02	0.890E-00	0.150E-02	0.900E-00	0.160E-02	0.895E-00	0.170E-02	0.890E-00
0.180E-02	0.900E-00	0.190E-02	0.900E-00	0.200E-02	0.905E-00	0.210E-02	0.905E-00
0.220E-02	0.910E-00	0.230E-02	0.910E-00	0.240E-02	0.915E-00	0.250E-02	0.925E-00
0.260E-02	0.920E-00	0.270E-02	0.920E-00	0.280E-02	0.915E-00	0.290E-02	0.920E-00
0.300E-02	0.920E-00	0.310E-02	0.915E-00	0.320E-02	0.925E-00	-0.	-0.

Emissivity Required 100 x 300 x 500 x Solar Absorptivity x other

200 x 400 x Carbon Arc Absorptivity

Emissivity (100 K) = 0.790861E-01	Summation Ratio = 0.288127E-01
Emissivity (300 K) = 0.127119E-00	Summation Ratio = 0.119718E-00
Emissivity (500 K) = 0.180942E-00	Summation Ratio = 0.177277E-00
Solar Absorptivity = 0.748876E-00	Summation Ratio = 0.748876E-00
Emissivity (200 K) = 0.977414E-01	Summation Ratio = 0.784249E-01
Emissivity (400 K) = 0.151117E-00	Summation Ratio = 0.144928E-00

TABLE 11-6

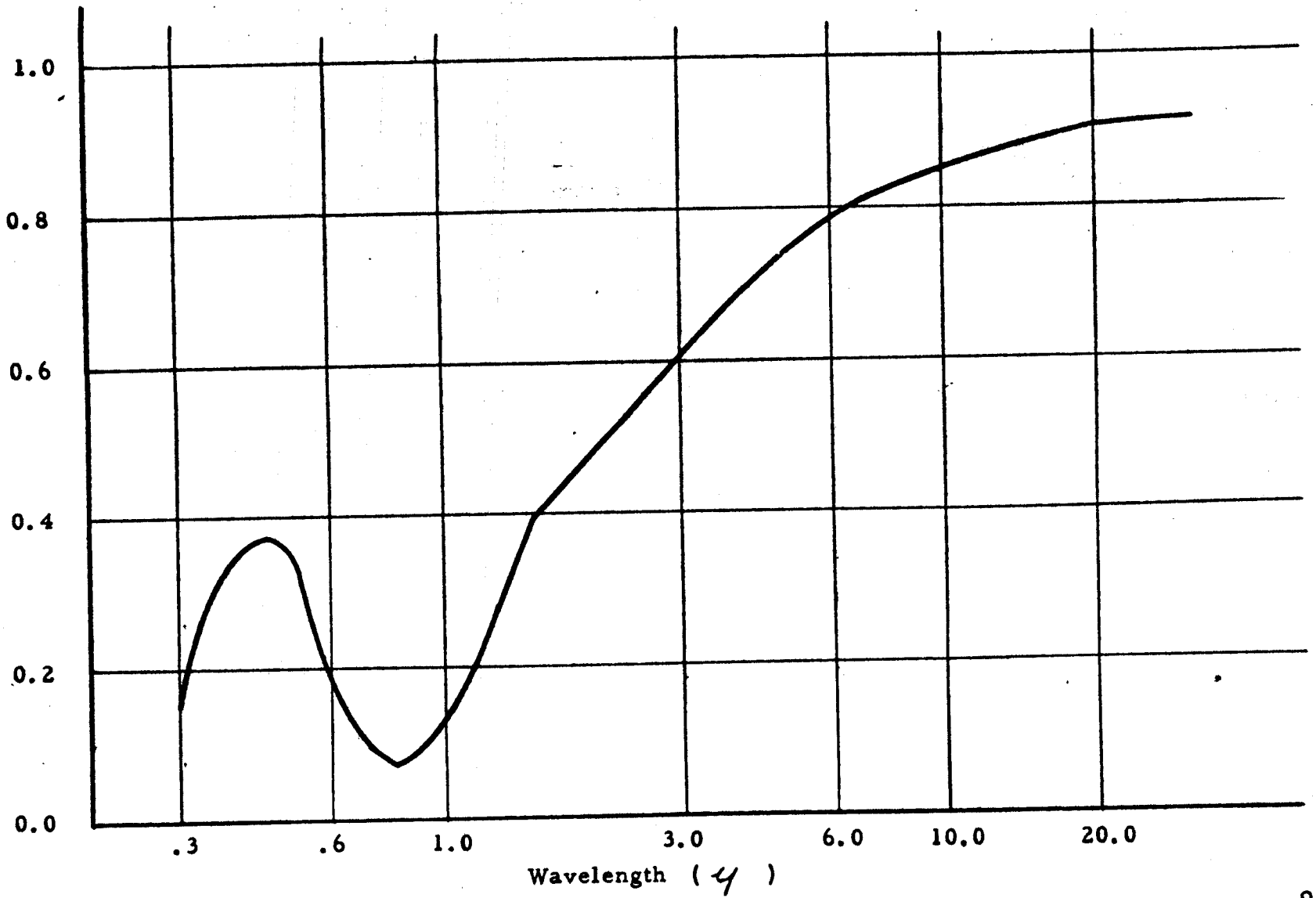

Normal Monochromatic Reflectance - Oxidized Titanium Beam Test Section - Oxidized @ 1000°F

Figure 11 - 18

Figure 11 - 18

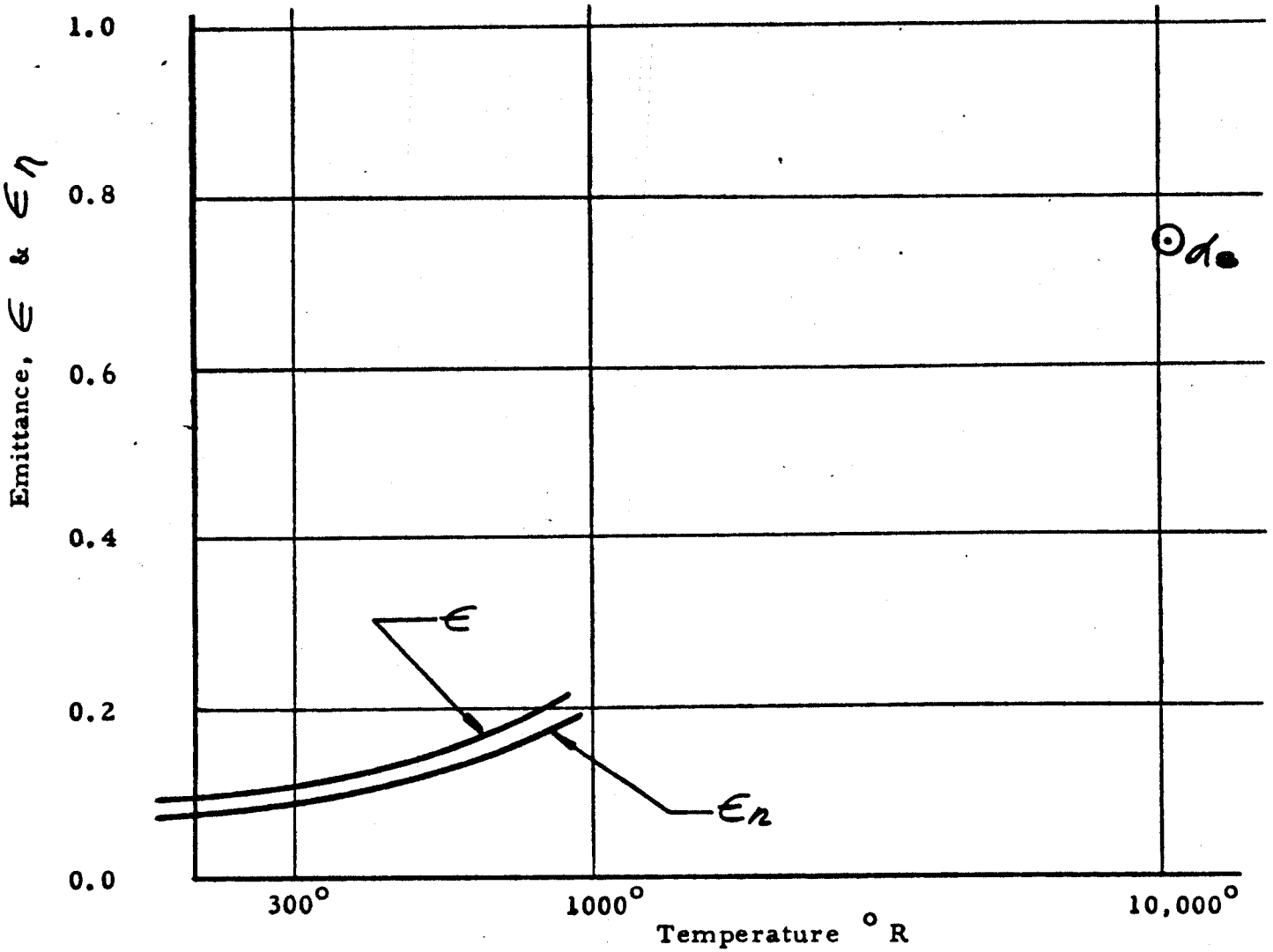

Figure 11 - 19

Total Normal & Total Emittance as a Function of Blackbody Temperature - Oxidized Titanium Beam Test Section

Figure 11 - 19

REFLECTIVITY DATA--OXIDIZED TITANIUM ALLOY, 1200-F 30 MIN

Wavelength	Reflectance	Wavelength	Reflectance	Wavelength	Reflectance	Wavelength	Reflectance
0.300E-00	0.960E-01	0.320E-00	0.960E-01	0.330E-00	0.940E-01	0.335E-00	0.930E-01
0.350E-00	0.950E-01	0.360E-00	0.104E-00	0.360E-00	0.116E-00	0.375E-00	0.130E-00
0.390E-00	0.149E-00	0.400E-00	0.152E-00	0.410E-00	0.153E-00	0.420E-00	0.153E-00
0.430E-00	0.155E-00	0.440E-00	0.157E-00	0.445E-00	0.155E-00	0.450E-00	0.156E-00
0.465E-00	0.179E-00	0.475E-00	0.186E-00	0.490E-00	0.202E-00	0.495E-00	0.272E-00
0.500E-00	0.279E-00	0.510E-00	0.280E-00	0.520E-00	0.282E-00	0.540E-00	0.283E-00
0.570E-00	0.284E-00	0.700E-00	0.193E-00	0.800E-00	0.335E-00	0.900E-00	0.464E-00
0.100E-01	0.488E-00	0.110E-01	0.490E-00	0.120E-01	0.489E-00	0.130E-01	0.487E-00
0.140E-01	0.380E-00	0.150E-01	0.332E-00	0.160E-01	0.290E-00	0.170E-01	0.250E-00
0.180E-01	0.212E-00	0.200E-01	0.180E-00	0.250E-01	0.165E-00	0.300E-01	0.255E-00
0.350E-01	0.340E-00	0.400E-01	0.480E-00	0.450E-01	0.550E-00	0.500E-01	0.605E-00
0.550E-01	0.650E-00	0.600E-01	0.680E-00	0.650E-01	0.695E-00	0.700E-01	0.720E-00
0.750E-01	0.735E-00	0.800E-01	0.760E-00	0.850E-01	0.770E-00	0.900E-01	0.775E-00
0.950E-01	0.775E-00	0.100E-02	0.780E-00	0.105E-02	0.790E-00	0.110E-02	0.790E-00
0.115E-02	0.790E-00	0.120E-02	0.795E-00	0.125E-02	0.810E-00	0.130E-02	0.815E-00
0.140E-02	0.840E-00	0.150E-02	0.835E-00	0.160E-02	0.840E-00	0.170E-02	0.850E-00
0.180E-02	0.850E-00	0.190E-02	0.860E-00	0.200E-02	0.850E-00	0.210E-02	0.855E-00
0.220E-02	0.865E-00	0.230E-02	0.875E-00	0.240E-02	0.880E-00	0.250E-02	0.890E-00
0.260E-02	0.885E-00	0.270E-02	0.890E-00	0.280E-02	0.885E-00	0.290E-02	0.890E-00
0.300E-02	0.895E-00	0.310E-02	0.885E-00	0.320E-02	0.890E-00	-0.	-0.

Emissivity Required 100 x 300 x 500 x Solar Absorptivity x other

200 x 400 x Cabron Arc Absorptivity

Emissivity (100 K) = 0.115056E-00	Summation Ratio = 0.413219E-01
Emissivity (300 K) = 0.187995E-00	Summation Ratio = 0.177139E-00
Emissivity (500 K) = 0.281357E-00	Summation Ratio = 0.275982E-00
Solar Absorptivity = 0.706926E-00	Summation Ratio = 0.706926E-00
Emissivity (200 K) = 0.143528E-00	Summation Ratio = 0.115197E-00
Emissivity (400 K) = 0.227680E-00	Summation Ratio = 0.218602E-00

TABLE 11-7

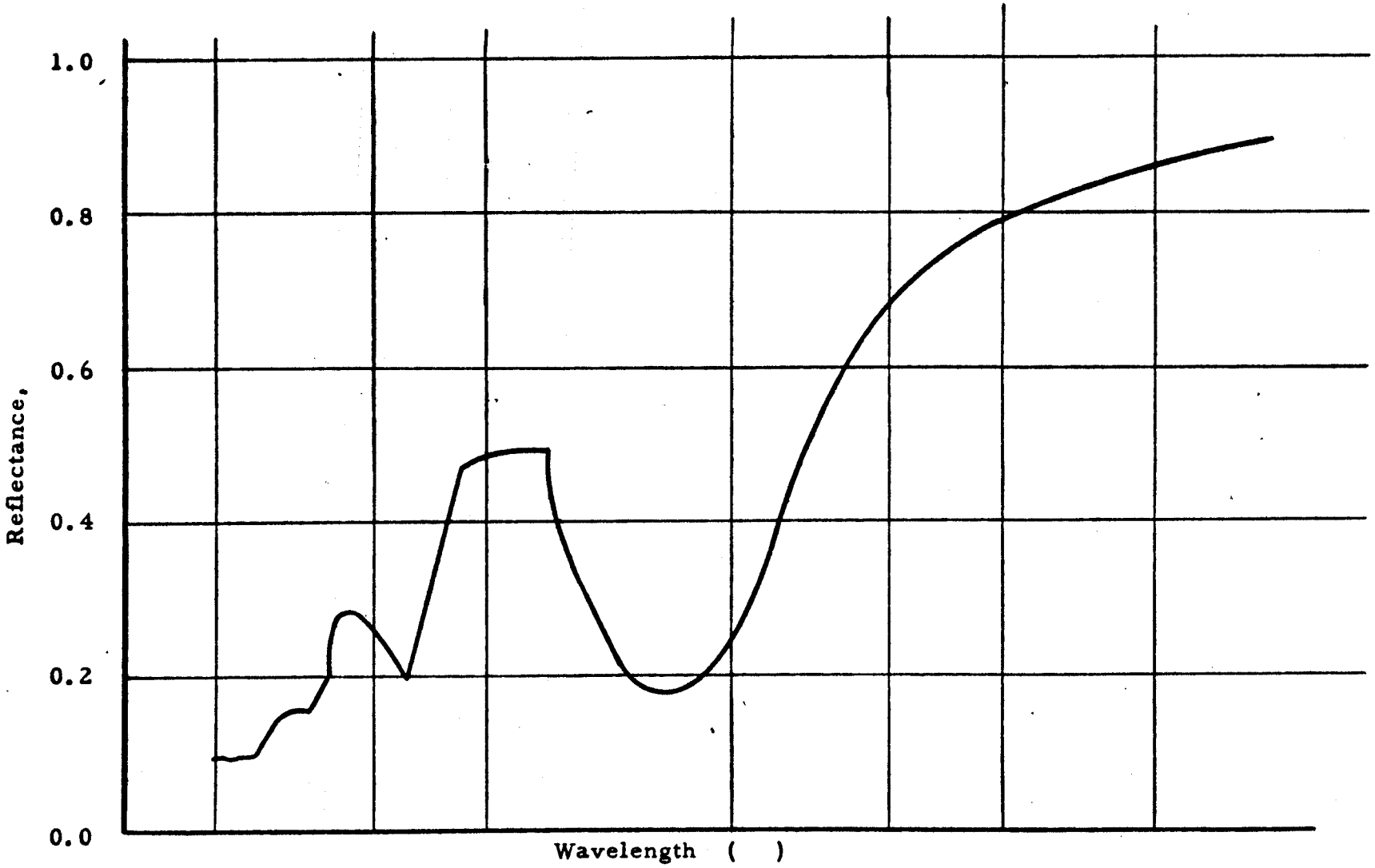

Figure 11-20

Normal Monochromatic Reflectance - Oxidized Titanium Sample Oxidized @ 1200°F - Blue - Brown (1200°F)

Figure 11-20

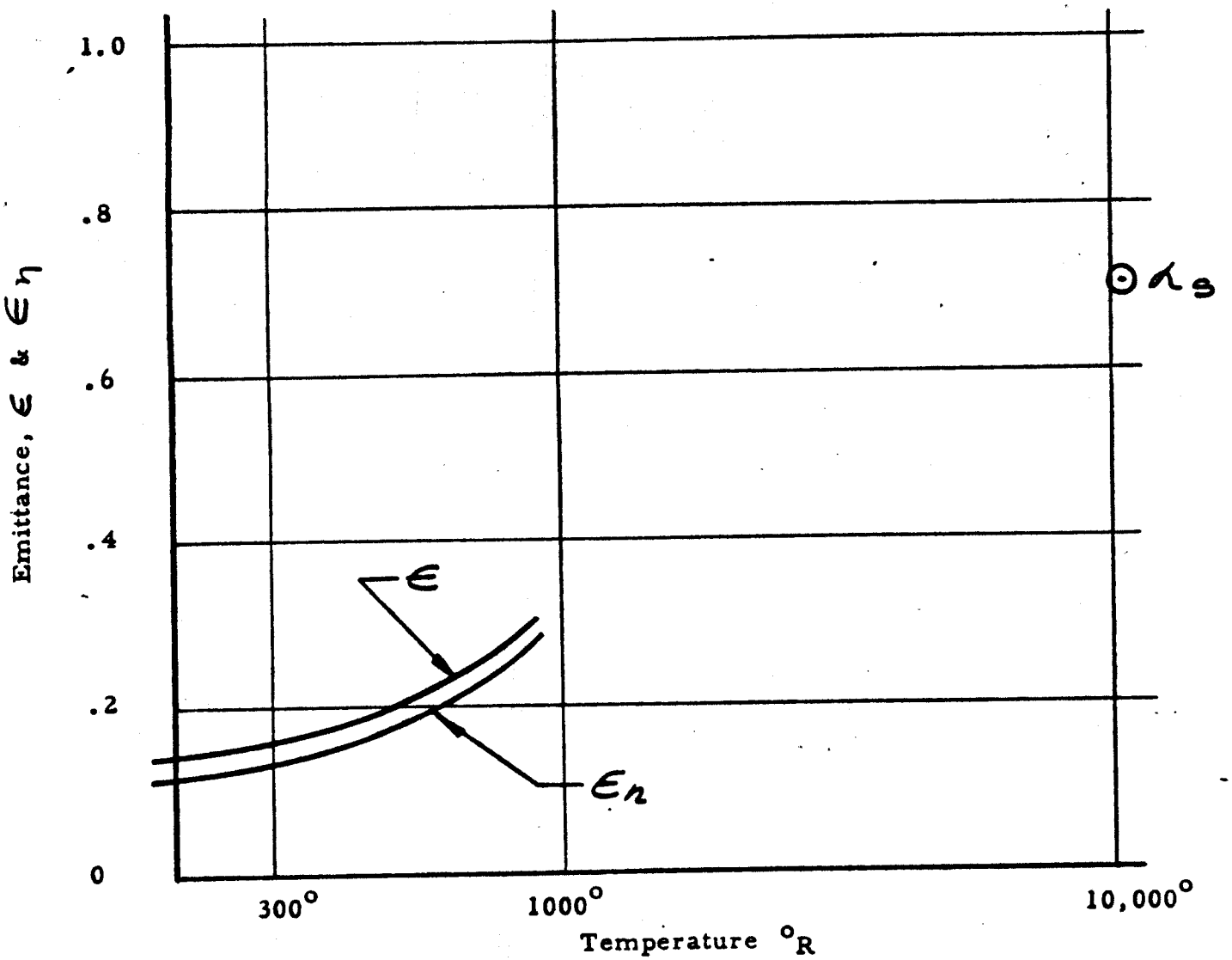

Figure 11 - 21

Total Normal & Total Emittance as a Function of Blackboy Temperature --

Oxidized Titanium -- Blue - Brown (1200°F)

Figure 11 - 21

REFLECTIVITY DATA--OXIDIZED TITANIUM ALLOY , BROWN, 1300-F 30 MIN

Wavelength	Reflectance	Wavelength	Reflectance	Wavelength	Reflectance	Wavelength	Reflectance
0.300E-00	0.106E-00	0.320E-00	0.105E-00	0.330E-00	0.104E-00	0.335E-00	0.102E-00
0.350E-00	0.980E-01	0.360E-00	0.960E-01	0.370E-01	0.375E-01	0.375E-00	0.950E-01
0.390E-00	0.960E-01	0.400E-00	0.990E-01	0.410E-00	0.100E-00	0.420E-00	0.104E-00
0.430E-00	0.105E-00	0.440E-00	0.106E-00	0.445E-00	0.109E-00	0.450E-00	0.110E-00
0.465E-00	0.115E-00	0.475E-00	0.112E-00	0.490E-00	0.133E-00	0.495E-00	0.130E-00
0.500E-00	0.124E-00	0.510E-00	0.130E-00	0.520E-00	0.150E-00	0.540E-00	0.142E-00
0.570E-00	0.150E-00	0.700E-00	0.194E-00	0.800E-00	0.220E-00	0.900E-00	0.262E-00
0.100E-01	0.290E-00	0.110E-01	0.335E-00	0.120E-00	0.350E-00	0.130E-00	0.346E-00
0.140E-01	0.388E-00	0.150E-01	0.440E-00	0.160E-00	0.457E-00	0.170E-01	0.455E-00
0.180E-01	0.472E-00	0.200E-01	0.455E-00	0.250E-01	0.395E-00	0.300E-01	0.410E-00
0.350E-01	0.530E-00	0.400E-01	0.650E-00	0.450E-01	0.670E-00	0.500E-01	0.610E-00
0.550E-01	0.545E-00	0.600E-01	0.450E-00	0.650E-01	0.405E-00	0.700E-01	0.380E-00
0.750E-01	0.410E-00	0.800E-01	0.460E-00	0.850E-01	0.520E-00	0.900E-01	0.570E-00
0.950E-01	0.605E-00	0.100E-02	0.660E-00	0.105E-02	0.710E-00	0.110E-02	0.710E-00
0.115E-02	0.715E-00	0.120E-02	0.720E-00	0.125E-02	0.715E-00	0.130E-02	0.745E-00
0.140E-02	0.770E-00	0.150E-02	0.790E-00	0.160E-02	0.800E-00	0.170E-02	0.795E-00
0.180E-02	0.790E-00	0.190E-02	0.780E-00	0.200E-02	0.635E-00	0.210E-02	0.620E-00
0.220E-02	0.735E-00	0.230E-02	0.795E-00	0.240E-02	0.820E-00	0.250E-02	0.830E-00
0.260E-02	0.785E-00	0.270E-02	0.800E-00	0.280E-02	0.845E-00	0.290E-02	0.865E-00
0.300E-02	0.870E-00	0.310E-02	0.860E-00	0.320E-02	0.875E-00	-0.	-0.

Emissivity Required 100 x 300 x 500 x Solar Absorptivity x other

200 x 400 x Carbon Arc Absorptivity

Emissivity (100 K) =	0.149032E-00	Summation Ratio =	0.652428E-01
Emissivity (300 K) =	0.301932E-00	Summation Ratio =	0.289595E-00
Emissivity (500 K) =	0.391823E-00	Summation Ratio =	0.385715E-00
Solar Absorptivity =	0.769047E-00	Summation Ratio =	0.769047E-00
Emissivity (200 K) =	0.212933E-00	Summation Ratio =	0.180738E-00
Emissivity (400 K) =	0.354890E-00	Summation Ratio =	0.344574E-00

TABLE 11-8

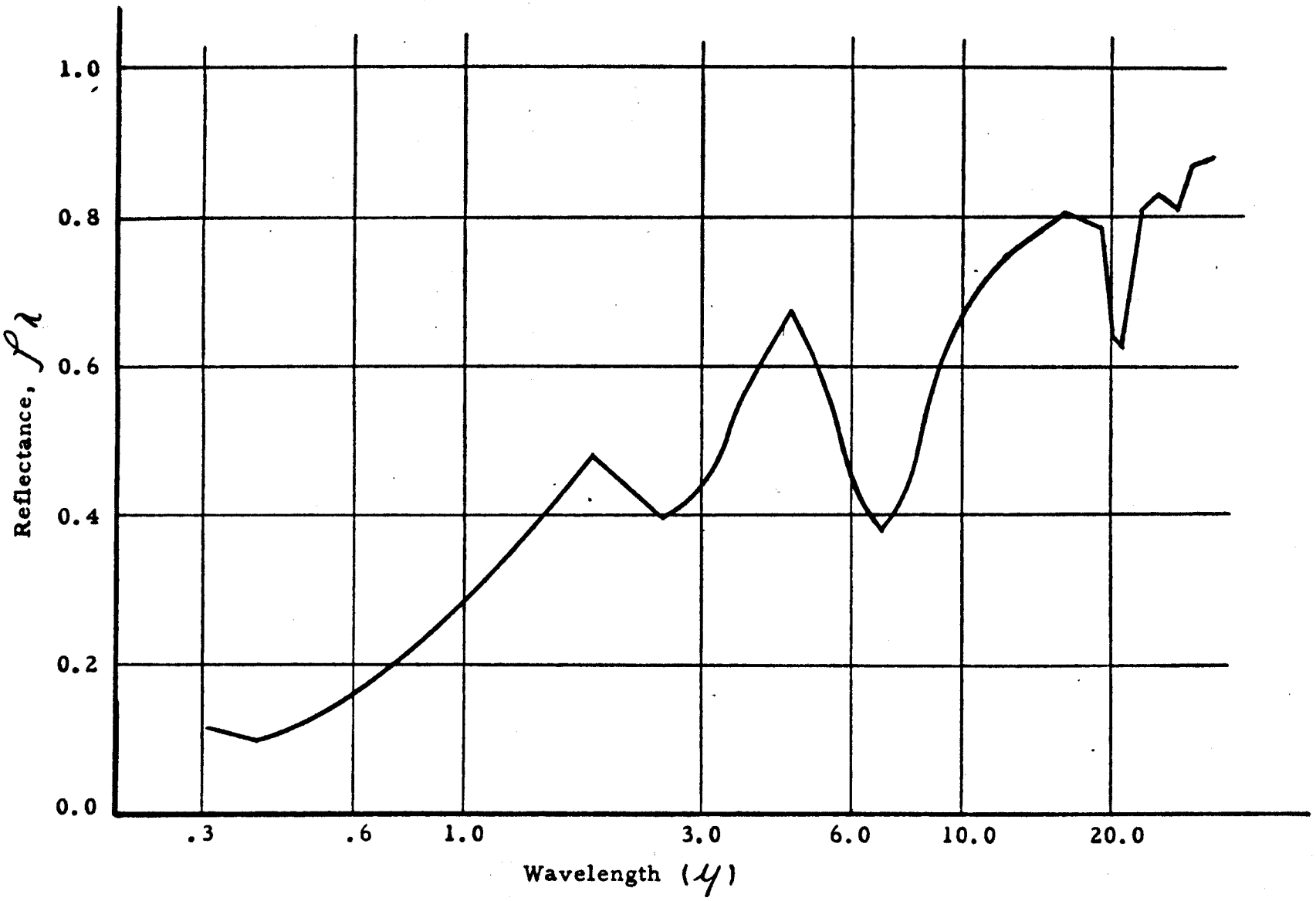

Figure 11 - 22

Normal Monochromatic Reflectance - Oxidized Titanium Sample Oxidized at 1300°F Brown

Figure 11 - 22

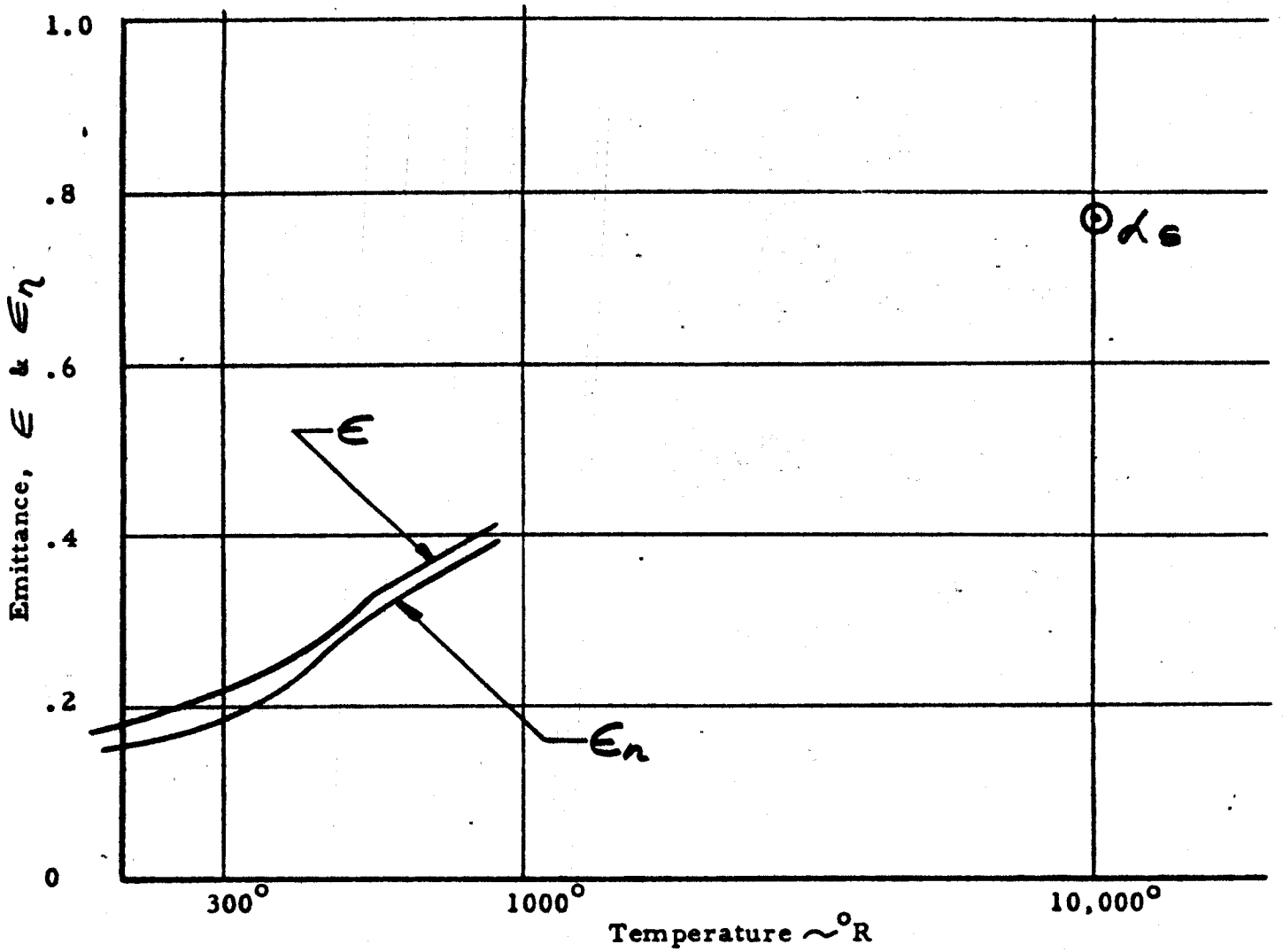

Figure 11 - 23

Total Normal & Total Emittance as a Function of Blackbody Temperature--
Oxidized Titanium - Brown (1300°F

Figure 11 - 23

REFLECTIVITY DATA--DUST BLAST OXIDIZED, 1300-F 10 MIN

Wavelength	Reflectance	Wavelength	Reflectance	Wavelength	Reflectance	Wavelength	Reflectance
0.300E-00	0.600E-01	0.320E-00	0.610E-01	0.330E-00	0.650E-01	0.335E-00	0.690E-01
0.350E-00	0.710E-01	0.360E-00	0.730E-01	0.370E-00	0.740E-01	0.375E-00	0.750E-01
0.390E-00	0.800E-01	0.400E-00	0.830E-01	0.410E-00	0.860E-01	0.420E-00	0.870E-01
0.430E-00	0.870E-01	0.440E-00	0.890E-01	0.445E-00	0.900E-01	0.450E-00	0.900E-01
0.465E-00	0.910E-01	0.475E-00	0.920E-01	0.490E-00	0.930E-01	0.495E-00	0.950E-01
0.500E-00	0.950E-01	0.510E-00	0.970E-01	0.520E-00	0.990E-01	0.540E-00	0.101E-00
0.570E-00	0.107E-00	0.700E-00	0.132E-00	0.800E-00	0.130E-00	0.900E-00	0.122E-00
0.100E-01	0.140E-00	0.110E-01	0.142E-00	0.120E-01	0.142E-00	0.130E-01	0.140E-00
0.140E-01	0.128E-00	0.150E-01	0.138E-00	0.160E-01	0.141E-00	0.170E-01	0.142E-00
0.180E-01	0.143E-00	0.200E-01	0.140E-00	0.250E-01	0.130E-00	0.300E-01	0.130E-00
0.350E-01	0.130E-00	0.400E-01	0.145E-00	0.450E-01	0.180E-00	0.500E-01	0.190E-00
0.550E-01	0.225E-00	0.600E-01	0.250E-00	0.650E-01	0.280E-00	0.700E-01	0.305E-00
0.750E-01	0.335E-00	0.800E-01	0.360E-00	0.850E-01	0.370E-00	0.900E-01	0.375E-00
0.950E-01	0.390E-00	0.100E-02	0.405E-00	0.105E-02	0.375E-00	0.110E-02	0.425E-00
0.115E-02	0.400E-00	0.120E-02	0.405E-00	0.125E-02	0.410E-00	0.130E-02	0.410E-00
0.140E-02	0.435E-00	0.150E-02	0.460E-00	0.160E-02	0.485E-00	0.170E-02	0.520E-00
0.180E-02	0.500E-00	0.190E-02	0.535E-00	0.200E-02	0.553E-00	0.210E-02	0.580E-00
0.220E-02	0.590E-00	0.230E-02	0.565E-00	0.250E-02	0.560E-00	0.250E-02	0.595E-00
0.260E-02	0.625E-00	0.270E-02	0.610E-00	0.280E-02	0.620E-00	0.290E-02	0.625E-00
0.300E-02	0.610E-00	0.310E-02	0.620E-00	0.320E-02	0.630E-00	-0.	-0.

Emissivity Required 100 x 300 x 500 x Solar Absorptivity x other

200 x 400 x Carbon Arc Absorptivity

Emissivity (100 K) = 0.385489E-00	Summation Ratio = 0.137473E-00
Emissivity (300 K) = 0.543862E-00	Summation Ratio = 0.507346E-00
Emissivity (500 K) = 0.648033E-00	Summation Ratio = 0.629953E-00
Solar Absorptivity = 0.882496E-00	Summation Ratio = 0.882496E-00
Emissivity (200 K) = 0.460438E-00	Summation Ratio = 0.365144E-00
Emissivity (400 K) = 0.596255E-00	Summation Ratio = 0.565718E-00

TABLE 11-9

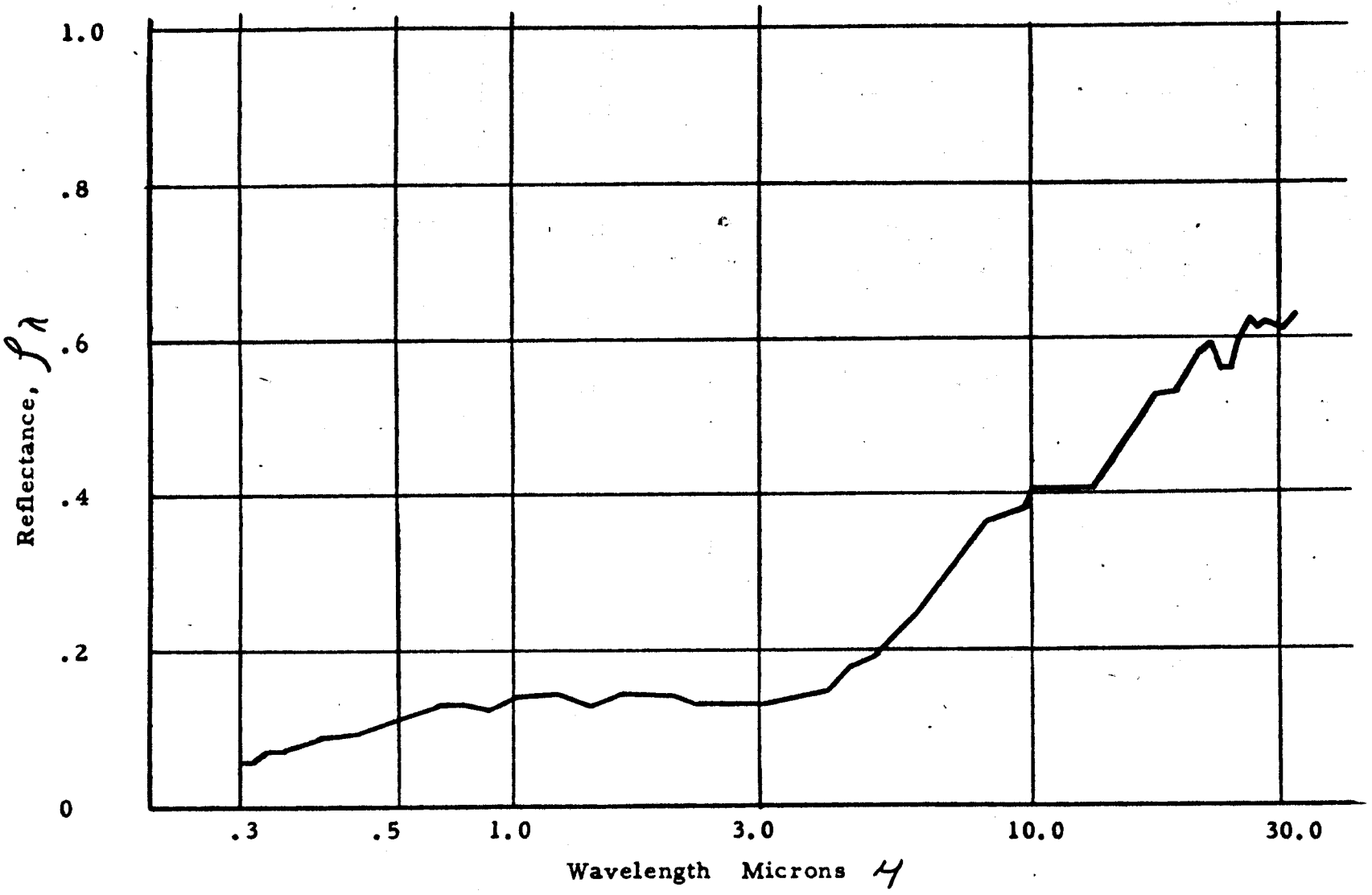

Normal Reflectance Vs. Wavelength for Titanium Alloy Ti-6AL-4V Dust Blasted & Oxidized 10 Minutes @ 1300°F

Figure 11 - 24

Figure 11 - 24

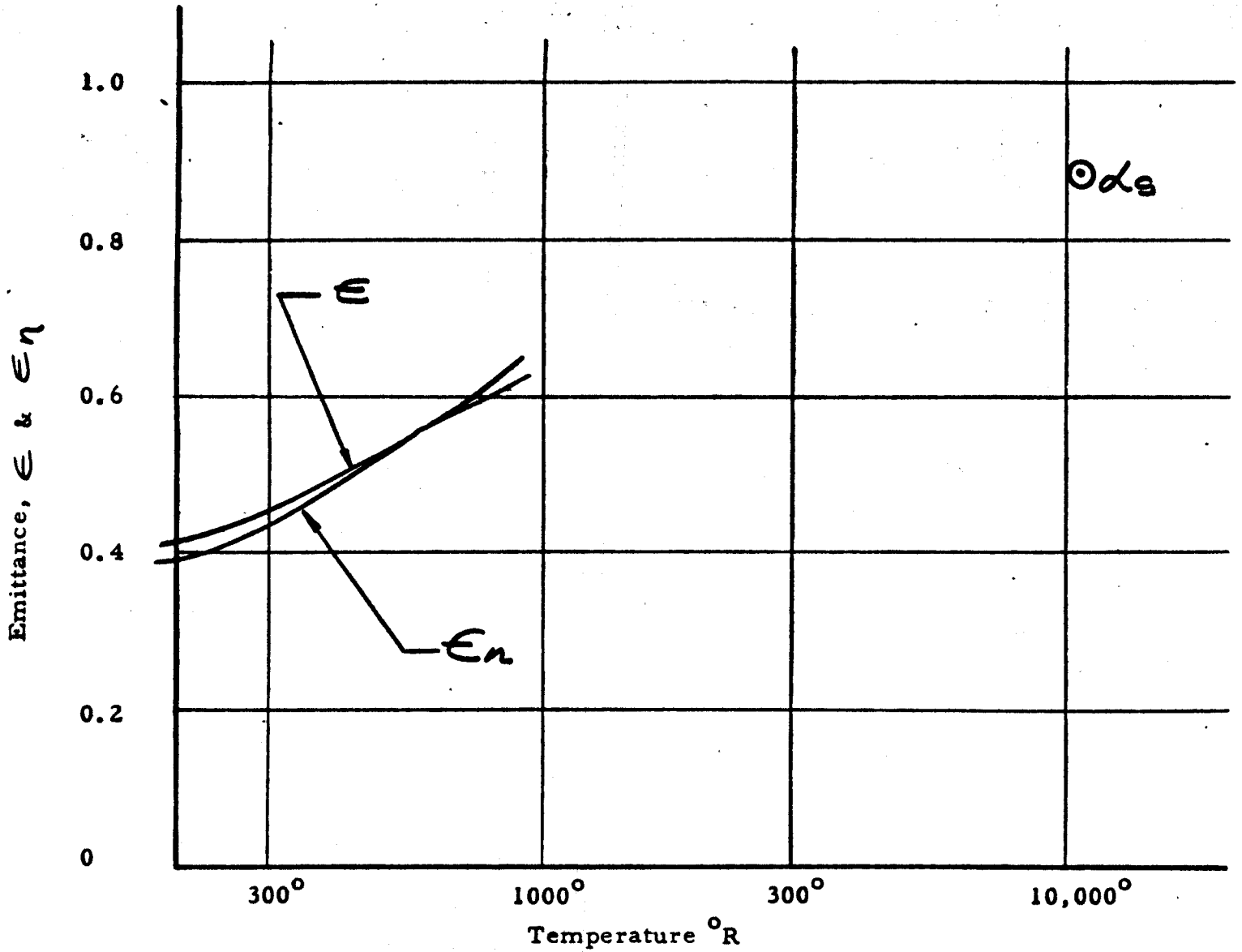

Figure 11 - 25

Total Normal Emittance & Total Emittance as a Function of Temperature,

Titanium Alloy Ti-6AL-4V Dust Blasted & Oxidized at 1300°F, for 10 minutes.

Figure 11 - 25

12.0 LIST OF REFERENCES

1. Engineering Data Sheet, No. 53, Fafnir Brg. Co., 1 Aug. 1957.
2. Roark, R. J. , Formulas for Stress and Strain, McGraw-Hill Book Co., Inc., New York, N. Y., 1954.
3. MIL-HDBK-5, Metallic Materials and Elements for Flight Vehicle Structures, Department of Defense, Washington 25, D.C., Aug. 1962.
4. Balckman, G. L., Circular Plates with Transverse or Moment Loading, Design News Magazine.
5. Honeycomb Sanwich Structures, Design News Magazine, 31 March 1965.
6. Structures Manual, Convair Aircraft Corporation, San Diego Division, San Diego, California.
7. Structures Manual, Report No. G-42-37, Ryan Aeronautical Company, Lindberg Field, San Diego 12, California, 1 Aug. 1957.
8. Preliminary Developmental Report - Deployable Large Area Solar Array Structure, Report No. 20869-1, Ryan Aeronautical Company, Lindberg Field, San Diego 12, California, 30 July 1965.
9. MIL-HBK-17, Plastics for Flight Vehicles, Part I Reinforced Plastics, Armed Forces Supply Support Center, Washington 25, D.C., 5 November 1959.
10. EPON Adhesives Manual, Shell Chemical Co., Pittsburg, Calif. pg. 52.
11. Gerard, G. and Becker, H., Handbook of Structural Stability, Article I, Buckling of Flat Plates, NACA TN-3781, Langley Aeronautical Lab., Langley, Virginia.
12. Air Force - Navy Aeronautical Standards
13. Alcoa Structural Handbook, Aluminum Company of America, Pittsburgh, Pennsylvania, 1960.
14. Bruhn, E. F., Analysis and Design of Aircraft Structures, Vol. 1, Tri-State Offset Co., Cincinnati 2, Ohio, 1958.
15. Structures Data Sheets, Volume 4, Royal Aeronautical Society, 1964.
16. Condensed D. R. M., Ryan Aeronautical Co., Lindberg Field, San Diego 12, California.
17. Saelman, B., Large Deflection of Cantilever Beams, Design News Magazine.
18. Timoshenko, S., Vibration Probelms in Engineering, 3rd. Edition, D. Van Nostrand Co., Inc. , New York, N. Y., 1955.
19. Burington, R. S., Handbook of Matehmatical Tables and Formulas, 3rd. Edition, Handbook Publishing Inc., Sandusky, Ohio, 1953.

20. Hartog, D., Mechanical Vibrations, 3rd Edition, McGraw-Hill Book Co., Inc., New York, N.Y., 1947.

21. Goetzel, Rittenhouse, and Singletary, Space Materials Handbook, Lockheed Missiles and Space Co., Addison-Wesley Publishing Co., Palo Alto, Calif., 1965.

22. Oleesky and Mohr, Handbook of Reinforced Plastics Reinhold Publishing Co., New York, N.Y., 1964.

23. Silastic RTV S-5370 Foam, Bulletin 08-019, Dow Corning Corp., Midland, Michigan.

24. Zerlaut, Harada, and Berman, Development of Space Stable Thermal Control Coatings, Report No. C6014-13, Illinois Institute of Technology Research Institute.

26. Silastic 140 Adhesive, Bulletin 9-407, Dow Corning Corp., Midland, Michigan.

27. Thermal Radiative Properties of Selected Materials, DMIC Report 177, Battele Memorial Institute, Nov. 1962.

28. Qualification of Dion RP-7A Epoxy Resin Hardener, Report No. WCLT R58-141, WADC, Wright Patterson AFB, Ohio.

29. Fralich, R. W. and Mayers, J., Behavior in Pure Bending of a Long Monocoque Beam of Circular Arc Cross-Section, NACA TN-2875, Langley Aeronautical Lab., Langley, Virginia., 1953.

30. Space Materials Data Book For Project Surveyor, Hughes Aircraft Co., Culver City, California.

31. Johnson, F. S., The Solar Constant, Journal of Meteorology, Vol. II, No. 6, Dec. 1964, p. 431.

32. Brandenberg, W. M. and Clausen, O.W., Spectral Reflectance Measurements (0.3 - .32), Aerospace Industries Round Robin Program, GD/A 63-0934 Space Science Lab.

33. Handbook of Adhesives, Bloomingdale Division, American Cyanimid Co., Aberdeen, Maryland.

34. Liquid Epoxy Hardeners Dion RP-7A and RP-22, Dion Data Sheet 302, Diamond Alkali Co., Western Division, Redwood City, California.